



**EFFECT OF PITCH RATIO FOR FINNED TUBE
IN CROSS-FLOW HEAT EXCHANGER ON FLUID
FLOW AND HEAT TRANSFER**

**2022
MASTER THESIS
MECHANICAL ENGINEERING**

Mohammed Khalid JAR AL-ISAWI

**Thesis Advisors
Prof. Dr. Kamil ARSLAN
Prof. Dr. Zena Khalefa KADHIM**

**EFFECT OF PITCH RATIO FOR FINNED TUBE IN CROSS-FLOW HEAT
EXCHANGER ON FLUID FLOW AND HEAT TRANSFER**

Mohammed Khalid Jar AL-ISAWI

**T.C.
Karabuk University
Institute of Graduate Programs
Department of Mechanical Engineering
Prepared as
Master Thesis**

**Thesis Advisors
Prof. Dr. Kamil ARSLAN
Prof. Dr. Zena Khalefa KADHIM**

KARABUK

July 2022

I certify that in my opinion the thesis submitted by Mohammed Khalid Jar AL-ISAWI titled “EFFECT OF PITCH RATIO FOR FINNED TUBE IN CROSS-FLOW HEAT EXCHANGER ON FLUID FLOW AND HEAT TRANSFER” is fully adequate in scope and quality as a thesis for the degree of Master of Science. Aug 15, 2022

Prof. Dr. Kamil ARSLAN

Thesis Advisor, Department of Mechanical Engineering

Prof. Dr. Zena Khalefa KADHIM

Thesis Co-Advisor, Department of Mechanical Engineering

This thesis is accepted by the examining committee with a unanimous vote in the Department of Mechanical Engineering as a Master of Science thesis. Aug 15, 2022

Examining Committee Members (Institutions)

Signature

Chairman : Dr. Öğr. Ü. Enes KILINÇ (KBU)

Member : Prof. Dr. Kamil ARSLAN (KBU)

Member : Prof. Dr. Zena Khalefa KADHIM (WAS)

Member : Dr. Öğr. Ü. Mutlu TEKİR (KBU)

Member : Dr. Öğr. Ü. Hüseyin KAYA (BU)

The degree of Master of Science by the thesis submitted is approved by the Administrative Board of the Institute of Graduate Programs, Karabuk University.

Prof. Dr. Hasan SOLMAZ

Director of the Institute of Graduate Programs

“I declare that all the information within this thesis has been gathered and presented in accordance with academic regulations and ethical principles and I have according to the requirements of these regulations and principles cited all those which do not originate in this work as well.”

Mohammed Khalid Jar AL-ISAWI

ABSTRACT

M. Sc. Thesis

INVESTIGATION ON EFFECT OF PITCH RATIO FOR FINNED TUBE IN CROSS-FLOW HEAT EXCHANGER ON FLUID FLOW AND HEAT TRANSFER

Mohammed Khalid Jar AL-ISAWI

Karabük University

Institute of Graduate Programs

Department of Mechanical Engineering

Thesis Advisors:

Prof. Dr. Kamil ARSLAN

Prof. Dr. Zena Khalefa KADHIM

August 2022, 153 pages

Heat exchangers are very important engineering applications in practical life. This situation has led researchers and scientists to study the types of heat exchangers, to develop new types and to increase their efficiency.

In this study, it was used integral medium finned tube with variable pitch fin to get the perfect aspect ratio that gives the largest possible amount of heat transfer, where a smooth model has been chosen to compare with three models with fin pitch. This study includes two parts; the first part consists of a theoretical study, where a designing program (SolidWorks 2018) and a simulation program (ANSYS Fluent 19R2) have been used to design and simulate the model, respectively.

Four different models (smooth tube, tube with pitch fins of $P= 1.6, 2.5,$ and 3.75 mm) have been used for the numerical analyses. Also, different water (2, 3, 4, 5, and 6 L/min) and air (1, 2, 3, and 4m/s) velocity conditions have been tried with different inlet temperatures (50, 60, 70°C). Variations of water and air velocity magnitudes and inlet temperature on convective heat transfer characteristics have been determined. The theoretical results show that the best model that gives the highest heat transfer rate is the finned tube with a fin pitch of ($P=1.6$ mm) compared to other models and according to the Enhancement Ratio ($ER= 341.84\%$). The effectiveness of the four models have been determined as 2.36%, 11.47%, 9.07%, 8.3% for the tubes of smooth, $P=1.6, 2.5,$ and 3.75 mm, respectively.

In the second part of the study, experimental analyses have been carried out for the condition of tube with $P=1.6$ mm condition. Variations of water and air velocity magnitudes and inlet temperature on convective heat transfer characteristics have also been determined in this section. It was obtained in the experimental analyses that; The value of pressure drops increases as the flow rate of hot water increases, the difference in water temperature decreases. The rate of heat transfer (Q) increases with the increase in the temperature of entering the hot water and the increase in air velocity for all models. Increasing the air velocity increases the temperature difference of hot water and air and increases the rate of heat transfer. The Nusselt number of the air increases with the flow rate of hot water and the velocity of the air. The finned tube is better than the smooth tube by the ratio of Nu number comparing with smooth tube of 68.1%, 73.5%, 80.4% for the models of $P=3.75, 2.5,$ and 1.6 mm, respectively.

At the conclusion, it was determined that the case of the finned tube with a fin pitch of $P=1.6$ mm has been determined as the best case for this study.

Key Words : Cross-Flow, Heat Exchanger, Heat Transfer, CFD, Integral Finned Tube.

Science Code : 91412

ÖZET

Yüksek Lisans Tezi

ÇAPRAZ AKIŞLI ISI EŞANJÖRÜNDE KULLANILAN KANATLI BORU İÇİN KANAT AÇIKLIK ORANININ AKIŞ VE ISI TRANSFERİNE ETKİSİNİN İNCELENMESİ

Mohammed Khalid Jar AL-ISAWI

Karabük Üniversitesi

Lisansüstü Eğitim Enstitüsü

Makine Mühendisliği Anabilim Dalı

Tez Danışmanları:

Prof. Dr. Kamil ARSLAN

Prof. Dr. Zena Khalefa KADHIM

Ağustos 2022, 153 sayfa

Isı eşanjörleri pratik yaşamda çok önemli mühendislik uygulamalarıdır. Bu durum, araştırmacıların ve bilim adamlarının ısı eşanjörlerinin türlerini incelemeye, yeni türler geliştirmeye ve verimlerini arttırmaya yönelik çalışmalar yapmalarına neden olmuştur.

Bu çalışmada, mümkün olan en büyük miktarda ısı transferi sağlayan mükemmel en-boy oranını elde etmek için değişken hatveli kanatçıklı kanat oranlarına sahip kanatlı boru kullanılmış ve kanat aralıklı üç modelle karşılaştırılmıştır. Bu çalışma iki bölümden oluşmaktadır; ilk bölüm, sırasıyla bir tasarım programının (SolidWorks 2018) ve bir simülasyon programının (ANSYS Fluent 19R2) modeli tasarlamak ve simüle etmek için kullanıldığı teorik bir çalışmadan oluşmaktadır.

Sayısal analizler için dört farklı kanatçıklı boru ($P= 1,6, 2,5$ ve $3,75$ mm) düz boru kullanılmıştır. Ayrıca farklı su ($2, 3, 4, 5$ ve 6 L/dk) ve hava ($1, 2, 3$ ve 4 m/s) hız koşulları farklı giriş

sıcaklıkları ($50, 60, 70^{\circ}\text{C}$) ile denenmiş, su ve hava hızı büyüklükleri ile giriş sıcaklığının taşınımıyla gerçekleşen ısı transfer özellikleri üzerindeki değişimleri belirlenmiştir. Teorik sonuçlar, diğer modellere göre ve İyileştirme Oranına göre ($ER= \%341,84$) en yüksek ısı transfer oranını veren en iyi modelin kanat aralığı $P= 1,6$ mm olan kanatlı boru olduğunu göstermiştir. Dört model (düz boru ve $P=1,6, 2,5$ ve $3,75$ mm) için etkinlik oranları sırasıyla $\%2,36, \%11,47, \%9,07, \%8,3$ olarak belirlenmiştir.

Çalışmanın ikinci bölümünde $P=1,6$ mm koşulunda kanatçıklı borunun durumu için deneysel analizler yapılmıştır. Su ve hava hızı büyüklüklerinin ve giriş sıcaklığının taşınımıyla ısı transfer özellikleri üzerindeki değişimleri de bu bölümde belirlenmiştir. Deneysel analizlerde sıcak suyun akış hızı arttıkça basınç düşüşlerinin değerinin arttığı ve su sıcaklığındaki farkın azaldığı belirlenmiştir. Tüm modeller için sisteme giren sıcak suyun sıcaklığın artması ve hava hızının artması ile ısı transfer hızının (Q) arttığı görülmüştür. Hava hızının artırılması, sıcak su ve havanın sıcaklık farkını arttırdığı ve ısı transfer oranını arttığı tespit edilmiştir. Havanın Nusselt sayısı, sıcak suyun debisi ve havanın hızı ile arttığı belirlenmiştir. Kanatlı boru ($P=3.75, 2.5$ ve 1.6 mm) modelleri için Nu sayısının artışı düz boruya kıyasla sırasıyla $\%68.1, \%73.5, \%80.4$ olarak elde edilmiştir.

Sonuç olarak, kanat aralığı $P= 1,6$ mm olan kanatlı boru modeli bu çalışma için en iyi durum olarak belirlenmiştir.

Anahtar Kelimeler : Çapraz Akış, Eşanjör, Isı Transferi, HAD, Kanatçıklı Boru.

Bilim Kodu : 91412

ACKNOWLEDGMENT

Firstly, I am happy to provide my thanks and appreciation to my dear supervisor Prof. Dr. Kamil ARSLAN for his valuable help and advice. Also, I would like to express my thanks and appreciation to my co-supervisor Prof. Dr. Zena Khalefa KADHIM for his valuable help and advice throughout my thesis journey.

Thanks to my first family my wife, children, mother, father, and sisters. To my friends, loved ones, and everyone who supported me. Finally, I would like to express my thanks and appreciation to everyone who helped in one way or another to implement this thesis.

CONTENTS

	<u>Page</u>
APPROVAL.....	ii
ABSTRACT.....	iv
ÖZET.....	vi
ACKNOWLEDGMENT.....	viii
CONTENTS.....	ix
LIST OF FIGURES	xiv
LIST OF TABLES	xxii
SYMBOLS AND ABBREVIATIONS	xxiii
PART 1	1
INTRODUCTION	1
1.1. BACKGROUND.....	1
1.2. MEDIUM INTEGRAL FINNED TUBE	2
1.3. MOTIVATION	3
PART 2	5
LITERATURE REVIEW.....	5
2.1. INTRODUCTION.....	5
2.2. NUMERICAL STUDIES.....	5
2.3. EXPERIMENTAL STUDIES.....	11
2.4. EXPERIMENTAL AND THEORETICAL STUDIES	16
PART 3	19
NUMERICAL SIMULATION	19
3.1. PHYSICAL MODEL	20
3.1.1. Air Zone	21
3.1.2. Pipes	21
3.1.3. Fins.....	22
3.2. GOVERNING EQUATIONS	25

	<u>Page</u>
3.2.1. Mesh Generation	27
3.2.1.1. Mesh Independence.....	31
3.3. SETTING OF MATERIALS	33
3.4. SETUP.....	33
3.5. ASSUMPTIONS	35
3.6. BOUNDARY CONDITIONS.....	35
3.7. ITERATION CONVERGENCE.....	36
3.8. SOLUTION AND RESULT	36
PART 4	37
EXPERIMENTAL WORK.....	37
4.1. GENERAL	37
4.2. LABORATORY EQUIPMENT COMPONENTS	37
4.3. INLET SECTION	39
4.3.1. Test Section.....	40
4.3.2. Centrifugal Pump	40
4.3.3. Water Heater Tank	41
4.3.4. Centrifugal Air Blower	42
4.3.5. Heat Exchanger Pipes	42
4.3.6. Measurement Tools.....	43
4.3.6.1. Thermometer	43
4.3.6.2. Datalogger	44
4.3.6.3. Pressure Meter.....	45
4.3.6.4. Thermocouples	45
4.3.6.5. Anemometer	46
4.3.6.6. Flowmeter	47
4.4. EXPERIMENTAL PROCEDURE	49
4.5. BASIC EQUATIONS	49
4.5.1. Logarithmic Mean Temperature Difference (LMTD):	50
4.5.2. Heat Capacity	50
4.5.3. Effectiveness of Heat Exchanger	51
4.5.4. Actual Rate of Heat Transfer	51

	<u>Page</u>
4.5.5. Overall Heat Transfer Coefficient.....	53
4.5.5.1. Heat Transfer Coefficient for Water side.....	54
4.5.5.2. Heat Transfer Coefficient for Air side	55
4.5.6. Enhancement Ratio for Finned Tube	56
4.5.7. Pressure Drop for heat exchanger	56
4.5.8. Error Analysis	57
 PART 5	 59
RESULTS AND DISCUSSION	59
5.1. GENERAL	59
5.2. NUMERICAL RESULTS.....	60
5.2.1. Results of the Smooth Tube	60
5.2.1.1. Effect of Inlet Water Temperature on Heat Transfer Rate.....	60
5.2.1.2. Effect of Air Velocity and Inlet Water Temperature on Heat Transfer Rate	61
5.2.1.3. Effect the Tube Inlet Temperature on Heat Transfer Coefficient.....	63
5.2.2. Effect of Fins on Heat Transfer Rate	65
5.2.2.1. Effect of Pitch Ratio for Medium Integral Fin on Heat Transfer Rate	66
5.2.2.2. Effect of the Pitch Ratio on NTU.....	68
5.2.2.3. Effect of Reynolds Number on the Effectiveness	69
5.2.2.4. Effect of Pitch Ratio on Temperature Difference	70
5.2.2.5. Effect of Pitch Ratio on Air side Overall Heat Transfer Coefficient	72
5.2.2.6. Effect of Pitch Ratio on Air side Overall Heat Transfer Coefficient	75
5.2.2.7. Effect of Air Velocity on Air side Overall Heat Transfer Coefficient	77
5.2.2.8. Effect of Pitch Ratio on Pressure Drop for Air Side.....	80
5.2.2.9. Velocity and Temperature Variations	83
5.2.2.10. Temperature Distribution for Finned Tube	86
5.2.2.11. Velocity Distribution in Smooth and Finned Tubes	95
5.3. EXPERIMENTAL RESULTS.....	104

	<u>Page</u>
5.3.1. The Effect of Different Inlet Temperature on Fluid Temperature Difference	104
5.3.2. The Effect of the Reynolds Number on Overall Heat Transfer Coefficient	108
5.3.3. The Effect of Inlet Temperature on the Effectiveness and Number of Transfer Units.....	113
5.3.4. The Effect of the Fluid Velocity on the Side Heat Transfer Coefficient	117
5.4. COMPARING THE THEORETICAL AND EXPERIMENTAL RESULT	121
5.5. THE VALIDATION FOR CURRENT STUDY WITH PREVIOUS STUDY	123
PART 6	126
CONCLUSIONS AND SUGGESTIONS	126
6.1. CONCLUSIONS	126
6.2. SUGGESTIONS FOR LATER STUDIES	127
REFERENCES.....	128
APPENDIX A: <u>UNCERTAINTY</u>	134
APPENDIX B: <u>THE TABLES FOR EXPERIMENT DATA</u>	140
APPENDIX C: <u>CALCULATION FOR ONE CASE FOR SMOOTH AND FINNED TUBE</u>	144
C.1. SMOOTH TUBE (EXPERIMENTAL DATA)	144
C.1.1. Data Case.....	144
C.1.2. The Rate of Heat Transfer	144
C.1.3. The Overall Heat Transfer Coefficient for Water	145
C.1.4. The Average Temperature for Surface	145
C.1.5. Inside Tube	146
C.1.6. Calculations for Air Side	146
C.1.7. Calculations Water Pressure Drop (ΔP)	147
C.1.8. Calculations for Number of Transfer Unit and Effectiveness	148

	<u>Page</u>
C.2. FINNED TUBE WITH PITCH FINNED 1.6 MM (EXPERIMENTAL DATA).....	148
C.2.1. Data Case.....	148
C.2.2. The Rate of Heat Transfer	149
C.2.3. The Overall Heat Transfer Coefficient for water	149
C.2.4. The Average Temperature for Surface	150
C.2.5. Inside Tube	150
C.2.6. Calculations for Air Side	150
C.2.7. Calculations Water Pressure Drop (ΔP)	152
RESUME	153

LIST OF FIGURES

	<u>Page</u>
Figure 1.1. Different types of integral finned tubes.	3
Figure 3.1. Numerical solution algorithm.	20
Figure 3.2. Air zone geometry and dimensions for heat exchanger.....	21
Figure 3.3. Dimensions of the tube passage of the study.....	22
Figure 3.4. Fins dimensions.	22
Figure 3.5. The number of fins according to change of pitch fin for test model. .	23
Figure 3.6. Direction for all flow.	24
Figure 3.7. Types of meshes.	27
Figure 3.8. Mesh shape for smooth tube.	29
Figure 3.9. Mesh for finned tube.....	30
Figure 3.10. Mesh independence between number of element and outlet water temperature for smooth tube.....	32
Figure 3.11. Mesh independence between number of element and outlet water temperature for finned tube with pitch fin (P= 1.6 mm).	32
Figure 3.12. Selection of the viscous model.	34
Figure 3.13. Selection of the boundary conditions.	34
Figure 4.1. The schematic diagram of the experimental setup.	38
Figure 4.2. Photograph of experimental setup.	39
Figure 4.3. Inlet section of the experimental setup.	39
Figure 4.4. Test section internal view for: (a) smooth tube, (b) Finned tube.....	40
Figure 4.5. Centrifugal pump.	41
Figure 4.6. Water heater tank.	41
Figure 4.7. Centrifugal air blower.....	42
Figure 4.8. Heat exchanger pipes for: (a) finned tube, (b) smooth tube.	43
Figure 4.9. Thermometer.....	44
Figure 4.10. Datalogger.....	44
Figure 4.11. Pressure meter.....	45
Figure 4.12. Thermocouple.	46

	<u>Page</u>
Figure 4.13. Termocouple calibration.....	46
Figure 4.14. Anemometer.	47
Figure 4.15. Flow meter of water.....	47
Figure 4.16. Flowmeter calibration.....	48
Figure 4.17. Temperature profiles in counter flow heat exchange.	50
Figure 5.1. Effect of inlet water temperature on heat transfer rate.	60
Figure 5.2. Variation of heat transfer rate with Re_{air} for different inlet hot water temperatures (50, 60, and 70oC) at flow rate of 2 L/min.	61
Figure 5.3. Variation of heat transfer rate with Re_{air} for different inlet hot water temperatures (50, 60, and 70oC) at flow rate of 3L/min.	62
Figure 5.4. Variation of heat transfer rate with Re_{air} for different inlet hot water temperatures (50, 60, and 70oC) at flow rate 4L/min.....	62
Figure 5.5. Variation of heat transfer rate with Re_{air} for different inlet hot water temperatures (50, 60, and 70oC) at flow rate 5L/min.....	63
Figure 5.6. Variation of heat transfer rate with Re_{air} for different inlet hot water temperatures (50, 60, and 70oC) at flow rate 6L/min.....	63
Figure 5.7. Variaiton of heat transfer coefficient with Re_w for different inlet water temperatures at air velocity 1m/s.	64
Figure 5.8. Variaiton of heat transfer coefficient with Re_w for different inlet water temperatures at air velocity 2m/s.	64
Figure 5.9. Variaiton of heat transfer coefficient with Re_w for different inlet water temperatures at air velocity 3m/s.	65
Figure 5.10. Variaiton of heat transfer coefficient with Re_w for different inlet water temperatures at air velocity 4m/s.	65
Figure 5.11. Variation of heat transfer rate with inlet water temperature for all models	66
Figure 5.12. Variation of heat transfer rate with water Reynolds number for constant air velocity (2m/s).....	67
Figure 5.13. Variation of heat transfer rate with water Reynolds number for constant air velocity (3m/s).....	67
Figure 5.14. Variation of heat transfer rate with water Reynolds number for constant air velocity (4m/s).....	68

	<u>Page</u>
Figure 5.15. Relation between number of transmission units with Reynolds number and constant air velocity 2m/s.	69
Figure 5.16. The relation between Reynolds number and effectiveness with different pitch ratio and constant air velocity 3m/s.....	69
Figure 5.17. The relation between the Reynolds number and the effectiveness with different pitch ratio and constant air velocity 4m/s.	70
Figure 5.18. Relationship between the temperature difference and Reynolds number for constant air velocity 2m/s.....	71
Figure 5.19. Relationship between temperature difference and Reynolds number for constant air velocity 3m/s.	71
Figure 5.20. Relationship between temperature difference and Reynolds number for constant air velocity 4m/s.	72
Figure 5.21. The relation between overall heat transfer coefficient and air velocity for all models.....	73
Figure 5.22. The relation between overall heat transfer coefficient and air velocity for all models.....	73
Figure 5.23. The relation between overall heat transfer coefficient and air velocity for all models.....	74
Figure 5.24. The relation between overall heat transfer coefficient and air velocity for all models.....	74
Figure 5.25. The relation between overall heat transfer coefficient and air velocity for all models.....	75
Figure 5.26. Air side overall heat transfer coefficient with Renolds number for all models.....	76
Figure 5.27. Air side overall heat transfer coefficient with Renolds number for all models.....	76
Figure 5.28. Air side overall heat transfer coefficient with Renolds number for all models.....	77
Figure 5.29. Internal overall heat transfer coefficient varies with air velocity for all models.....	78
Figure 5.30. Internal overall heat transfer coefficient varies with air velocity for all models.....	78

	<u>Page</u>
Figure 5.31. Internal overall heat transfer coefficient varies with air velocity for all models.....	79
Figure 5.32. Internal overall heat transfer coefficient varies with air velocity for all models.....	79
Figure 5.33. Internal overall heat transfer coefficient varies with air velocity for all models.....	80
Figure 5.34. Effect of air side velocity on pressure drop at varies pitch ratio and smooth tubes with constant water mass flow rate 2L/min.....	81
Figure 5.35. Effect of air side velocity on pressure drop at varies pitch ratio and smooth tubes with constant water mass flow rate 3L/min.....	81
Figure 5.36. Effect of air side velocity on pressure drop at varies pitch ratio and smooth tubes with constant water mass flow rate 4L/min.....	82
Figure 5.37. Effect of air side velocity on pressure drop at varies pitch ratio and smooth tubes with constant water mass flow rate 5L/min.....	82
Figure 5.38. Effect of air side velocity on pressure drop at varies pitch ratio and smooth tubes with constant water mass flow rate 6L/min.....	83
Figure 5.39. Temperature distribution in the smooth tube.....	84
Figure 5.40. Temperature distribution in finned tube with pitch fin (P=1.6 mm)	84
Figure 5.41. Temperature distribution in finned tube with pitch fin (P= 2.5 mm). .	85
Figure 5.42. Temperature distribution in finned tube with pitch fin (P=3.75 mm).	85
Figure 5.43. Temperature distribution of water in smooth tube.	87
Figure 5.44. Temperature distribution of water in ntegral finned tube with pitch fin (P=1.6 mm).....	88
Figure 5.45. Temperature distribution of water in integral finned tube with pitch fin (P=2.5 mm).	89
Figure 5.46. Temperature distribution of water in integral finned tube with pitch fin (P=3.75 mm).	90
Figure 5.47. Temperature distribution of air and water for smooth tube.....	91
Figure 5.48. Temperature distribution of air and water for meduim integral finned tube with pitch fin (P=1.6 mm).....	92
Figure 5.49. Temperature distribution of air and water for medium integral finned tube with pitch fin(P= 2.5 mm).....	93

	<u>Page</u>
Figure 5.50. Temperature distribution of air and water for medium integral finned tube with pitch fin(P= 3.75 mm).....	94
Figure 5.51. Velocity distribution of air in smooth tube.....	96
Figure 5.52. Length of the vortex after the smooth tube.....	97
Figure 5.53. Velocity distribution of air in medium itegral finned tube with pitch fins (P=1.6 mm).	98
Figure 5.54. Length of the vortex after the medium itegral finned tube with pitch fins (P=1.6 mm).	99
Figure 5.55. Velocity distribution of air in medium itegral finned tube with pitch fins (P=2.5 mm).	100
Figure 5.56. Length of the vortex after the medium itegral finned tube with pitch fins (P=2.5 mm).	101
Figure 5.57. Velocity distribution of air in medium itegral finned tube with pitch fins (P=3.75 mm).	102
Figure 5.58. Length of the vortex after the medium itegral finned tube with pitch fins (P=3.75 mm).	103
Figure 5.59. The relationship between the hot water temperature difference and the Reynolds number at air velocity (1 m/s) for all temperatures(50, 60, and 70oC) for smooth tube.	104
Figure 5.60. The relationship between the hot water temperature difference and the Reynolds number at air velocity (2m/s) for all temperatures(50, 60, and 70oC) for smooth tube.	105
Figure 5.61. The relationship between the hot water temperature difference and the Reynolds number at air velocity (3 m/s) for all temperatures(50, 60, and 70oC) for smooth tube.	105
Figure 5.62. The relationship between the hot water temperature difference and the Reynolds number at air velocity (4 m/s) for all temperatures(50, 60, and 70oC) for smooth tube.	106
Figure 5.63. The relationship between the hot water temperature difference and the Reynolds number at air velocity (1 m/s) for all temperatures (50, 60, and 70oC) medium integral finned tube with pitch(P= 1.6 mm).....	106

Figure 5.64. The relationship between hot water temperature difference and Reynolds number at air velocity (2m/s) for all temperatures (50, 60, and 70oC) medium integral finned tube with pitch(P= 1.6 mm).	107
Figure 5.65. The relationship between hot water temperature difference and the Reynolds number at air velocity (3 m/s) for all temperatures (50, 60, and 70oC) medium integral finned tube with pitch(P= 1.6 mm).	107
Figure 5.66. The relationship between hot water temperature difference and the Reynolds number at air velocity (4m/s) for all temperatures (50, 60, and 70oC) medium integral finned tube with pitch(P= 1.6 mm).	108
Figure 5.67. The relationship between overall heat transfer coefficient and Reynolds number at air velocity (1 m/s) for all inlet hot water temperatures for smooth tube	109
Figure 5.68. The relationship between overall heat transfer coefficient and Reynolds number at air velocity (2 m/s) for all inlet hot water temperatures for smooth tube	109
Figure 5.69. The relationship between overall heat transfer coefficient and Reynolds number at air velocity (3 m/s) for all inlet hot water temperatures for smooth tube.	110
Figure 5.70. The relationship between overall heat transfer coefficient and Reynolds number at air velocity (4 m/s) for all inlet hot water temperatures for smooth tube.	110
Figure 5.71. The relationship between overall heat transfer coefficient and Reynolds number at air velocity (1 m/s) for all inlet hot water temperatures for integral finned tube with (P=1.6).	111
Figure 5.72. The relationship between overall heat transfer coefficient and Reynolds number at air velocity (2 m/s) for all inlet hot water temperatures for integral finned tube with (P=1.6).	111
Figure 5.73. The relationship between overall heat transfer coefficient and Reynolds number at air velocity (3 m/s) for all inlet hot water temperatures for integral finned tube with (P=1.6).	112

Figure 5.74. The relationship between overall heat transfer coefficient and Reynolds number at air velocity (4 m/s) for all inlet hot water temperatures for integral finned tube with (P=1.6).	112
Figure 5.75. The effectiveness and NTU at air velocity (1 m/s) for all inlet hot water temperatures for smooth tube.	113
Figure 5.76. The effectiveness and NTU at air velocity (2 m/s) for all inlet hot water temperatures for smooth tube.	114
Figure 5.77. The effectiveness and NTU at air velocity (3 m/s) for all inlet hot water temperatures for smooth tube.	114
Figure 5.78. The effectiveness and NTU at air velocity (4 m/s) for all inlet hot water temperatures for smooth tube.	115
Figure 5.79. The effectiveness and NTU at air velocity (1 m/s) for all inlet hot water temperatures for medium integral finned tube with (P=1.6).	115
Figure 5.80. The effectiveness and NTU at air velocity (2 m/s) for all inlet hot water temperatures for medium integral finned tube with (P=1.6).	116
Figure 5.81. The effectiveness and NTU at air velocity (3 m/s) for all inlet hot water temperatures for medium integral finned tube with (P=1.6).	116
Figure 5.82. The effectiveness and NTU at air velocity (4 m/s) for all inlet hot water temperatures for medium integral finned tube with (P=1.6).	117
Figure 5.83. The effect of hot water flow rate on the outlet heat transfer coefficient at air velocity (1 m/s) at different inlet temperatures for smooth tube. ..	118
Figure 5.84. The effect of water flow rate on the outlet heat transfer coefficient at air velocity (2 m/s) at different inlet temperatures for smooth tube.	118
Figure 5.85. The effect of water flow rate on the outlet heat transfer coefficient at air velocity (3 m/s) at different inlet temperatures for smooth tube.	119
Figure 5.86. The effect of water flow rate on the outlet heat transfer coefficient at air velocity (4 m/s) at different inlet temperatures for smooth tube.	119
Figure 5.87. The effect of water flow rate on the outlet heat transfer coefficient at air velocity (1 m/s) at different inlet temperatures for integral finned tube with pitch (P= 1.6 mm).	120

	<u>Page</u>
Figure 5.88. The effect of water flow rate on outlet heat transfer coefficient at air velocity (2 m/s) at different inlet temperatures for integral finned tube with pitch (P=1.6 mm).....	120
Figure 5.89. The effect of water flow rate on outlet heat transfer coefficient at air velocity (3 m/s) at different inlet temperatures for integral finned tube with pitch (P=1.6mm).....	121
Figure 5.90. The effect of water flow rate on outlet heat transfer coefficient at air velocity (4 m/s) at different inlet temperatures for integral finned tube with pitch (P=1.6 mm).....	121
Figure 5.91. Comparing the theoretical and experimental results of the relationship between the outlet heat transfer coefficient at different flow rats for a smooth tube.	123
Figure 5.92. Comparing theoretical and experimental results of relationship between the outlet heat transfer coefficient at different flow rate for a integral finned tube with pitch fin (P=1.6 mm).....	123
Figure 5.93. Comparing relationship between numerical results for internal heat transfer coefficient with the water entry temperatures between the current study and comparative research	124
Figure 5.94. Comparing relationship between numerical results for Nusselt number with Renolds number between the current study and comparative research	125
Figure 5.95. Comparing relationship between numerical results for pressure drop with the water entry temperatures between current study and comparative research.....	125
Appendix A.1. Pictures of central of standardization and quality control for calibrating reader temperature.....	136
Appendix A.2. Image for Quality control of a calibration of K-type thermocouples	137
Appendix A.3. Calibration of thermometer type (HT-9815).....	139

LIST OF TABLES

	<u>Page</u>
Table 3.1. The specifications of the meshes.	28
Table 3.2. Mesh independence for smooth tube.	31
Table 3.3. Mesh independence for finned tube (P= 1.6 mm).....	32
Table 3.4 . Boundary conditions.	35
Table 5.1. The comparative between the present research and Mardan study.....	60
Table 5.2. Variation of heat transfer rate with inlet water temperature.	66
Table Appendix B.1. Smooth tube.....	140
Table Appendix B.2. Finned tube.	142
Table Appendix C.1. Data case.....	144
Table Appendix C.2. Data case.....	148

SYMBOLS AND ABBREVIATIONS

SYMBOLS

A_i	: Internal surface area of tube
A_o	: External surface area of tube
av.	: Average
Cp_a	: Specific heat
Cp_w	: Specific heat
d	: Diameter
d_z	: Diameter of air section
F	: Correction factor
f	: Friction n factor
h_i	: Heat transfer coefficient of interior side tube
h_o	: Heat transfer coefficient of exterior side tube
K_l	: Loss coefficient
K_w	: Thermal conductivity of water
\dot{m}_w	: Mass flow rate of water
Nu_w	: Nusselt number
Pr_w	: Prandtl number
Q	: Heat transfer rate
Re_w	: Reynolds number
s	: Surface
T_{ai}	: Inlet temperature of air
T_{ao}	: Outlet temperature of air
T_{hi}	: Outlet temperature of fluid hot
T_{ho}	: Inlet temperature of fluid hot
T_s	: Temperature of exterior surface tube
U_i	: Overall heat transfer coefficient of interior side tube
u_w	: Water velocity
γ_a	: Kinematic viscosity of air

ε : Effectiveness
 μ : Dynamic viscosity
 ρ : Density
% : Percent Sign.
 ΔP_{fitt} : Pressure drops in fittings
 ΔP_{tube} : Pressure drops for pipes
 ΔP_{total} : Total pressure drops
 α_a : Thermal diffusivity of air

ABBREVIATIONS

CFD : Computational Fluid Dynamics
ER : Enhancement Ratio
HEX : Heat exchanger
HVAC : Heating, Ventilation and Air Conditioning
LMTD : Logarithmic Mean Temperature Difference
NTU : Number of Transfer Units

PART 1

INTRODUCTION

1.1. BACKGROUND

The heat exchangers can be defined as a device which is used to exchange heat between two fluids without mixing them. This device is considered one of the primary parts for the heat systems. There is an increasing demand for heat exchanger for wide applications in various areas of life such as, aviation, automobiles etc. Heat exchanger is mainly used in power generation, ecological building, air conditioning systems, electronic chip cooling, refrigeration, ventilation, and heating. An air conditioning unit improvement depends on the performance of its devices consisting of the heat exchangers, compressors, and fans. Most researchers and scientists work to improve the performance of heat exchanger and reduce its consumption of the electrical power. There are many techniques used to increase the thermal performance of heat exchangers and thus increase its energy and decrease the size and cost. The mentioned techniques are named the heat transfer enhancement techniques and they usually include three classifications [1]:

- **Passive Methods:** This type of techniques does not require external power. It includes gaseous additives, surface-tension devices, evacuated improvement devices, swirl-flow devices, treated surfaces, liquids additives, extended surfaces, coiled tubes, and rough surfaces.
- **Active Methods:** This type of techniques requires external power and includes electrostatic fields, mechanical aids, injection involves, fluid vibration, and surface vibration.
- **Compound Methods:** This type of techniques includes two or more techniques including active and passive concurrently to improve the devices of heat transfer.

The above-mentioned enhancement techniques are used to reduce the thermal resistance of heat exchanger and obtain higher heat transfer coefficient. This requires the reduction of size, heat exchange increase and reduce the pumping heat exchanger power [2].

Finned tubes are used to improve the performance of the heat exchanger by excess of the surface space (area) to tubes of heat exchanger. There are several types of fins such as cylindrical, square, rectangular, pin and annular fins [3-5].

1.2. MEDIUM INTEGRAL FINNED TUBE

The integral finned tubes are tubes which are formed by the ring fins on their outside surface to improve heat transfer [6]. Area rate is typical in order to determine the type fins:

- Low integral finned tube ($A_o/A_i=3$)
- Medium integral finned tube ($A_o/A_i=5$)
- High integral finned tube ($A_o/A_i=14$)

The ratio means the total exterior surface area of the tube with fins to the total interior tube area [7]. These include fin height more than pitch (Figure 1.1). These types of integral finned tubes are used to heat the pressurized gases and condensation water bath treatment and hydrocarbons cooling [8]. Medium integral finned tube has been used in this study.

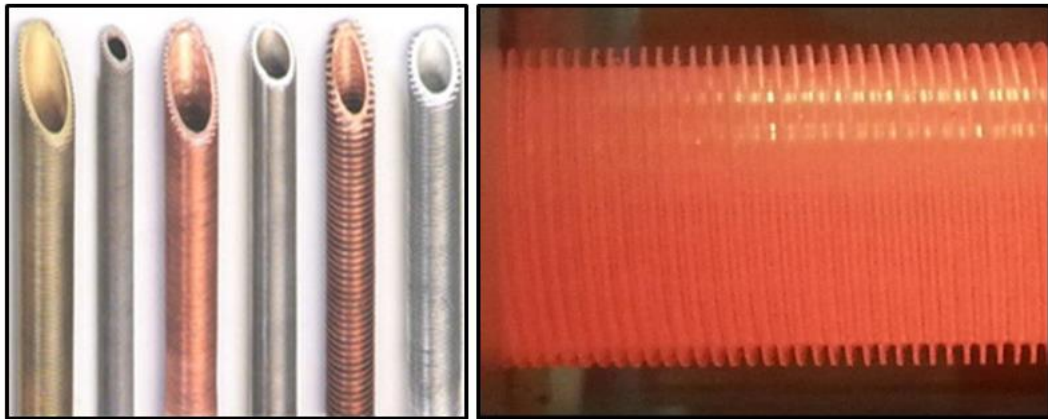


Figure 1.1. Different types of integral finned tubes.

1.3. MOTIVATION

The high uses and importance of heat exchangers in manufactural applications motivated many researchers to think about enhancing the heat exchangers performance. The goal of this study is to decrease the thermal resistance of heat exchangers and get higher convective heat transfer coefficients and decreasing the exchanger volume using the finned tubes with different pitches. Enhance the heat transfer coefficient of heat exchanger by the use of different pitches ratio to the fins on the air side. In order to reach the goal specified in the research, the study involves the implementation of a survey of previous research literature relevant to the research topic in addition to the following:

The numerical side includes the following:

- Using computational fluid dynamic program (ANSYS Fluent 19.2R2) to simulate 3D geometry for smooth tube and integral finned tubes with various pitch for cross flow heat exchanger.
- Find the best pitches which give the maximum heat transfer coefficient.
- Comparing the results with the smooth tube as well as with the findings of literature.

The experimental side includes the following:

- Smooth tube and integral finned tube of $P=1.6$ mm have been used for the experiments.
- Studying the effects of various inlet water temperature, air and water velocities on the convective heat transfer of a smooth and integral finned tube.
- Finding the cases that improve the heat transfer of many ranges of air and water velocities.
- Developing the experimental correlations for Nu and f of integral finned tubes as a function of Re .
- Comparing the experimental results with the findings of other researchers in the literature and numerical results.

PART 2

LITERATURE REVIEW

2.1. INTRODUCTION

This part of our study shows many prior related studies to improve the heat transfer rate in crossflow heat exchangers. The main objective of using integrated fins on smooth tubes of heat exchangers is to raise the area exposed to heat transfer by these fins and from this idea is presented in previous investigations and studies to improve heat transfer, where the focus will be on a number of experimental and theoretical studies regarding the improvement of heat transfer by the use of various approaches and techniques.

2.2. NUMERICAL STUDIES

Mon and Gross [12] investigated numerical study for the effects of fin spacing on tube bundles in-line and staggered arrangement. Three different fins have been used with pitches of ($P=1.6$ mm, $P=2$ mm, and $P=4$ mm) at a fixed height of 5 mm with a tube diameter of 24 mm. The boundary in the fins and the surface of the tube depends largely on the aspect ratio (spacing of the fin relative to its height). For using $P=1.6$ mm spacing Reynolds number ($Re= 8.6 \times 10^3$) two boundary layers were found from the front edge of the fins to the highest thickness near the intersection of the base of the fin in the middle of the tube where these vortices develop at the intersections, which are more visible in large distances ($P=2$ mm and $P=4$ mm) mm, and after increasing the Reynolds number to ($Re= 4.3 \times 10^4$) at a distance of 4 mm spacing, with increasing speed. The result shows that the coefficient of heat transfer raises in both tube arrays when aspect ratio was raised.

Jung and Assanis [13] studied the development of a predictive numerical model for the crossflow fin type crossflow fin heat exchanger, depending on the rate of total transfer and air flow resistance on the design of fins and vents. The final goal of studying the design of the heat exchanger is to maximize the heat expulsion rate while reducing the flow resistance. Two cases were studied to evaluate the performance after obtaining the results where the dimensions of the cooler core were changed from 0.5 to 1.5 while keeping the interface area. The front as it is 0.25 shows that the heat expulsion rate increases by 8% when increasing the percentage of (0.5 to 1.5 mm) with the same basic volume of air velocity 8 m/s because the coolant is exposed to more heat transfer during the passage of air flow through longer tubes.

Wais [14] presented a three-dimensional numerical study of fluid flow in the heat exchanger of the strongest finned tube, where three models of radial fins were used, ignoring the resistance generated among the base of the fin and the surface of the tube, as the fin was homogeneous from the same metal tube, and the distance between the fins was 2.6 mm and the distance between the diameters of the tubes 80 mm and a variable air inlet velocity (0.5, 1, and 1.5) m/s and an air inlet temperature of 10°C and a liquid inlet temperature of 90°C were selected. Through the results obtained, it was found that the best of the three solutions that were worked on is the third model in terms of the highest air entry velocity, and the resulting efficiency was higher than the other models, and the best air entry velocity for the best improvement equation was calculated at the air entry velocity at 1 m/s.

Bhuiyan and Islam, [15] presented a study to determine the characteristics of the fin and tube heat exchanger for the plain and corrugated fin configurations without neglecting the lined and overlapping tube arrangements for the laminar flow system by using commercial computational fluid dynamics. The results were expressed in terms of the friction factor (f), Colburn factor (j) and efficiency index (j/f). The longitudinal and transverse inclination leads to a decrease in the thermal and hydraulic performance of the heat exchanger due to the low Reynolds number ($400 \leq Re_H \leq 1200$), and the reduction in the pitch of the fins leads to a significant decrease in the heat transfer and friction properties. In this study, air was used as a working fluid assuming its constant properties and that there is a constant incompressible three-

dimensional flow, and through the results it was found that the efficiency increases with the increase of the pitch of the tube.

Gunnasegaran et al [16] presented research about the impact of the engineering variables on the heat transfer properties of the open fin compact heat exchanger, where a model was used consisting of an entry and exit hole with three pitches for fins (1.0 mm, 2.0 mm, and 4.0 mm) where the fins were designed in a way that has the greatest role to produce the maximum effectiveness for [CHE]. These fins include five different rings with different arrangement of the slot angles ($+2^\circ$, $+4^\circ$, -2° , -4° , and uniform angle 20°). Through the results obtained and after conducting the simulation, it was found that there is a highest and lowest value of Reynolds number ($100 < Re < 1000$) in each ventilation opening and along the flow due to the recurrent development and destruction of the boundary layer. ($+2^\circ$, -4°) was higher than the case for the uniform aperture angle (20°) and the highest value of the pressure drop coefficient was in the case ($+4^\circ$) in addition to that the Nusselt's number and the pressure drop coefficient are directly proportionate to the Reynolds number and inversely with the decrease in the fin pitch.

Ocloń et al [17] conducted an experimental study on the impact of surface fouling of the interior tube on thermal performance of a high-temperature fin-tube heat exchanger. For an exchanger where two rows of successive finned tubes with gas flow were selected to analyze the results assuming that the thickness of the sedimentation layer is 1 mm and the wall thickness of the tube made of carbon steel is 2 mm. For the wall of pipe, when the water is not filtered appropriately, it greatly decreases the heat transfer capacity and raises the temperature of the pipe and fin. According to the obtained calculations, the flue gas outlet temperature can rise by 122 K when silicate scale is deposited within the pipe. These foulings are more visible when the pipe wall temperature is 163 K and this high increase may lead to the generation of excessive high thermal stress that leads to the fracture of the pipe.

Dev and Ardhapurkar [18] presented a numerical study to examine the multi-flow heat exchanger by the use of the computational fluid dynamics [CFD]. The study included two cold streams, one of these cold tubes passes in the opposite direction of the hot

fluid through the interior region, and the other passes in the intersecting direction with the hot fluid above the exterior tube. It was assumed that the mass flow for both cold streams is 0.25 kg. Assuming that the two coolant fluids are mixed after the heat exchange process, a different simulation was conducted for the mass flow of the coolant through the opposite direction and the cross-flow direction of the hot fluid. Through the results obtained, it was shown that the heat transfer rate is greater in the case of the cross-flow heat exchanger where the present arrangement is 22.6% more efficient than the counter flow heat exchanger and 54.44% more efficient than the cross-flow heat exchanger.

Wais [19] carried out the accuracy of the air-side connections of a heat exchanger through the heat flow of a tube and fin exchanger at different thicknesses of the fins. Three-dimensional models were implemented to detect the heat transfer properties among the finned tube and the air for various shapes of fins to detect the heat transfer ratio among the air and the fin. During the flow of air in the cross-flow heat exchanger at a mass flow ratio of 4 m/s inlet velocity and inlet fluid temperature of 300°C and the interior tube surface temperature is 70°C and by obtaining the results and analyze the outputs established from the digital computations with the combined outputs, it was detected that heat transfer is decreased when the fin thickness and variations are increased inside standard deviation. Experimental techniques may forecast the coefficients of heat transfer with satisfactory accuracy.

For the purpose of introducing improvements in heat transfer for many engineering, industrial and scientific fields, Kumar [20] analyzed the three-dimensional geometry of the heat exchanger of smooth cross tube and finned tube in which hot water passes within the tube and cooling air outside the tube by the use of ANSYS-Fluent 15.0 program. Three-dimensional models were implemented that allow looking at the heat transfer in three directions, based on the mass flow rate at a speed (4m/s), the liquid inlet temperature (300°C), the interior tube surface temperature (70°C) and the air velocity (1m/s). Through the results that appeared, it was found that there is a gradient of the diagram in the distribution of temperature accompanied by the test tube, and the temperature difference appears in all cases that the temperature gradient in the finned

tube is higher than the smooth tube, and this means that the fin has an important impact on the increase of temperature difference inside the test tube.

Xu et al. [21] investigated the flow and heat transfer features of a rectangular external tube bank aligned with six rows of tubes using commercial fluid dynamics software, and after imposing data such as the Reynolds number, fin height, longitudinal tube pitch, transverse tube pitch, fin pitch in the axial direction and fin width. By using the program (ANSYS Fluent), the findings revealed that the heat transfer ability and friction loss in the external bank of the 3D finned rectangular tube were higher than those of the smooth tube bank. The increase of the longitudinal tube inclination, fin width and fin height or reducing the transverse tube inclination and fin inclination in the axial direction increased heat transfer and flow loss in the exterior rectangular fin tube bank. In spite that the finned tube bank performance was not always larger to the smooth tube bank, but it provides the possibility of greater heat transfer comparing with the smooth tube under the same conditions.

Due to the urgent need to develop a more effective and stable heat exchanger, the heat transfer and temperature gradient were studied in a cross-flow heat exchanger using various fin thicknesses by Rajput and Arya [22]. A three-dimensional model consisting of an eight-pass copper tube with dimensions (250 × 500 × 1200) mm width, height and length, was adopted. The tube is of the integrated low fin tube type with an interior diameter (19 mm), a root diameter (21) mm and an exterior diameter (24) mm. Variable fin height (1.5, 3 mm) was used to compare the results. The imposed air velocity was limited (1, 2, 3, 4) m/s and the flow rate was limited (2, 3, 4, 5, 6) L/min and the inlet air temperature was the temperature of the room whereas the side fluid temperature was limited (50, 60, 70, 80) °C and after running the simulation on the (ANSYS Fluent 14.5) program. The results showed that by changing the dimensions of the fins, the heat transfer will increase, and the water outlet temperature will decrease significantly, in addition to the temperature gradient in the finned tube 3 mm greater than the finned tube is 1.5 mm and smooth, and the heat transfer rate has increased by 15% when using 3 mm fin height instead of 1.5 mm fin height.

Ismail et al. [23] made a three-dimensional study on a cross-flow heat exchanger by the use of air as an external turbulent flow in the form of a cold liquid with the range of velocity (1 to 6) m/s and hot water as an internal flow assumed laminar with Reynolds 1200. The tube diameter is (1mm and 10mm). The results indicated that the small tube had better performance with a controlled pressure drop for each, where the heat flow rate increased by 20% per unit volume while the heat rate per unit volume increased by 800 to 1200% with the increase of air speed from the lowest speed to the highest given speed. The efficiency of the fin was different according to the diameter of the tube, where it is from 97% to 91% for a tube diameter of 10 mm and 99.98% to 99.99% for a tube diameter of 1 mm, and the findings also clarified that the fins effect is profitable and beneficial only in the case of the normal exchanger, while the small exchanger is not profitable or useful.

Sahel et. al. [24] presented an experimental study to test the impact of tube shape on heat transfer in a finned heat exchanger tube. Different shapes were chosen for the purpose of comparison in the study (circular, flat, oval and oval in both directions). Using simulations for two-dimensional flow inside the range of Reynolds numbers (3000 to 20000). The results showed that the shape of the tube directly affects the thermal and dynamic behavior of the fin and tube heat exchanger. 10% under the same conditions, however the elliptical tube produces the lowest pressure losses compared to other models.

Merdan and Kadhim [25] presented a study dealing with the impacts of many tubes and directions of flow on the heat transfer coefficient by examining five models of smooth copper tubes of various lengths and with various corridors (2,4,6,8,10) for a cross-flow heat exchanger to reach the best suitable length for the transfer of heat. Using ANSYS Fluent 14.2 program, when the exterior and interior pipe diameters are fixed (24,19 mm) correspondingly and a constant volumetric flow for all models (5) L/m and the same temperature of the cold and hot liquid (25, 80) °C, respectively. The results found that the heat transfer ratio increased with the increase in the lengths of the tubes, as the surface area will increase and therefore the air is spread through a wider area, but this increase was on the expense of increasing the pressure drop. A single triangular soft tube model consisting of (4) finned tubes to enhance the

transmission heat was also used. The results of this model showed that the finned tube delivered a higher heat transfer rate compared with the smooth tube, by increasing the air velocity, the increase of the external heat transfer coefficient, as well as increasing the volumetric flow ratio, the pressure drop increased. Flow does not affect heat transfer. The researcher suggested that the ideal and best length for heat transfer between these models is the 4-pipe model.

2.3. EXPERIMENTAL STUDIES

Hofmann et al. [26] experimentally tested the heat transfer and pressure flux in tubes with fins, serrated, rigid and cross-sectional different in cross-flow intended to enhance the heat exchanger performance. They tested three different geometries of fin tube within different fin geometric constants (height, pitch, thickness and width) for a heat exchanger consisting of eight consecutive rows of finned tubes and 11 tubes arranged on top of each other. After verifying the validity of the measurements and comparing the results obtained from the experimental results, it was found that there was a difference between rigid and threaded finned tubes within the range of Reynolds number (10000 to 20000) and an overall rise in the heat transfer coefficient from the air side within the same Reynolds number. The validated measurement of threaded and rigid finned tubes was in arrangement with formulas in the literature.

Nuntaphan and Kiatsiriroat [27] focused on studying the impact of fly ash deposits on the cross-flow heat exchanger performance that contains many spiral finned tubes used as a heat transfer surface. Warm air passes at a temperature of 40°C, which contains a high percentage of fly ash, to exchange heat with the cold-water stream at a temperature of 5°C inside the pipes at a flow ratio of 10 L/min. Through the experimental results, it was found that the thermal resistance resulting from pollution increased with time. Thus, it is the main reason to decrease the ratio of heat transfer and the percentage of ash deposited on the surface of the tube depends on the amount of ash, the amount of condensate, the quality of the fins used, their geometric shape and the pitch of the fin on the surface of the exchanger.

Experimental investigations were carried by Hofmann et. al. [28] for the pressure drop heat and transfer at the turbulent flow of combustion gases in tubes with transverse fins with serrated transverse fins in the transverse flow. The engineering designs of the fins were considered where there was a difference in the geometrical constants of the fins such as the height, fin pitch, thickness and width for the designs of heat exchangers with tubes and transverse fins for cross flow. It is necessary to take into consideration the shortcomings and benefits of the elements that affect the pressure drop and heat transfer. By analyzing and evaluating the measurements and information resulting from the experiment, the correlation of heat transfers and pressure drop was obtained. The comparison with some correlations showed a good application in which the Reynolds number was specified in three fields (10000 to 20000) to evaluate performance.

Agrawal and Bhagoria [29] tested an experimental study to assess the properties of heat transfer of the copper-nickel multi tube with corrugated fins in a cross-flow heat exchanger. The heat transfer ratio of the heat exchanger is increased either by aggregating the surface area by raising the fins number or by creating a disturbance. In the flow, the experiment was conducted on a heat exchanger with copper fins and after conducting an assessment of the cross-flow heat exchanger with copper fins for a temperature ranging between 38-64°C and the speed of water from 0.077 m/s to 0.271 m/s and a velocity of Air 3.194 m/s to 14.52 m/s. It was found that the coefficient of heat transfer increased constantly on the air and water side according to the concept of different flow of water and air.

Prognosis et al. [30] presented a study of the impact of the fin pitch and fin materials on the air side performance of heat exchangers under high Reynolds numbers (4000, 13000) using 6 samples for testing made of copper and aluminum with fin pitch difference (3.2, 4.2, 6.2) mm. For a fin thickness of 0.4 mm and an exterior tube diameter of 34.8 mm for two rows of tubes, the main objective of the experiment was to increase the front air velocity to 6 m/s and its effect on the performance of the fins and the metal of the fins. After conducting the experiment, it was found that when increasing the fin pitch to 6.2 mm there is a height notable in the friction factor. Changing the metal of the fins has no noticeable effect on the performance of the fins,

and it was found that the effect of Coburn j factor is very little because the higher Reynolds number gives good mixing, which generates better heat transfer performance regardless of the change in the pitch of the fins.

To study the heat transfer properties and the resistance to air flow through a helical tube heat exchanger, Fajiang et al. [31] examined 13 bundles of tubes for helical fin heat exchangers for samples with an external diameter of 32 mm and a various transverse tube pitch ($S1/d=2- 3.31$), fin height ($h/d=0.22- 0.5$), longitudinal tube pitch ($S2/d=2 - 3.31$) and fin pitch ($t/d = 0.22- 0.5$). The tests were implemented inside the range of fluid flowing Re number ($Re=5\times 10^3\sim 5.5\times 10^4$). After conducting the experiment, it was found that Heat transfer, Nu number rose with the rising of fluid flowing Re number, transverse tube pitch $S1$ and fin pitch t ; reduced with the increase of transverse tube pitch $S2$ and fin pitch h . The flowing resistance Euler number correlation with fluid flowing Re number, fin pitch t , fin height h , transverse tube pitch $S1$, longitudinal tube pitch $S2$ is practical.

Ikpotokin and Osueke [32] studied the coefficient of heat transfer as the function of pressure drop and pipe position of a bank of pipes embedded in the supply flow, where the experimental method was mainly used to create logarithmic mean curves and pressure ends up and down the test part stream. After calculating the heat transfer and flow coefficients besides obtaining the correlations for heat transfer by fitting the power law curve for every subject of the tube and using the simulation program FEMLAB 3.0, it was found that the Nusselt's number increased by 12.49% from the first column to the second and 11.85% from the second to the third column and 5.27% from the third to the fourth column and this was because of the increase in the turbulence rate resulting from a successive column of pipes. Despite this increase, we find it in a decreasing rate downstream from the third column, where the heat transfer is stable and there is a slight change in the convection of the tube after the fourth tube. Thus, this will ease compact heat exchanger design and discourage to use a large number of tubes which save space and energy, and after comparing the numerical and experimental results, there was a clear perception about the flow of the boundary layer developments and the formation of the eddy between the tubes where it was found that the progress of boundary layer and vortices among surrounding tube surfaces are

highly depending on Reynolds number. Vortex formation arises among the tube shaft and the fourth tube shaft and this explains the increase in heat transfer resistance and the rate of decreasing Reynolds number.

Due to the increasing demand for efficient heat exchanger design, Chaudhari et al. [33] investigated the impact of a finned heat exchanger on the total heat transfer coefficient with a variable velocity of air (3, 4, 5, 6) m/s and a variable flow of coolant (180, 260, 340, 420, 500) L/min. After conducting calculations through a well-verified classification and providing a full set of numerical information in this study, it was concluded that the total heat transfer ratio of the finned heat exchanger is larger than that of the finless heat exchanger, as with increasing the air speed the heat transfer rate of the heat exchanger increases for the finned tube. This increase makes the Reynolds number increase the Nusselt's number also because the Nusselt's number is directly relative to the coefficient of heat transfer, so the heat transfer ratio raises.

Abdul Hassan et al. [34] studied the improvement of heat transfer properties of a flow heat exchanger using an experimental integrated low fin tube. The study included the design and manufacture of two test sections, the first consisted of a smooth copper tube with the internal diameter of 19 mm and the external diameter of 24 mm, and the second consisted of a finned tube bottoms with a diameter of 19 mm, a root diameter of 21 mm and an exterior diameter of 24 mm for a fin height of 1.5 mm, thickness of 1 mm and a fin pitch of 2 mm. The coolant used was the air that passed through the test tube with a speed range (1, 2, 3, 4, 5, 6) liters / minute, the temperature of the water when entering the test tube was (50, 60, 70, 80) °C. It is shown from these figures that the finned tube has a higher heat dissipation rate comparing with the smooth tube and under similar circumstances. This is due to the increase in the cooling surface area and the penetration of the boundary layers near the tube wall because of the formation of the fins, as the improvement rate is 72% for the finned tube over the smooth tube.

Dhangar [35] presented an experimental study to test the heat transfer and air-side friction properties of five types of fin-tube heat exchangers with 12 rows of 18 mm tube diameter. These samples included five types of fin conformations to test the best type that provides the highest heat transfer rate from these fin models consisted of (slit

fin, plain fin, crimped spiral fin, fin with delta-wing longitudinal VGs and assorted fin with front 6-row vortex-generator fin and rear 6-row slit fin), based on the correlation of numerical data and Reynolds number in the range from 4000 to 10000. It is detected that the curly helical fin delivered better heat transfer rate and pressure drop comparing with other four fins, and the mixed fin heat exchanger (front vortex generator fin and rear fin) had good performance comparing with the heat exchanger fin with delta wing vortex generators. Increasing the Reynolds number increases the pressure drop, the outlet temperature of the fluid decreases, and the heat transfer reduces and this is due the increase in turbulence.

For the high demand and immediate need to design an efficient hot heat exchanger, Kumar et al. [36] examined the effect of a finned heat exchanger on a heat exchanger without fins on the examined heated total return coefficient, where the heated total return coefficient was examined for each of the hot exchange at an air rate (3, 4, 5, 6) m/s and coolant flow (180, 260, 340, 420, 500) L/min. This study shows a combined systematic, practical and statistical analysis of the total heated return coefficient of the coolant using a circular finned tube with finless tube heat exchanger. The experience is that with the increase in the speed of air exchange, the performance of the finned tube heat exchanger improves because the Reynolds variable improves the Nusselt's variable as the relationship between the Nusselt's variable and the Reynolds variable is direct with the warm exchange coefficient, so the warm exchange value improves.

Arshad et al. [37] carried out an experimental study on a group of parallel triangular fin tubes with a rate of (P/D_{eff}) 1.62 to show the impact of the fin geometry on the response to vibration caused by the flow. The presence of fins on the tubes increased the heat transfer ratio and thus affected the fluid dynamics around the tubes. An empirical analysis of fluid-elastic vibration of the parallel triangular fin tube array that is subject to a single-phase cross-flow of air was carried out and by evaluating the effect of different fin elements such as the thickness of the used fin (1.3, 1.7, 2.3) mm and fin density (4.5, 5, 5.5, 6, 6.5) mm. It was found that there is no unpredictability in utmost of the finned tubes for the present range of free flow velocity when they are put in the first, second and fourth rows, but the capacity of the finned tubes raised suddenly in the third row and thus the tube is exposed to the maximum vibration in

this row. The comparison between the exposed tube and the finned tube vibration response indicated that the vibration fullness of the exposed tube is less than that of the finned tube and there is a high difference in the profile between the vortex shedding in the finned tube compared with the exposed tube.

Aefan et. al. [38] has experimentally studied the heat exchanger through flow to transfer heat energy from the hot to cold liquid. The method of recording the average temperature differences was chosen to determine the heat transfer. The findings showed that the heat transfer increased when increasing the air mass flow rate. On the other hand, the efficiency decreased with the increase in the air mass flow ratio and the increase in the speed will increase Reynolds. This will increase the amount of air used to contact the surface of the heat exchanger to reduce heat.

2.4. EXPERIMENTAL AND THEORETICAL STUDIES

Tripathi and Singh [39] carried out a review that involved carrying out high number of numerical studies to enhance heat transfer of air-side. Among the factors it was mentioned that affect the performance of solid round finned tubes are (tube spacing, row effects, fin thickness, fin spacing, tube diameter, tube bundle arrangement and fin height). Through this study and the studies that preceded it, they agreed that the heat transfer coefficient nearby the fin and from one row to another varies according to the depth of the beam. The results indicated that the heat transfer coefficient and flow distribution differ across a tube in a bundle from an individual tube, and that the distribution of temperature on fin surfaces and flow structures between fins.

Muna and Hadeer [40] presented numerical and experimental research to improve the heat transfer features for single and low integral fins tube multi passes cross-flow heat exchanger by the use of silica as a nanofluid with oil and water base fluid. The numerical study carried out using of “ANSYS FLUENT 14.5”. Three concentrations of silica nanoparticles (SiO_2) had been investigated (0.3, 0.5, 0.7) % with oil and water as the base fluid. The experimental test rig was designed and manufactured where test sections and wind tunnel. The tested tubes are smooth and low integral finned tubes and the distance from center to center of two adjacent tubes are 55 mm. The tested

tubes have (19, 21 and 24) mm interior, root and exterior. The integral finned have a rectangular geometry with dimension (1.5, 1 and 1 mm) height, thickness and pitch, respectively. The cooling fluid (air) flew through air tunnel across tested tubes at velocities (1, 1.8, 2.6 and 3.4) m/s. The hot fluid (oil, water, and Nano fluids) flew through tested tubes at (2, 3, 4 and 5) L/min with inlet temperatures of (50, 60, 70 and 80) °C. Oxide silicon SiO₂ nanoparticle powder with average diameter 15 and 17.5 nm is dispersed in hydraulic oil (ISO VG 32) and distilled water with the optimum volume concentration of 0.7 % VOL from the numerical is used as nanofluid. The results show that, using low integral fins lead to a significant enhancement of heat liberated. The oil and water side heat transfer coefficient investigated experimentally and numerically without Nano fluid. The result shows that, using enhanced tube surface (finned tubes) raises oil and waterside (hi) with maximum enhancement (+21.03 and +25.2) %. The heat liberated investigated experimentally and numerically for oil and waterside heat exchanger without Nano fluid. The overall enhancement of heat liberated of (+71.88 and +103.9) % for oil and water heat exchanger. The heat transfer coefficient of oil and water are investigated experimentally with optimum concentrations (0.7) % of SiO₂ and numerically with concentrations (0.3, 0.5, and 0.7). Based on results adding SiO₂ nanoparticle to base fluid (oil or water) enhance the interior side of (+6.05 and +8.3) % for oil and water Nano fluid respectively.

Taher [41] provided a practical study of the heat transfer of tangential flow heat exchangers and the impact of fins on enhancing the heat transfer for an eight-pass heat exchanger for four models (smooth, low, medium and high fin tubes) that are air-cooled, which were manufactured from pure copper metal for testing and installed inside the test section. The test was conducted in working circumstances where the air velocity was (1, 1.7, 2.3) m/s, flow rates (2-6) L/min, and the water entry temperature (50, 60, 70) °C, and through the findings, it was concluded that the coefficient of heat transfer is directly proportional to air velocity and water inlet temperature for the entire cases. It was found that the heat transfer rate of the three integral finned tubes was greater than that of the smooth tube, and the highest results were achieved from the tube with high integrated fins. As well as the maximum enhancement of the heat transfer ratio at the volumetric flow rate of the three-finned tubes to the smooth tube is (50.7%, 203.9%, 329.9%) for the finned tubes (low, medium and high) respectively.

The heat transfer coefficient from the water side it is directly proportional to the water flow rate and water entry temperature and for all cases, where it was found that the tubes with integrated fins have a heat transfer coefficient from the water side less than the heat transfer coefficient of the smooth tube.

Two models of cross-flow heat exchangers with four finned smooth tubes were used to improve the heat transfer coefficient by Mardan [42]. The fins are practically shaped on the exterior surface of the tube with a circular and triangular cross-section with a tube length of 25 cm, a flow rate of (2, 3, 4, 5) L/min, an air speed of (1, 2, 3) m/s and a hot inlet temperature (50, 60, 70, 80) °C and the water entry temperature for the theoretical study is (25) °C. ANSYS 16.1 and SolidWorks 2017 programs used to study different lengths of tubes to reach the best length to analyze the flow direction and study the different shapes of fins within the range of Reynolds number (4022 - 50194). Through the findings it was found that the increase in the length of the lanes will lead to increase the heat transfer ratio and the best length of the heat exchanger is (2.5m), which can provide the largest amount of heat transfer with a value of (654.6) watts, but this is at the expense of the pressure drop gradient (651) Pa, because the longer the pipeline or the number of passages increases, the pressure drop increases, and the flow direction does not affect heat transfer. The best fins were the circular fins with a rectangle in terms of heat transfer rate of 32.98 %.

In this study we focus on the best pitch-fin ratio that gives the highest heat transfer rate on a four-pass heat exchanger and compare it to a smooth tube through experimental and theoretical application.

PART 3

NUMERICAL SIMULATION

-This part of the study aims to provide a numerical solution and mathematical formulation of all operations for the heat transfer and fluid flow in cross-flow heat exchanger of all types (smooth and finned tube). Where the shape geometry was designed by the usage of SolidWorks 2018 program, and the Gambit 2.4.6 program was used in preparing the mesh and the numerical simulations were solved using the ANSYS Fluent 19R2 program. This part provides an integrated study of the convection heat transfer in the heat exchangers used in this study, which consists of four models (smooth tube heat exchanger and three finned heat exchangers). The finned tubes have been used different among themselves in terms of the pitch fin in order to determine the best spacing between the fins that gives the best heat transfer rate.

The numerical analysis based on the CFD are used to solve the continuity, momentum, and energy equations, in addition to adopting the turbulence model. Finite volume technique is used for obtaining the solutions in the fluid simulation system. The model in this study is designed in a three-dimensional. There are several factors that affect the performance of the heat exchanger and the heat transfer coefficient (inlet temperature, fluid velocity inside the tubes, and fluid velocity on the surface of the exterior tube). Another important parameter is the pressure drop inside the heat exchanger.

The wide use of cross-flow heat exchangers triggers the attention of the researcher's interest to study them in order to improve the rate of heat transfer. The preparing practical models for studies, need high costs and long time involved in experimenting with them, most researchers have tended to use numerical analyses to reach the best simulation model and use it to get practical results which enabled researchers to secure economy with the time and cost needed to study, and to

determine the best model in simulation and to conduct a practical study on it. The CFD provides an accurate and detailed description of the flow and heat transfer characteristics of the model. The solution algorithm is given in Figure 3.1.

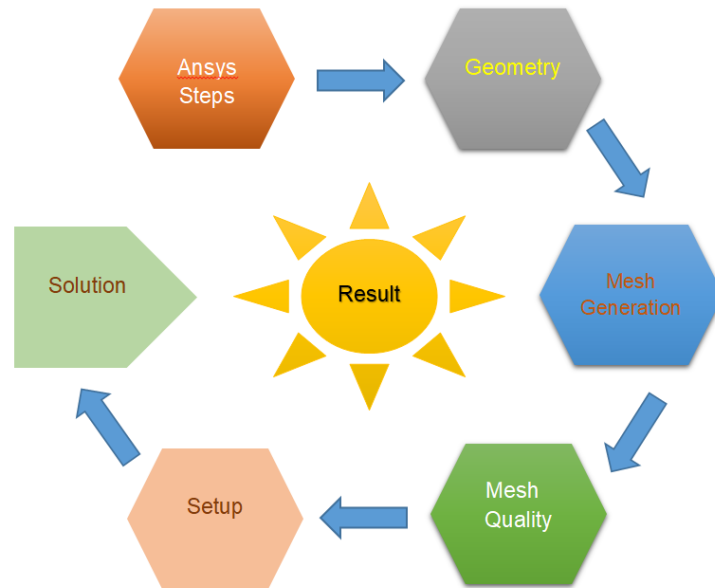


Figure 3.1. Numerical solution algorithm.

3.1. PHYSICAL MODEL

The aim of this model is to determine the ideal pitch fins in the heat exchanger tube as well as to compare it with other models through a four-pass heat exchanger. Pitches of the fins have been selected as ($P= 1.6, 2.5,$ and 3.75 mm). The interior tube diameter for all the models is 19 mm and the exterior diameter of the smooth tube is 21 mm, the finned tube has a diameter of 28.5 mm. The working fluids used in the study are the hot fluid (water) inside the tube and the cold fluid (air) outside the tubes. The water flow rates have been varied from 2 l/min to 6 l/min with inlet temperature of 70°C , while air velocity rates are (1, 2, 3, and 4 m/s) with inlet temperature of 20°C . Within these ranges Reynolds numbers for water flow has been varied with ($3985 < \text{Re}_w < 16032$) and air flow has been changed with ranges Reynolds numbers ($17390 < \text{Re}_a < 73060$).

Using Solid Works 2018 program, the heat exchanger and its surrounding parts have been prepared. They consist of the exchanger that contains four passages of tubes in

which the hot liquid interior and the exterior part in which the cold liquid interior (air) and touches the surface of the exterior tubes of the heat exchanger and the body is formed. It is divided into three main parts as follows:

3.1.1. Air Zone

This part is considered the largest part in terms of measurements as its length (800 mm), width (250 mm) and height (275 mm) as shown in Figure 3.2. Exterior surface is in contact with the air in order to achieve the process of heat exchange and be isolated from the outside where there is no radiation or heat generation.

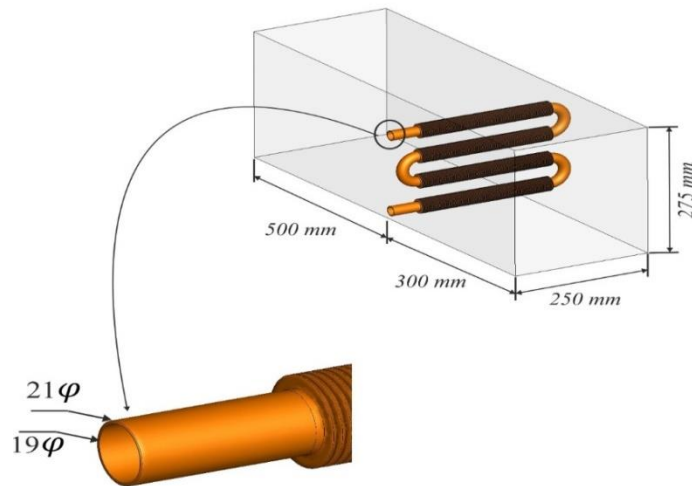


Figure 3.2. Air zone geometry and dimensions for heat exchanger.

3.1.2. Pipes

This part is a test section which is considered the most important part of the study. The test section shown in Figure 3.3, consists of four passages tube with an interior diameter of 19 mm, through which hot water passes. Exterior diameter of 21 mm, which passes air touching its exterior surface and a length of 250 mm for one corridor is used.

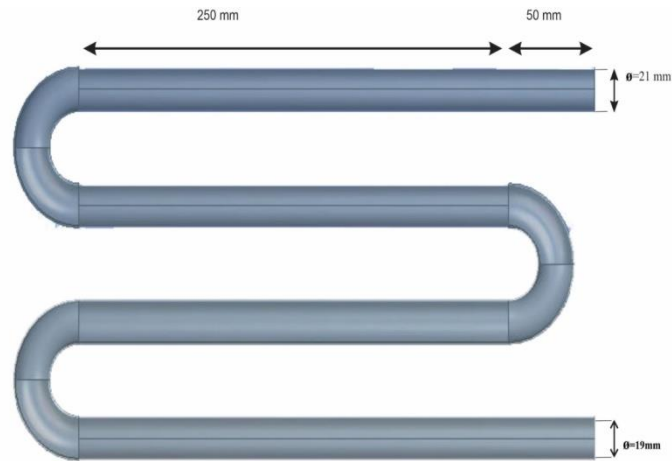


Figure 3.3. Dimensions of the tube passage of the study.

3.1.3. Fins

The fins are the important additions to the smooth tube. As they increase the surface area, the rate of heat transfer increases, too. The design of these fins has been made with the program of Solid Works 2018. The shape of fins is a circular shape with rectangular cross section with a height of 3.75 mm and a width of 1 mm as shown in Figure 3.4.

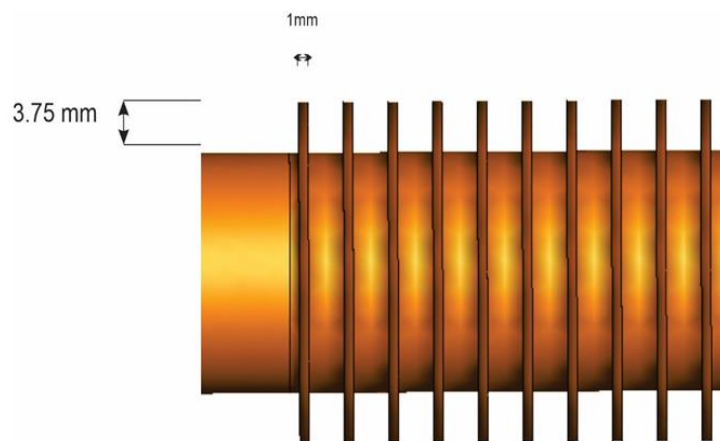


Figure 3.4. Fins dimensions.

In this study, three types of finned tubes were used with different pitches of fins. Different pitch ratios have been used to obtain the best ideal case that gives the highest heat transfer rate. The pitches of fins were taken as ($P= 1.6, 2.5,$ and 3.75 mm). The

number of fins with these pitches of fins are 380, 284, and 212 as shown in Figure 3.5. Direction of the fluid flows in the tubes and heat exchanger are also given in Figure 3.6.

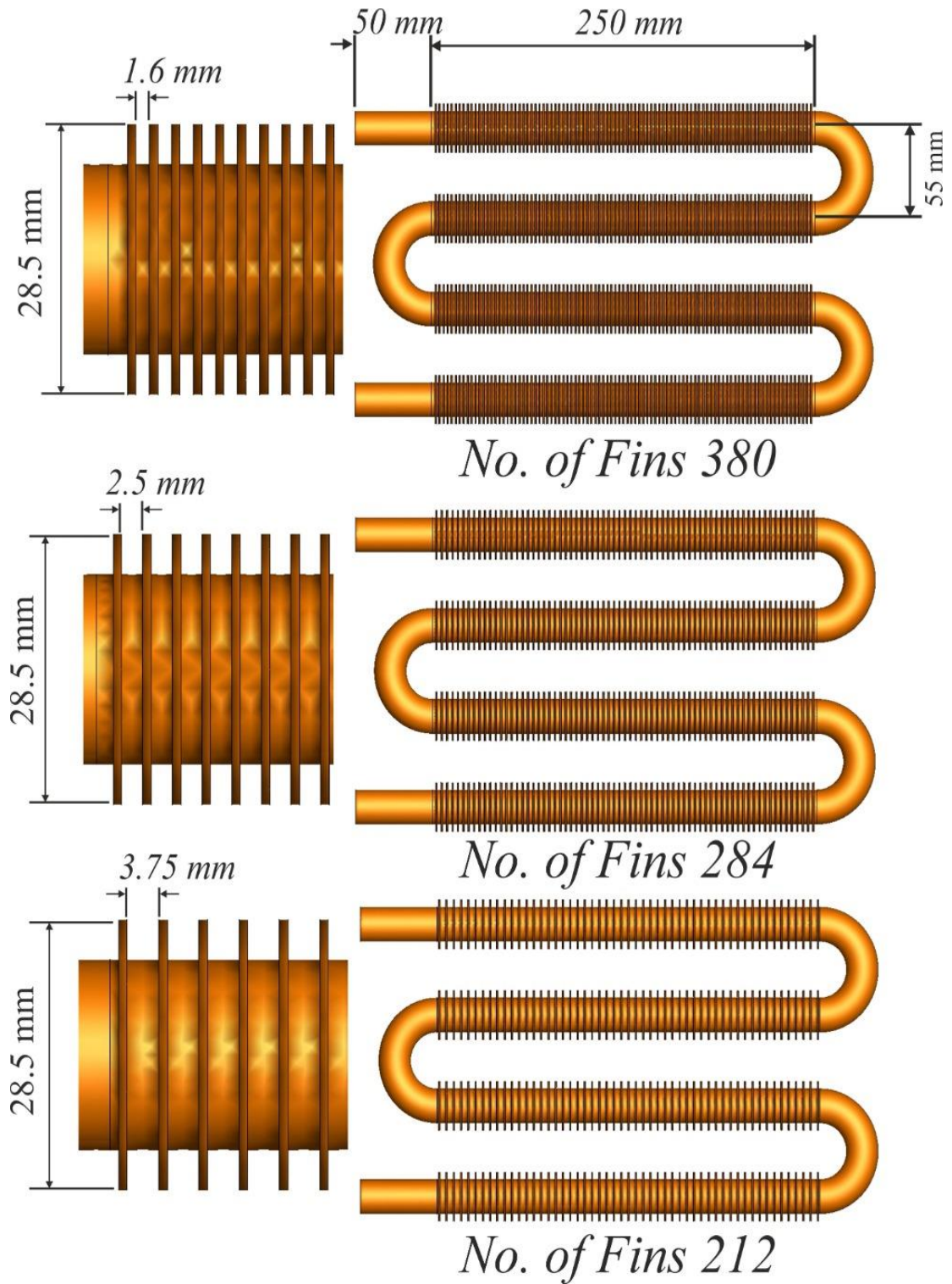


Figure 3.5. The number of fins according to the change of pitch fin for the test model.

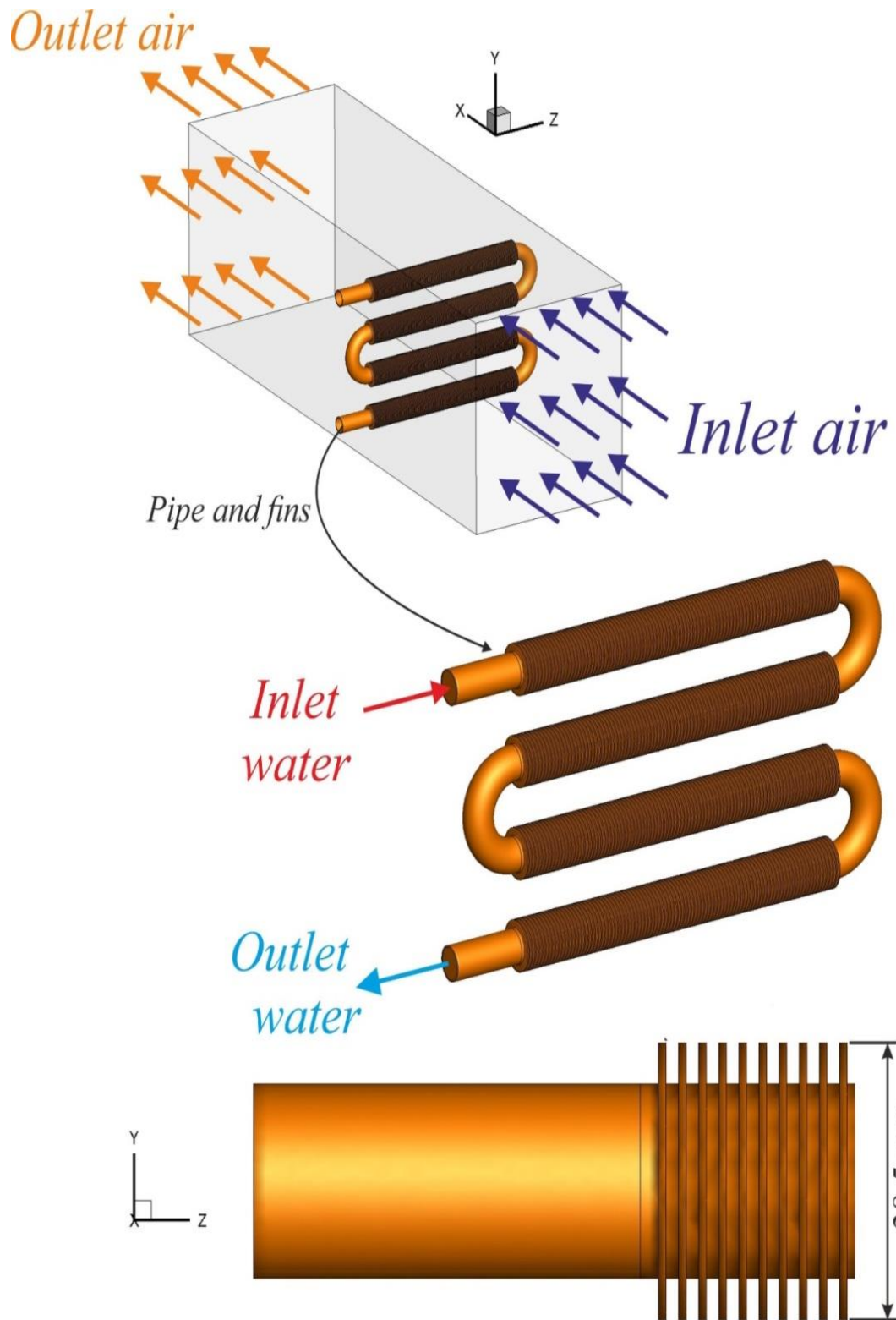


Figure 3 6. Direction for all flow.

3.2. GOVERNING EQUATIONS

Governing equations have been used to find the results and to reach the best model for this study. These equations include the continuity equation, momentum equation, energy equation as well as turbulence equation. From model list in Fluent, energy equation and viscous k-epsilon, RNG, Standard wall functions were chosen because it can improve the accuracy of the rapidly fatigued flows and enhance the accuracy of the eddy's flows using two equations of $k - \varepsilon$.

Two types of energy and viscosity equations (k- ε and k- ω) are usually used, which are the most common among engineering application. The first type (k- ω) is used in high flows. This method is characterized by a quick solution, but it is not accurate. The second method (k- ε) is widely used in tube flow to solved the complex problems of turbulent and have a high resolution and slow speed. Dependent on the previous serve [25][34][41][51] it was chosen for the solution in this study.

- **Mass Conservation (Continuity equation):**

$$\left[\frac{\partial \bar{u}}{\partial x} + \frac{\partial \bar{v}}{\partial y} + \frac{\partial \bar{w}}{\partial z} = 0 \right] \quad (3.1)$$

- **Conservation of Momentum:**

$$\left[\left(\bar{u} \frac{\partial \bar{u}}{\partial x} + \bar{v} \frac{\partial \bar{u}}{\partial y} + \bar{w} \frac{\partial \bar{u}}{\partial z} \right) + \left(\frac{\partial}{\partial x} (\overline{u^2}) + \frac{\partial}{\partial y} (\overline{uv'}) + \frac{\partial}{\partial z} (\overline{uw'}) \right) = -\frac{1}{\rho} \frac{\partial P}{\partial x} + \right. \quad (3.2)$$

$$\left. \frac{\mu}{\rho} \left(\frac{\partial^2 \bar{u}}{\partial x^2} + \frac{\partial^2 \bar{u}}{\partial y^2} + \frac{\partial^2 \bar{u}}{\partial z^2} \right) \right]$$

$$\left[\left(\bar{u} \frac{\partial \bar{v}}{\partial x} + \bar{v} \frac{\partial \bar{v}}{\partial y} + \bar{w} \frac{\partial \bar{v}}{\partial z} \right) + \left(\frac{\partial}{\partial x} (\overline{uv'}) + \frac{\partial}{\partial y} (\overline{v^2}) + \frac{\partial}{\partial z} (\overline{vw'}) \right) = -\frac{1}{\rho} \frac{\partial P}{\partial y} + \right. \quad (3.3)$$

$$\left. \frac{\mu}{\rho} \left(\frac{\partial^2 \bar{v}}{\partial x^2} + \frac{\partial^2 \bar{v}}{\partial y^2} + \frac{\partial^2 \bar{v}}{\partial z^2} \right) \right]$$

$$\left[\left(\bar{u} \frac{\partial \bar{w}}{\partial x} + \bar{v} \frac{\partial \bar{w}}{\partial y} + \bar{w} \frac{\partial \bar{w}}{\partial z} \right) + \left(\frac{\partial}{\partial x} (\overline{uw'}) + \frac{\partial}{\partial y} (\overline{vw'}) + \frac{\partial}{\partial z} (\overline{w^2}) \right) \right] \quad (3.4)$$

$$= -\frac{1}{\rho} \frac{\partial P}{\partial z} + \frac{\mu}{\rho} \left(\frac{\partial^2 \bar{w}}{\partial x^2} + \frac{\partial^2 \bar{w}}{\partial y^2} + \frac{\partial^2 \bar{w}}{\partial z^2} \right) \right]$$

- **Conservation of Energy:**

$$\begin{aligned} & [(\bar{u} \frac{\partial \bar{T}}{\partial x} + \bar{v} \frac{\partial \bar{T}}{\partial y} + \bar{w} \frac{\partial \bar{T}}{\partial z}) + (\frac{\partial}{\partial x} (\overline{uT'}) + \frac{\partial}{\partial y} (\overline{vT'}) + \frac{\partial}{\partial z} (\overline{wT'}))] = \\ & \alpha (\frac{\partial^2 \bar{T}}{\partial x^2} + \frac{\partial^2 \bar{T}}{\partial y^2} + \frac{\partial^2 \bar{T}}{\partial z^2}) \end{aligned} \quad (3.5)$$

- **Turbulence Kinetic Energy Equation:**

$$\begin{aligned} & [\rho (\bar{u} \frac{\partial k}{\partial x} + \bar{v} \frac{\partial k}{\partial y} + \bar{w} \frac{\partial k}{\partial z}) \\ & = \left[\left(\mu + \frac{\mu_t}{\sigma_k} \right) \cdot \left(\frac{\partial^2 k}{\partial x^2} + \frac{\partial^2 k}{\partial y^2} + \frac{\partial^2 k}{\partial z^2} \right) \right] + G_k - \rho \epsilon \end{aligned} \quad (3.6)$$

- **Dissipation Rate (ϵ) Equation:**

$$\begin{aligned} & [\rho (\bar{u} \frac{\partial \epsilon}{\partial x} + \bar{v} \frac{\partial \epsilon}{\partial y} + \bar{w} \frac{\partial \epsilon}{\partial z}) \\ & = \left[\left(\mu + \frac{\mu_t}{\sigma_{\epsilon\epsilon}} \right) \cdot \left(\frac{\partial^2 \epsilon}{\partial x^2} + \frac{\partial^2 \epsilon}{\partial y^2} + \frac{\partial^2 \epsilon}{\partial z^2} \right) \right] + C_{1\epsilon} \frac{\epsilon}{k} G_k - C_{2\epsilon} \rho \frac{\epsilon}{k} \end{aligned} \quad (3.7)$$

- **The Eddy Viscosity of Turbulent:**

$$[\mu_t = \rho C_\mu \frac{k^2}{\epsilon}] \quad (3.8)$$

- **Turbulent Intensity:**

$$[I = \frac{\dot{u}}{u_{ave}} = 0.16 \times (Re)^{(-1/8)}] \quad (3.9)$$

3.2.1. Mesh Generation

In order to obtain accurate results and very close to reality, the mesh generation must be accurate, as it is a very important thing in the work of the ANSYS Fluent program, as using the program Gambit 2.4.6 the mesh is created. This program gives us the best preparation for it after determining the areas of entry and exit of the hot fluid and cold, pipe walls and areas of concentration of turbulence for fluids. Then the geometry is exported to the program ANSYS Fluent 19R2 program.

The ANSYS Fluent program provides several models, and these models are the ones that determine the type of the object, the size of the mesh, the number of nodes that are formed in the body, and the accuracy of the results that will be obtained. Figure 3.7 shows these models. Each of these mesh is specific to the model on which the study will be conducted. Since the model used in this study is of a complex type and has small dimensions, choosing a tetrahedron and an irregular wedge is the optimal choice in order to take the shape of the entire body and give us the best mesh system to obtain ideal and real results.

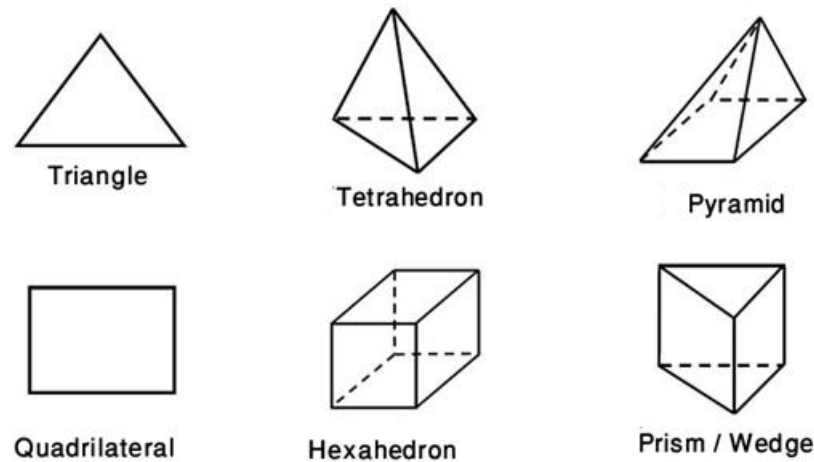


Figure 3.7. Types of meshes.

In this part of the program, it is preferred that the number of cells is high, as the greater the number of cells, the more accuracy, but this increase in the number of cells has a high impact on the time needed to obtain the results, which may take days of

continuous work on the computer to obtain the results. There are several options to determine the simulation's accuracy and efficiency and its impact on the stability of viscous flows and the quality of the mesh.

Including Skewness, as the closer to unity, is the best quality. In this study, the maximum Skewness is 0.913, which indicates that the quality is very good as shown in Table 3.1. Also, mesh structures of the smooth and finned tubes are given in Figure 3.8 and Figure 3.9, respectively. Mesh adaptation study has been carried out before the solution. In this study, optimum mesh numbers and structures have been determined for smooth and finned tube types.

Table 3.1. The specifications of the meshes.

Setup	Specifications	
	Smooth Pipe	Pipe with fins
Physics Preference	CFD	CFD
Solver Preference	ANSYS Fluent 19R2	ANSYS Fluent 19R2
Growth Rate	Default (1.2)	Default (1.2)
Sizing	fine	fine
Max Skewness	0.902	0.913
Node	813167	985850
Elements	4481282	4975702
Transition	Slow	slow
The Shape of The Mesh	The structure of computational grid is Tetrahedral	The structure of computational grid is Tetrahedral

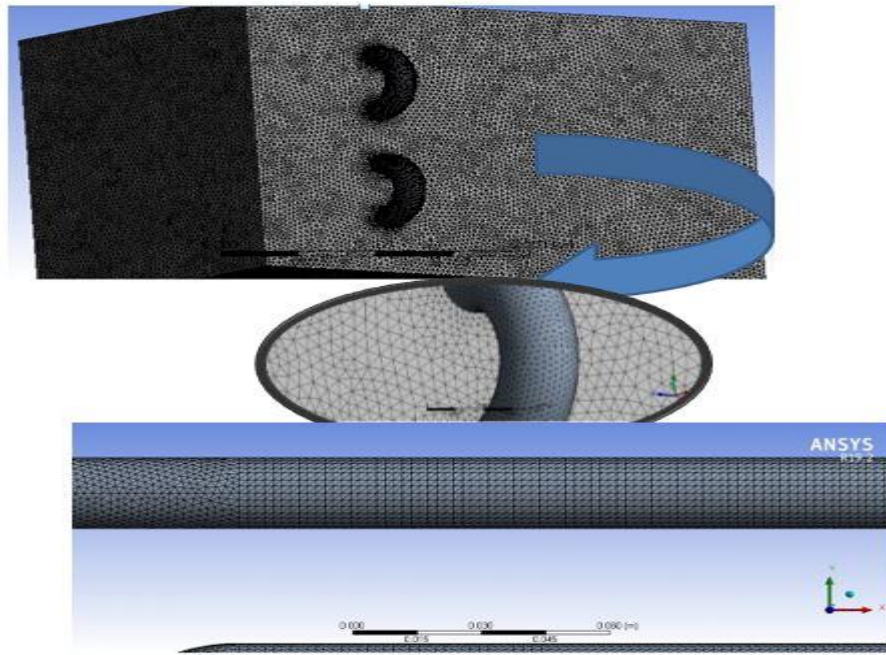


Figure 3.8. Mesh shape for smooth tube.

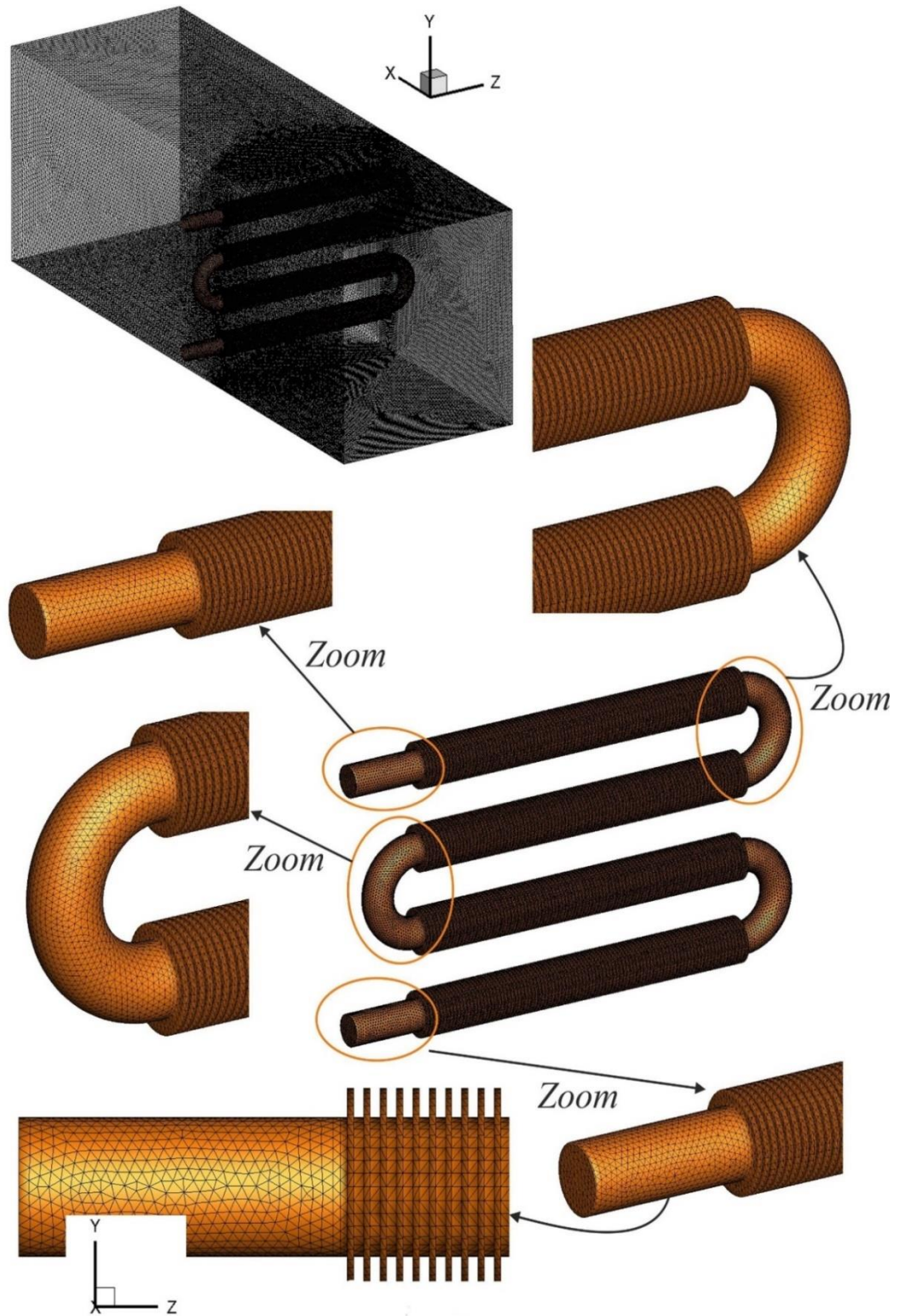


Figure 3.9. Mesh for finned tube.

3.2.1.1. Mesh Independence

Grid independence test plays an important role in the reliability of mesh because the poor design of the grid lead to decrease in the accuracy of the simulation results. The Mesh for this study is examined by changing the parameters and repeating the simulation work to ensure the validity of the results, the main method used in this test is to increase number of elements by increasing the element size of the pipe, until it reached a point where the results were not noticeable figure (3.10) and (3.11) show the variation in the temperature are not significant with the increase in the elements number. The mesh size (4481282) for smooth tube and (4975702) for finned tube with pitch (P=1.6 mm) are the best sizes chosen for the simulation calculation process, and it takes less time to complete the process as shown in table (3.2) and (3.3).

Table 3.2. Mesh independence for smooth tube.

Elements	Nodes	Outlet water temperature
1765720	299368	322.122
2438392	362415	322.268
2708849	420598	322.341
3652275	634257	322.578
4481282	813167	322.775
4625561	897263	322.778

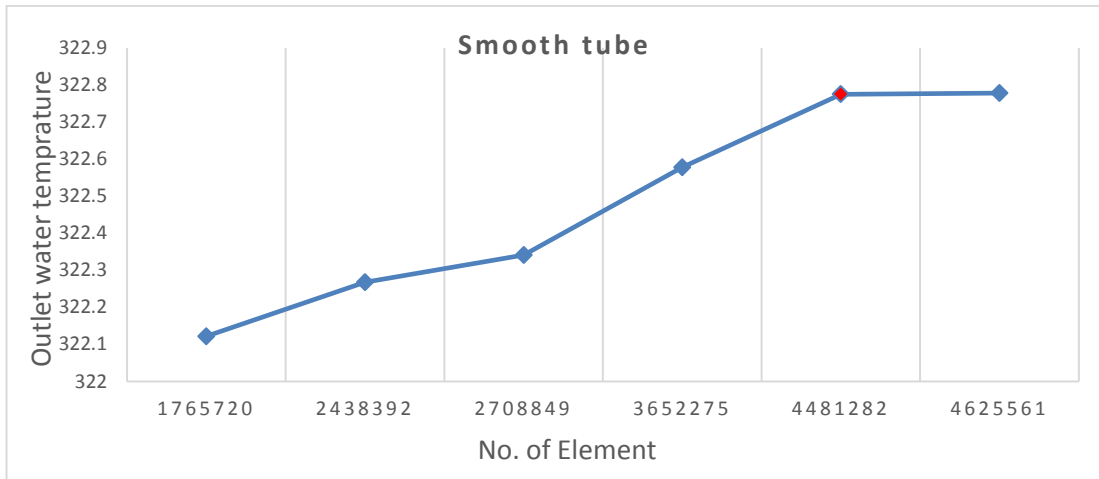


Figure 3.10. Mesh independence between number of element and outlet water temperature for smooth tube.

Table 3.3. Mesh independence for finned tube (P= 1.6 mm).

Elements	Nodes	Outlet water temperature
1865422	299368	321.128
2574317	362415	321.245
2967542	420598	321.377
3788971	634257	321.478
4975702	985850	321.597
4981312	1081544	321.599

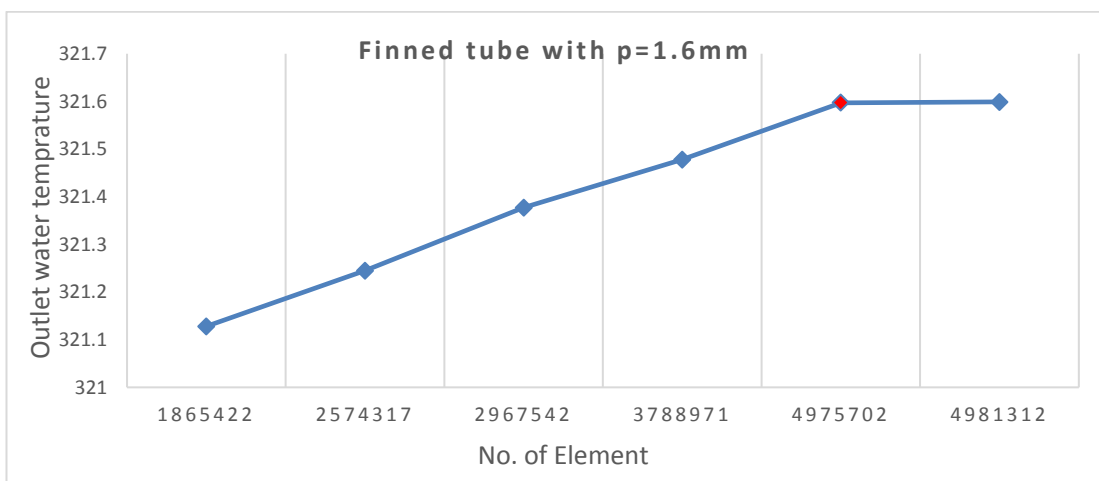


Figure 3.11. Mesh independence between number of element and outlet water temperature for finned tube with pitch fin (P= 1.6 mm).

3.3. SETTING OF MATERIALS

The first step in creation of a CFD model is the definition of the fluid and material parameters. In order for the results obtained in the program to be similar to the actual results, it must be used the properties of materials, whether solid or liquid, in the program, as we are dealing with three types of materials, one of which is solid and the other two are liquid.

3.4. SETUP

After completing the preparation of the mesh, at this stage, the boundary conditions that must be adopted to obtain the required results are determined, such as the velocity and temperature of the air and the velocity and temperature of the water. The properties of air, water and copper, and some important assumptions must be applied to determine the type of results that will appear, such as activating the energy equation and turbulence model as shown in Figure 3.12 and Figure 3.13, respectively. The condition is stable and the body is semi-isolated. There is no heat generation, the properties of water, air and copper are fixed, and the flow in this study is turbulent.

The fluids used in this study are of two types, including water, which passes through pipes with an interior diameter of 19 mm and turbulent flow of 4% and temperatures as shown in the Table 3.2, and air that passes outside of the pipes inside the walls of the space with a turbulent flow rate of 5% and an internal diameter of the flow space is 261.9 mm.

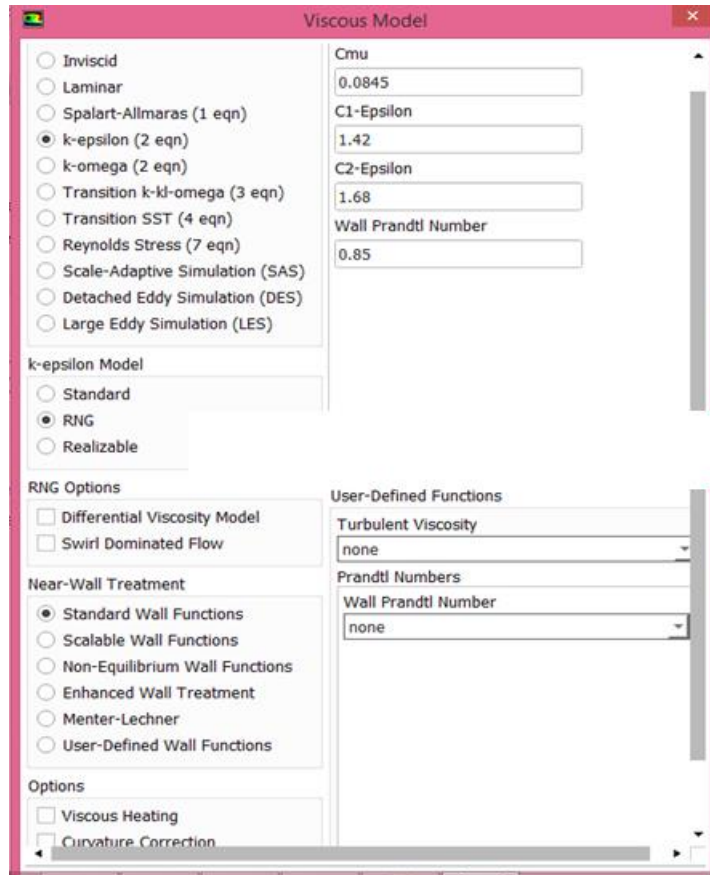


Figure 3.12. Selection of the viscous model.

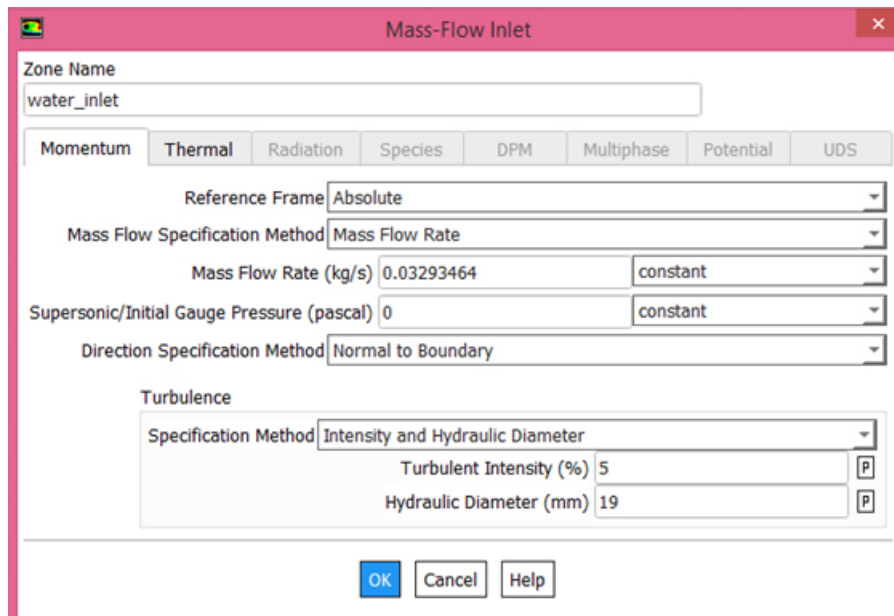


Figure 3.13. Selection of the boundary conditions.

3.5. ASSUMPTIONS

The assumptions must be applied to solve the equations of flow and heat transfer. In addition to the fact that the body is three-dimensional, the liquid is incompressible and the general condition is stable. The type of flow is turbulent. Assuming that the properties of the fluid are constant. The external part (elbow) for pipes to be insulated, as the heat generation inside the pipes in them is very little in addition to ignoring heat radiation, assuming that the walls are completely insulated.

3.6. BOUNDARY CONDITIONS

Using fluid conditions with the program ANSYS Fluent 19R2, it is possible to obtain results that give us a clear and accurate depiction of the models used in this study by solution the equations of mass, momentum, energy and turbulence with boundary conditions. Table 3.2 presents all the boundary conditions that applied to this study.

Table 3.4 . Boundary conditions.

Inlet boundary condition for air		
1	Temperature	20 °C
2	Inlet velocities	(1, 2, 3, 4) m/s
3	Turbulent intensity	4%
4	Hydraulic diameters	261.9 mm
Outlet boundary condition for air		
1	Pressure outlet	0 (Pa)
2	Turbulent intensity	4%
3	Hydraulic diameters	261.9 (mm)
Inlet boundary condition for water		
1	Temperature	70 °C
2	volume flow rate	2, 3, 4, 5, 6 (L/min)
3	Turbulent intensity	5%
4	Hydraulic diameters	19 (mm)
Outlet boundary condition for water		

1	Pressure outlet	0 (Pa)
2	Turbulent intensity	5%
3	Hydraulic diameter	19 (mm)
Tube wall boundary condition		
1	Thermal condition	Coupled
2	Wall motion	Stationary motion
3	Shear condition	No slip wall
4	Material	Copper

3.7. ITERATION CONVERGENCE

The method by which it reaches to check for convergence of the solution is known as monitoring the residuals. Convergence occurs when the convergence condition for some variables is reached. More than 15000 iterations are sometimes required to get the results, which take around 48 to 56 hours on a computers cluster consisting of eight 1.65 GHz, Intel® CORE (TM) i7, RAM 16 GB personal computers. Five computers were used in research to guarantee quick access to solutions. In order to obtain perfect accuracy, all equations are solved in the program and repeatedly. The properties of water and air are calculated at each point and continuously until it approaches the correct solution in each iteration.

3.8. SOLUTION AND RESULT

After completing all the steps of the program and completing the treatment, the diagrams and temperature distributions on the heat exchanger, inlet and outlet temperatures, pressure drop in the pipes, in addition to the velocity distribution of water and air have been taken from program.

PART 4

EXPERIMENTAL WORK

4.1. GENERAL

This chapter involves the clarification of the operational procedure and the set-up of the experimental work that are down in university of Wasit at postgraduate laboratories of the college of engineering at ambient conditions (temperature 20°C and pressure 1 bar). The purpose of practical work is to investigate the effect of changing the tube shape from smooth to integral finned mid tubes with different pitches between the fins on heat transfer enhancement for cross-flow heat exchanger, consisting of four tubes. Also calculating the heat transfer coefficient with compared to smooth tube at different working conditions, the inlet water temperatures have been taken as 50-70°C, and various amounts of water mass flow rates with (2-6 l/min), while the air velocity is (1, 2, 3, and 4 m/s) with its temperature of 20°C with range of Reynolds numbers for water side ($3985 < Re_w < 16032$) and for air side ($17390 < Re_a < 73060$).

4.2. LABORATORY EQUIPMENT COMPONENTS

The schematic diagram of the test setup is presented in Figure 4.1. It shows the parts that make up the laboratory devices on which the practical experiment was conducted. Figure 4.2 also shows a realistic photograph of the experimental setup for showing the parts of the experimental devices as follows:

1. Inlet section.
2. Test section.
3. Pipe Polyvinyl Chloride (PVC).
4. Centrifugal water pump.
5. Water heater tank.

6. Centrifugal air blower.
7. Heat exchanger.
8. Tools of measurement.
9. Heat insulator.

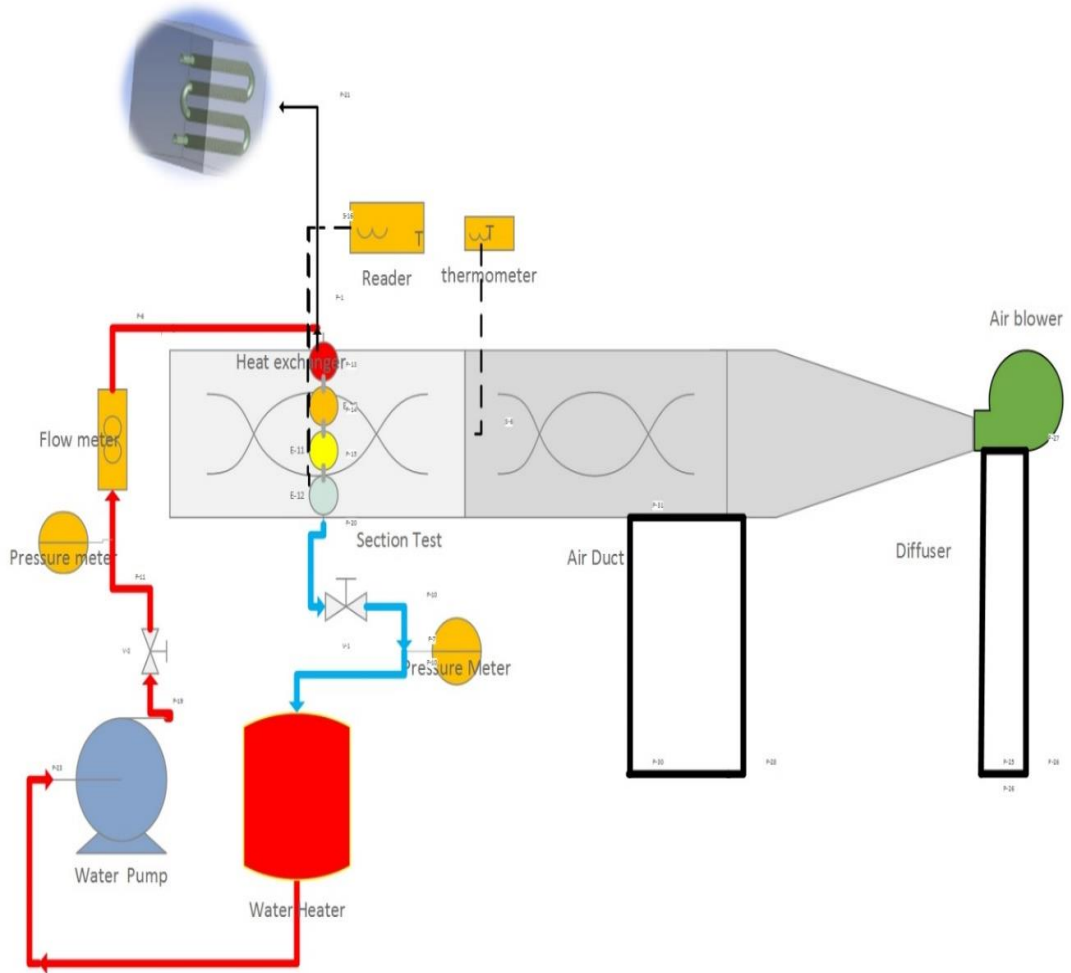


Figure 4.1. The schematic diagram of the experimental setup.



Figure 4.2. Photograph of experimental setup.

4.3. INLET SECTION

This part consists of two sections made of galvanized steel. The first is of a rectangular conical shape with dimensions of 750 mm in length, 250 mm in width and 275 mm in height. It relates to a fan where the air is pushed to the other part, which is in the form of a rectangle, with dimensions of 800 mm length, 250 mm width, and 275 mm height. Its purpose is to distribute air and deliver it to the examination section as shown in Figure 4.3.



Figure 4.3. Inlet section of the experimental setup.

4.3.1. Test Section

This part is considered one of the important parts of this experiment as it contains most of the examination devices made of Pyrex glass material with a thickness of 6 mm within the measurements of 400 mm length, 250 mm width and 275 mm height. After installing the measuring tubes consisting of four tubes and as shown in the Figure 4.4, the gaps are sealed with silicon material to prevent air leakage from them.

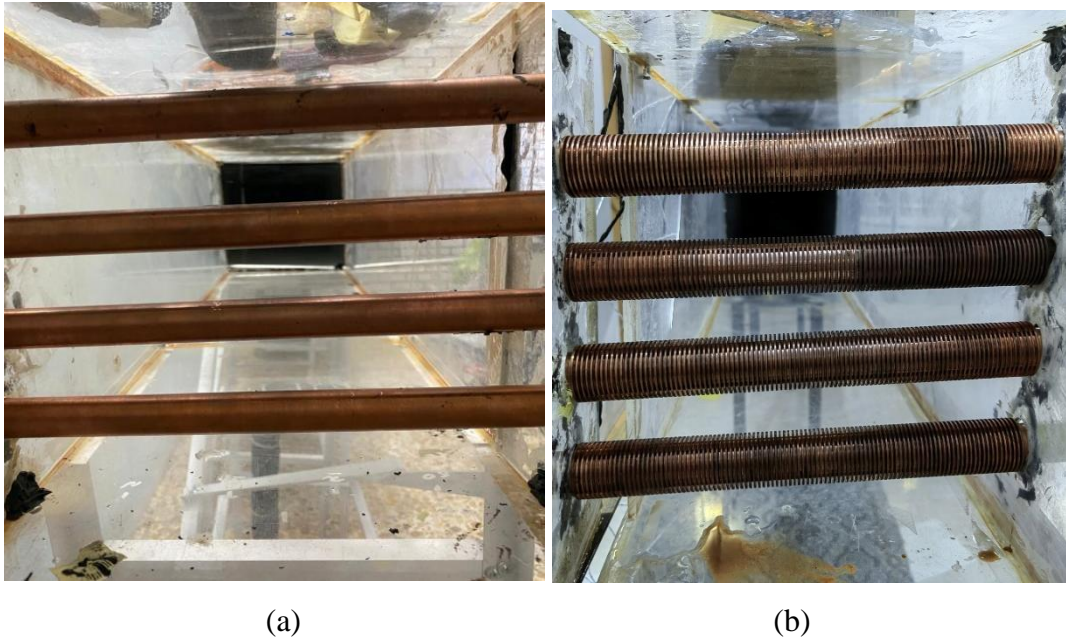


Figure 4.4. Test section internal view for: (a) smooth tube, (b) Finned tube.

4.3.2. Centrifugal Pump

For the purpose of pushing water into the pipes and obtaining water pressure readings, a centrifugal water pump is used that is operated by an electric current as shown in Figure 4.5. The pump operates with an electrical power of 330 watts and a flow rate of 20 L/min. To control the amount of flow, the regulator valve is placed after the pump, and the flowmeter device is located after the valve.



Figure 4.5. Centrifugal pump.

4.3.3. Water Heater Tank

A water heater that works on an electric heater with a capacity of 1000 watts and a voltage of 220 volts. It contains an insulated interior tank in which the water is heated through the heater. The heater contains a heating temperature controller. The capacity of the internal water tank is 80 liters and is connected before the pump to heat the water in it and pass it to the pump to be push it into the test tubes as shown in the Figure 4.6.



Figure 4.6. Water heater tank.

4.3.4. Centrifugal Air Blower

Air blower has been used which works by centrifugal on electric current with a capacity of 750 watts and a voltage of 220 volts and contains side slots to control the speed of the air coming out of the blower, as the total speed of the air is $15 \text{ m}^3/\text{min}$ as shown in the Figure 4.7.



Figure 4.7. Centrifugal air blower.

4.3.5. Heat Exchanger Pipes

In order to conduct the examination and test the heat transfer rate through the tubes and the heat transfer coefficient and the extent of the effect of temperature change and flux change on it, so two types of tubes were selected for the experimental examination: a smooth tube and a finned tube with a pitch of ($P= 1.6 \text{ mm}$) as shown in Figure 4.8 for comparison in what is between them and theoretical readings.

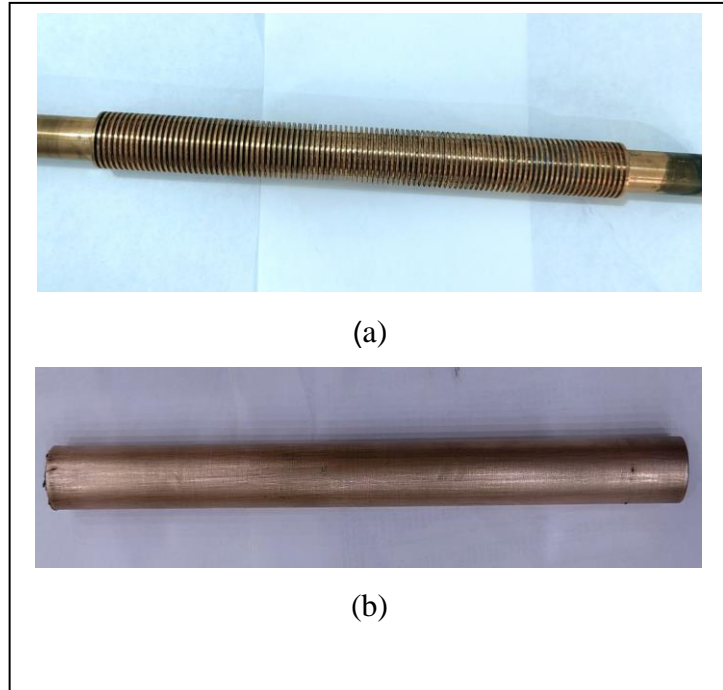


Figure 4.8. Heat exchanger pipes for: (a) finned tube, (b) smooth tube.

4.3.6. Measurement Tools

In order to obtain the real readings related to this research from the used examination device, a number of devices were used that show us the readings, each according to its specialization, such as measuring air and water temperatures, measuring air velocity, water flow rate and pressure drop, as shown below:

4.3.6.1. Thermometer

In the experiment, it has been used a digital thermometer type (TPM-10) to measure the temperature of the air outside through the pipes (Figure 4.9). It measures the highest temperature of 110°C and the lowest temperature of -50°C . It has an accurate reading resolution with 0.1°C and accuracy of $\pm 1^{\circ}\text{C}$.

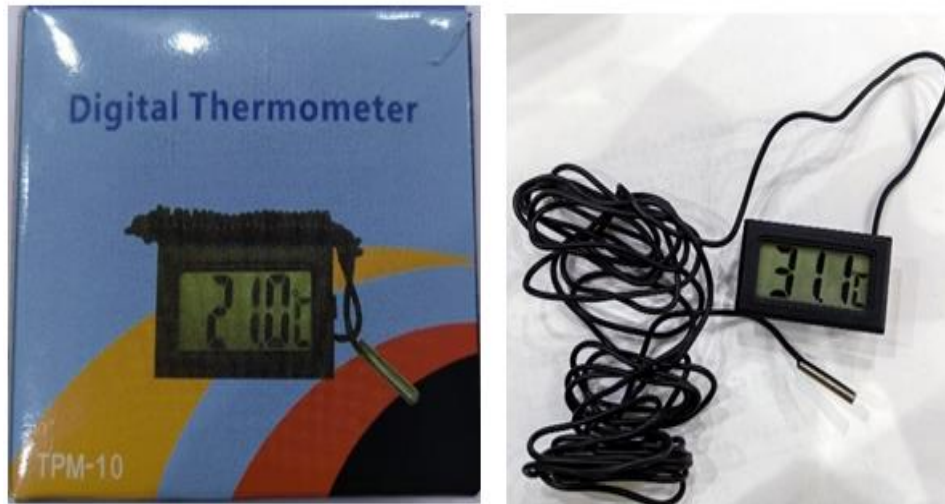


Figure 4.9. Thermometer.

4.3.6.2. Datalogger

A datalogger with the type of HT-9815 as shown in the Figure 4.10 has been used for reading temperature measurements. It works with an accuracy of $\pm 0.1^{\circ}\text{C}$ and reads the temperatures of four zones at the same time and for the necessity of using six points for examination. The thermocouples of Type-K have been used for the temperature measurement. The device calibration certificate is given in Appendix A.1 [25].



Figure 4.10. Datalogger.

4.3.6.3. Pressure Meter

Type pressure gauge (En 837-1) connects to the inlet and exit pipe heat exchanger in order to measure the pressure difference for the test section. Highest measured pressure (150) Psi with measurement accuracy ($\pm 0.3\%$) and respond time (0.5s) as shown in Figure 4.11.

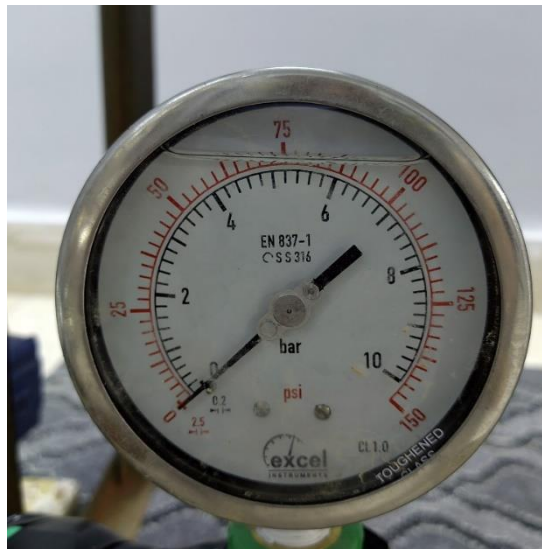


Figure 4.11. Pressure meter.

4.3.6.4. Thermocouples

It is a wire length of 1 m type K, which is of the type that measure wide range temperatures between (T1, T2, T3...T8), it contains two ends, the first is a socket connected to the temperature reader device and the second end is the measuring point, which is in the form of a sphere with a diameter of 2 mm, is connected with the surface of the heat exchanger and as shown in the Figure 4.12.

The thermocouples were calibrated using different degrees of temperature according to the thermocouple and thermometer which calibrated in the Central of Standardization and Quality Control according to the previous study [25], as shown in Appendix A.2. Figure 4.13 shows a picture of the calibration of the first thermocouple and the other forms of calibrations are in the Appendix A.2.



Figure 4.12. Thermocouple.

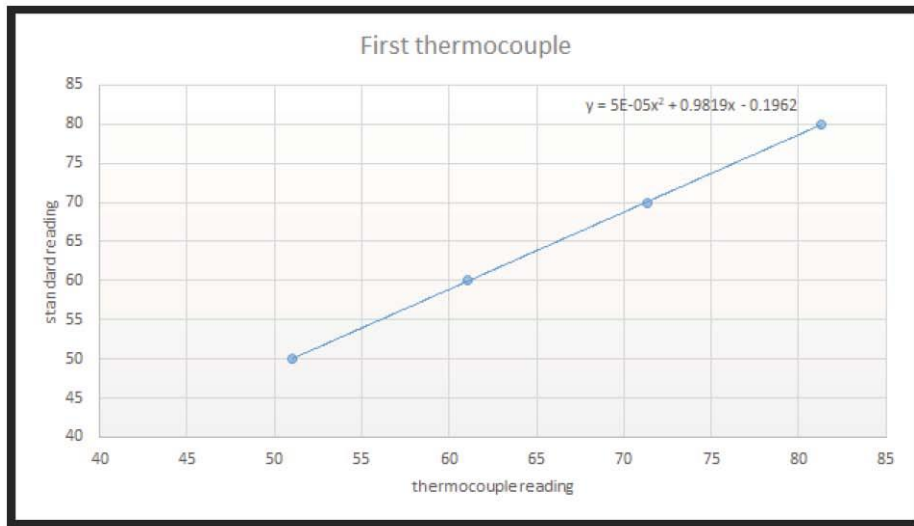


Figure 4.13. Thermocouple calibration.

4.3.6.5. Anemometer

Anemometer has been used for measuring the air velocity entering the test section, with a range of air speed (0.4-30 m/s). The resolution of the anemometer is 0.01 and the accuracy is $\pm 2\%$ as shown in Figure 4.14.



Figure 4.14. Anemometer.

4.3.6.6. Flowmeter

Mechanical flow meter, the principle of operation of this meter is based on the theory of buoyancy, where it is made of polished glass, containing inside it a circular piece with a conical shape that floats when the flow increases to rise at each flow on the reading scale that is a pointer on the surface of the exterior glass. The fluid flow in it usually from the bottom to up, and the measuring amount ranges from 1 liter per minute to 7 liters per minute, as shown in the Figure 4.15 The device was calibrated according to the Table 4.1 and Figure 4.6 [25].



Figure 4.15. Flow meter of water.

Table 4.1. The experimental values for flowmeter calibration.

Flow meter Reading (L/min)	Experience 1			Experience 2			Experience 3			\dot{v}_{av} (L/min)	Diff. %
	Volume (L)	Time (sec)	\dot{v} (L/min)	Volume (L)	Time (sec)	\dot{v} (L/min)	Volume (L)	Time (sec)	\dot{v} (L/min)		
5	5	59.35	5.05	5	58.69	5.11	5	59.41	5.04	5.06	-1.2
4	5	59.32	4.04	5	59.15	4.05	5	59.54	4.03	4.04	-1
3	5	58.8	3.06	5	58.91	3.05	5	59.64	3.01	3.04	-1.3
2	5	57.8	2.07	5	59.41	2.01	5	58.83	2.03	2.03	-1.5

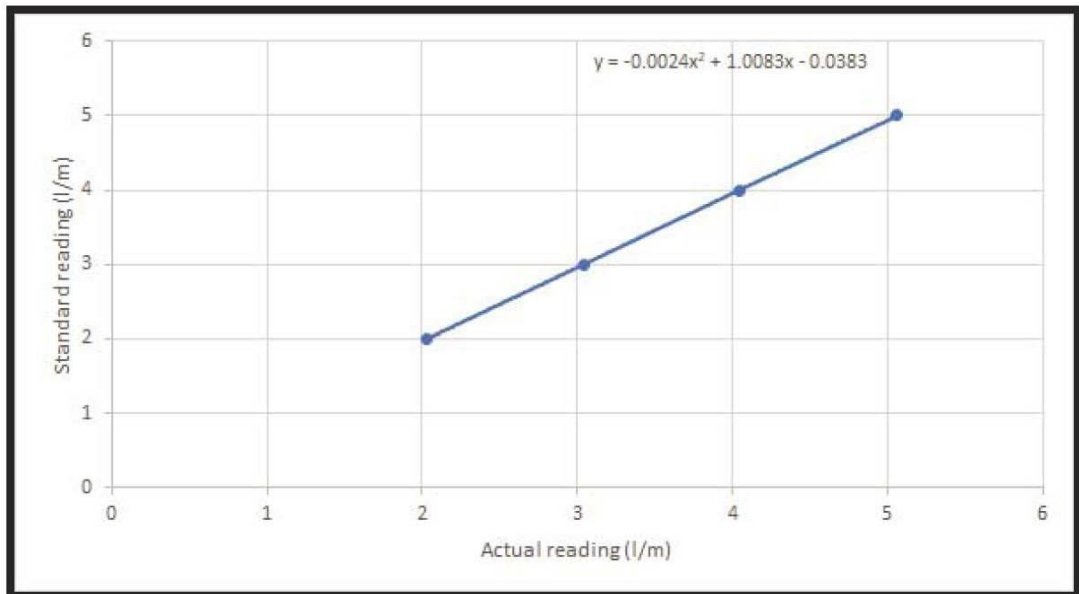


Figure 4.16. Flowmeter calibration.

4.4. EXPERIMENTAL PROCEDURE

Before starting the experiment, a trial test of the device must be carried out to obtain accurate results and to ensure that there are no problems during the trial test. These steps include:

1. Fill the water heater completely.
2. Ensure that the electrical wires are connected correctly, that the pump and heater are running, and that the heater temperature is adjusted for each case.
3. Make sure the air temperature is set to 20°C.
4. Ensure there are no leaks.
5. Make sure the fan is working and control the air speed limited in this study.
6. Connect the measuring devices and take preliminary readings to ensure their validity.
7. Repeat the first case three times to ensure the accuracy of the readings and to calculate the percentage of accuracy.
8. Each case takes two hours from the time until reach the steady state, and after two minutes, the temperatures and pressure difference are recorded for each case.

4.5. BASIC EQUATIONS

Figure 4.18 represents the logarithm of the average temperature difference, which is the appropriate form to use in analyzing the work of heat exchangers, where we notice in the above figure the difference in the temperatures of the two liquids at entry and exit, and it can be calculated by all the equations below were applied for smooth and finned tubes for one case as shown in the Appendix (C).

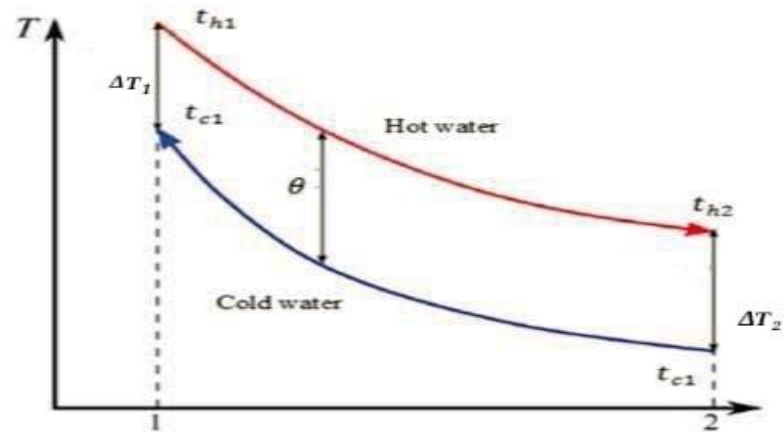


Figure 4.17. Temperature profiles in counter flow heat exchange.

4.5.1. Logarithmic Mean Temperature Difference (LMTD):

The logarithmic average of the temperature difference at both ends of the heat exchanger.

$$\text{LMTD} = \frac{\Delta T_1 - \Delta T_2}{\ln\left(\frac{\Delta T_1}{\Delta T_2}\right)} \quad (4.1)$$

$$\Delta T_1 = t_{hi} - t_{co} \quad (4.2)$$

$$\Delta T_2 = t_{ho} - t_{ci} \quad (4.3)$$

4.5.2. Heat Capacity

C_{\max} it means maximum heat capacity.

$$C_{\max} = (\dot{m} \times C_p)_{\max} \quad \text{and} \quad C_{\min} = (\dot{m} \times C_p)_{\min} \quad (4.4)$$

Number of transfer unit

$$\text{NTU} = U_o \times \frac{A_{os}}{C_{\min}} \quad (4.5)$$

4.5.3. Effectiveness of Heat Exchanger

$$\varepsilon = \frac{Q_{actual}}{Q_{max}} \quad (4.6)$$

$$Q_{actual} = Q = \dot{m}_h \times C_{ph} \times (t_{hi} - t_{ho}) = \dot{m}_c \times C_{pc} (t_{co} - t_{ci}) \quad (4.7)$$

$$Q_{max} = C_{min} (t_{hi} - t_{ci}) \quad (4.8)$$

The C_{min} is mean the minimum heat capacity for hot or cold fluid effectiveness (ε) with number of transfer unit (NTU) [7].

$$\varepsilon = \left(\frac{1}{C_r} \right) (1 - \exp((-C_r)(1 - e^{-NTU})) \quad (4.9)$$

$$C_{max} = C_{hot} \text{ and } C_{max} = C_{cold} \quad (4.10)$$

$$\varepsilon = (1 - \exp\left(-\frac{1}{C_r}\right)(1 - e^{-NTU.C_r}))$$

$$\text{The ratio of heat capacity is } C_r = \frac{C_{min}}{C_{max}} \quad (4.11)$$

4.5.4. Actual Rate of Heat Transfer

$$Q = \dot{m}_w \times Cp \times \Delta t \quad (4.12)$$

And

$$Q = \dot{m}_a \times Cp_a \times \Delta t \quad (4.13)$$

and we can the rate of heat transfer can be expressed as:

$$Q = U \times A \times \Delta t_{lmt} \quad (4.14)$$

The factors (R & S) are the ratio of temperature

$$R = \frac{T_{hi} - T_{ho}}{T_{co} - T_{ci}} \quad (4.15)$$

$$S = \frac{T_{co} - T_{ci}}{T_{hi} - T_{ci}} \quad (4.16)$$

$$F = \frac{(\sqrt{R^2 + 1}) \times \ln\left(\frac{1 - S}{1 - RS}\right)}{(R - 1) \times \ln\left(\frac{2 - S(R + 1 - (\sqrt{R^2 + 1}))}{2 - S(R + 1 + (\sqrt{R^2 + 1}))}\right)} \quad (4.17)$$

$$\left[\Sigma R = R_{tot} = R_i + R_{wall} + R_o = \left(\frac{1}{h_i A_{is}}\right) + \left(\frac{\ln \frac{r_o}{r_i}}{2\pi k_t L}\right) + \left(\frac{1}{h_o A_{os}}\right) \right] \quad (4.18)$$

As

$$A_{is} = \pi d_i L \quad (4.19)$$

$$A_{os} = \pi d_o L \quad (4.20)$$

$$R_{wall} = \left(\frac{\ln \frac{r_o}{r_i}}{2\pi k_{cop} L}\right) \quad (4.21)$$

R_{wall} : Thermal resistance for wall tube.

k_{cop} : Thermal conductivity for tube material

L: length of tube

To find rate of heat transfer between two fluids in the heat exchanger we used:

$$Q = \frac{\Delta T_{lmtd}}{R_{tot}} = U A \Delta T_{lmtd} \quad (4.22)$$

$$Q = U_o A_o \Delta T_{lmtd} = U_i A_i \Delta T_{lmtd} \quad (4.23)$$

$$\frac{1}{UA} = \frac{1}{U_i A_i} = \frac{1}{U_o A_o} = \Sigma R = \frac{1}{U_i A_i} + R_{wall} + \frac{1}{U_o A_o} \quad (4.24)$$

By Substituting equation (4.18) into equation (4.21) we get:

$$U_o = \frac{1}{\left(\frac{A_o}{h_i A_i}\right) + \left(\frac{A_o \ln \frac{d_o}{d_i}}{2\pi k_{cop} L}\right) + \left(\frac{1}{h_o}\right)} \quad (4.25)$$

4.5.5. Overall Heat Transfer Coefficient

The overall heat transfer coefficient for interior and exterior (U_o), (U_i) is the product of the two surface areas of the heat exchanger, which in general are not equal except by the method of Eq. (4.23).

$$U_o A_o = U_i A_i \quad (4.26)$$

$$U_o \neq U_i$$

$$U_o = \frac{1}{\left(\frac{A_{of}}{h_i A_i}\right) + \left(\frac{A_{of} \ln \frac{d_r}{d_i}}{2\pi k_{cop} L}\right) + \left(\frac{1}{h_o}\right)} \quad (4.27)$$

$$A_{of} = \pi d_{of} L \quad (4.28)$$

where, A_{of} is external area of tube surface at the integral finned tube,

$$U_o = \frac{1}{\left(\frac{d_{of}}{h_i d_i}\right) + \left(\frac{d_{of} \ln \frac{d_r}{d_i}}{2k_{cop}}\right) + \left(\frac{1}{h_o}\right)} \quad (4.29)$$

Then the Eq. (4.26) applies to clean surfaces as recommended by [56] which was presented to predict the turbulent heat transfer coefficient in the pipe, which is:

$$Nu = 0.023 Re^{0.8} Pr^n \quad (4.30)$$

The Prandtl number for cooling processes is equal to 0.3 and for turbulent flow this number is ($0.6 < Pr < 100$)

$$Pr = \frac{\mu C_p}{K} \quad (4.31)$$

$$Nu = h \cdot \frac{d}{k} \quad (4.32)$$

$$h_i = 0.023 Re_w^{0.8} \frac{Pr^n K_w}{d_i} \quad (4.33)$$

$$Re_w = \frac{\rho_w u_w d_i}{\mu_w} \quad (4.34)$$

$$u_w = \frac{Q}{A_{ic}} \quad (4.35)$$

$$A_{ic} = \frac{\pi}{4} d_i^2 \quad (4.36)$$

$$Pr_w = \frac{\mu_w C_{pw}}{K_w} \quad (4.37)$$

4.5.5.1. Heat Transfer Coefficient for Water side

$$Q = \dot{m}_w \times C_{pw} \times \Delta t \quad (4.38)$$

And the rate of heat transfers from an isothermal surface

$$Q = \dot{h}_{av,w} \times A_{s,w} \times (T_{s,av} - T_b) \quad (4.39)$$

$$\dot{m}_w \times C_{pw} \times \Delta t = \dot{h}_{av,w} \times A_{s,w} \times (T_{s,av} - T_b)$$

$$h_{av,w} = \frac{\dot{m}_w \times C_{pw} \times \Delta t}{A_{s,w} \times (T_{s,av} - T_b)} \quad (4.40)$$

Average Temperature for Surface

$$T_s = \frac{T_1 + T_2 + T_3 + \dots + T_n}{n} \quad (4.41)$$

And surface area for tube is

$$A_s = \pi d_o L \quad (4.42)$$

$$T_b = \frac{T_{wi} + T_{wo}}{2} \quad (4.43)$$

$$Nu_{av} = \frac{h_{av,w} d_i}{K_w} \quad (4.44)$$

4.5.5.2. Heat Transfer Coefficient for Air side

For smooth tube

$$h_o = \frac{1}{\left(\frac{1}{U_o}\right) - \left(d_o \times \frac{\ln\left(\frac{d_o}{d_i}\right)}{2 \times K_{cop}}\right) - \left(\frac{d_o}{h_i \times d_i}\right)} \quad (4.45)$$

For finned tube

$$h_o = \frac{1}{\left(\frac{1}{U_o}\right) - \left(d_{of} \times \frac{\ln\left(\frac{d_r}{d_i}\right)}{2 \times K_{cop}}\right) - \left(\frac{d_{of}}{h_i \times d_i}\right)} \quad (4.46)$$

Then U_o calculated by

$$U_o A_{os} = U_i A_{is} \quad (4.47)$$

$$U_i = \frac{Q}{A_{is} \times F \times LMTD} \quad (4.48)$$

To calculate Reynolds number for air we can use:

$$Re_a = \frac{\rho_a u_a d_z}{\mu_a} \quad (4.49)$$

And the hydraulic diameter calculated by

$$d_z = \frac{2 W \times H}{(W + H)} \quad (4.50)$$

4.5.6. Enhancement Ratio for Finned Tube

Enhancement Ratio (Er) is the ratio whose purpose is to know the extent of improvement and enhancement in increasing the heat transfer coefficient from the smooth model to the finned model. It is the ratio of the heat transfer coefficient of the finned tube minus the heat transfer coefficient of the smooth tube divided by the heat transfer coefficient of the smooth tube.

$$Er = \frac{h_{of} - h_{os}}{h_{os}} \times \%100 \quad (4.51)$$

4.5.7. Pressure Drop for heat exchanger

$$\Delta P_{Total} = \Delta P_{fitt} + \Delta P_{tube} \quad (4.52)$$

From Darcy–Weisbach Equation

$$\Delta P_{tube} = f \times \left(\frac{L}{d_i}\right) \times \left(\frac{\rho_w \times U_w^2}{2}\right) \quad (4.53)$$

$$f = \frac{0.316}{(Re)^{0.25}} \quad (4.54)$$

which is the $Re \geq 10^5$

$$\Delta P_{fitt} = N \times K_l \times \left(\frac{\rho_w \times U_w^2}{2}\right) \quad (4.55)$$

Where (K_l) is the loss coefficient and is equal to (1.9) the return curve at the interior diameter (0.19) mm, as shown in the Appendix (A).

4.5.8. Error Analysis

For the purpose of calculating the percentage of accuracy and knowing the percentage of error, we use the equations below, where we show the percentage of error in the first three values that are taken to evaluate the accuracy of the device, this uncertainty analysis is based on the method is suggested by Kline [57] and Moffat [58] which are covered by the reference [59] and the percentages were as shown in Table 4.2 and according to the equations below:

$$X_{av} = \frac{\sum_1^n X_i}{n} \quad (4.56)$$

Where is

(X_i) is the measurement value of each case

(n) It is the number of cases that have been taken

(σ) standard deviation value

$$\sigma = \frac{\sqrt{(\sum_1^n (X_i - X_{av})^2)}}{n - 1} \quad (4.57)$$

(σ_a) is the mean standard deviation.

$$\sigma_a = \frac{\sigma}{\sqrt{n}} \quad (4.58)$$

So (X) represents the real value measured by the equation below:

$$X = X_{av} \pm \sigma_a \quad (4.59)$$

The total accuracy of the system has been calculated between -10.7525 and 8.583007.

Table 4.2. Results of calculated error rates.

Var.	X_1	X_2	X_3	X_{av}	σ	σ_a	X+	%
							X-	
Q	42.91	34.107	47.173	41.396	6.663	3.847	45.243	8.502
							37.549	-10.245
U_i	25.513	20.251	28.11	24.625	4.004	2.312	26.937	8.583
							22.313	-10.36
h_i	798.402	798.65	798.283	798.445	0.187	0.108	798.554	0.0136
							798.337	-0.0136
Re_w	3987.781	3989.745	3986.831	3988.12	1.486	0.858	3988.977	0.0215
							3987.261	-0.0215
Nu_w	23.524	23.53	23.521	23.525	0.004	0.0027	23.528	0.0116
							23.522	-0.0116
U_o	23.083	18.322	25.433	22.279	3.623	2.092	24.371	8.583
							20.188	-10.36
h_o	23.96	18.87	26.502	23.110	3.886	2.243	25.354	8.849
							20.867	-10.75
Re_a	17309.67	17310.53	17304.51	17308.24	3.259	1.88	17310.12	0.011
							17306.36	-0.011
Nu_a	19.457	15.324	21.518	18.766	3.1545	1.8213	20.588	8.846
							16.945	-10.75

PART 5

RESULTS AND DISCUSSION

5.1. GENERAL

This chapter involves all the experimental and theoretical results. The flow is turbulent with five different mass flow rates for water side from 2, 3, 4, 5, 6 L/min, velocity for the air side 1, 2, 3, 4 m/s over the tubes, Reynolds numbers for water side ($3985 < Re_w < 16032$), and for air side ($17390 < Re_a < 73060$) investigated both numerically and experimentally. The ANSYS Fluent 19 R2 program has been used to simulate single-phase turbulent flows and in order to confirm the validity of the outcomes. 126 analyses were done. These results clarify the effect of temperature and pressure drop, heat transfer rate, Nusselt number, Reynolds number in addition to the internal and external heat transfer coefficient among them through changing the air velocity and fluid flow used in this numerical study. The experimental part involves four models which are studied smooth tube, finned tube with pitch fins as ($P= 1.6, 2.5,$ and 3.75 mm) to obtain the best model that provides the highest heat transfer rate and the highest efficiency. In the experimental side the effect of the seam parameter study for medium integral finned tube with h_e ($P=1.6$ mm) and smooth tube with inlet temperature (50, 60, and 70°C).

Through comparison and adoption of the previous study [25] almost identical results are reached with a little difference, as the researcher in the previous study use an air temperature of 25°C , while in this study it was used an air temperature of 20°C , which indicates the accuracy of the program and as shown in Table 5.1, which illustrates the comparison form between the two studies. The numerical results are compared with the experimental results at the last part.

Table 5.1. The comparative between the present research and Mardan study [25].

	U air m/s	m ³ w Kg/s	Thi °C	Tci °C	Tho °C	Tco °C	ΔTw	Δta	Qw Watt
The Previos Study	1	0.033	50	25	49.561	25.725	0.438	0.725	60.338
The Present reserch	1	0.033	50	20	49.607	21.862	0.393	1.88	54.049

5.2. NUMERICAL RESULTS

5.2.1. Results of the Smooth Tube

5.2.1.1. Effect of Inlet Water Temperature on Heat Transfer Rate

Figure 5.1 shows the relation between the flow rate water on convective heat transfer rate at different inlet temperatures of hot water (50, 60, and 70°C). This figure shows that the heat transfer rate increases with inlet temperature. This attributed to increase the temperature difference.

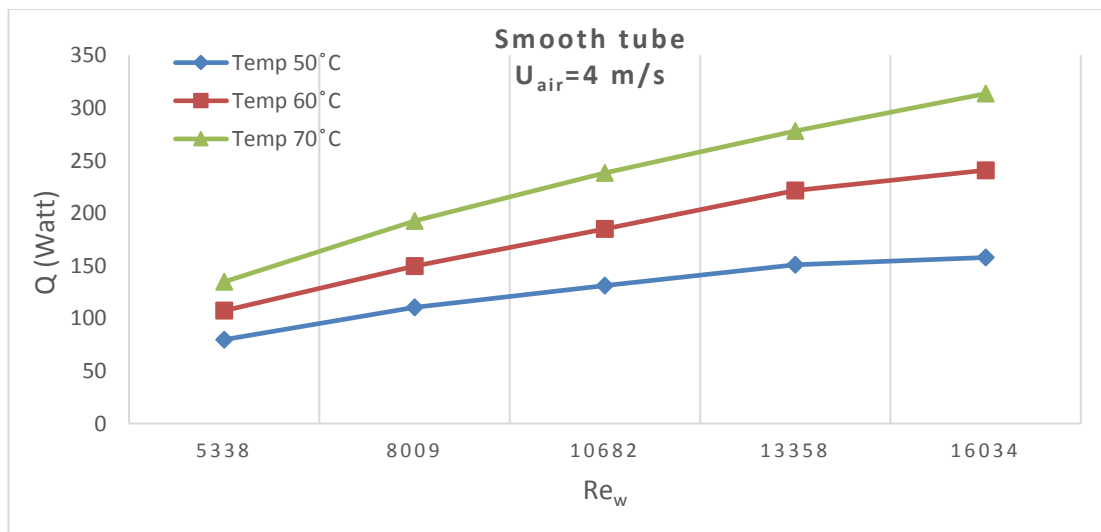


Figure 5.1. Effect of inlet water temperature on heat transfer rate.

5.2.1.2. Effect of Air Velocity and Inlet Water Temperature on Heat Transfer Rate

The effect of air velocity on heat transfer rate for different inlet water temperatures is shown in Figure 5.2 to Figure 5.6. From this figure it is noted obvious increase in the heat transfer rate when the air velocity increases under constant water flow rate and varies inlet temperature. The higher heat transfer rate of the heat exchanger of air side due to the higher the air velocity on the tube surface, which drawn large amount of heat dissipation of the heat exchanger.

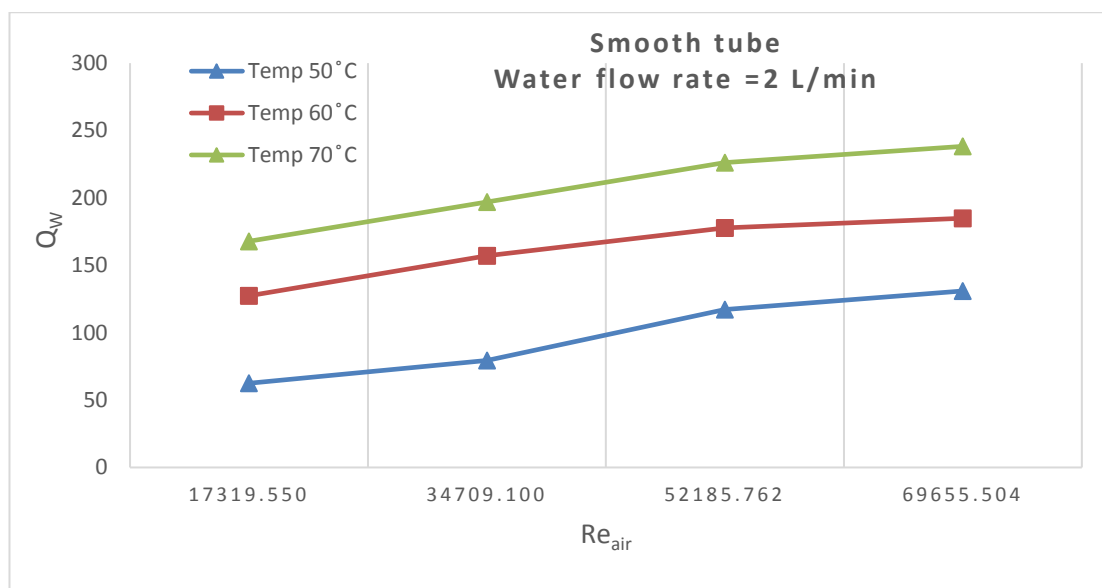


Figure 5.2. Variation of heat transfer rate with Re_{air} for different inlet hot water temperatures (50, 60, and 70oC) at flow rate of 2 L/min.

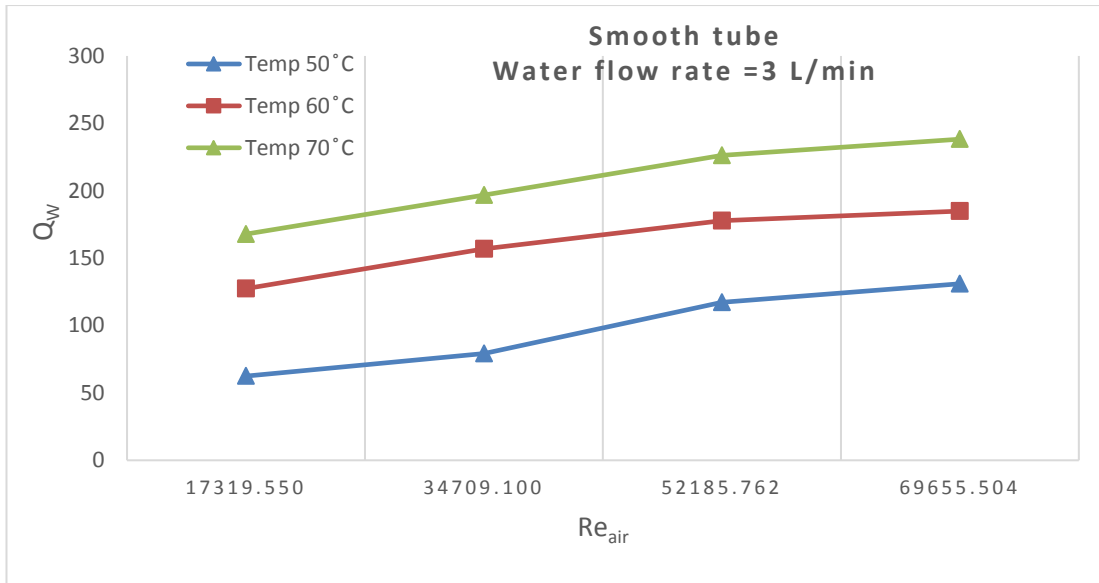


Figure 5.3. Variation of heat transfer rate with Re_{air} for different inlet hot water temperatures (50, 60, and 70°C) at flow rate of 3L/min.

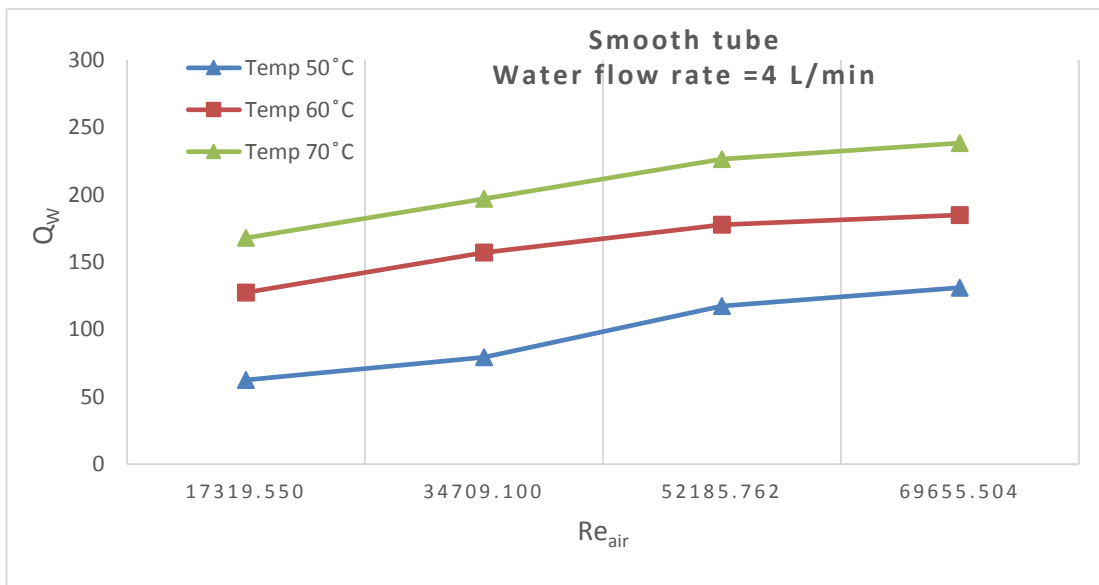


Figure 5.4. Variation of heat transfer rate with Re_{air} for different inlet hot water temperatures (50, 60, and 70°C) at flow rate 4L/min.

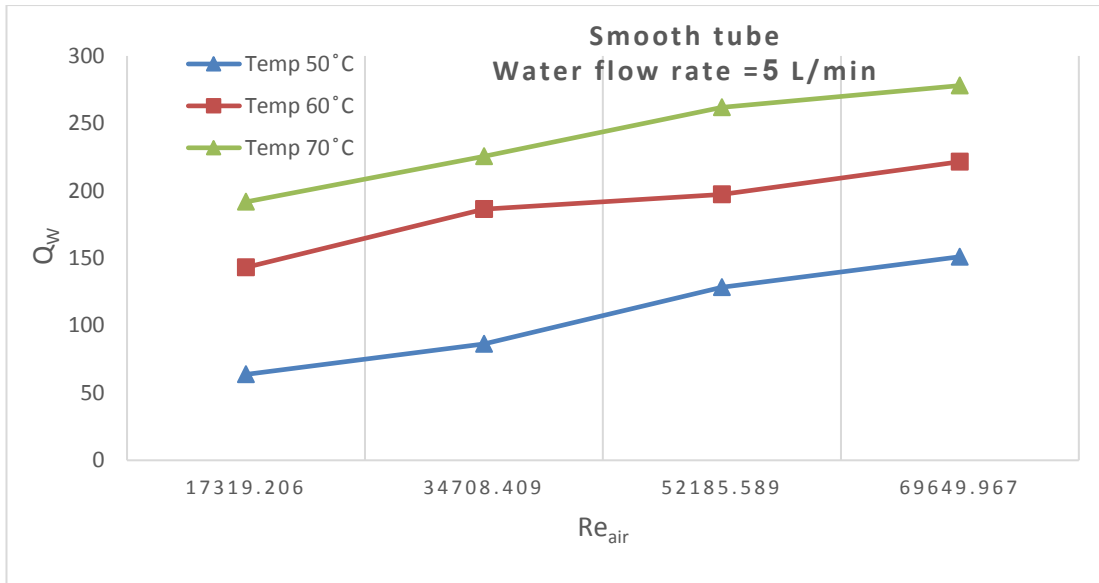


Figure 5.5. Variation of heat transfer rate with Re_{air} for different inlet hot water temperatures (50, 60, and 70°C) at flow rate 5L/min.

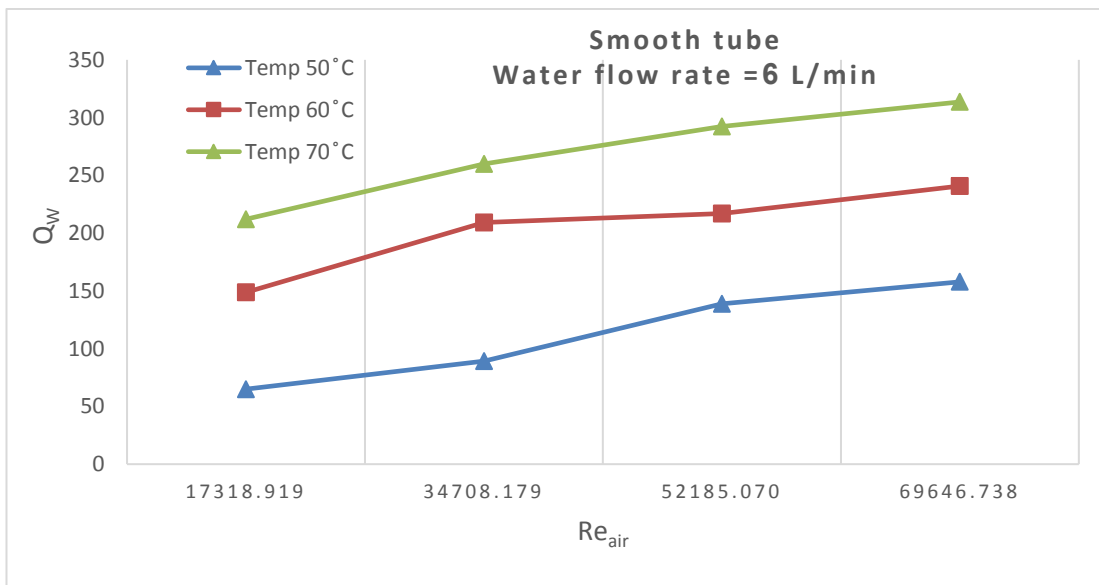


Figure 5.6. Variation of heat transfer rate with Re_{air} for different inlet hot water temperatures (50, 60, and 70°C) at flow rate 6L/min.

5.2.1.3. Effect the Tube Inlet Temperature on Heat Transfer Coefficient

Through the Figure 5.7 to Figure 5.10, which show the relationship between the heat transfer coefficient with the temperatures of hot water inside the pipe. As these diagrams confirmed that the heat transfer coefficient increases with increasing temperatures and the flow rate of the incoming water when the velocity of the outside

air remains constant. The reason for this increase is the turbulence resulting from an increase in the turbulence of the water and the effect of thermal conductivity, which rises with the increase in water temperatures.

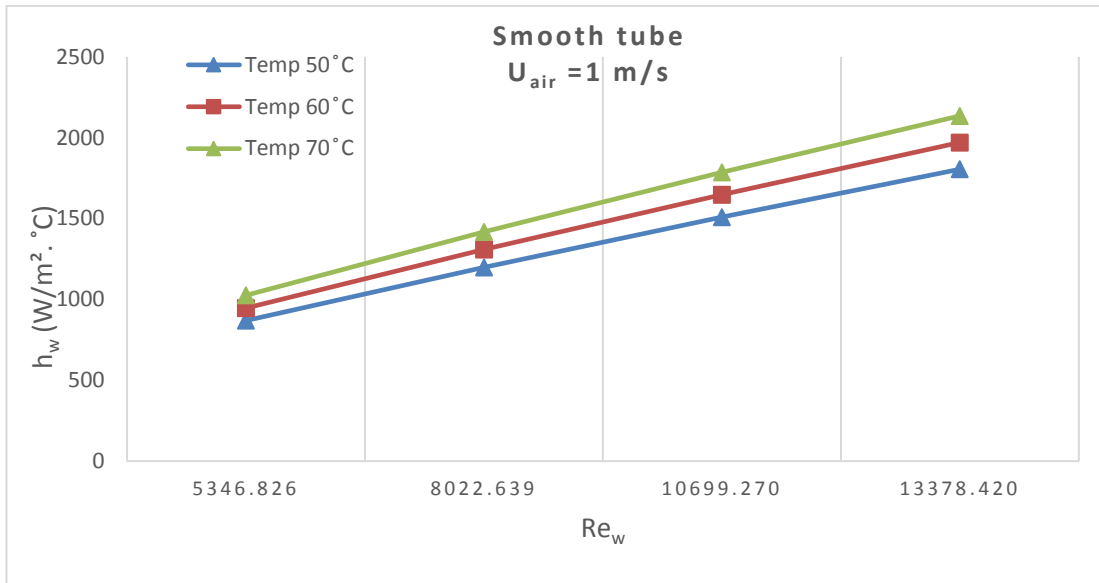


Figure 5.7. Variaiton of heat transfer coefficient with Re_w for different inlet water temperatures at air velocity 1m/s.

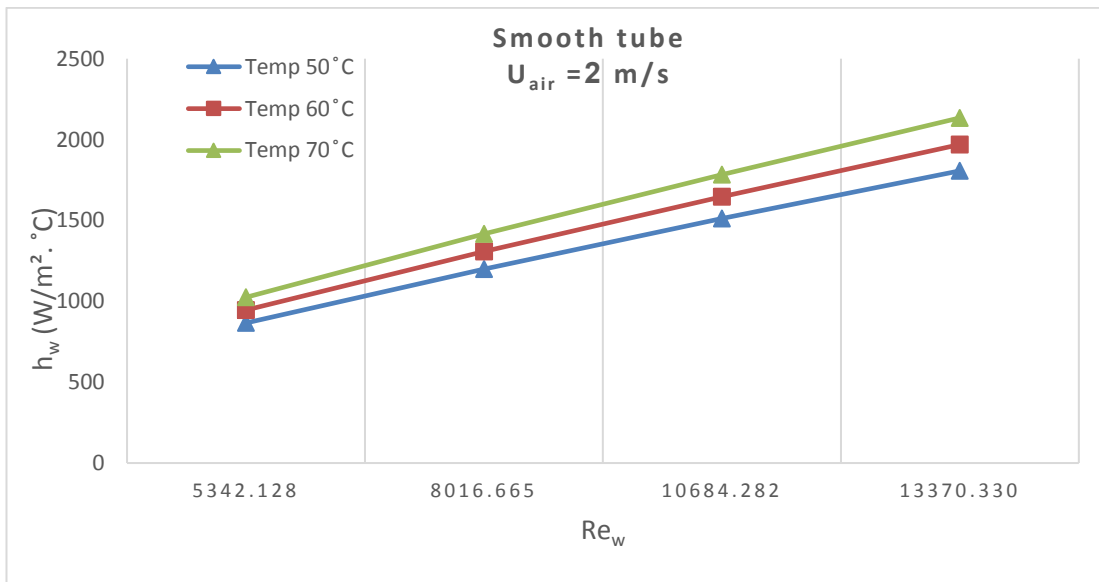


Figure 5.8. Variaiton of heat transfer coefficient with Re_w for different inlet water temperatures at air velocity 2m/s.

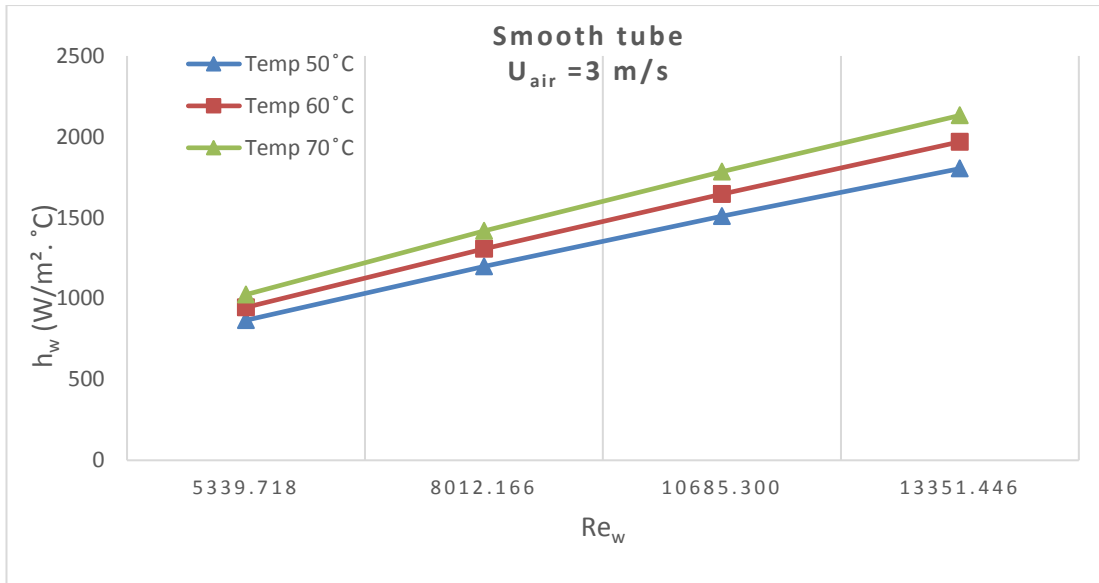


Figure 5.9. Variaiton of heat transfer coefficient with Re_w for different inlet water temperatures at air velocity 3m/s.

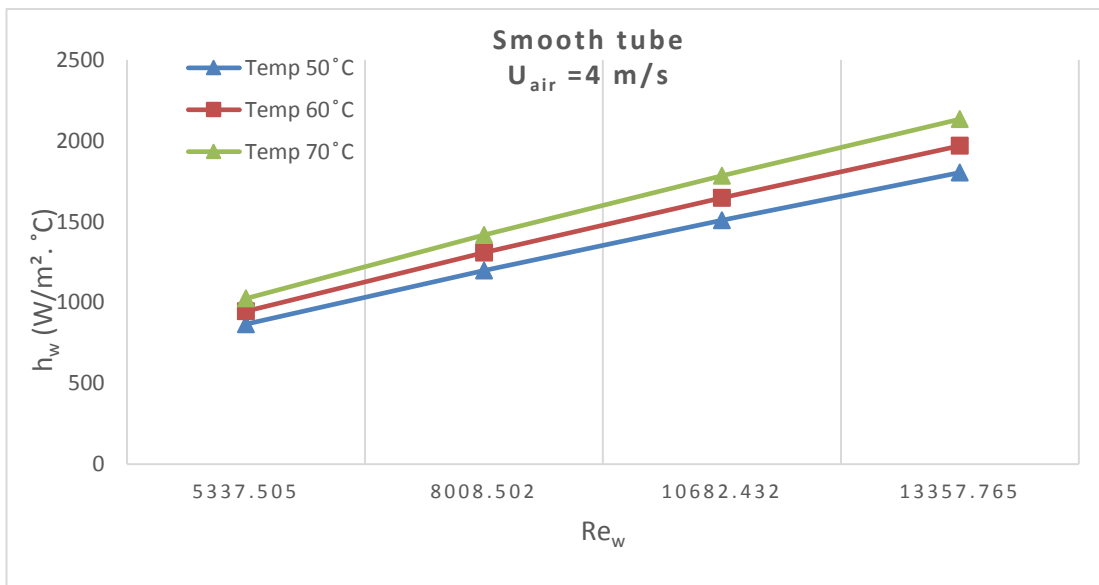


Figure 5.10. Variaiton of heat transfer coefficient with Re_w for different inlet water temperatures at air velocity 4m/s.

5.2.2. Effect of Fins on Heat Transfer Rate

Through the study and the results obtained, it was found that the finned tubes give more heat transfer rate than the smooth tubes with different number and shape of the fins. The fins used in this study were rectangular fins, based on the previous study [41], which confirmed that the rectangular circular fins give the best heat transfer rate than

other shapes, as the higher the surface area of the tubes, the heat transfer rate will also increase, and thus this increase will be a reason in increasing the actual efficiency of the tubes. Table 5.2 and Figure 5.11 shows the effect of the rate of heat transfer for each type.

The boundary conditions are applied to two models (the first model smooth tube, and the second models involve three model medium integral finned tube, with fin pitch ($P=1.6, 2.5,$ and 3.75 mm), respectively, to obtain the best heat transfer rate, best heat transfer coefficient and efficiency were obtained for inlet water temperature as $70\text{ }^{\circ}\text{C}$.

Table 5.2. Variation of heat transfer rate with inlet water temperature.

T_{hi} ($^{\circ}\text{C}$)	U_a (m/s)	\dot{v}_w (L/min)	Q_w (W)			
			Smooth	Finned tube with 1.6 mm	Finned tube with 2.5 mm	Finned tube with 3.75 mm
50	1	2	54.049	213.629	172.077	152.954
60	1	2	75.754	289.814	233.752	207.026
70	1	2	108.207	369.254	296.462	226.689

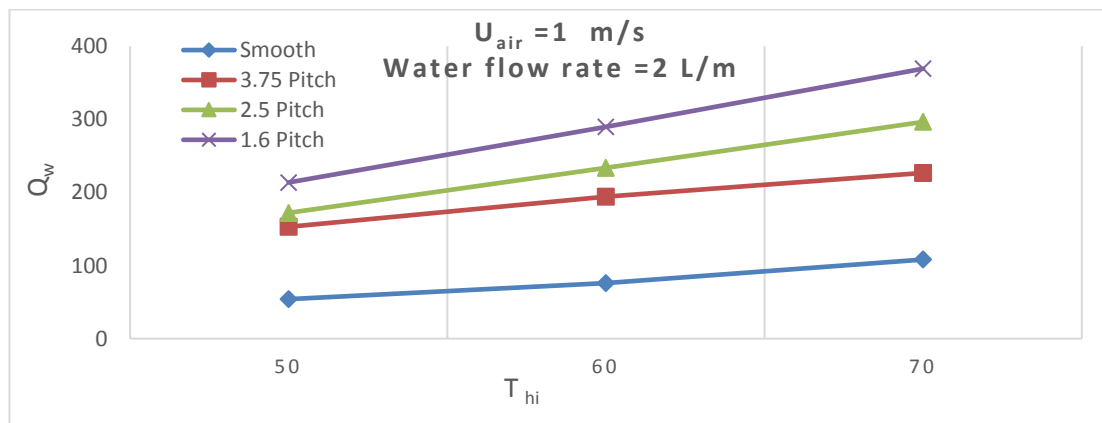


Figure 5.11. Variation of heat transfer rate with inlet water temperature for all models.

5.2.2.1. Effect of Pitch Ratio for Medium Integral Fin on Heat Transfer Rate

The effect of fin pitch ratio on heat transfer rate when changing the flow of water and changing the temperature with constant air velocity is shown between Figures (5.12, 5.13, and 5.14). It turns out that the heat transfer rate increases with the increase

Reynolds number for generally and fins pitch ratio respect to the smooth tube, where it was found that the best model is obtained with integral medium finned tube with the pitch is ($P= 1.6$ mm). When the distance between the fins is reduced, it leads to an increase the number of fins, this led to increases the surface area for heat exchange and generates more air turbulences prevent the thermal boundary layer, which tend to increases the rate of heat transfer.

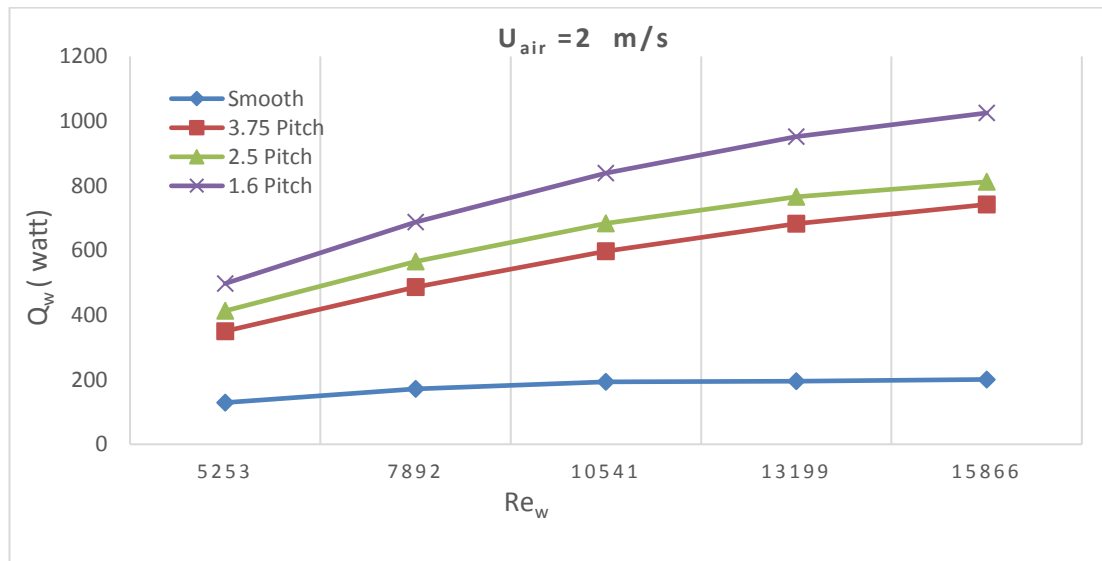


Figure 5.12. Variation of heat transfer rate with water Reynolds number for constant air velocity (2m/s).

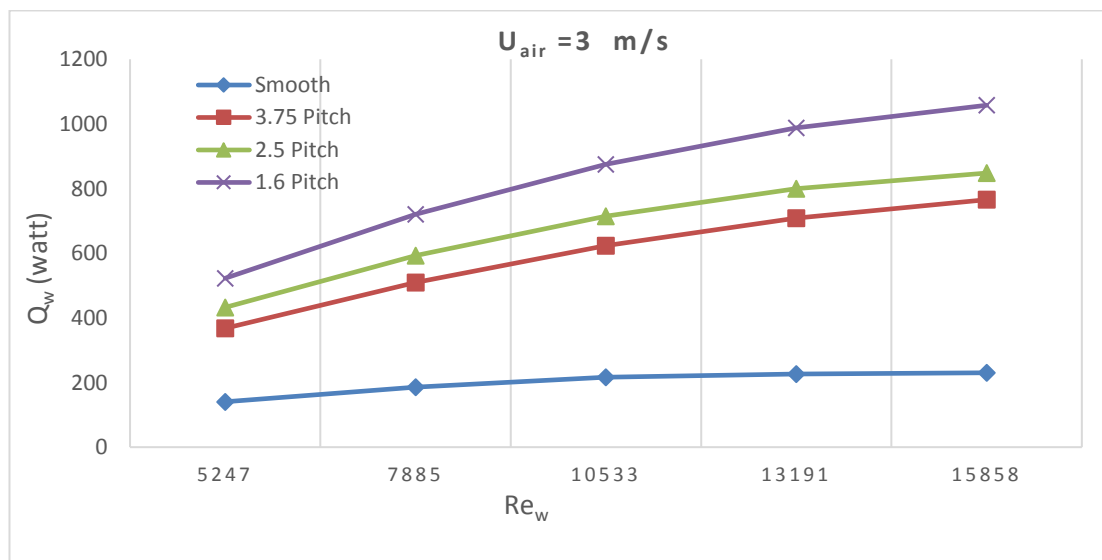


Figure 5.13. Variation of heat transfer rate with water Reynolds number for constant air velocity (3m/s)

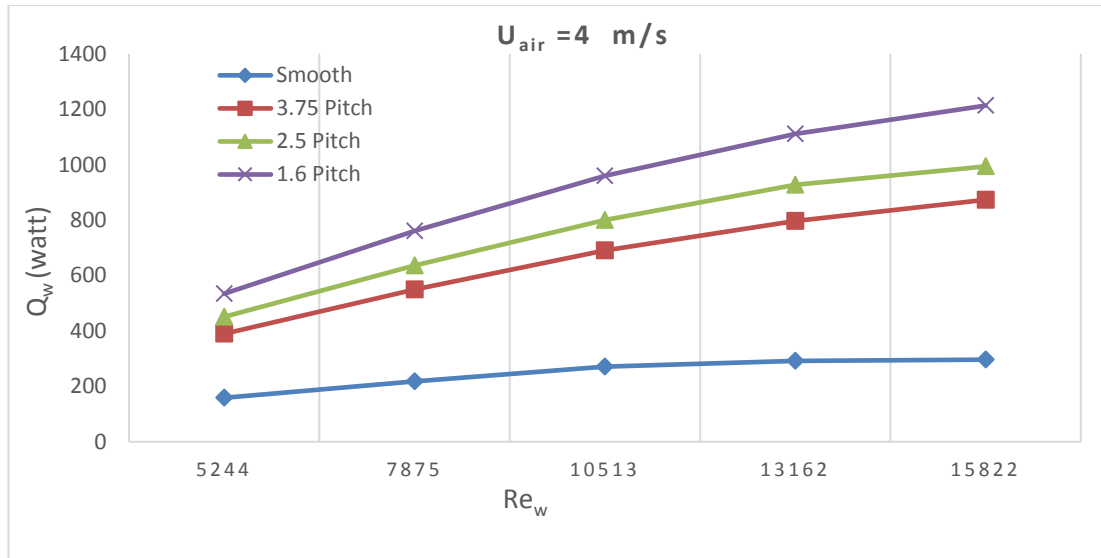


Figure 5.14. Variation of heat transfer rate with water Reynolds number for constant air velocity (4m/s).

5.2.2.2. Effect of the Pitch Ratio on NTU

Figure 5.15 shows the relationship between the number of transmission units (*NTU*) with Reynolds number for integrated medium finned tubes and smooth tube.

It was defined that increasing the value of the Reynolds number increases the *NTU* and the greater the number of fins, the greater the ratio. Also, thermal efficiency with respect to smooth tubes in general is the same trend. This is due to the increase in the total heat transfer coefficient. It was found from this condition that the tube with a pitch of ($P= 1.6$ mm) gives a higher value of *NTU* than the others, due to the increase in the surface area and the number of fins as it works to direct the movement of air, which leads to an increase in thermal energy dissipation from the air side to the air flow.

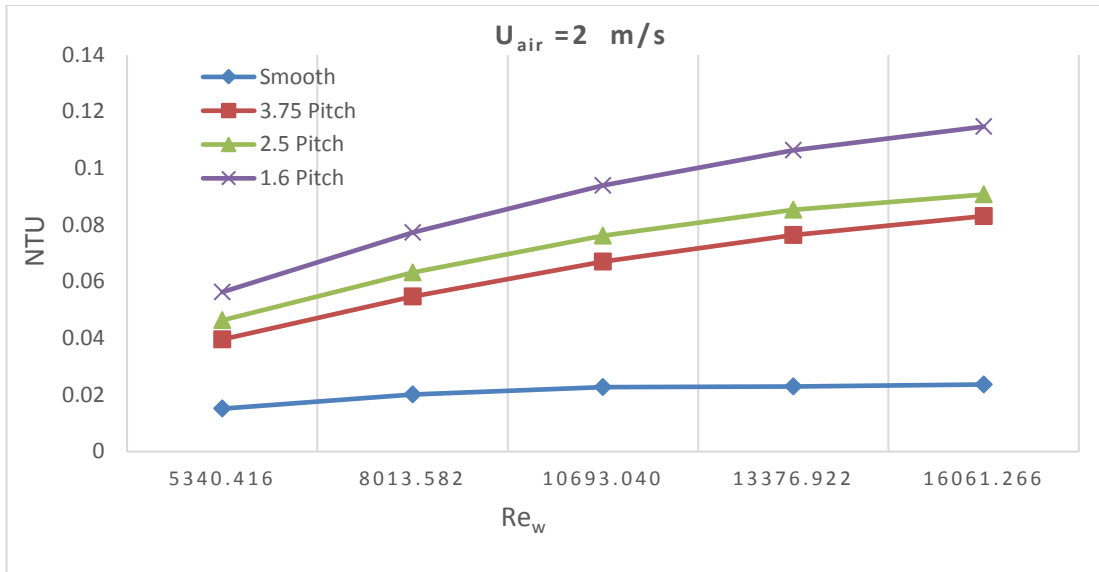


Figure 5.15. Relation between the number of transmission units (NTU) with Reynolds number and constant air velocity 2m/s.

5.2.2.3. Effect of Reynolds Number on the Effectiveness

Figure 5.16 and Figure 5.17 show the relation between the Reynolds number and the effectiveness of cross flow heat exchanger for all model which studied. The results showed that as the Reynolds number increases, the effectiveness of the heat exchanger decreases. In turn, this increases the heat transfer coefficient and improves the effectiveness of the heat exchanger.

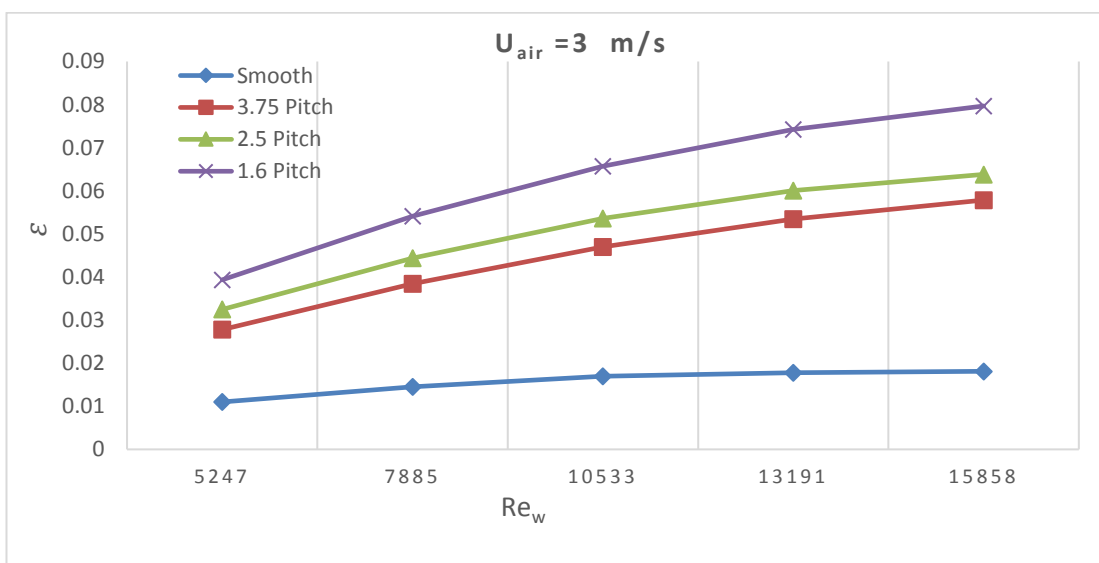


Figure 5.16. The relation between the Reynolds number and the effectiveness with different pitch ratio and constant air velocity 3m/s.

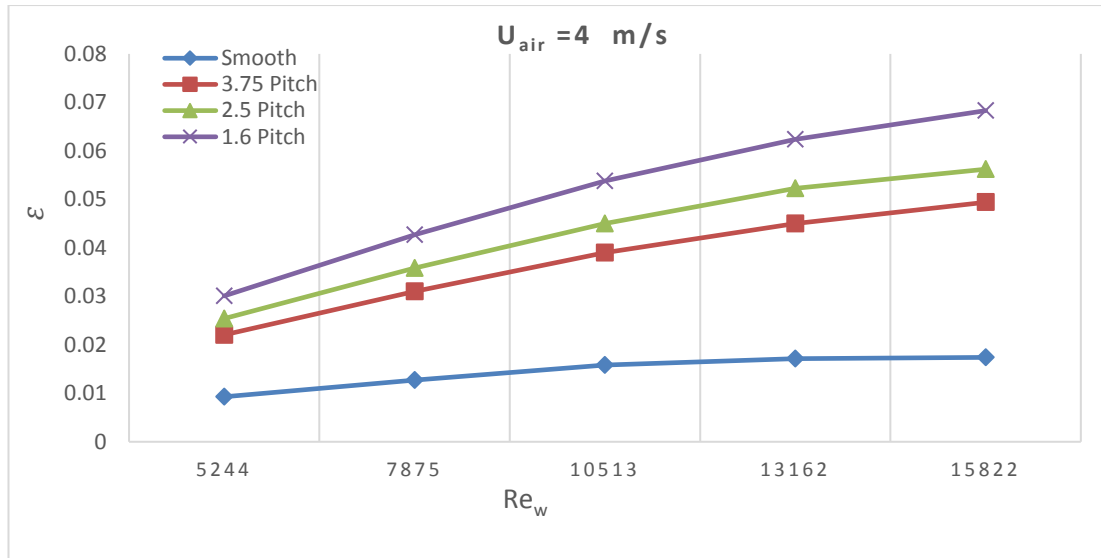


Figure 5.17. The relation between the Reynolds number and the effectiveness with different pitch ratio and constant air velocity 4m/s.

5.2.2.4. Effect of Pitch Ratio on Temperature Difference

Figure 5.18 to Figure 5.20 shows the relationship between the temperature difference and pitch ratio. The temperature difference decreases with the increase of the Reynolds number for all test models and for the various pitch ratios in general, relative to the smooth tube. It is also noted that the pitch ratio of (P=1.6 mm) gives the highest temperature difference at low velocity. This is attributed to the increase in the Reynolds number which means an increase in the water mass flow rate and the lack of sufficient time for the heat transfer between the hot fluid on the interior side of the tube and the air on the fins side, in addition to an increase in the surface area of the finned tubes.

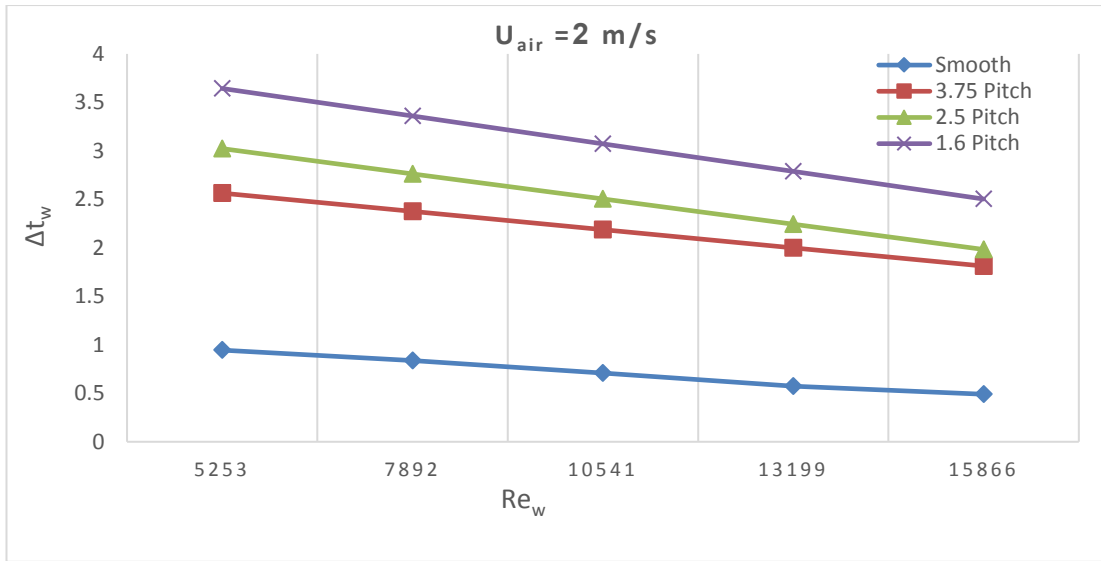


Figure 5.18. Relationship between the temperature difference and Reynolds number for constant air velocity 2m/s.

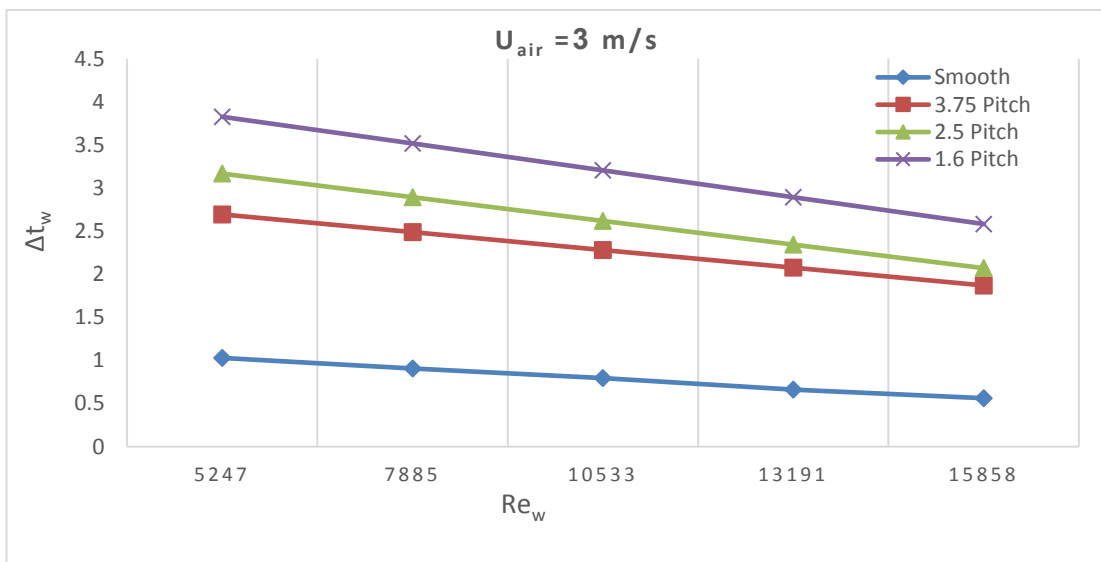


Figure 5.19. Relationship between the temperature difference and Reynolds number for constant air velocity 3m/s.

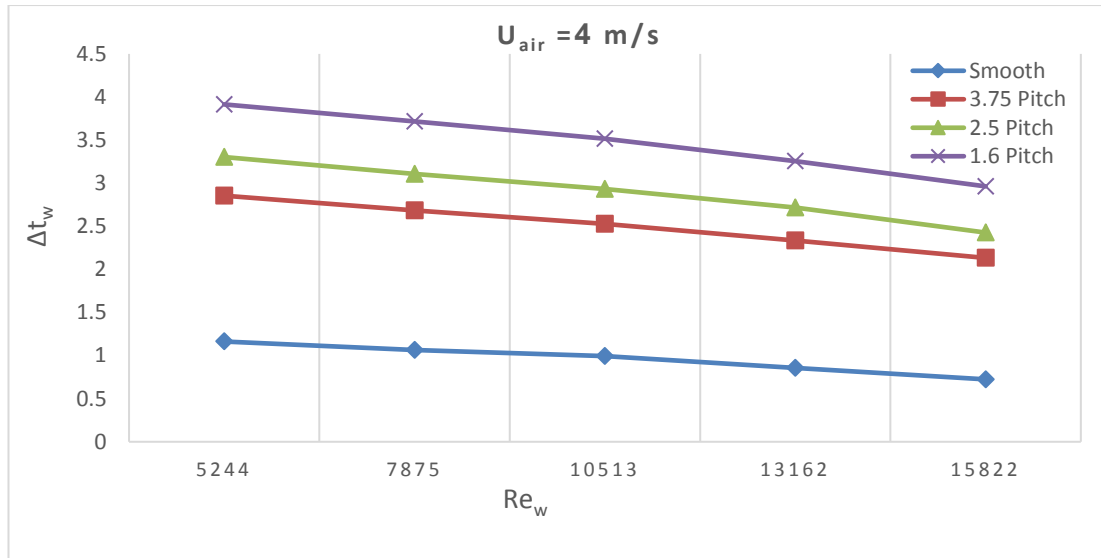


Figure 5.20. Relationship between the temperature difference and Reynolds number for constant air velocity 4m/s.

5.2.2.5. Effect of Pitch Ratio on Air side Overall Heat Transfer Coefficient

Figure 5.21 to Figure 5.25 shows the relationship between the air side overall heat transfer coefficient with the different inlet air velocity at constant water flow rate. It was found that decreasing the pitch ratio between the fins, their number will increase. As a result, it increases the surface area, which works to regulate the flow direction and tend to prohibit growth the thermal boundary layer. It also shows that as Reynolds number increases, the total heat transfer coefficient for air side will also increase under changing water flow rate and air velocity.

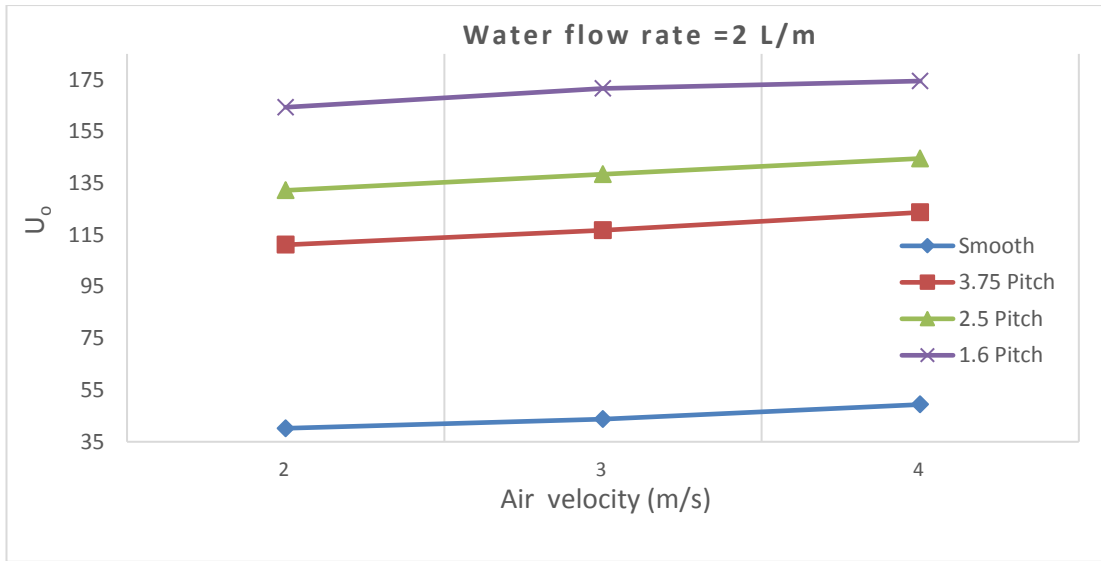


Figure 5.21. The relation between overall heat transfer coefficient and air velocity for all models.

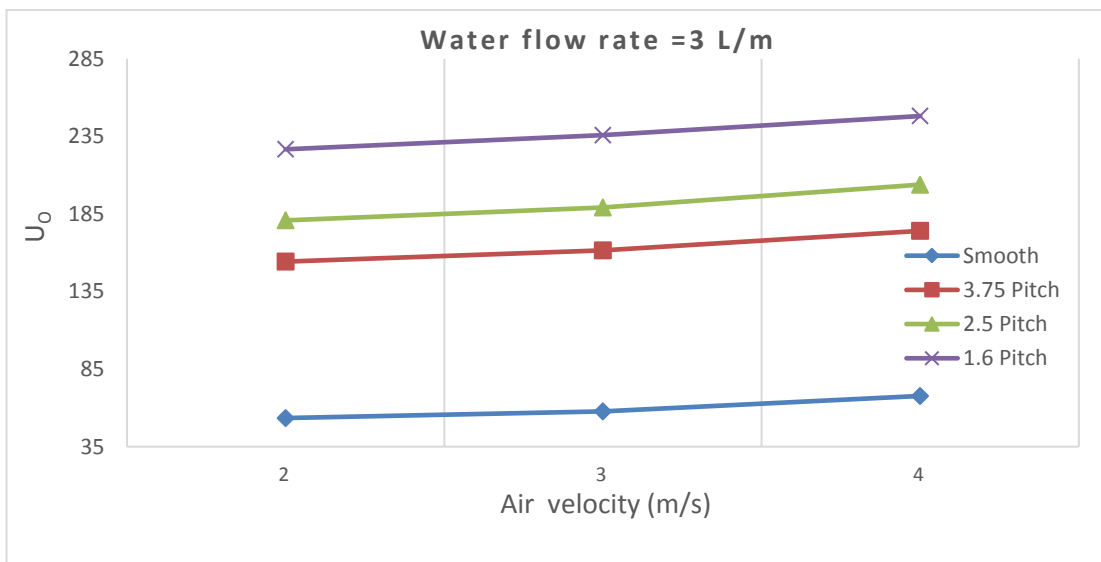


Figure 5.22. The relation between overall heat transfer coefficient and air velocity for all models.

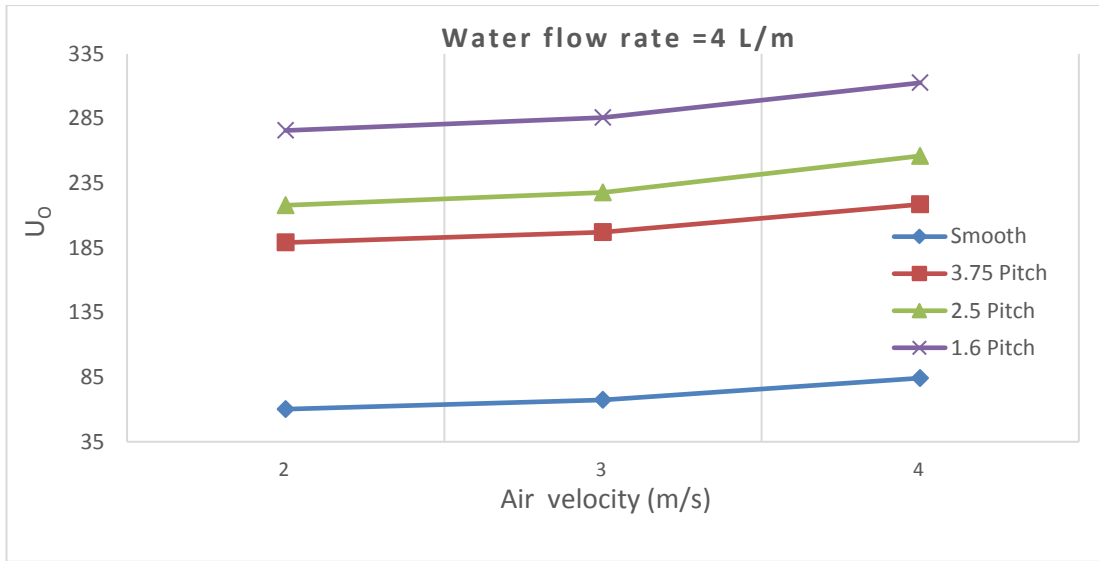


Figure 5.23. The relation between overall heat transfer coefficient and air velocity for all models.

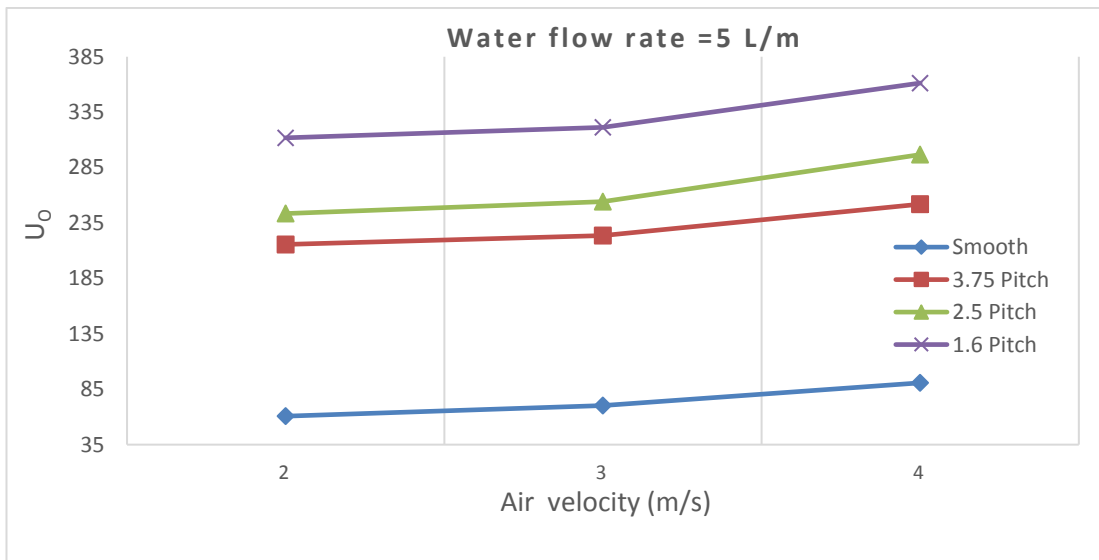


Figure 5.24. The relation between overall heat transfer coefficient and air velocity for all models.

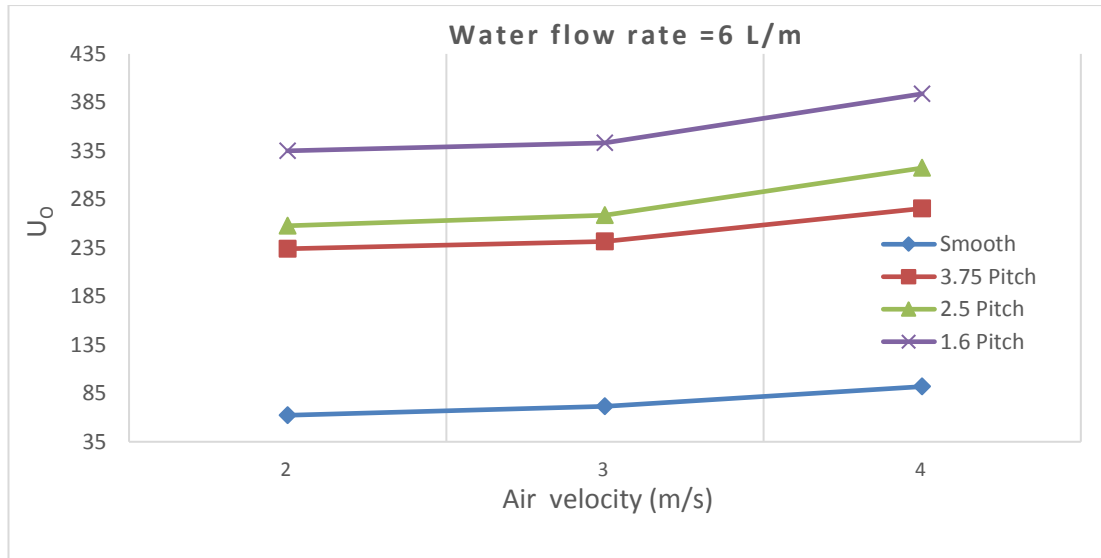


Figure 5.25. The relation between overall heat transfer coefficient and air velocity for all models.

5.2.2.6. Effect of Pitch Ratio on Air side Overall Heat Transfer Coefficient

Figure 5.26 to Figure 5.28 shows the relationship between the air side overall heat transfer coefficient and pitch ratio. It shows that as Reynolds number inside tube increases, the air side overall heat transfer coefficient will also increase under constant air velocity generally for all integral fins tube with different pitch ratio. From this obtained phenomenon the higher overall heat transfer coefficient at higher Reynolds number and air velocity at pitch ratio of (P=1.6 mm). This is due to effectiveness for integral finned tube with large number of fins as well as increases the surface area for these tubes.

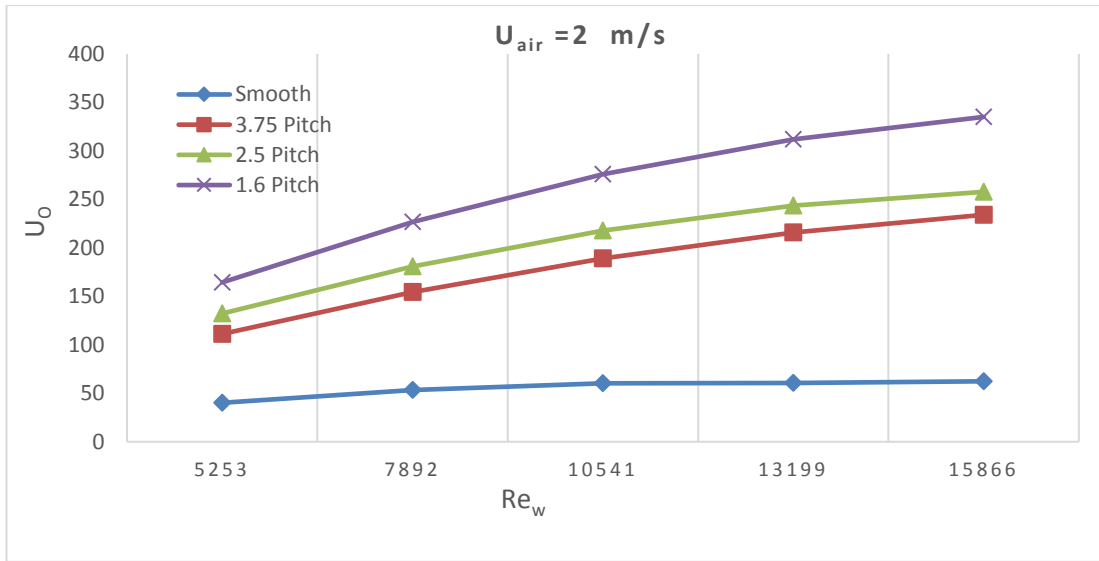


Figure 5.26. Air side overall heat transfer coefficient with Reynolds number for all models.

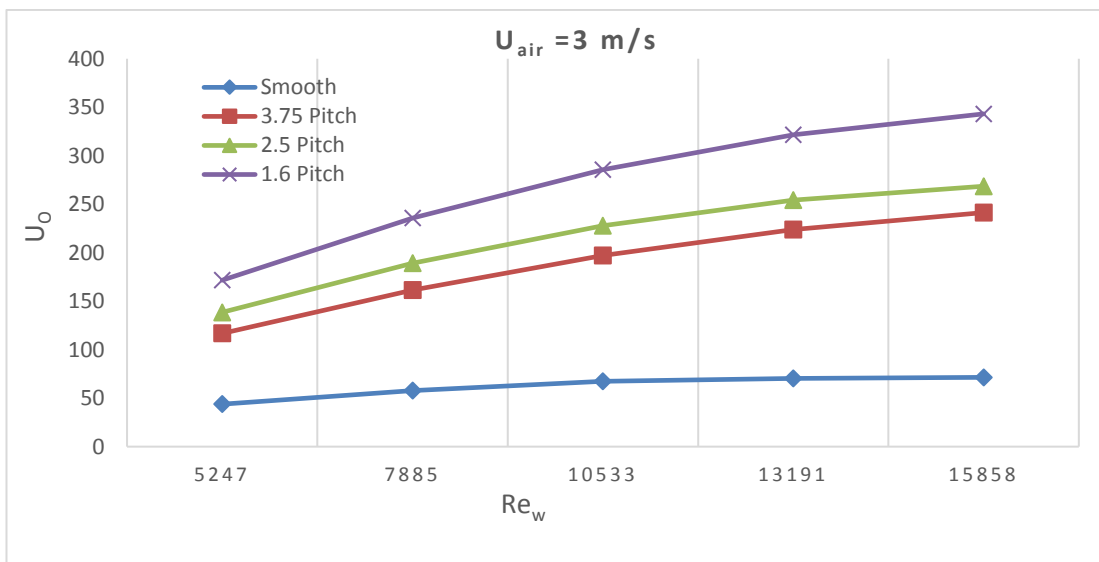


Figure 5.27. Air side overall heat transfer coefficient with Reynolds number for all models.

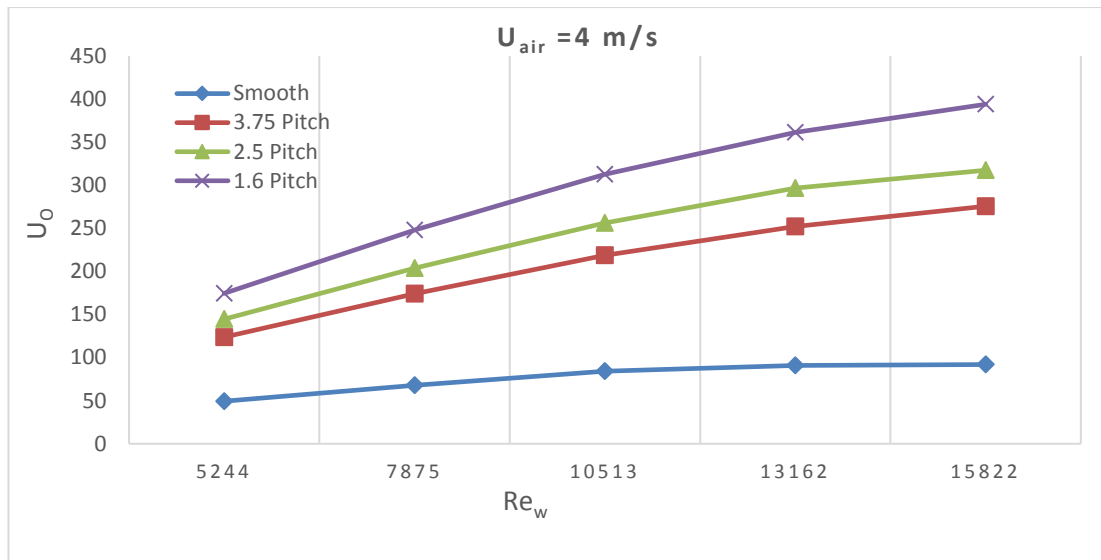


Figure 5.28. Air side overall heat transfer coefficient with Reynolds number for all models.

5.2.2.7. Effect of Air Velocity on Air side Overall Heat Transfer Coefficient

Concerning figure (5.29 to 5.33), it shows the relationship between the interior overall heat transfer coefficient with the change in air velocity at constant temperature and the flow rate of water. It shows that the higher air velocity, the higher overall heat transfer coefficient for all test model. This increase is very clear at the increase in the mass flow rate inside tube. Prior to it, the three forms mentioned above show that the best tube that gives the best overall external and internal heat transfer coefficient is the tube with a fin pitch of (P=1.6 mm).

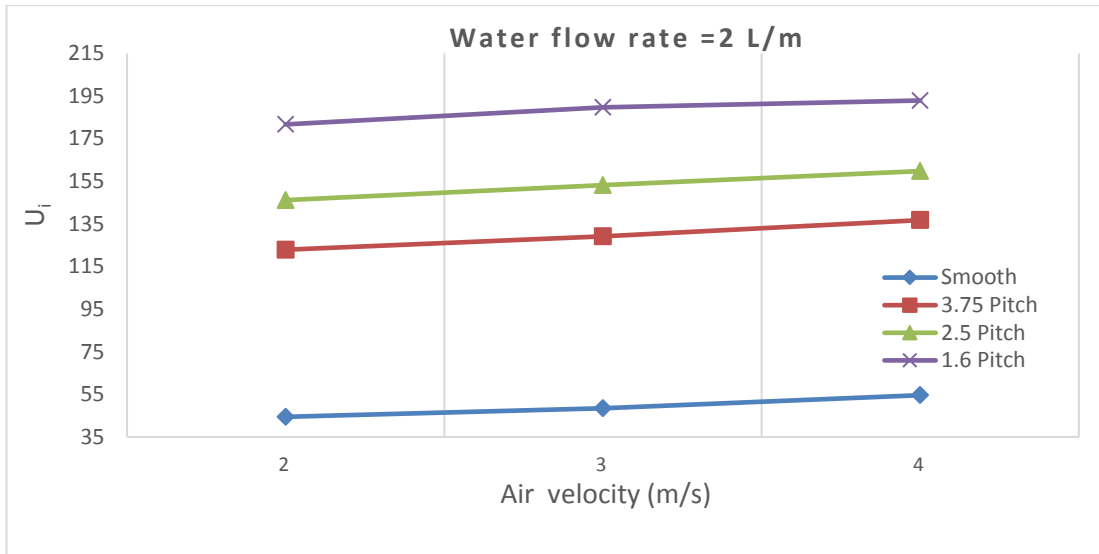


Figure 5.29. Internal overall heat transfer coefficient varies with air velocity for all models.

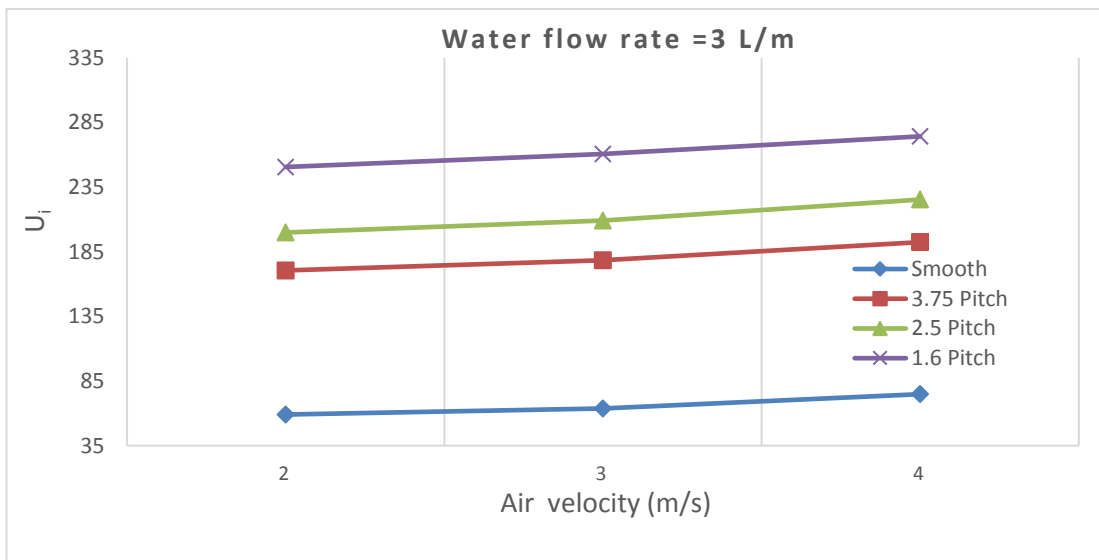


Figure 5.30. Internal overall heat transfer coefficient varies with air velocity for all models.

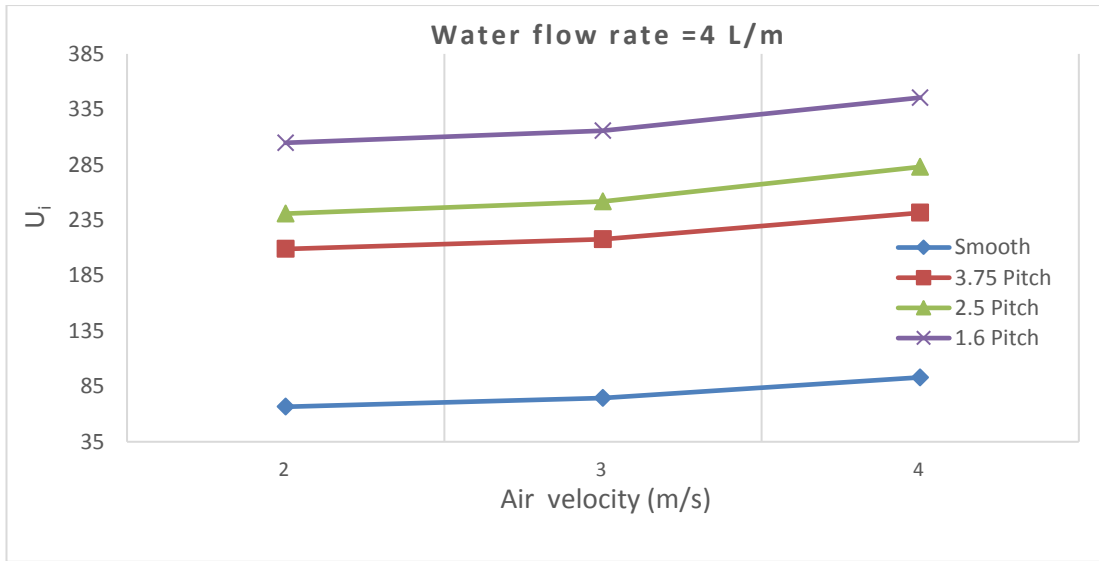


Figure 5.31. Internal overall heat transfer coefficient varies with air velocity for all models.

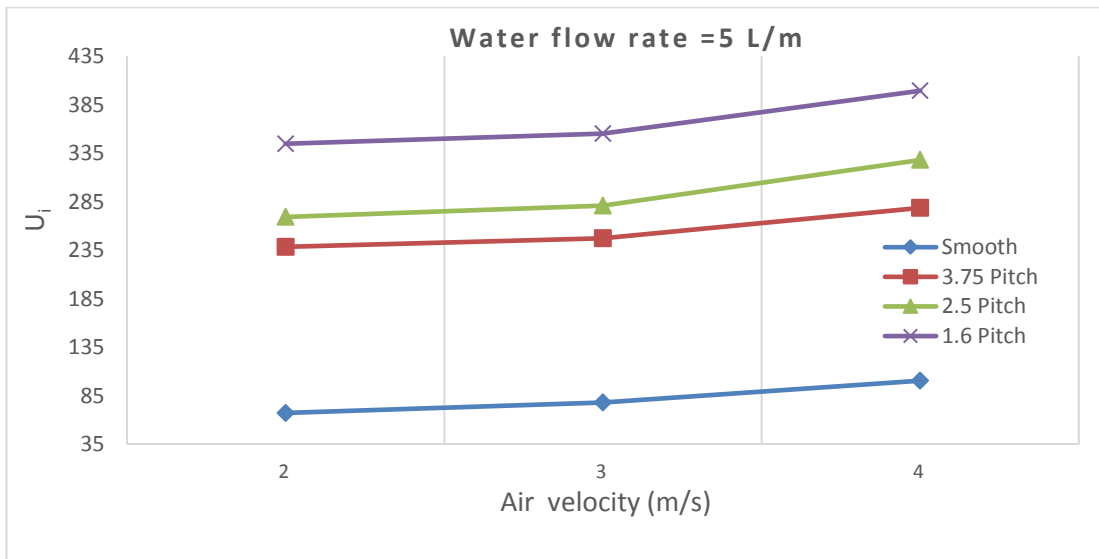


Figure 5.32. Internal overall heat transfer coefficient varies with air velocity for all models.

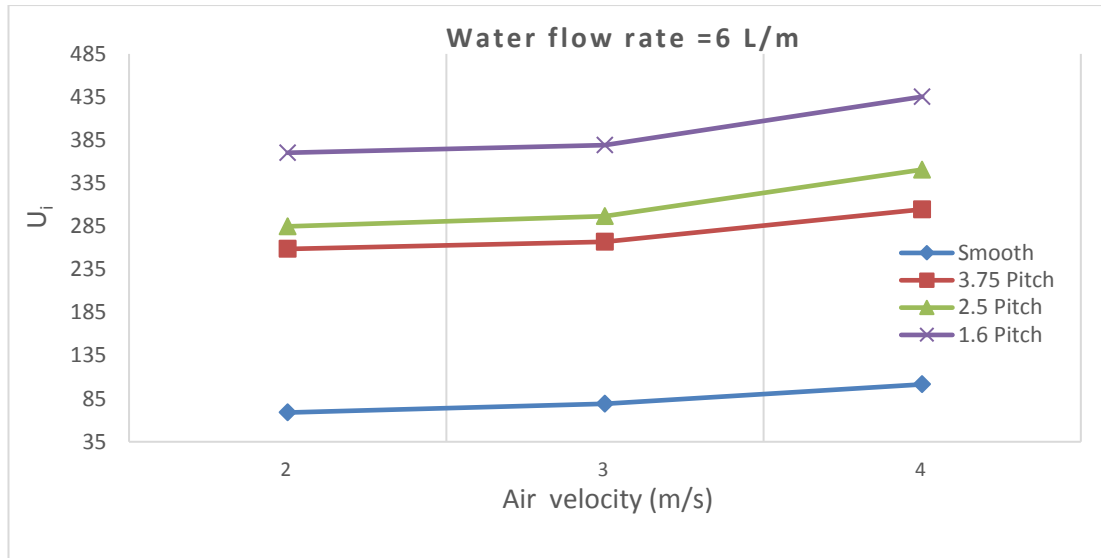


Figure 5.33. Internal overall heat transfer coefficient varies with air velocity for all models.

5.2.2.8. Effect of Pitch Ratio on Pressure Drop for Air Side

The relationship between pressure drops and air velocity at constant water flow rate and inlet temperature of 70 °C is shown in figures (5.34 to 5.38). We find that the pressure drops for air side increases with increasing air velocity and pitch ratio for all integral medium finned tubes. The highest pressure drops in tube with a pitch fin (P=1.6, 2.5, 3.75 mm) and then the smooth tube, respectively.

This is attributed to an increase in the number of fins at the pitch ratio of (P= 1.6 mm) and an increase in the surface area, in turn to an increase in surface resistance and the friction factor, which in turn to an increase in the pressure gradient. On the other hand, the percentage of improvement in the heat transfer coefficient from the air side, which is the main factor in this study, to the increase in the pressure drop ratio, is acceptable.

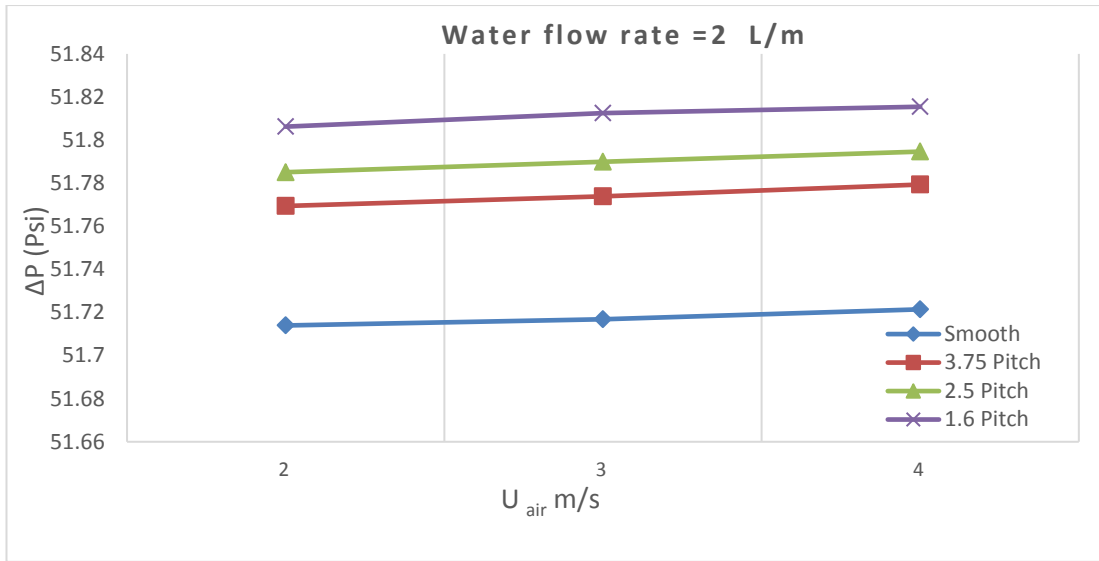


Figure 5.34. Effect of air side velocity on pressure drop at varies pitch ratio and smooth tubes with constant water mass flow rate 2L/min.

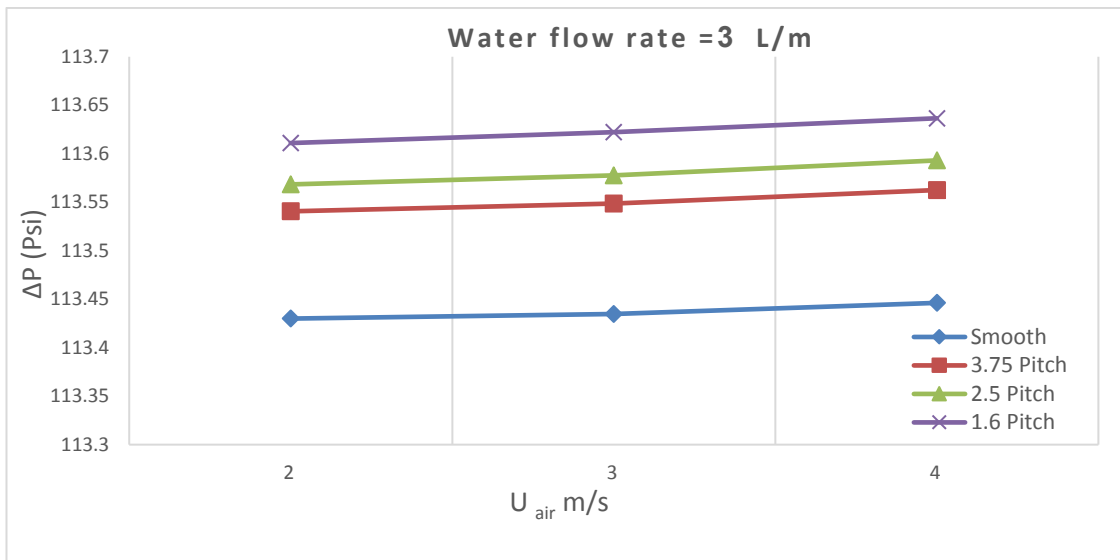


Figure 5.35. Effect of air side velocity on pressure drop at varies pitch ratio and smooth tubes with constant water mass flow rate 3L/min.

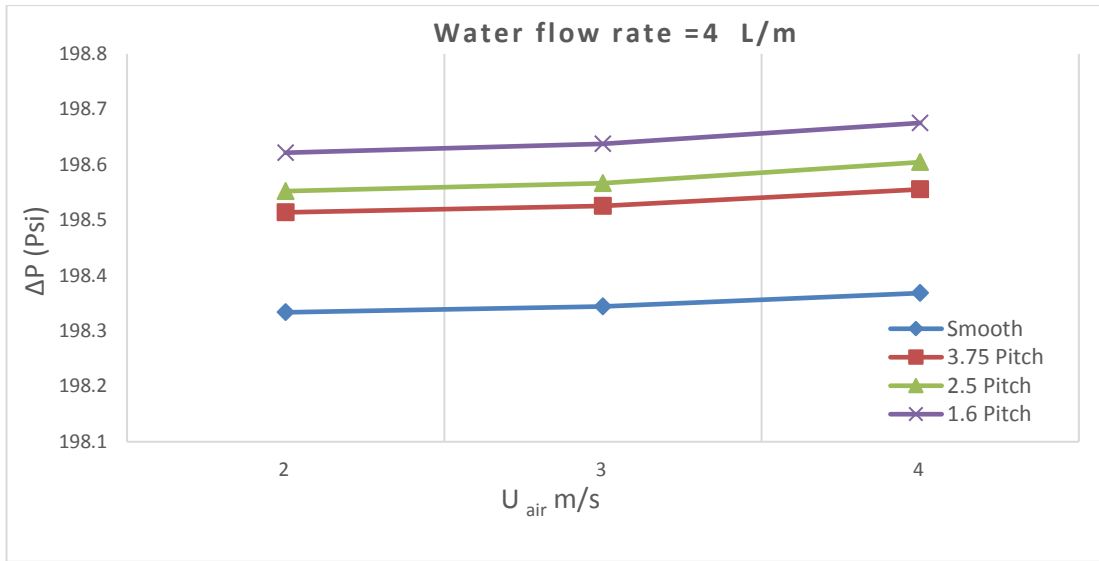


Figure 5.36. Effect of air side velocity on pressure drop at varies pitch ratio and smooth tubes with constant water mass flow rate 4L/min.

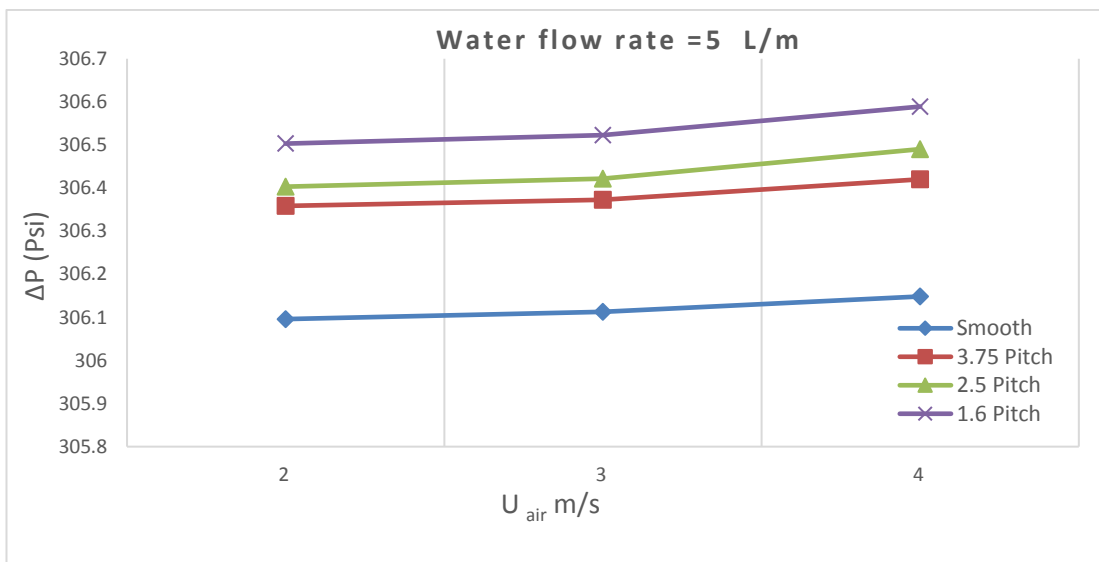


Figure 5.37. Effect of air side velocity on pressure drop at varies pitch ratio and smooth tubes with constant water mass flow rate 5L/min.

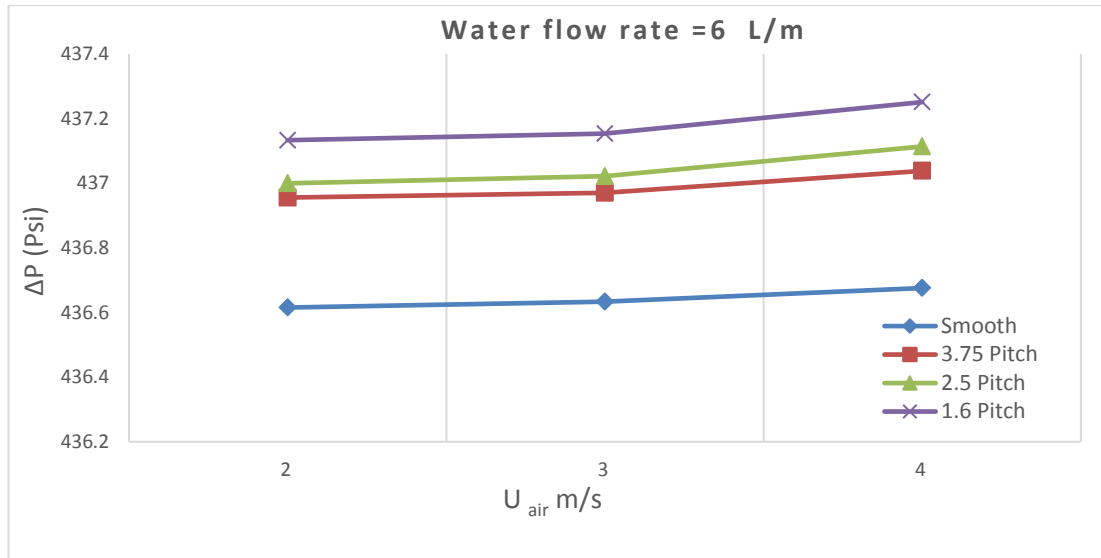


Figure 5.38. Effect of air side velocity on pressure drop at varies pitch ratio and smooth tubes with constant water mass flow rate 6L/min.

5.2.2.9. Velocity and Temperature Variations

Through the Figure 5.39 to Figure 5.42, which show the temperature distribution on the surface of the tubes, whether smooth or finned, where we notice that the temperature rises at the entrance to the tube and gradually decreases until it ends at the outlet of the tube. It was also noted that the tube with a pitch fin (P=1.6 mm) gives the highest temperature gradation for the surface, next is the tube with pitch fin (P=2.5 mm), then the tube with pitch fin (P=3.75mm), and then the smooth tube, as the heat exchange increases with increasing the number of fins.

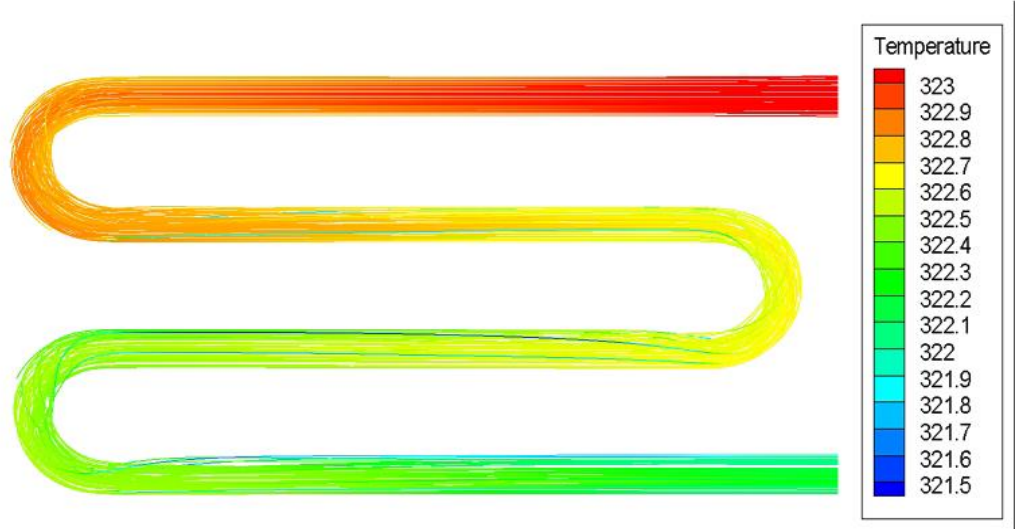


Figure 5.39. Temperature distribution in the smooth tube.

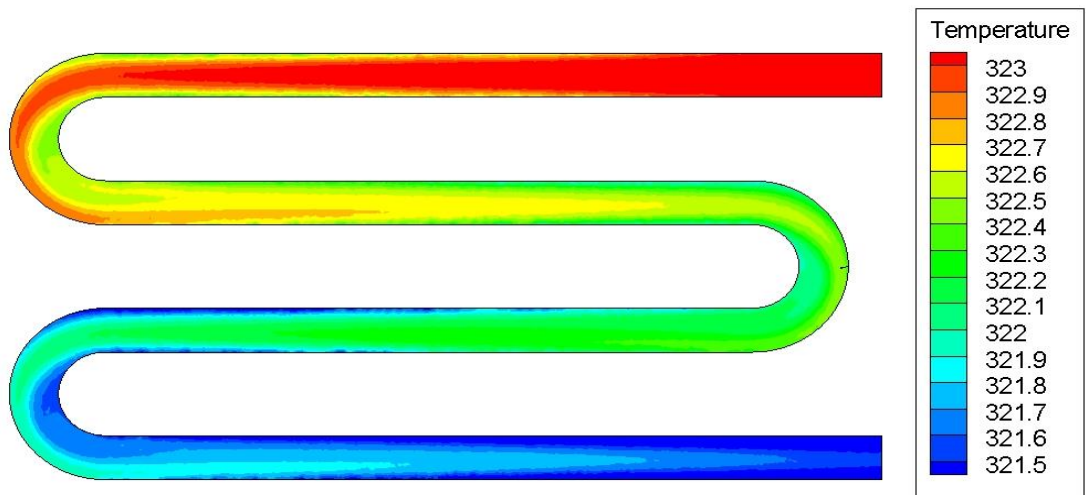


Figure 5.40. Temperature distribution in the finned tube with pitch fin ($P=1.6$ mm).

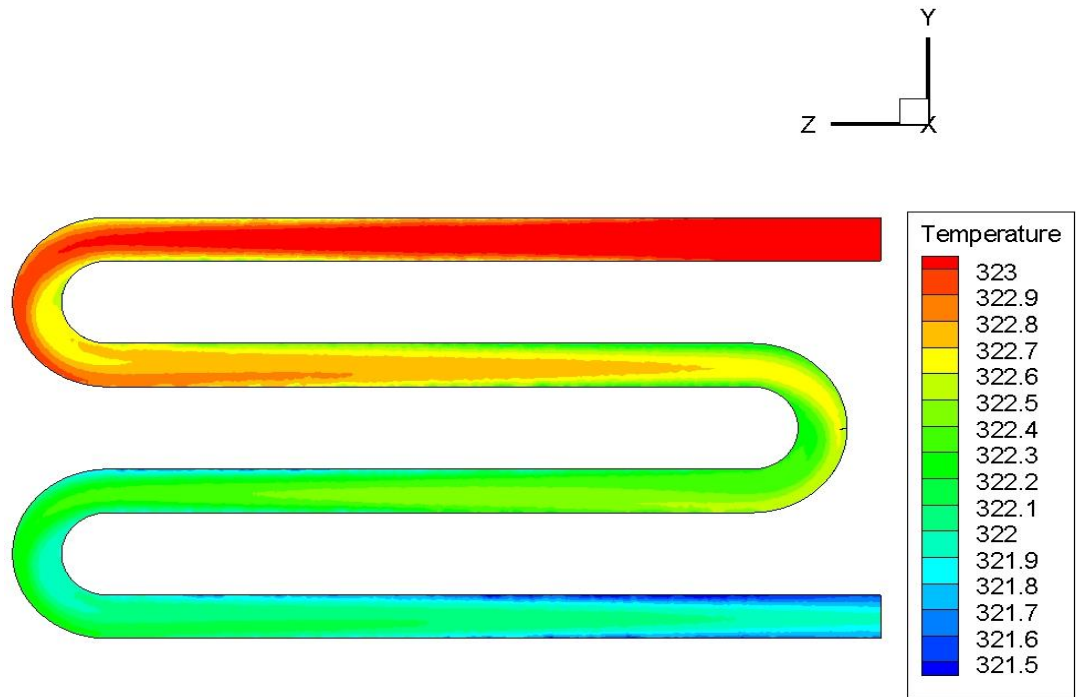


Figure 5.41. Temperature distribution in the finned tube with pitch fin ($P=2.5$ mm).

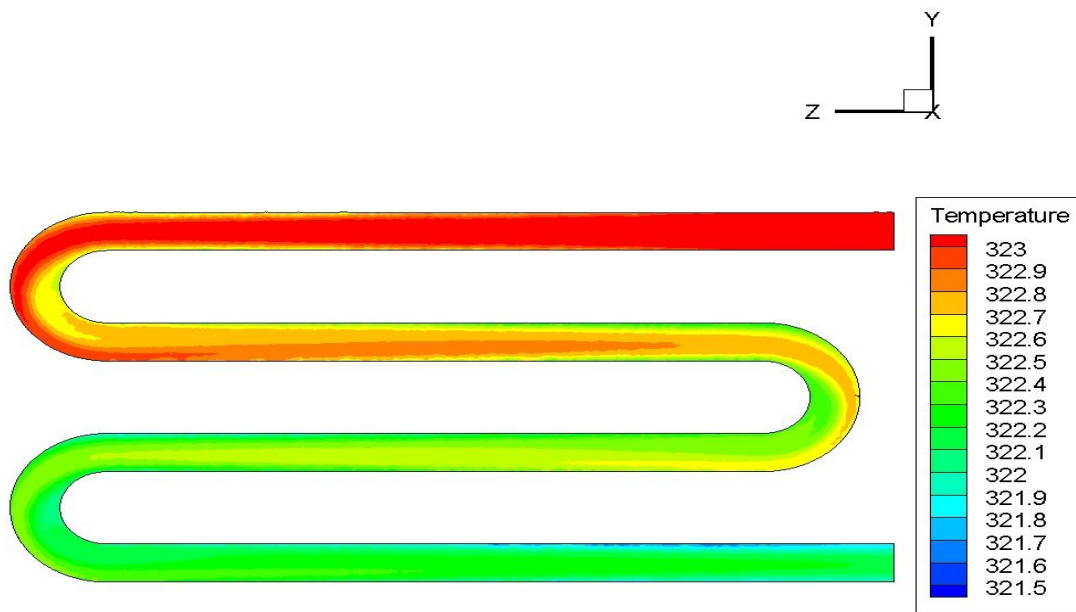


Figure 5.42. Temperature distribution in the finned tube with pitch fin ($P=3.75$ mm).

5.2.2.10. Temperature Distribution for Finned Tube

Figure 5.43 to Figure 5.46 show the numerical results which are obtained to explain the distribution of water temperatures on the test tube inside plane where the temperatures reach their highest value at the entrance to the tube and their lowest at the outlet. The heat gradually loses part of its value from the connection with the tube wall while it is exposed to the air temperature, which is less than the maximum water temperature. As for the Figure 5.47 to Figure 5.50 represent the temperature distribution in a cross-section of the tubes. It shows the level of air distribution that passes over the pipes from the air side. These figures show us a clear and gradual decrease in temperature across the cross-section of the tubes. It was noted from all of integral finned tube mentioned above, that the best decrease at temperatures is at the tube with a pitch fin ($P=1.6$ mm).

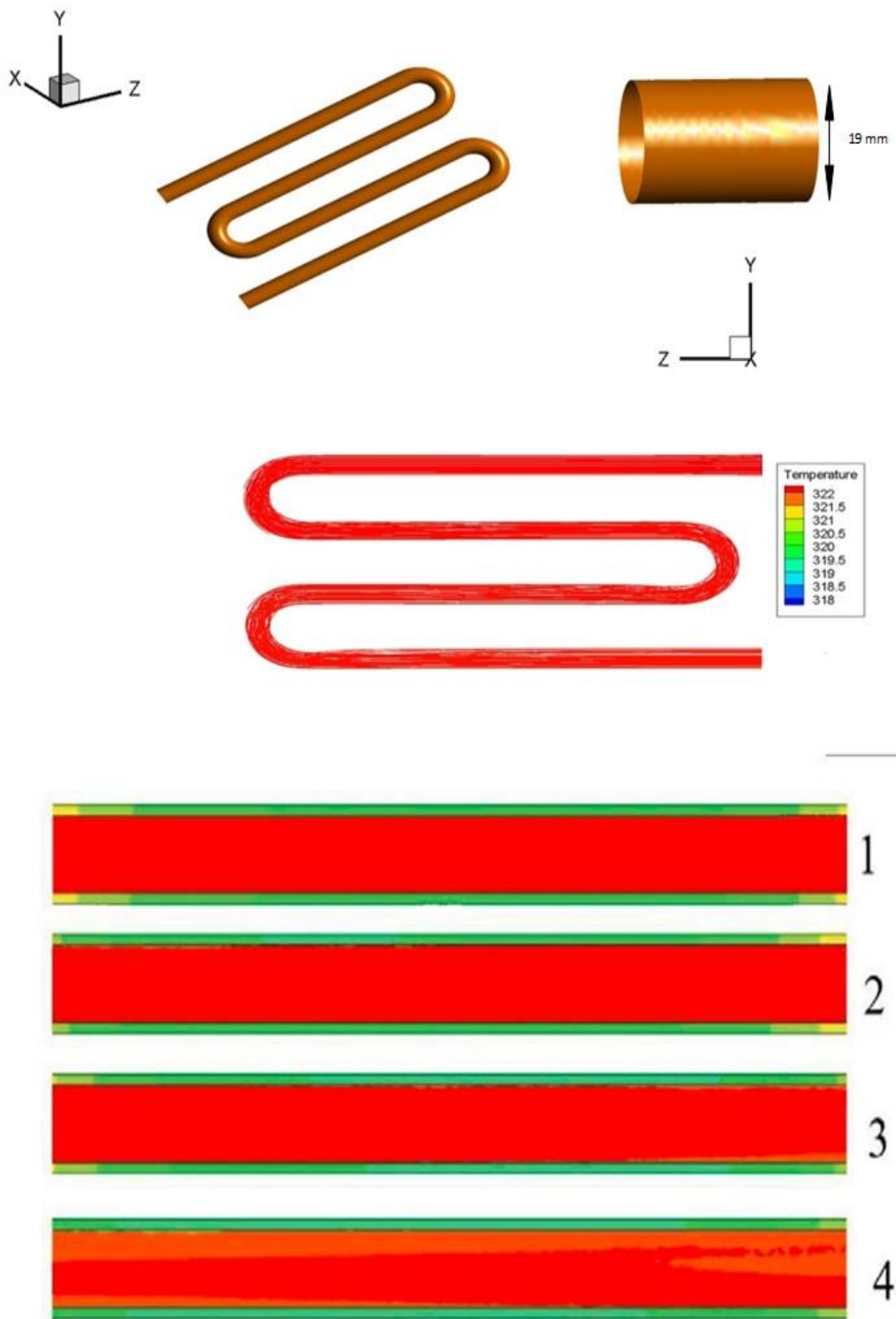


Figure 5.43. Temperature distribution of water in smooth tube.

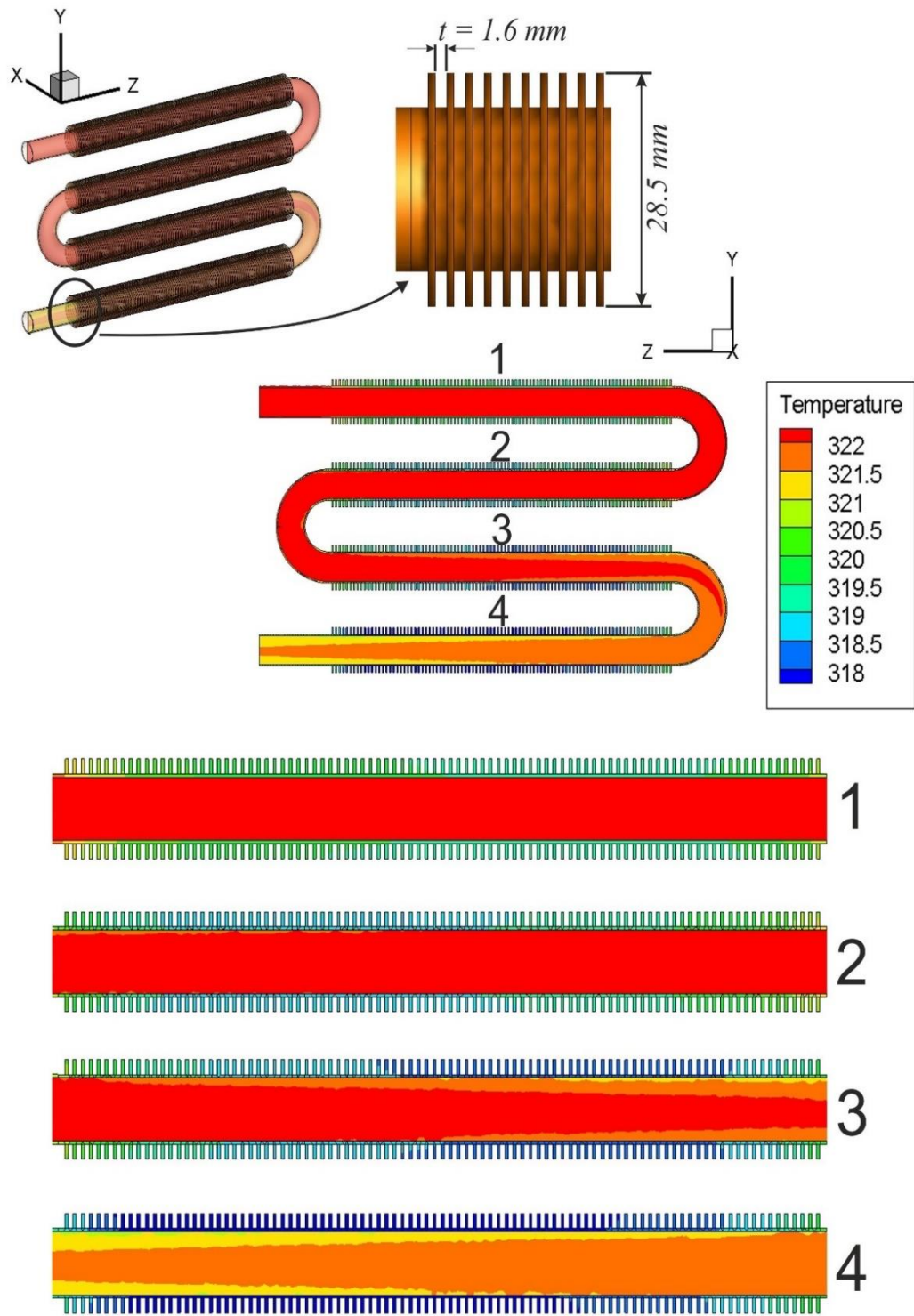


Figure 5.44. Temperature distribution of water in ntegral finned tube with pitch fin (P=1.6 mm).

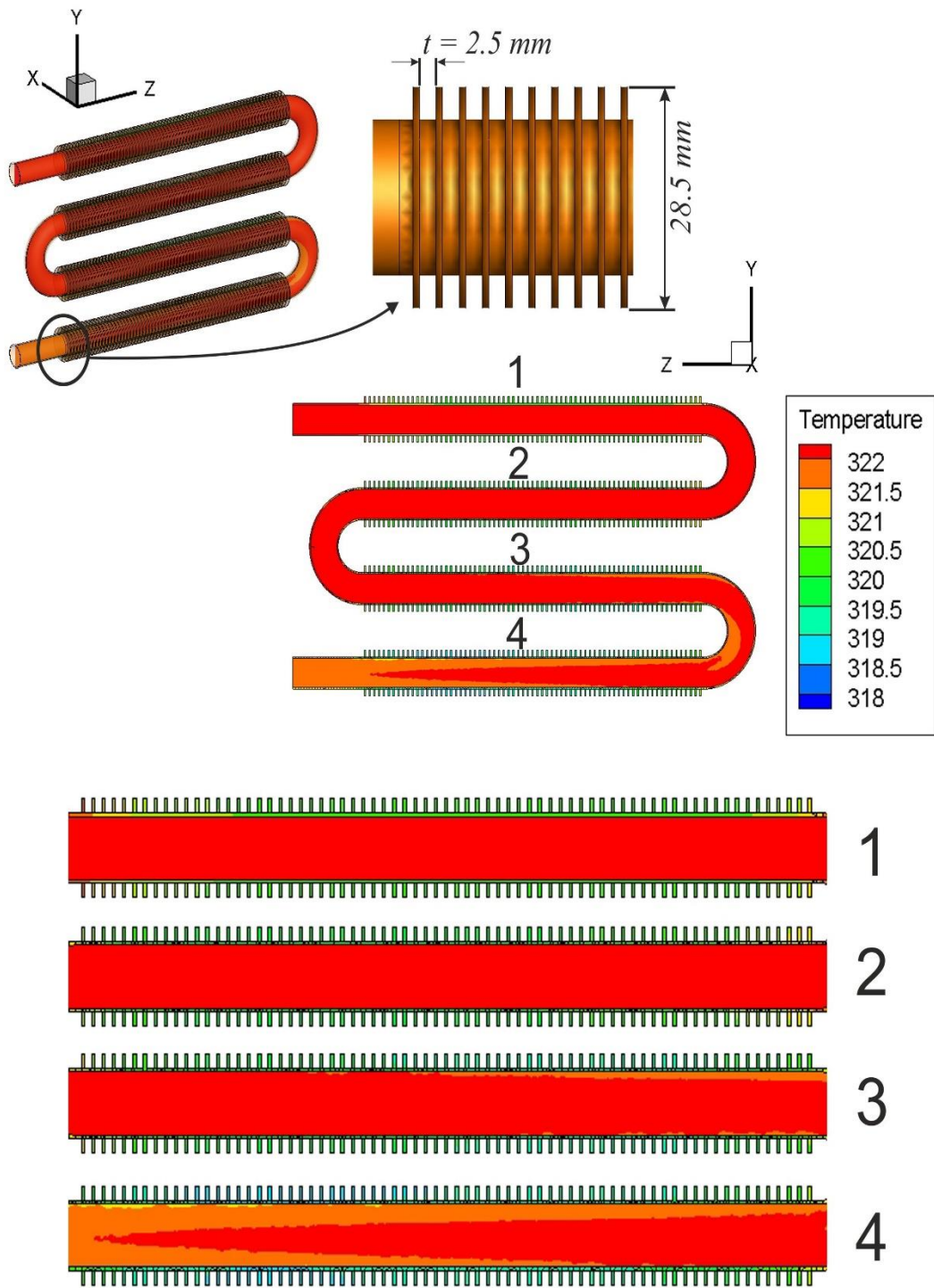


Figure 5.45. Temperature distribution of water in integral finned tube with pitch fin ($P=2.5 \text{ mm}$).

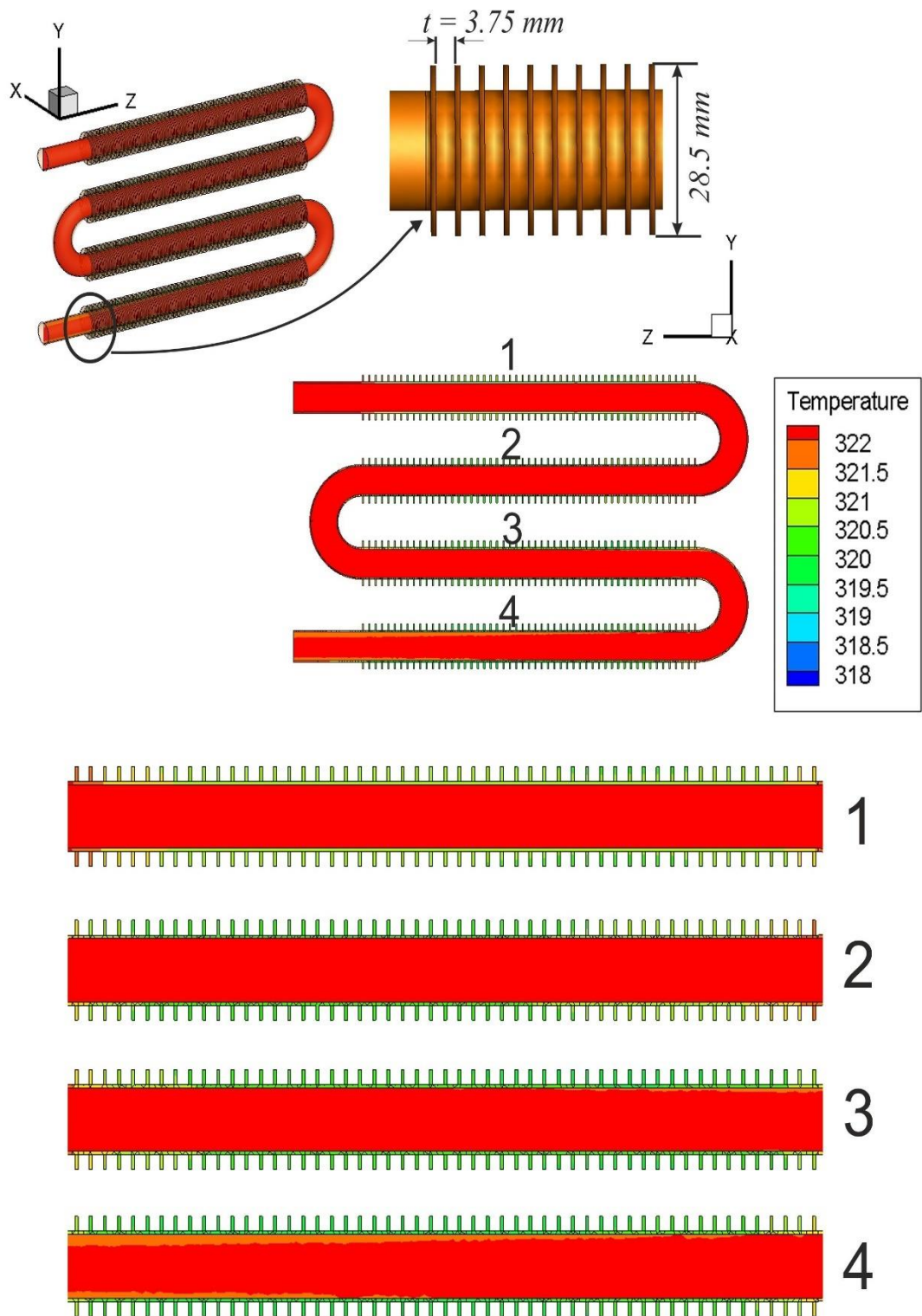


Figure 5.46. Temperature distribution of water in integral finned tube with pitch fin ($P=3.75$ mm).

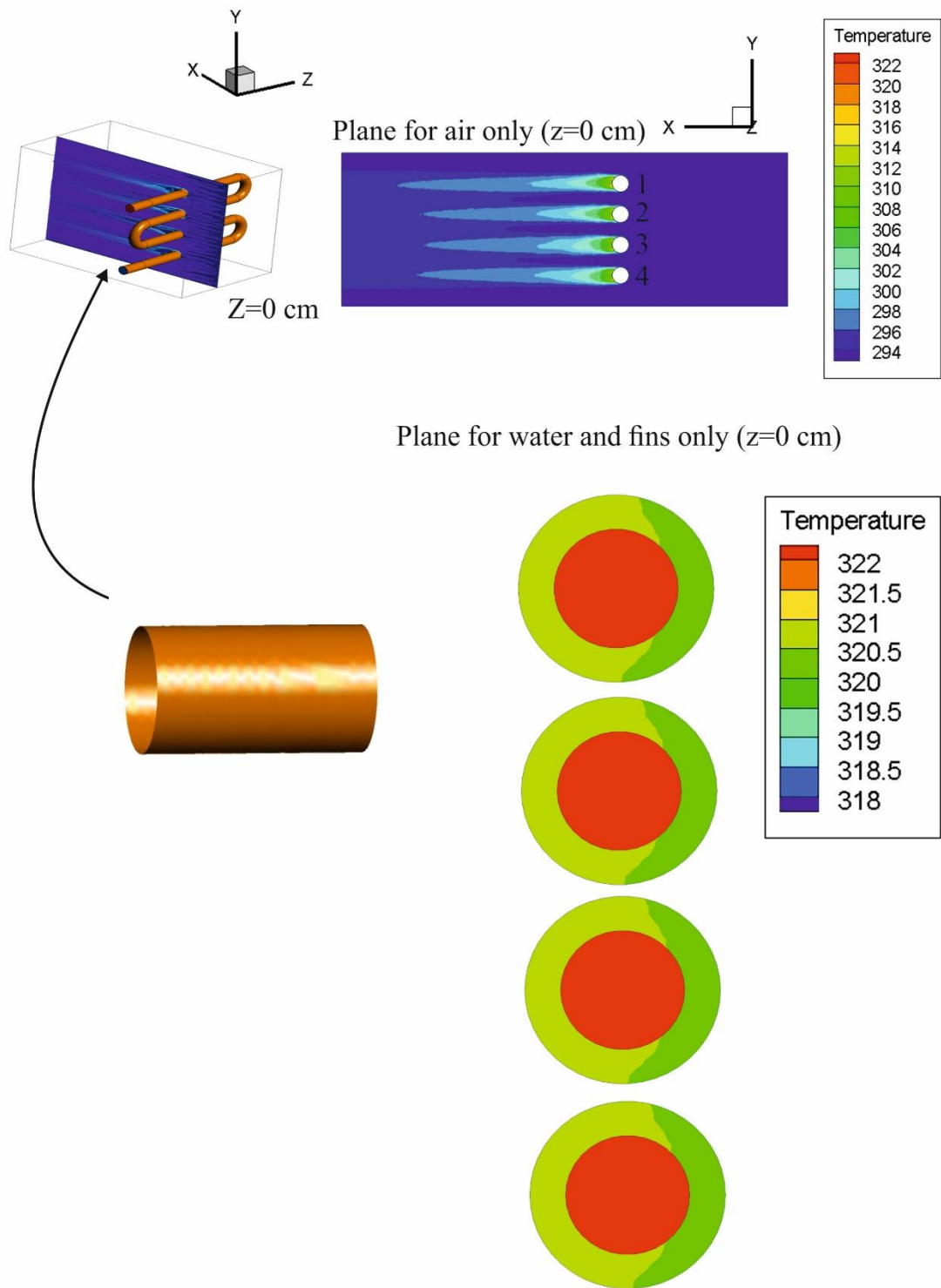


Figure 5.47. Temperature distribution of air and water for smooth tube.

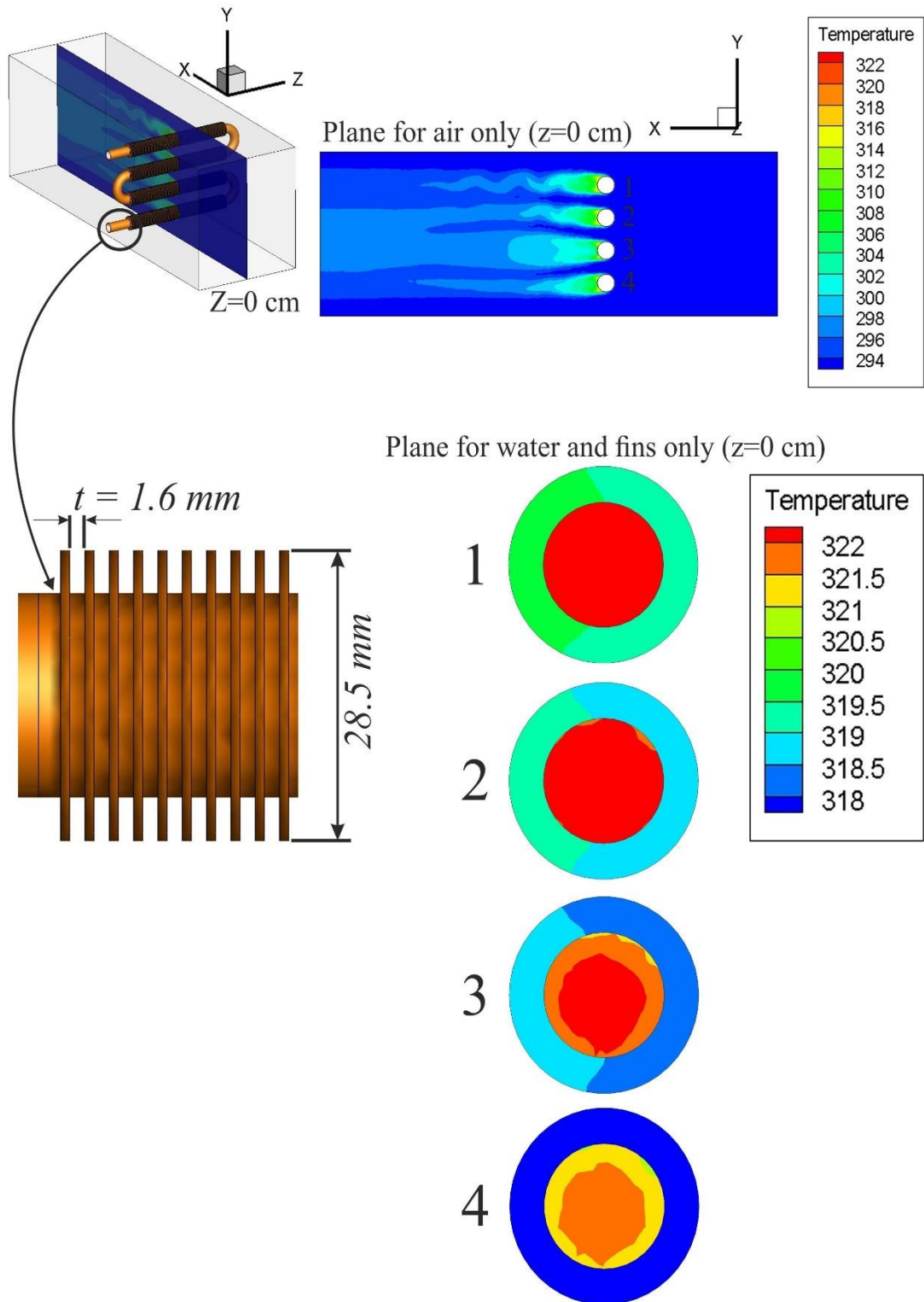


Figure 5.48. Temperature distribution of air and water for medium integral finned tube with pitch fin ($P=1.6 \text{ mm}$).

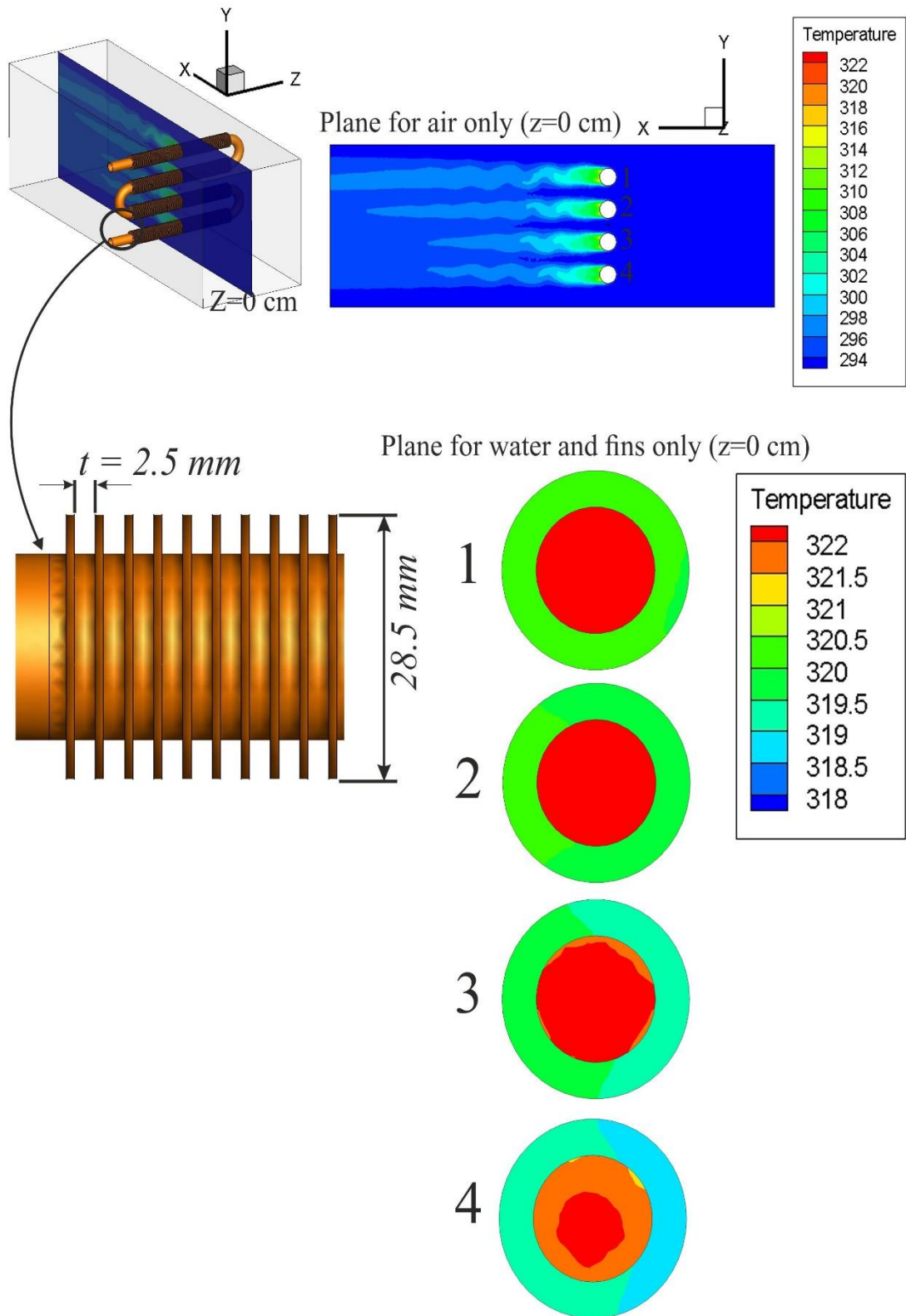


Figure 5.49. Temperature distribution of air and water for medium integral finned tube with pitch fin($P= 2.5$ mm).

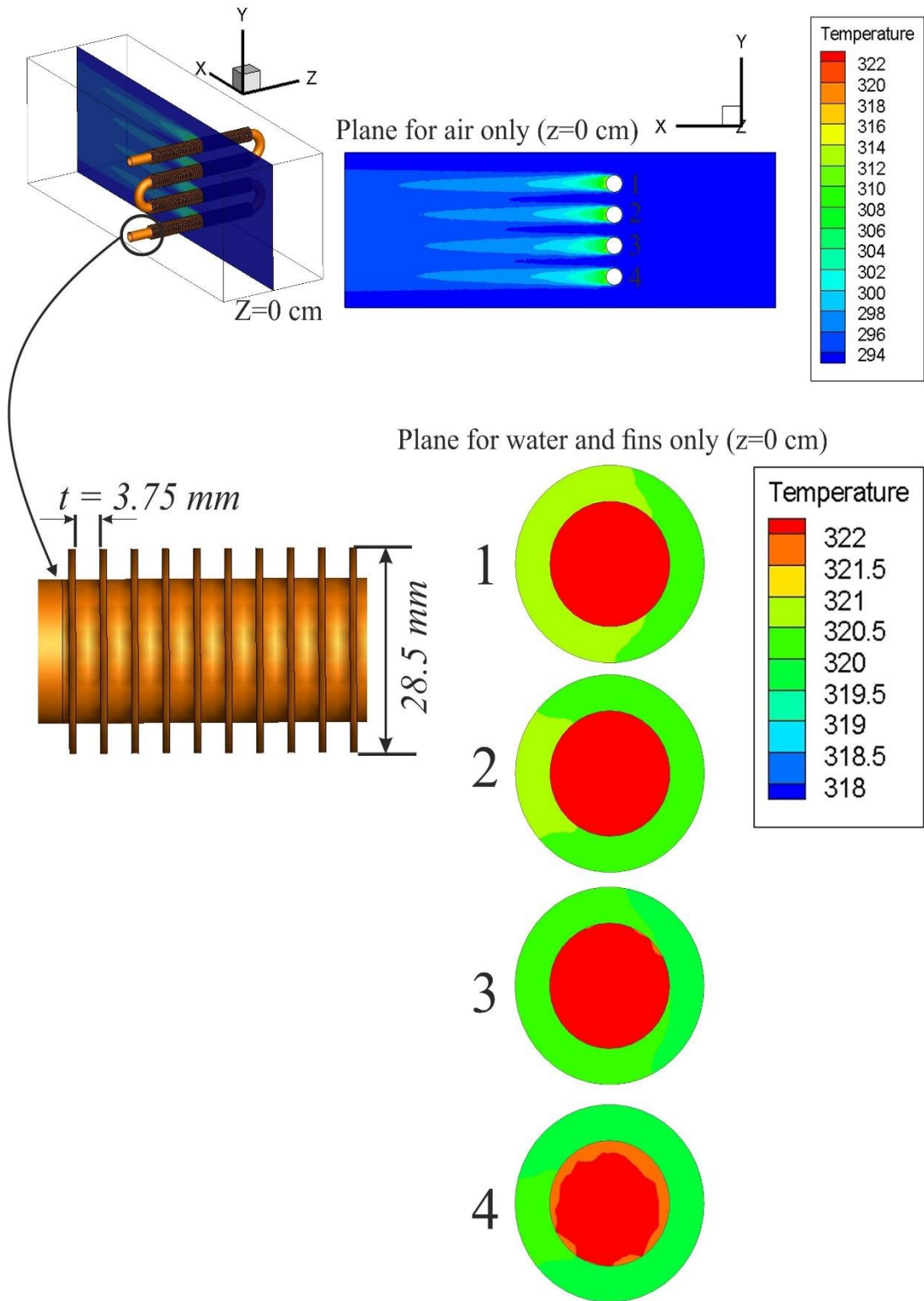


Figure 5.50. Temperature distribution of air and water for medium integral finned tube with pitch fin($P= 3.75 \text{ mm}$).

5.2.2.11. Velocity Distribution in Smooth and Finned Tubes

The figures (5.51), (5.53), (5.55) and (5.57) show the distribution of the air stream on the tubes. They show us the shape of the air passage on the test tubes and its distribution. Here we note that the air velocity will vary from the entry section beyond the test tubes, as it will narrow the air entry opening at the test tubes due to the reduction in the area of the air section which causes turbulence and eddies in the air flow after the tubes. The extension and length of this turbulence depends on the distance between the tubes, as the increase the number of fins increase the length of the turbulence also increases.

Figures (5.52), (5.54), (5.56) and (5.58) show us that the vortex in smooth tube disappears at a distance of (5 cm) after pipe, while a tube with a fin pitch of ($P=3.75$ mm) disappears at a distance of (10 cm) after pipe. A tube with a fin pitch of ($P=2.5$ mm), the vortex disappears at a distance of (20 cm), and in a tube with a fin pitch of ($P=1.6$ mm), the vortex in it disappears at a distance of (30 cm), as shown earlier.

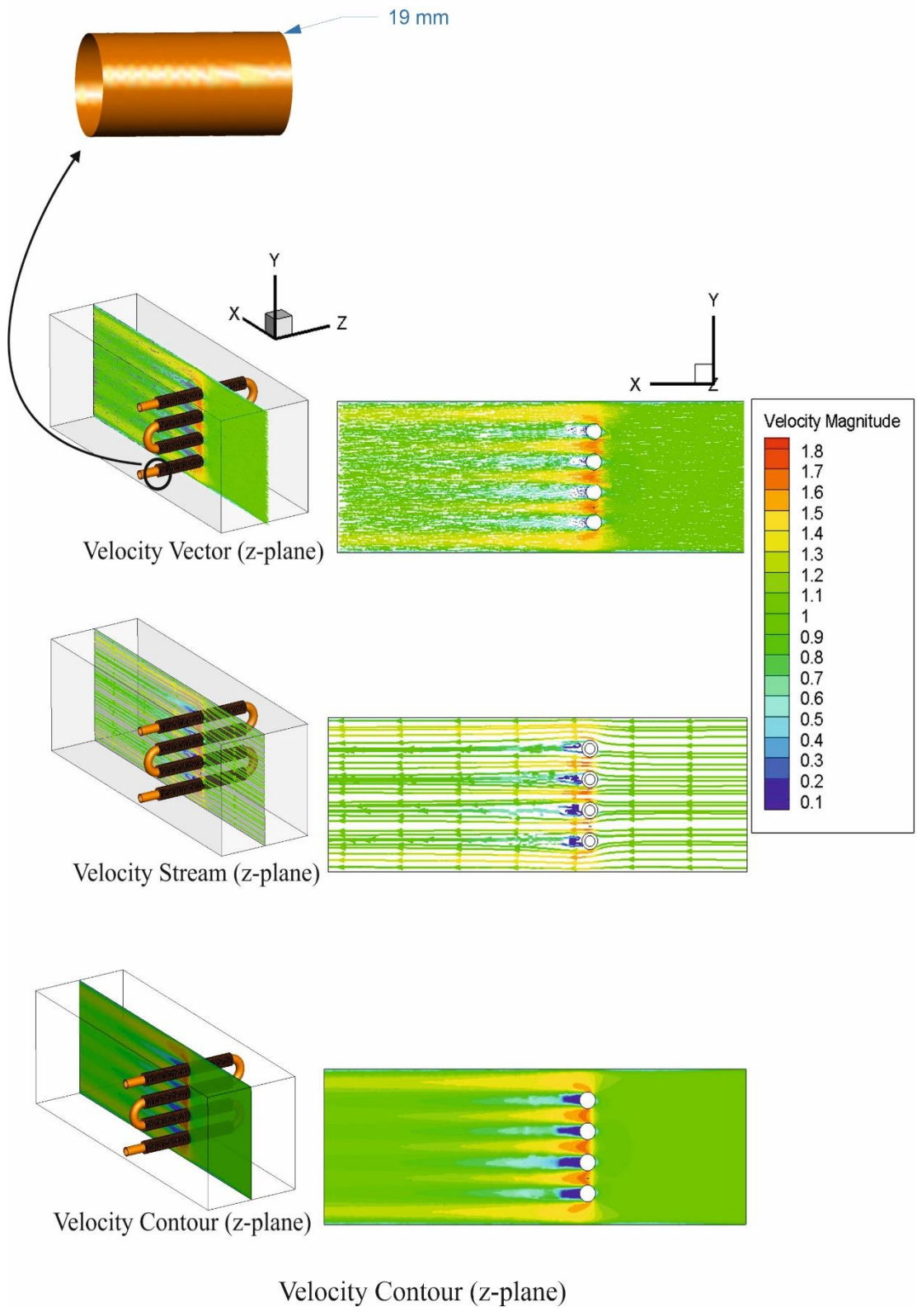


Figure 5.51. Velocity distribution of air in smooth tube.

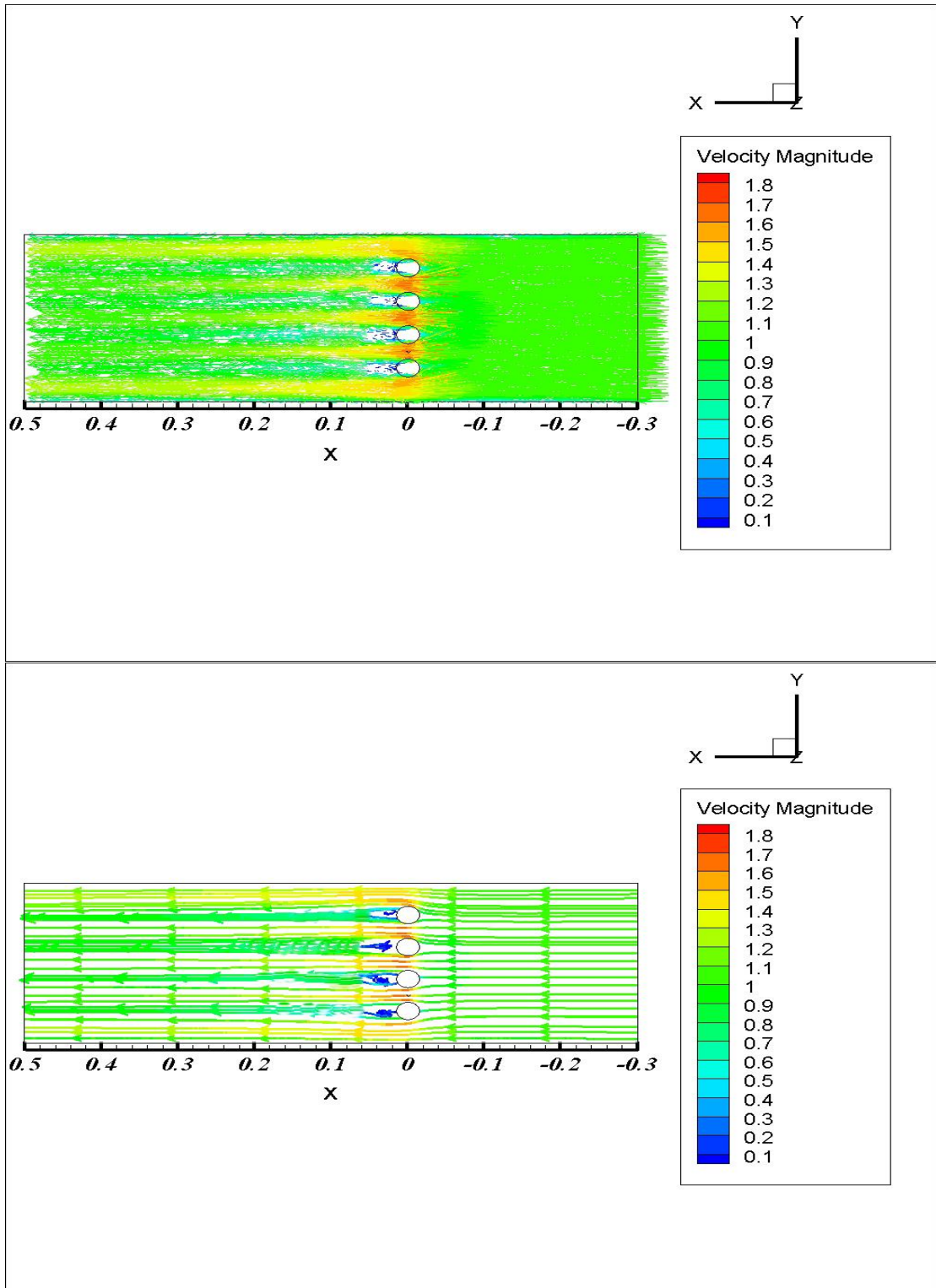


Figure 5.52. Length of the vortex after the smooth tube.

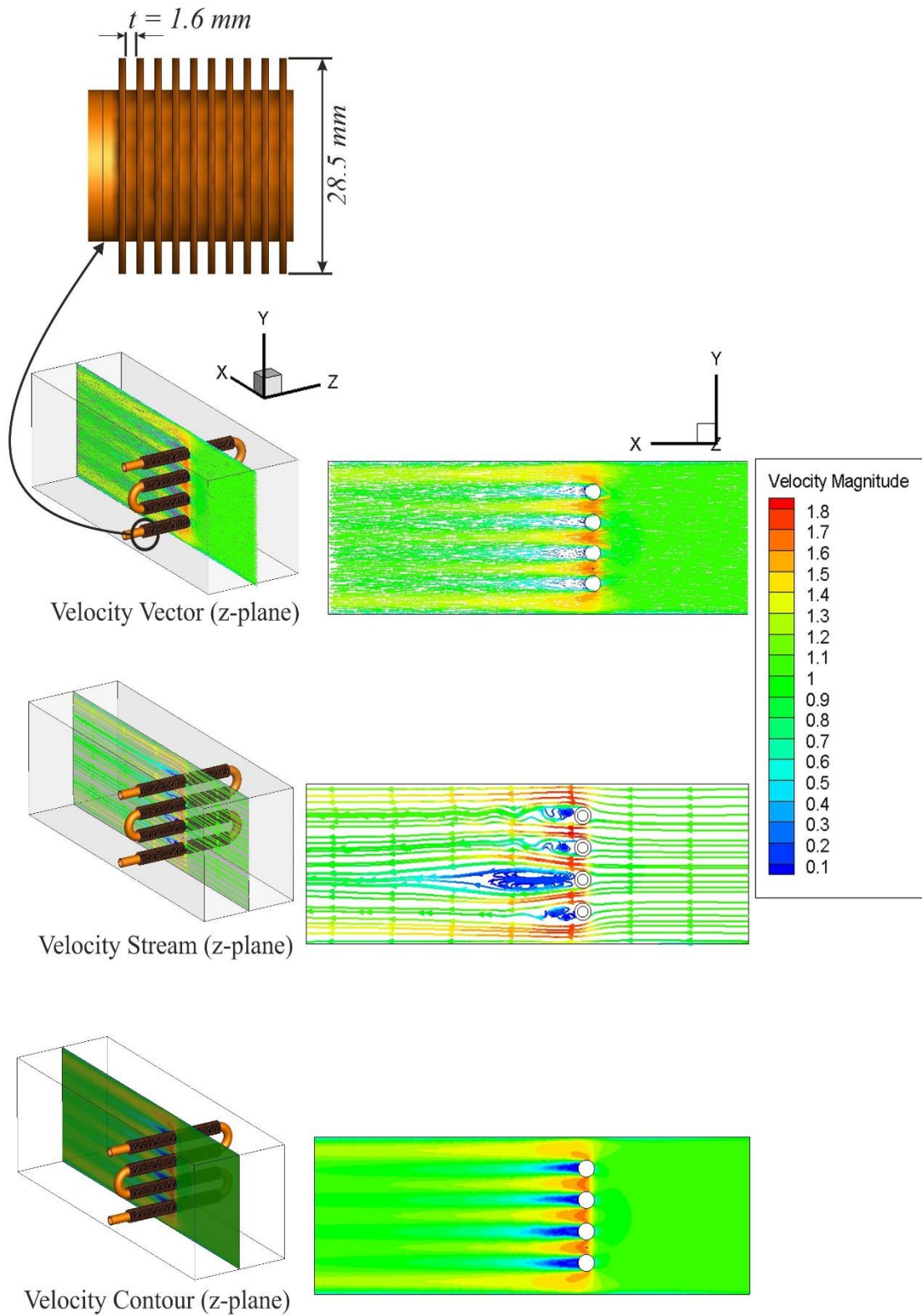


Figure 5.53. Velocity distribution of air in medium integral finned tube with pitch fins ($P=1.6$ mm).

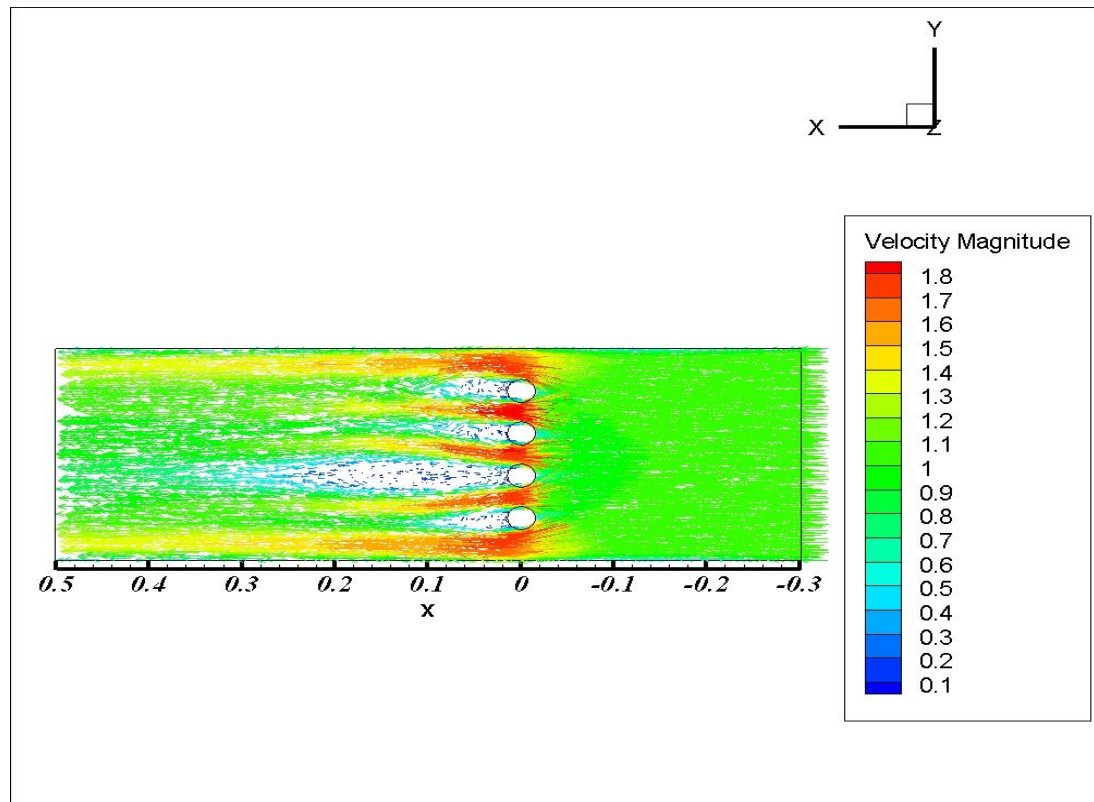
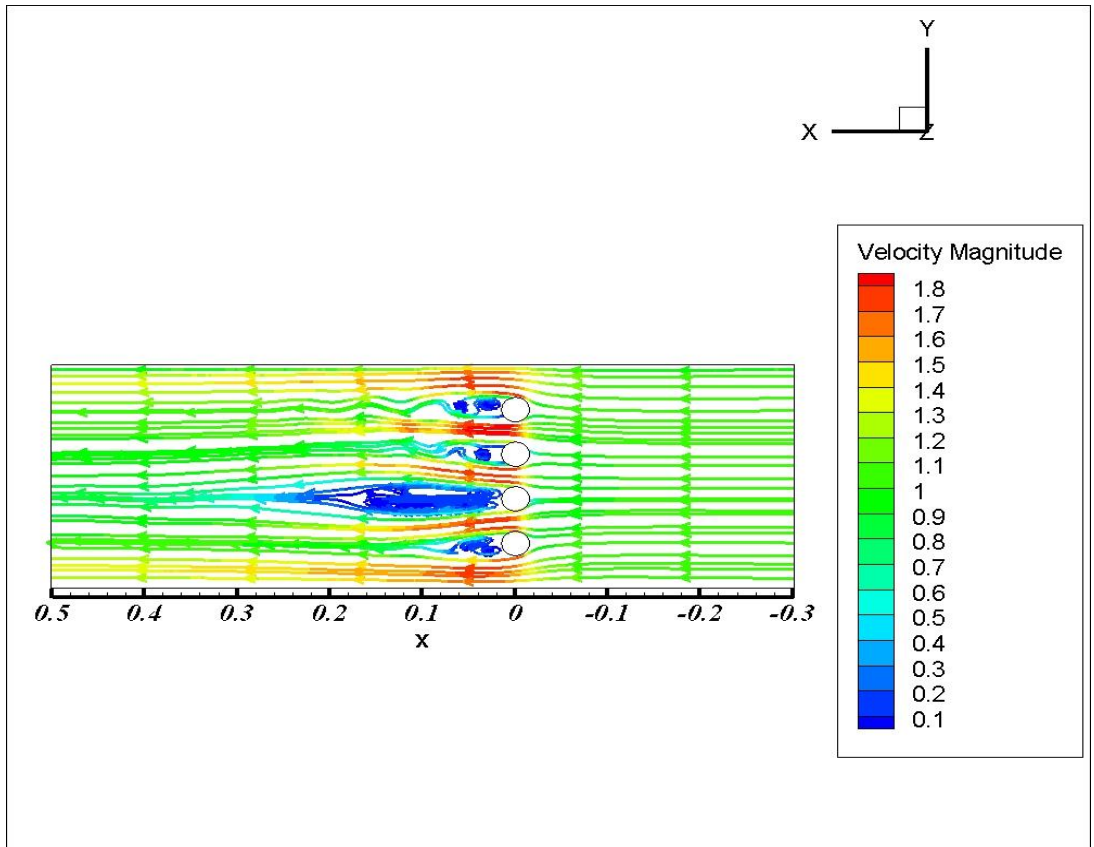


Figure 5.54. Length of the vortex after the medium integral finned tube with pitch fins ($P=1.6$ mm).

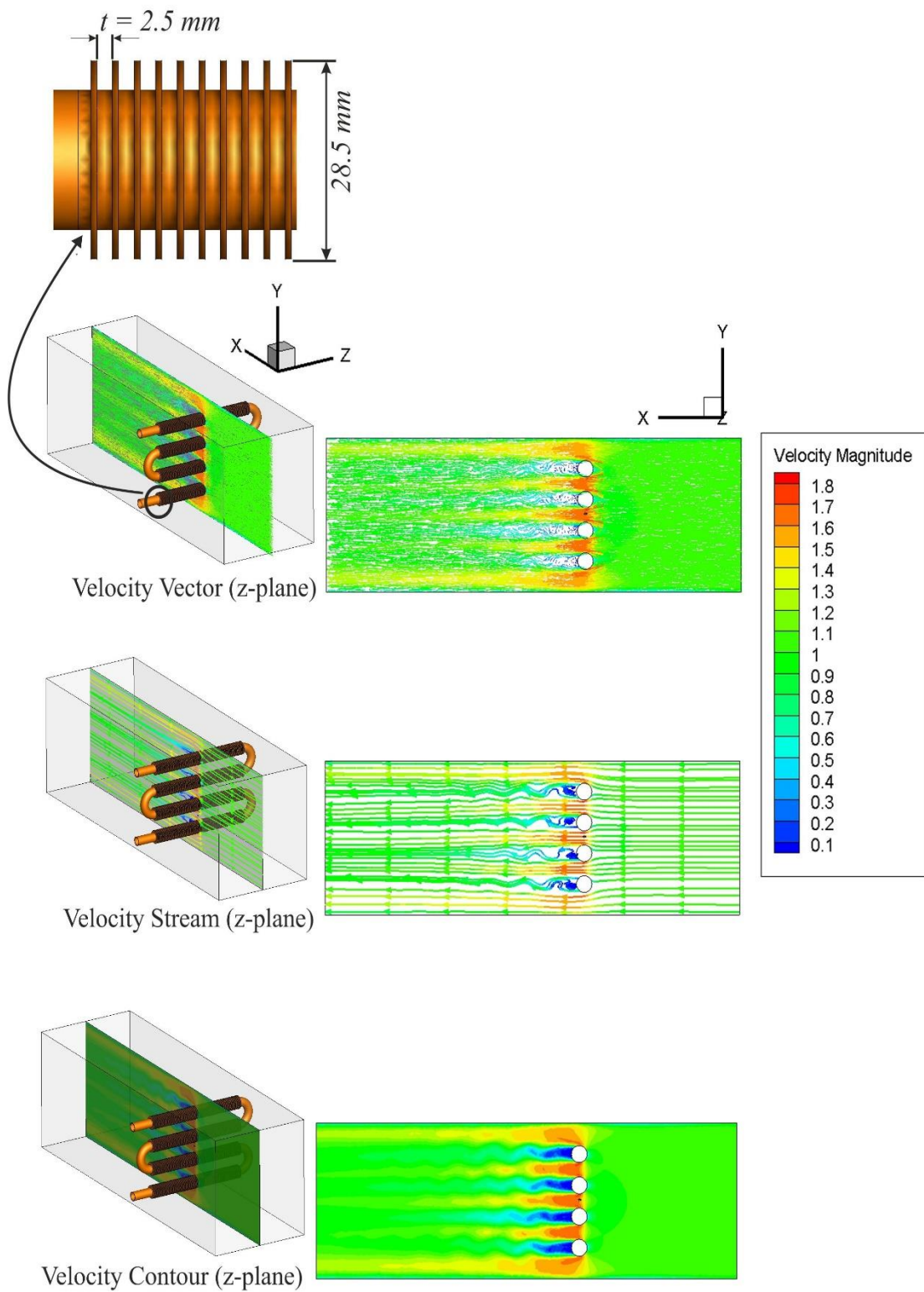


Figure 5.55. Velocity distribution of air in medium integral finned tube with pitch fins ($P=2.5$ mm).

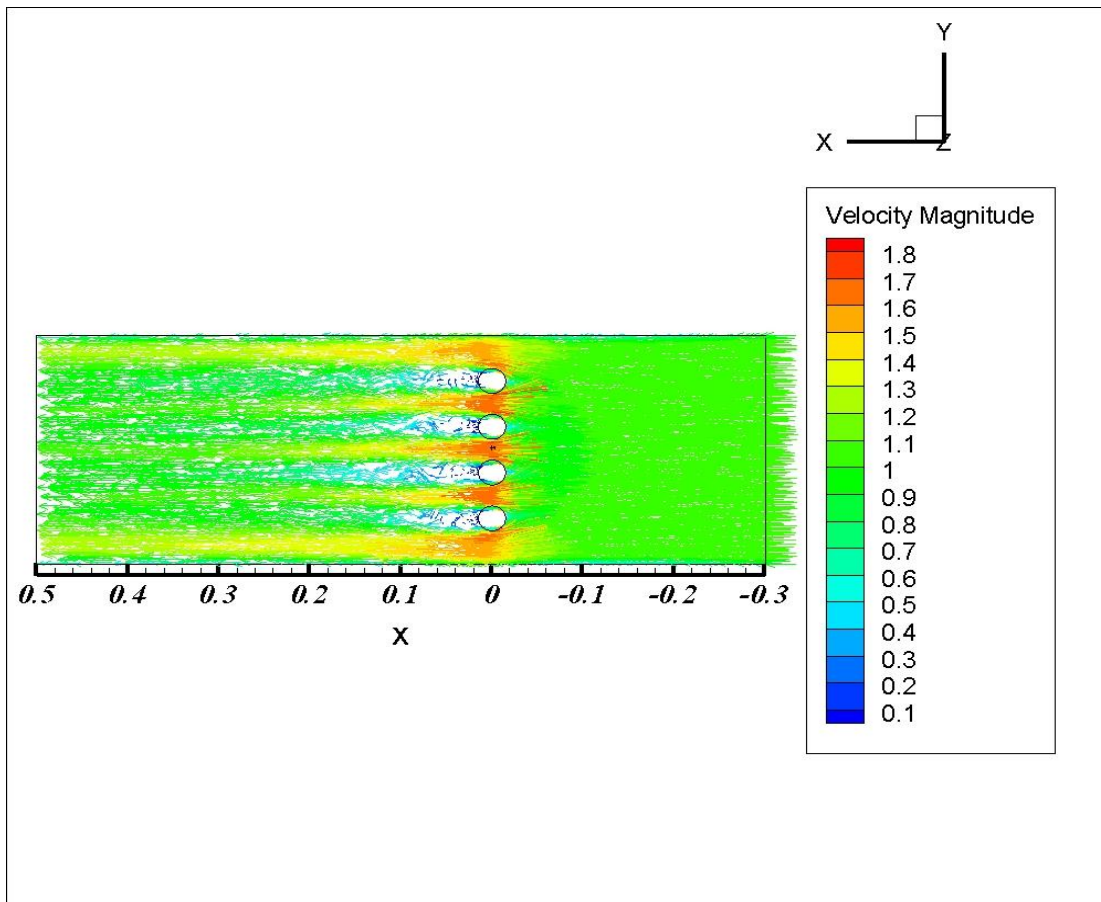
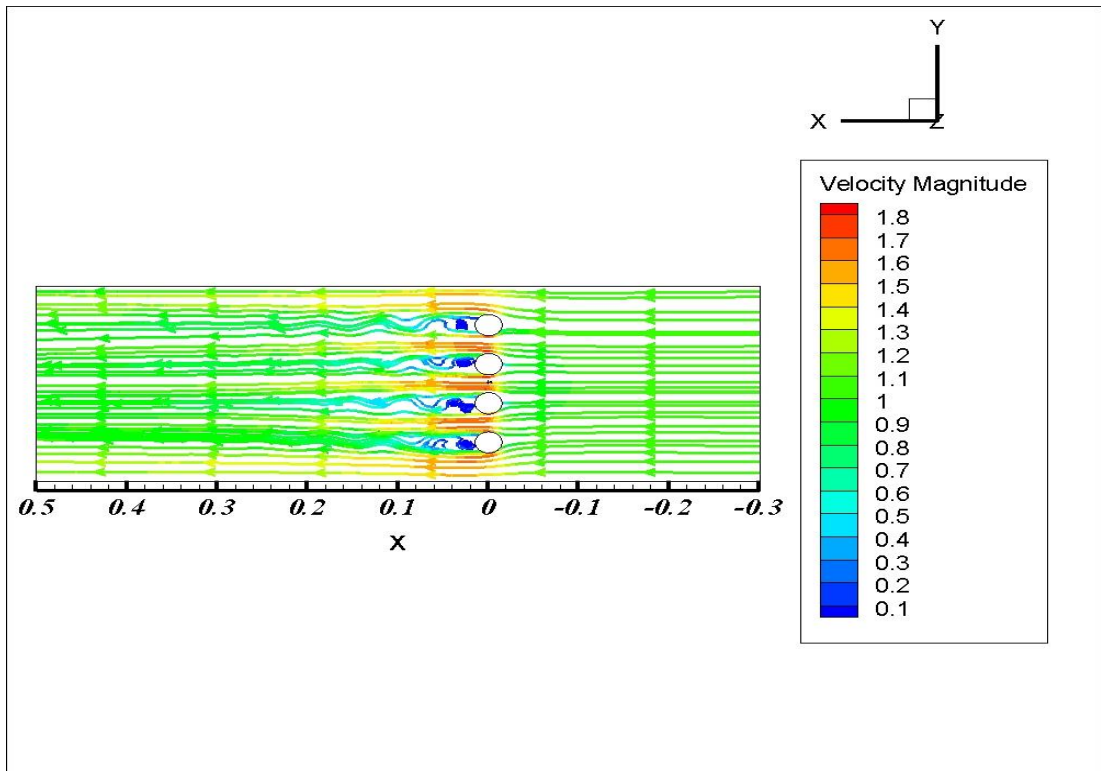


Figure 5.56. Length of the vortex after the medium integral finned tube with pitch fins ($P=2.5$ mm).

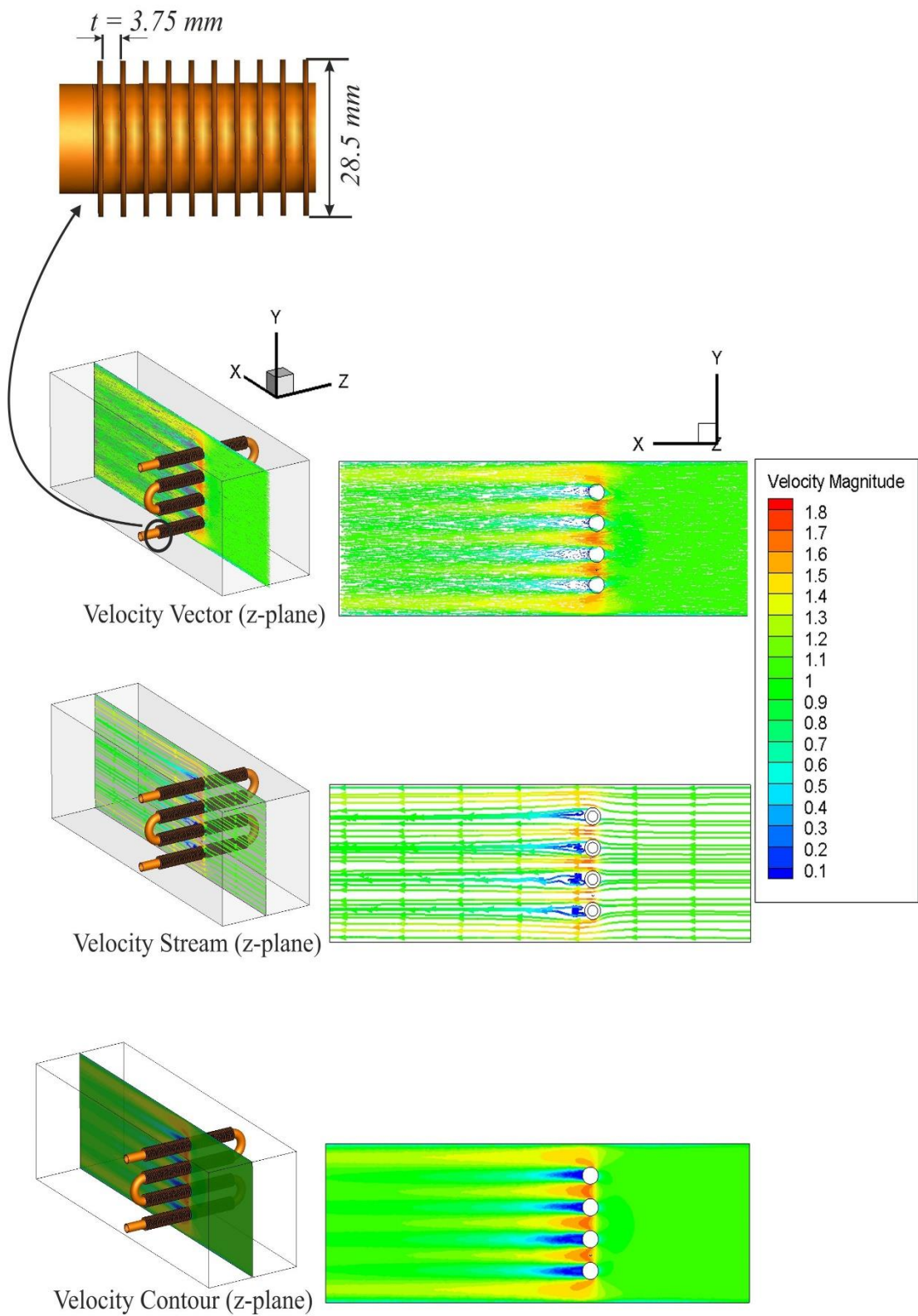


Figure 5.57. Velocity distribution of air in medium itegral finned tube with pitch fins ($P=3.75 \text{ mm}$).

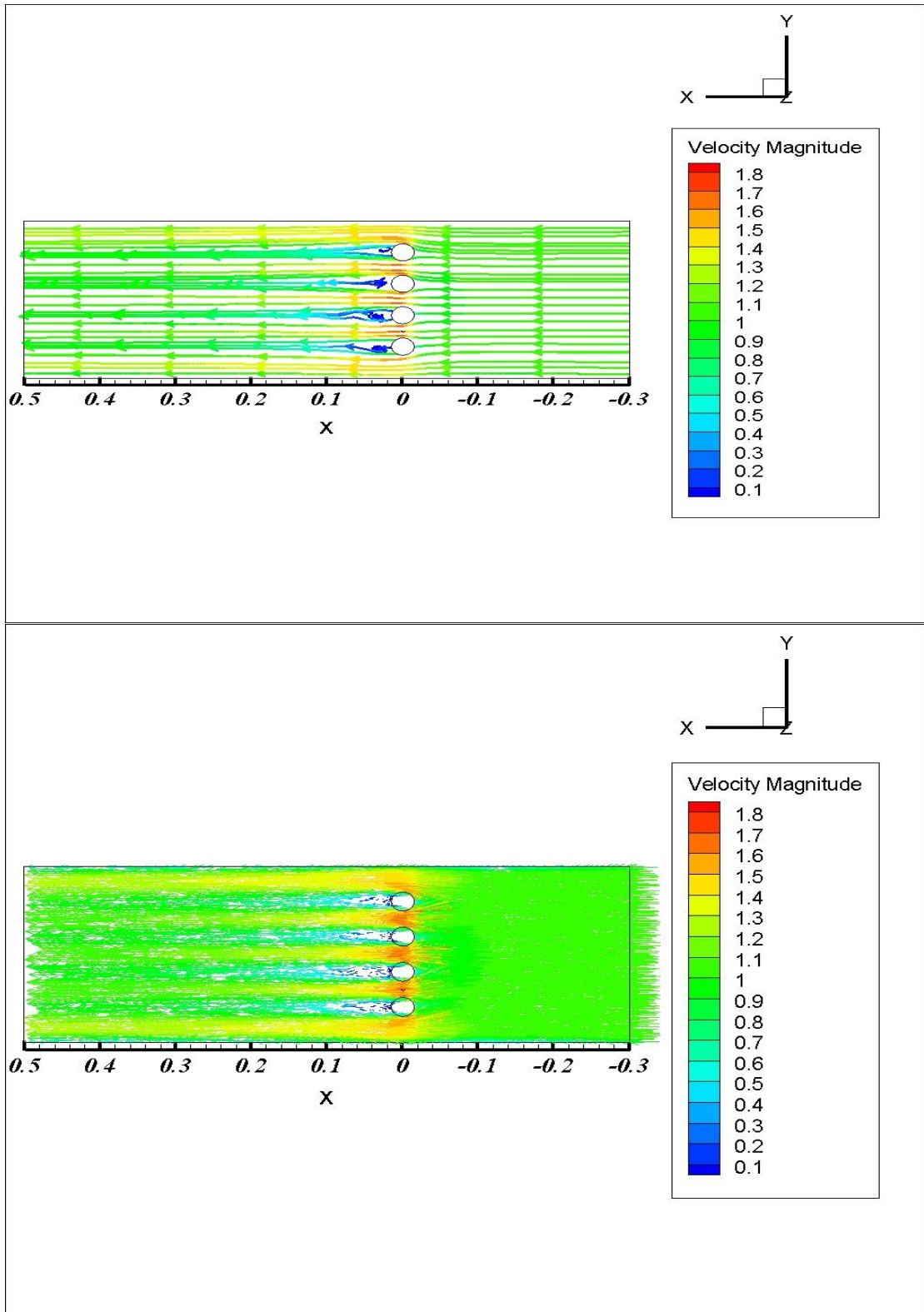


Figure 5.58. Length of the vortex after the medium integral finned tube with pitch fins ($P=3.75$ mm).

5.3. EXPERIMENTAL RESULTS

5.3.1. The Effect of Different Inlet Temperature on the Fluid Temperature Difference

The relationship between the water temperature difference and Reynolds number at air velocities (1, 2, 3, 4 m/s) for all inlet water temperatures and the flow rate of the smooth tube is shown in Figures. (5.59 to 5.66). We note from these figures that the temperature difference decreases with the increase Reynolds number in general. This behavior increases with the increase in the temperature of the inlet hot water and the air velocity. Increasing the hot water flow rates reduces the time required for heat transfer through the heat exchanger, therefore the temperature difference decreases. In addition, it becomes clear that the increase in the temperature difference in the medium finned tubes with a pitch ratio ($P= 1.6\text{mm}$) gives a higher temperature difference than the smooth tube for all flow rates and inlet temperatures. This is due to the increase in the surface area and the work of the fins as guiding passages for the flow that displace high thermal energy relative to the smooth tube.

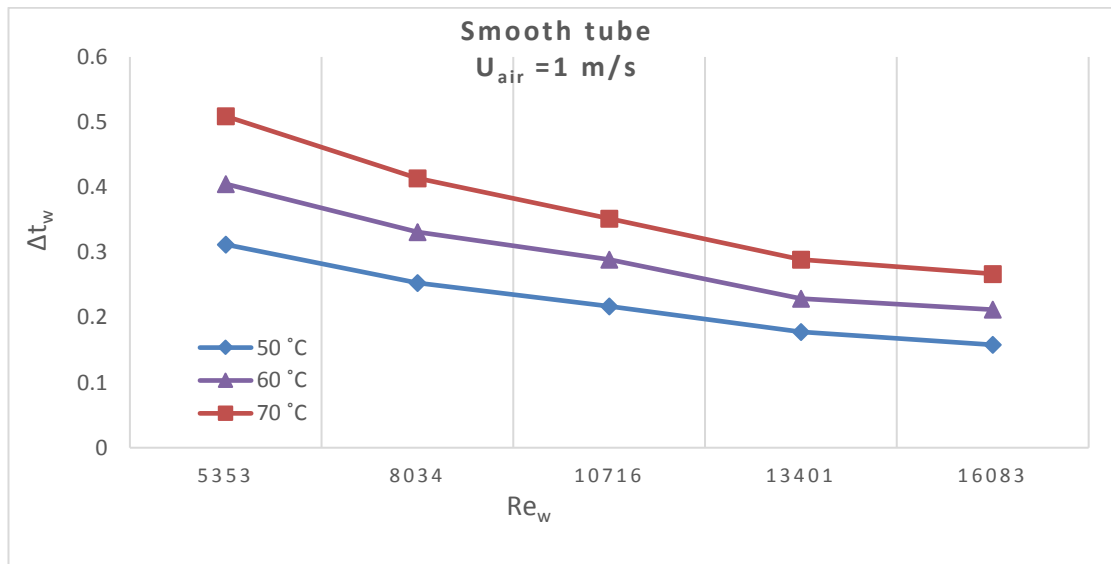


Figure 5.59. The relationship between the hot water temperature difference and the Reynolds number at air velocity (1 m/s) for all temperatures(50, 60, and 70oC) for smooth tube.

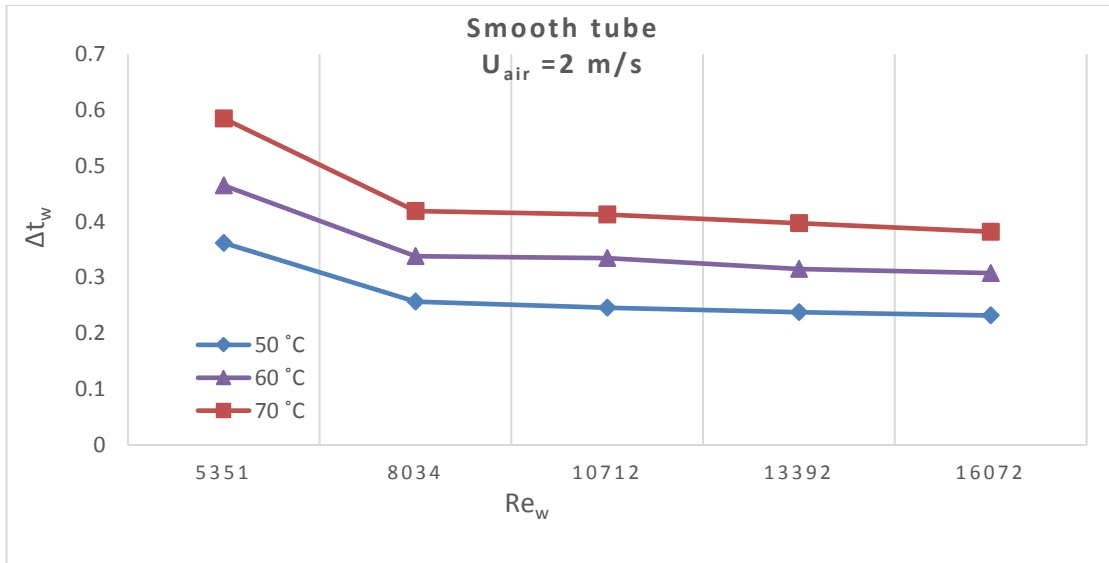


Figure 5.60. The relationship between the hot water temperature difference and the Reynolds number at air velocity (2m/s) for all temperatures(50, 60, and 70oC) for smooth tube.

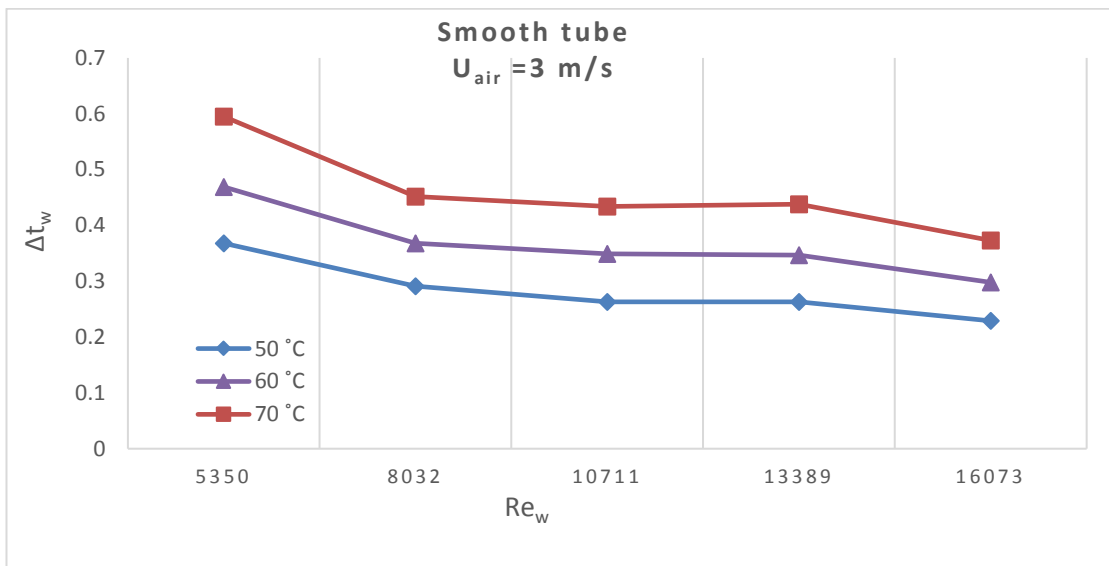


Figure 5.61. The relationship between the hot water temperature difference and the Reynolds number at air velocity (3 m/s) for all temperatures(50, 60, and 70oC) for smooth tube.

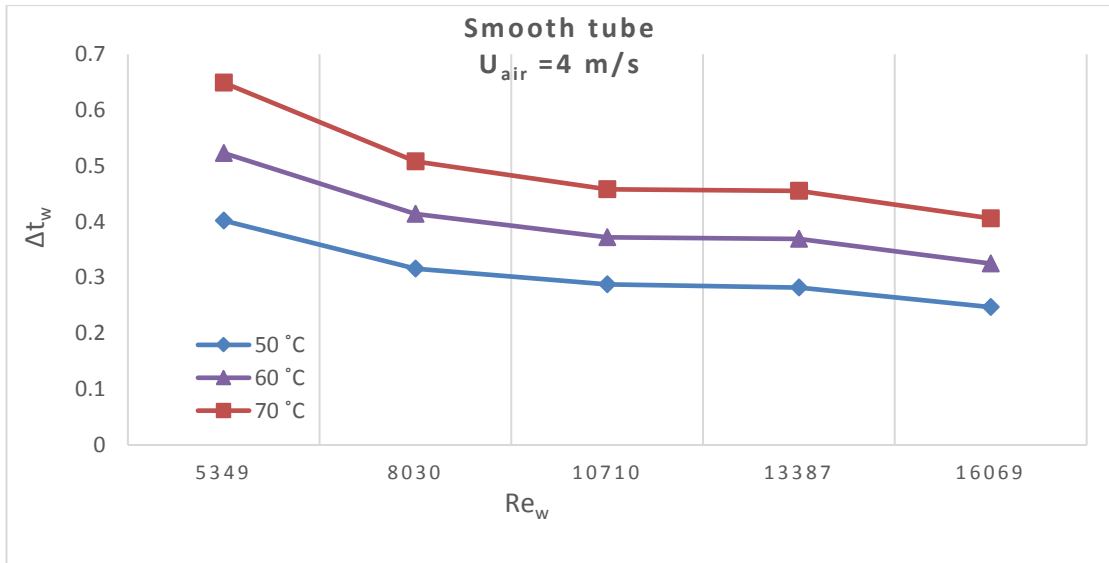


Figure 5.62. The relationship between the hot water temperature difference and the Reynolds number at air velocity (4 m/s) for all temperatures (50, 60, and 70°C) for smooth tube.

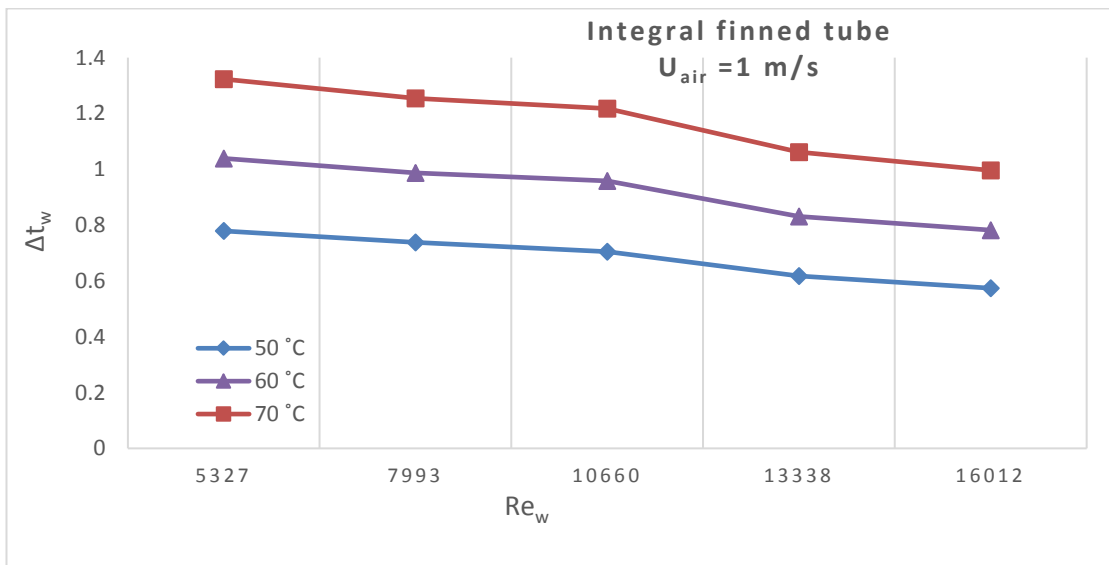


Figure 5.63. The relationship between the hot water temperature difference and the Reynolds number at air velocity (1 m/s) for all temperatures (50, 60, and 70°C) medium integral finned tube with pitch ($P = 1.6 \text{ mm}$).

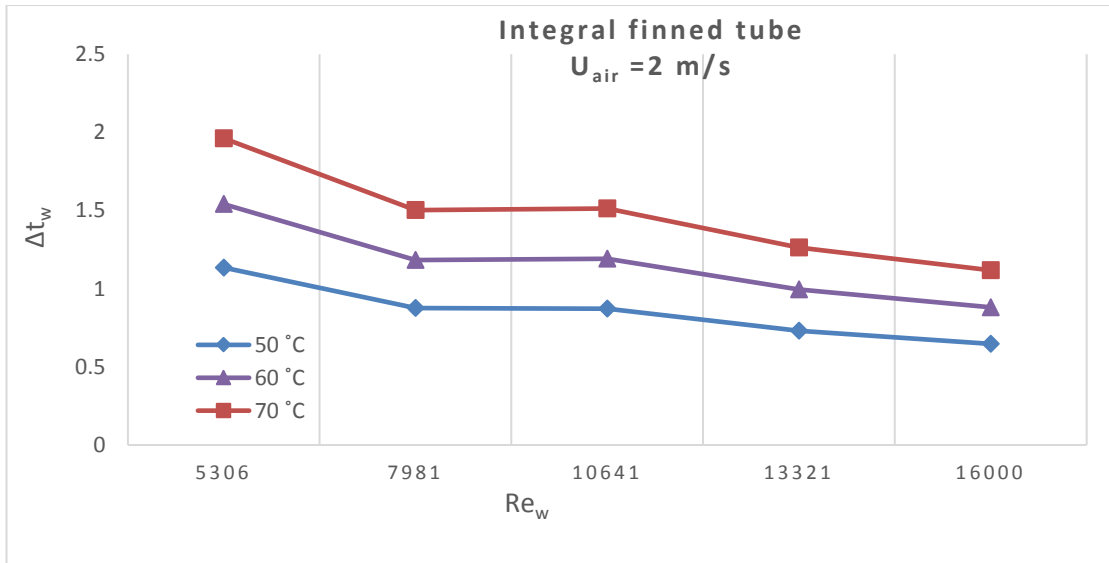


Figure 5.64. The relationship between the hot water temperature difference and the Reynolds number at air velocity (2m/s) for all temperatures (50, 60, and 70oC) medium integral finned tube with pitch(P= 1.6 mm).

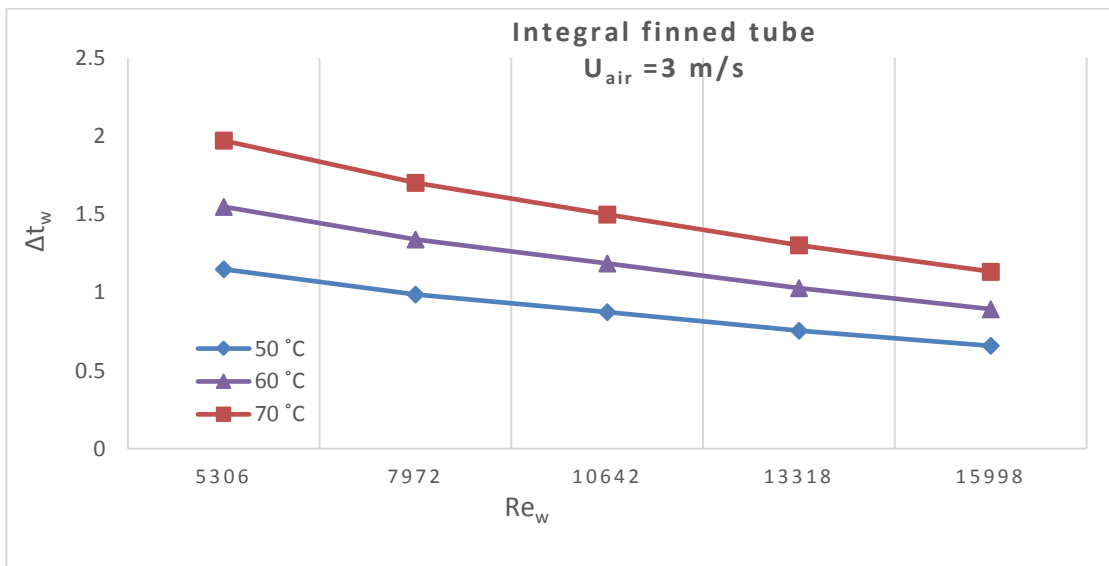


Figure 5.65. The relationship between the hot water temperature difference and the Reynolds number at air velocity (3 m/s) for all temperatures (50, 60, and 70oC) medium integral finned tube with pitch(P= 1.6 mm).

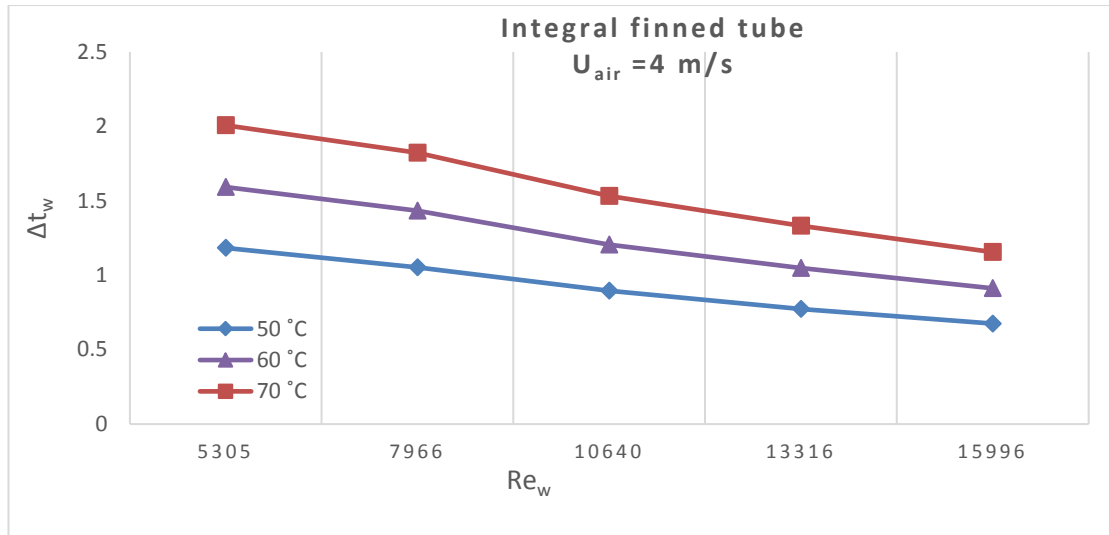


Figure 5.66. The relationship between the hot water temperature difference and the Reynolds number at air velocity (4m/s) for all temperatures (50, 60, and 70oC) medium integral finned tube with pitch(P= 1.6 mm).

5.3.2. The Effect of the Reynolds Number on the Overall Heat Transfer Coefficient

The relationship between the overall heat transfer coefficient and Reynolds number at air velocity (1, 2, 3, and 4 m/s) for all inlet hot water temperature (50, 60, 70°C) and at different water flow rates (2, 3, 4, 5, and 6L/min), for smooth and medium integral finned tube shown in figures (5.67 to 5.74).

It is clear from this figures that the total heat transfer coefficient increases with the increase of the Reynolds number in general. This effect increases with the increase in the inlet hot water temperature, and air velocities. The increase in the total heat transfer coefficient for the integral finned tube for all operating conditions is higher than for the smooth tube, this attributed to the fact that the heat transfer rate is higher in the finned tube due to increase in the surface area.

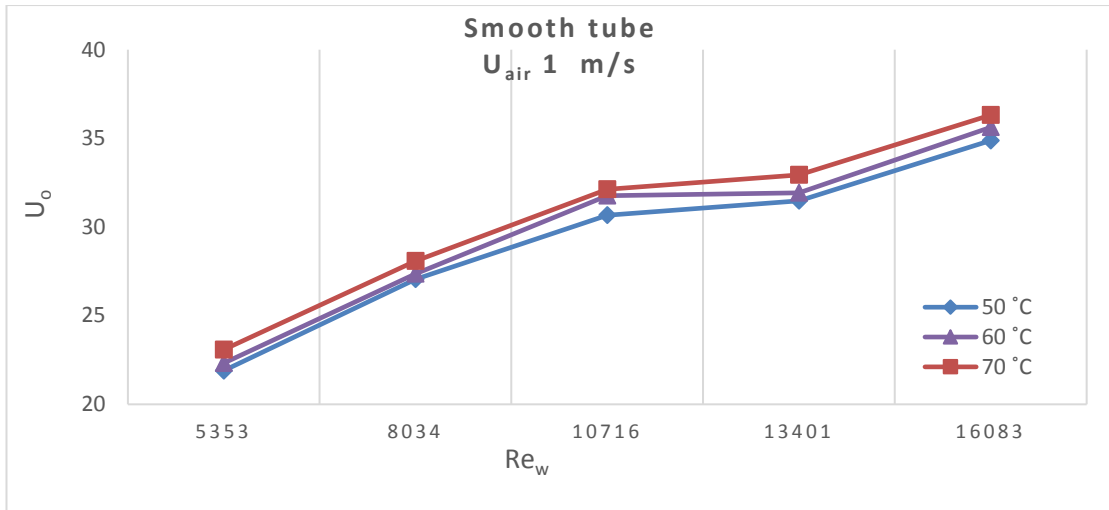


Figure 5.67. The relationship between the overall heat transfer coefficient and Reynolds number at air velocity (1 m/s) for all inlet hot water temperatures for smooth tube.

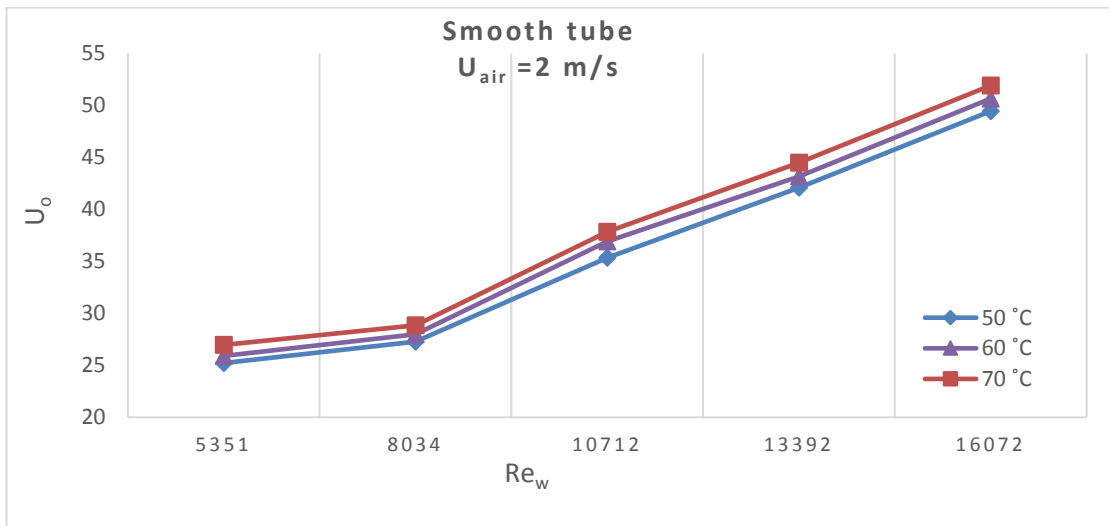


Figure 5.68. The relationship between the overall heat transfer coefficient and Reynolds number at air velocity (2 m/s) for all inlet hot water temperatures for smooth tube.

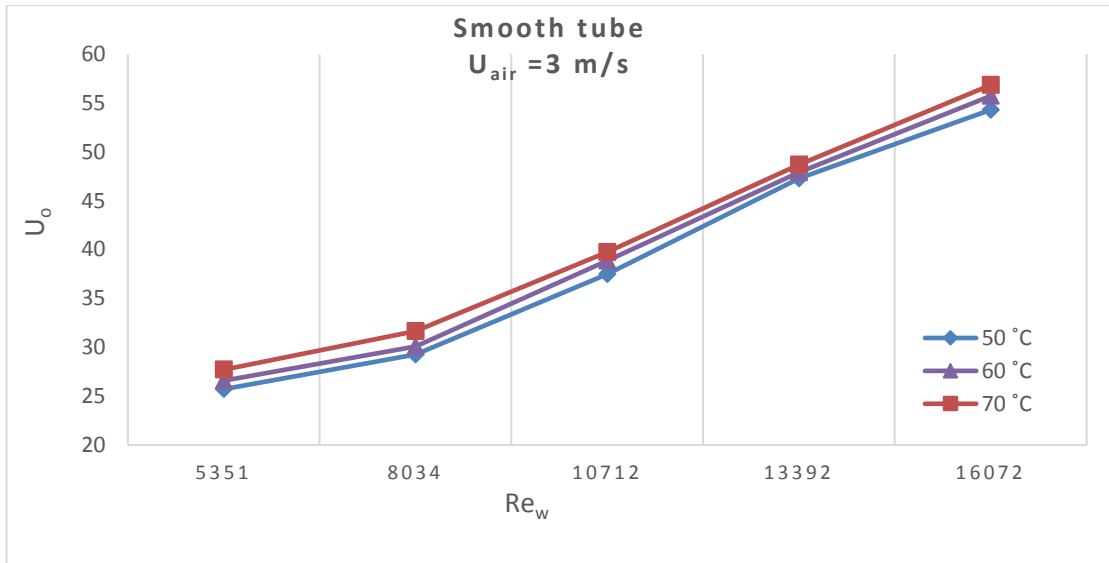


Figure 5.69. The relationship between the overall heat transfer coefficient and Reynolds number at air velocity (3 m/s) for all inlet hot water temperatures for smooth tube.

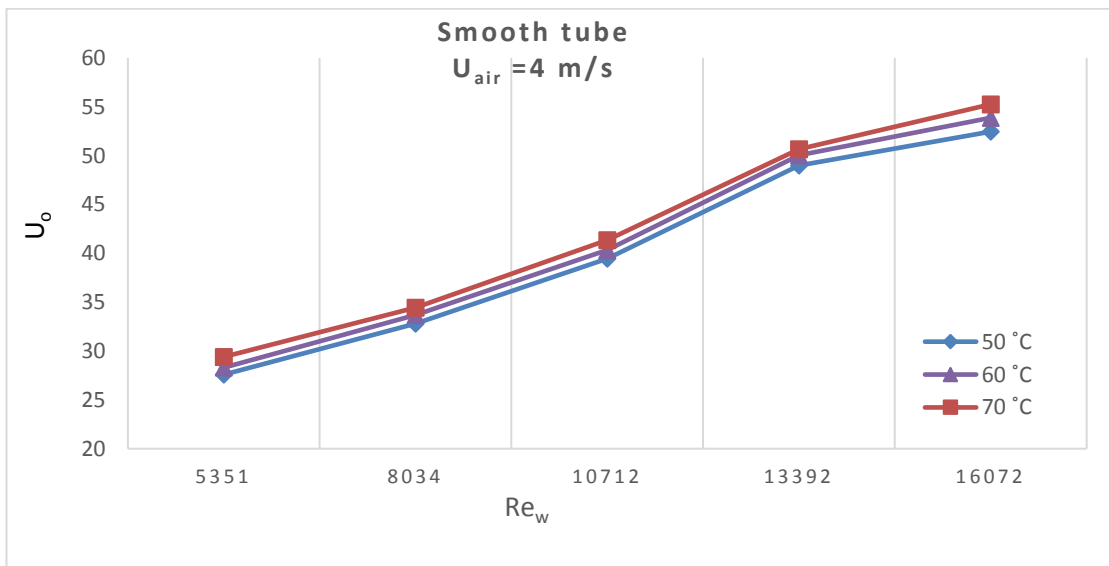


Figure 5.70. The relationship between the overall heat transfer coefficient and Reynolds number at air velocity (4 m/s) for all inlet hot water temperatures for smooth tube.

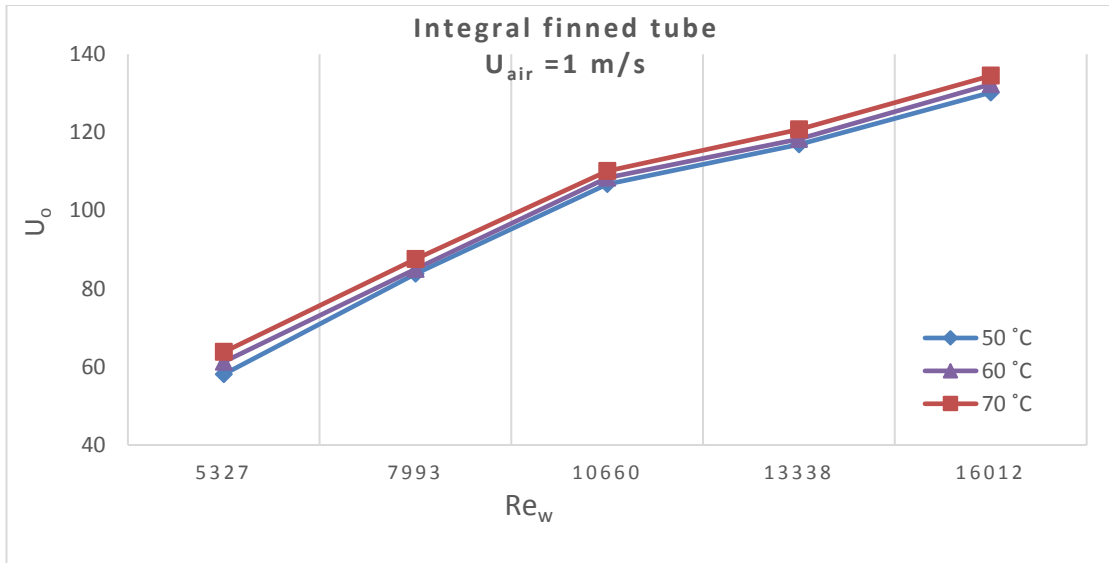


Figure 5.71. The relationship between the overall heat transfer coefficient and Reynolds number at air velocity (1 m/s) for all inlet hot water temperatures for integral finned tube with (P=1.6).

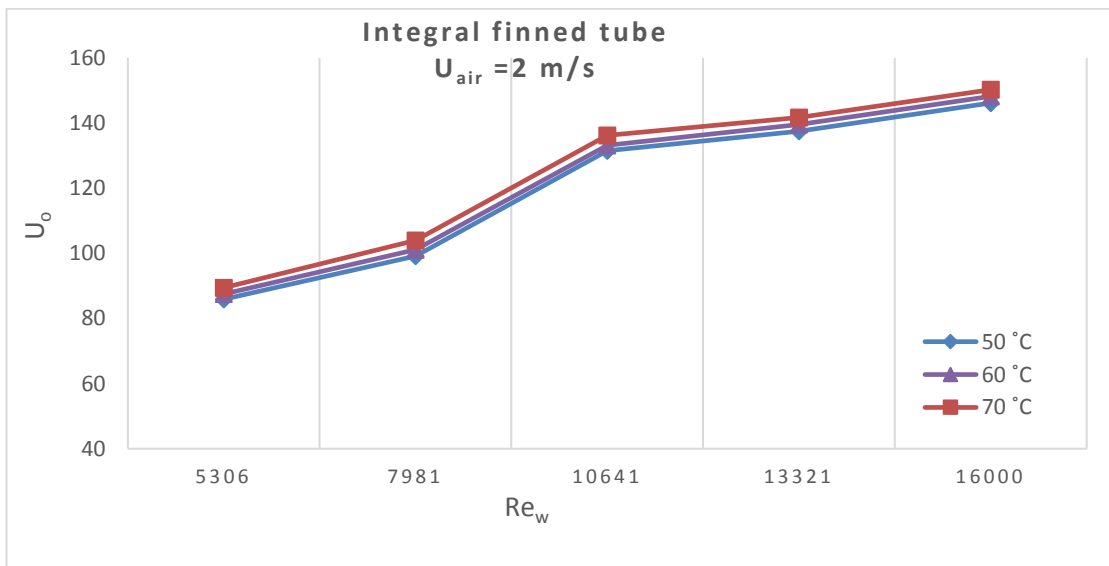


Figure 5.72. The relationship between the overall heat transfer coefficient and Reynolds number at air velocity (2 m/s) for all inlet hot water temperatures for integral finned tube with (P=1.6).

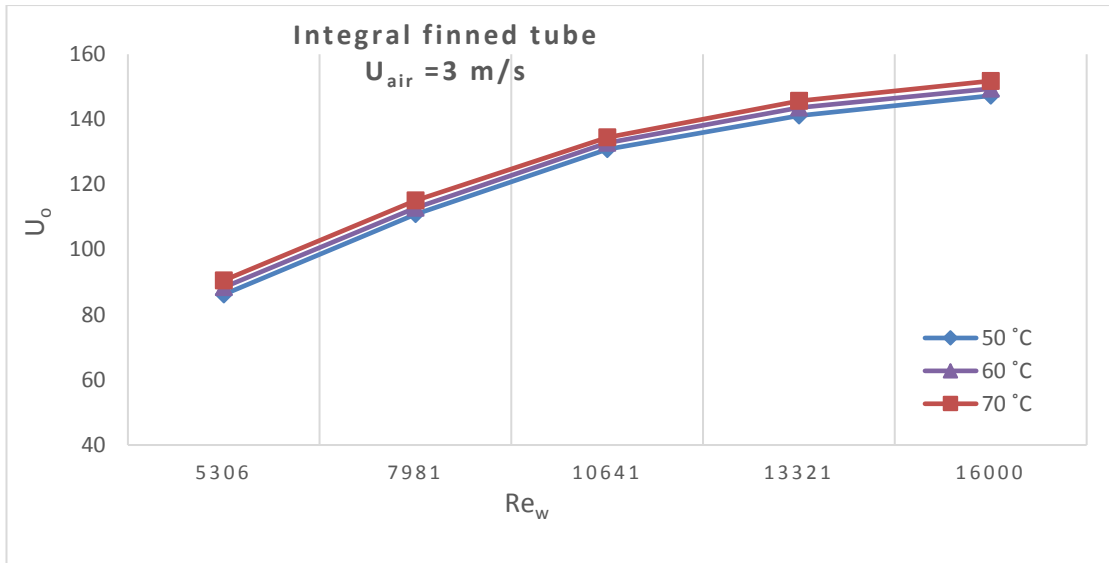


Figure 5.73. The relationship between the overall heat transfer coefficient and Reynolds number at air velocity (3 m/s) for all inlet hot water temperatures for integral finned tube with (P=1.6).

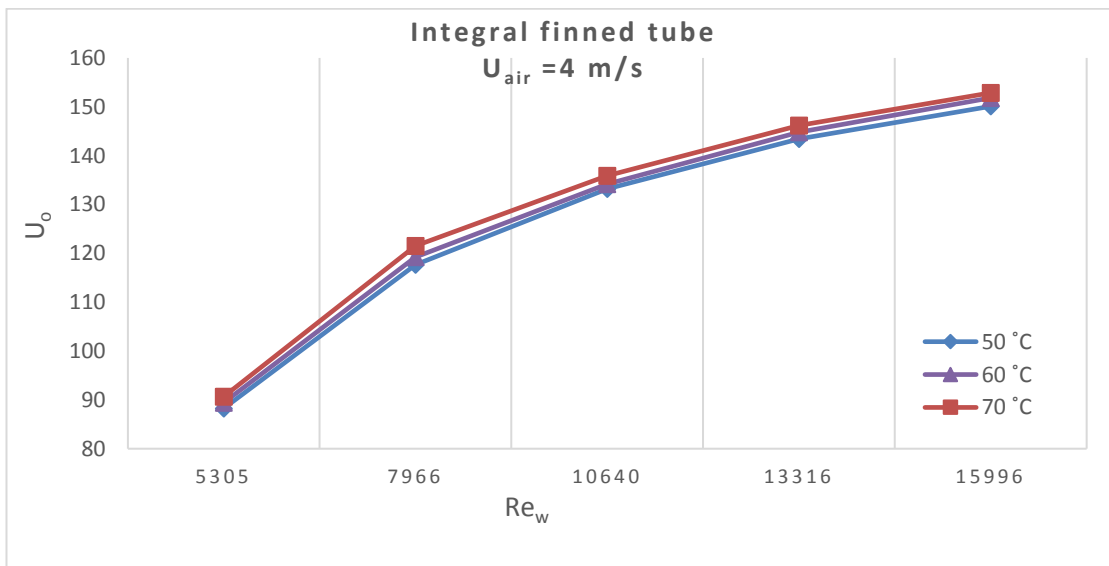


Figure 5.74. The relationship between the overall heat transfer coefficient and Reynolds number at air velocity (4 m/s) for all inlet hot water temperatures for integral finned tube with (P=1.6).

5.3.3. The Effect of Inlet Temperature on the Effectiveness and the Number of Transfer Units

Figures (5.75 to 5.82) demonstrate the relationship between the number of heat transfer units (NTU) and the effectiveness of the heat exchanger for each of the smooth and finned tubes with a pitch ratio ($P= 1.6$ mm), for inlet hot water temperatures (50, 60,70 °C), and air velocity (1, 2, 3, 4 m/s). The increase in the number of transfer units leads to an increase in effectiveness due to the increase in (U_o). The effectiveness of the finned tube great than of the smooth tube with the percentage (66.2%, 69.4%, 72.2%, and 73.6%) respectively.

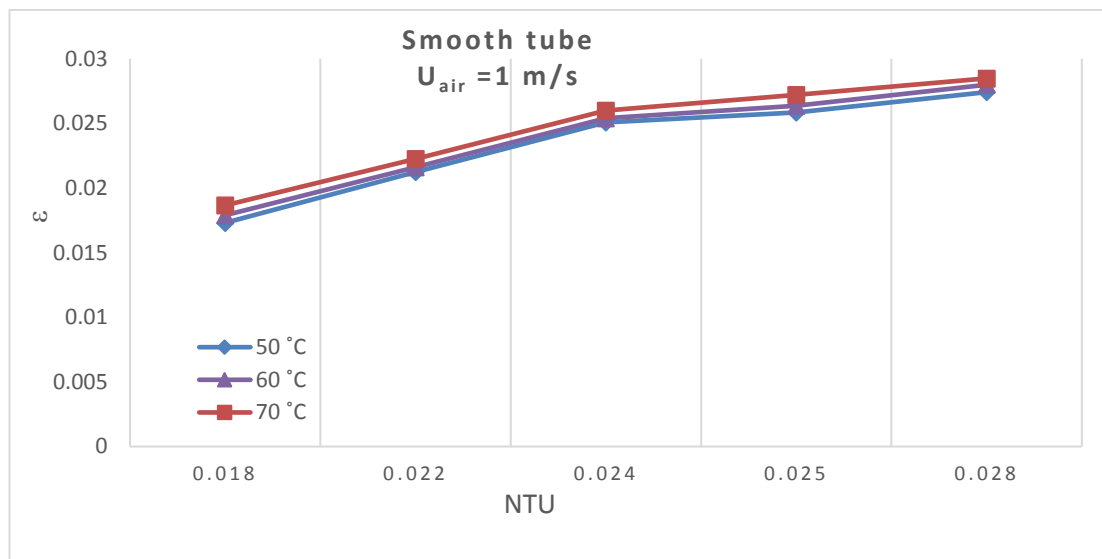


Figure 5.75. The effectiveness and NTU at air velocity (1 m/s) for all inlet hot water temperatures for smooth tube.

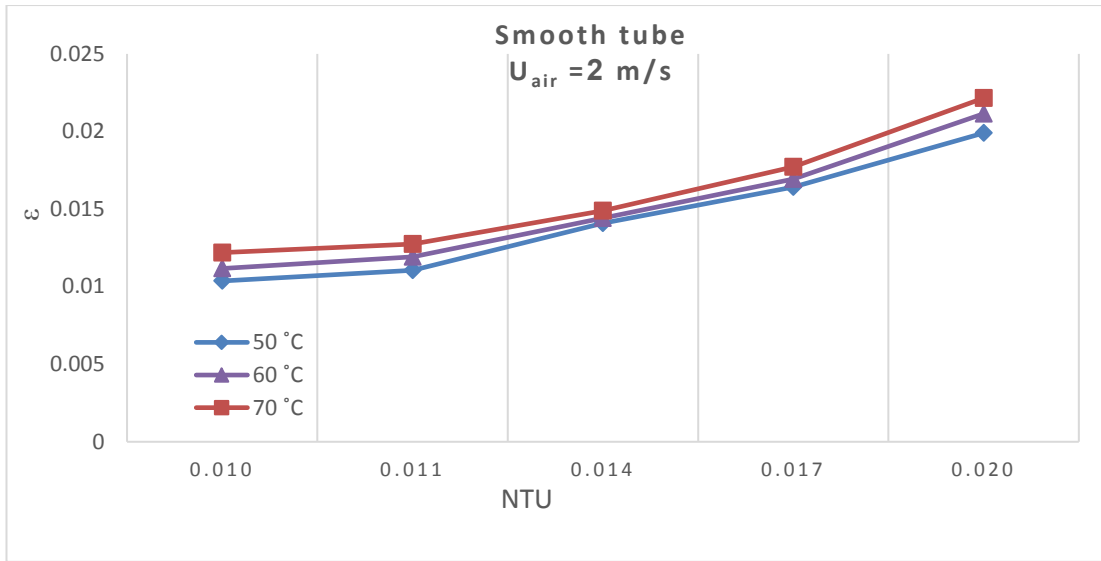


Figure 5.76. The effectiveness and NTU at air velocity (2 m/s) for all inlet hot water temperatures for smooth tube.

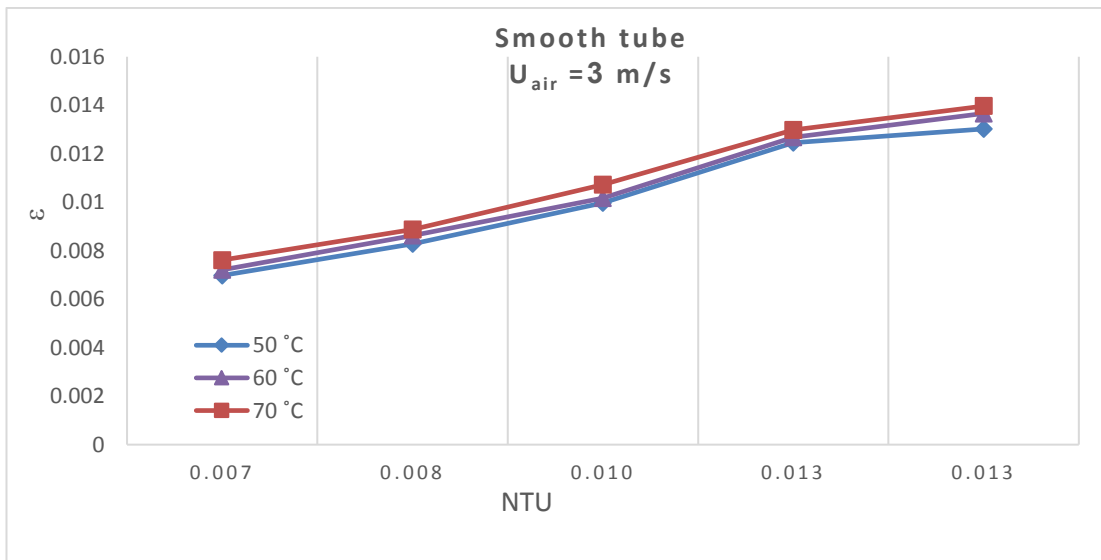


Figure 5.77. The effectiveness and NTU at air velocity (3 m/s) for all inlet hot water temperatures for smooth tube.

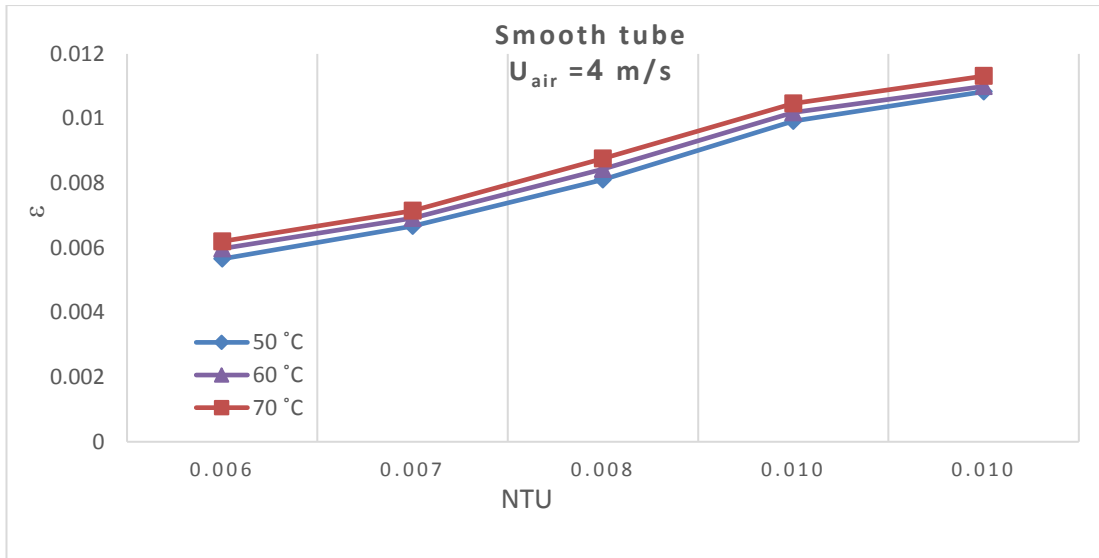


Figure 5.78. The effectiveness and NTU at air velocity (4 m/s) for all inlet hot water temperatures for smooth tube.

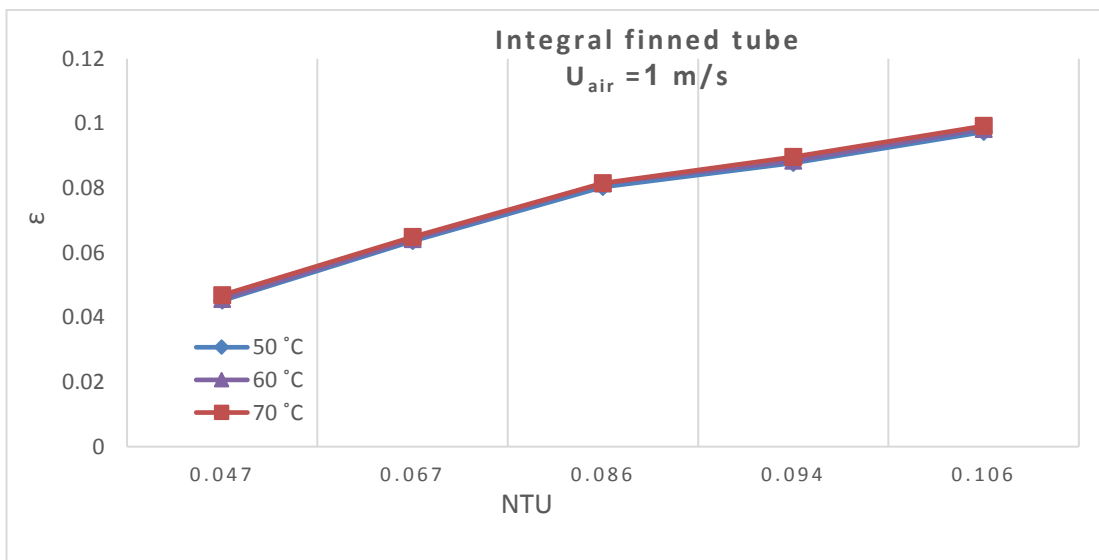


Figure 5.79. The effectiveness and NTU at air velocity (1 m/s) for all inlet hot water temperatures for medium integral finned tube with (P=1.6).

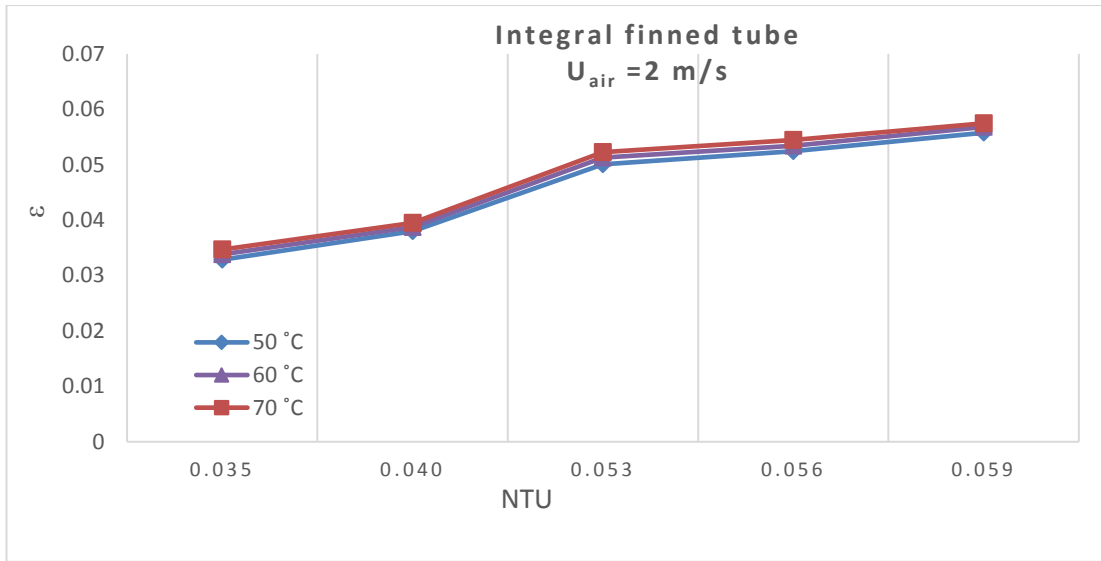


Figure 5.80. The effectiveness and NTU at air velocity (2 m/s) for all inlet hot water temperatures for medium integral finned tube with (P=1.6).

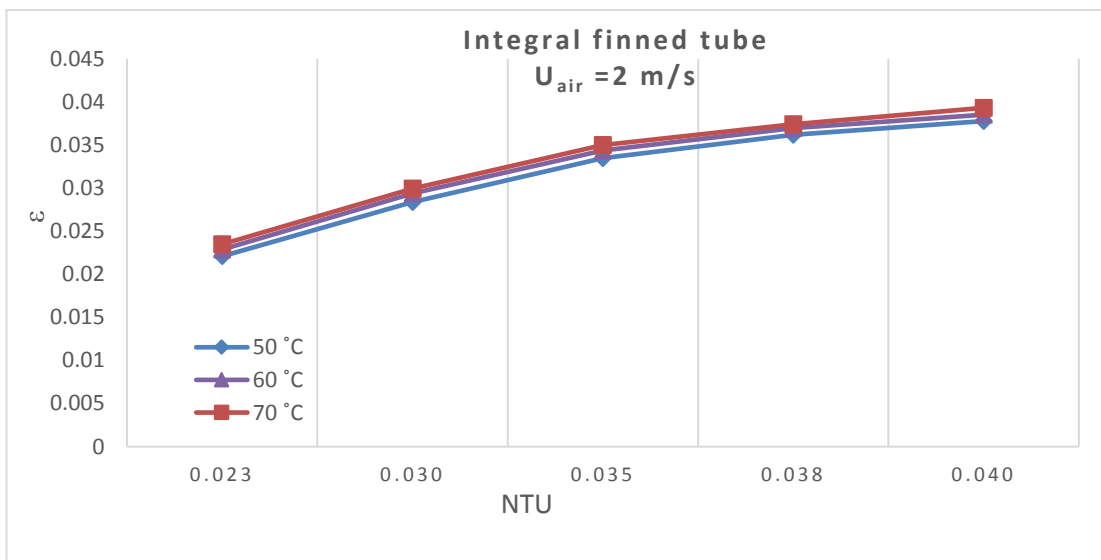


Figure 5.81. The effectiveness and NTU at air velocity (3 m/s) for all inlet hot water temperatures for medium integral finned tube with (P=1.6).

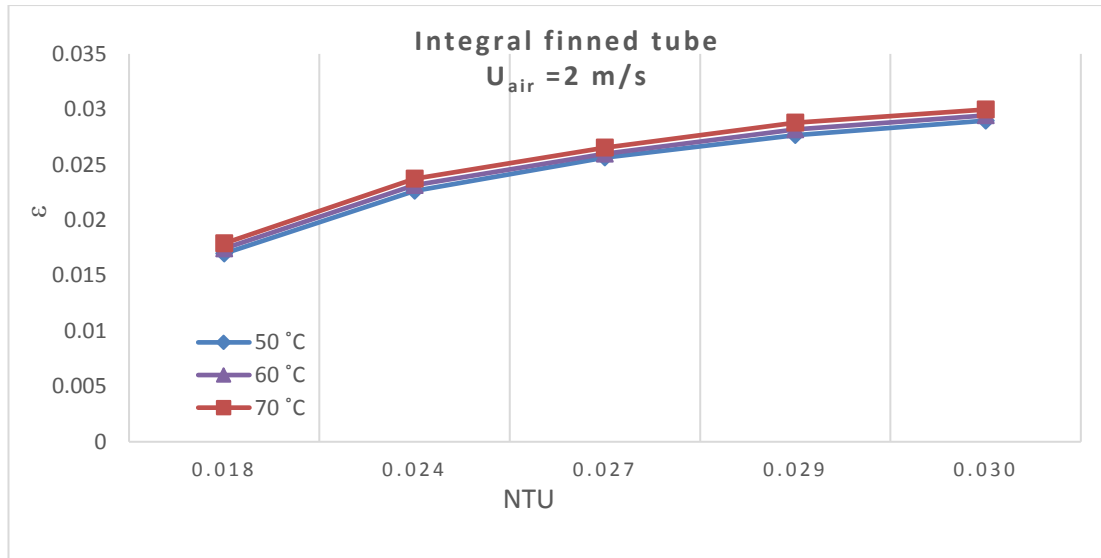


Figure 5.82. The effectiveness and NTU at air velocity (4 m/s) for all inlet hot water temperatures for medium integral finned tube with (P=1.6).

5.3.4. The Effect of the Fluid Velocity on the Air Side Heat Transfer Coefficient

The effect of hot water flow rate on the air side heat transfer coefficient at air velocity (1, 2, 3, 4 m/s) at different inlet hot water temperatures (50, 60, 70 oC) for smooth tube and medium integral finned tube with pitch ratio (P= 1.6 mm), shown in figures (5.83 to 5.90). This figure displays the relation between the inlet water temperature, the mass flow rate on air side heat transfer coefficient for smooth and integral finned tube. The results declare that when the inlet hot water temperature and flow rate increase, the heat transfer coefficient for air side (h_o) increases, due to the increase in the internal heat transfer. For the finned tube, the same behavior with the smooth tube can be observed but with higher value for percentage (124%, 142%, 159%, and 171%) respectively.

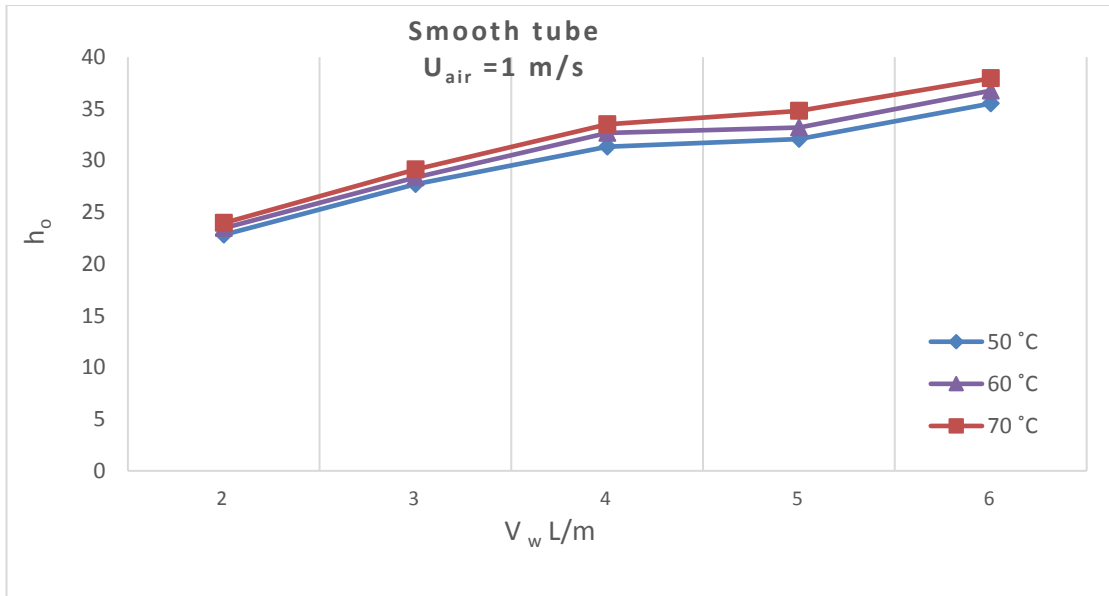


Figure 5.83. The effect of hot water flow rate on the outlet heat transfer coefficient at air velocity (1 m/s) at different inlet temperatures for smooth tube.

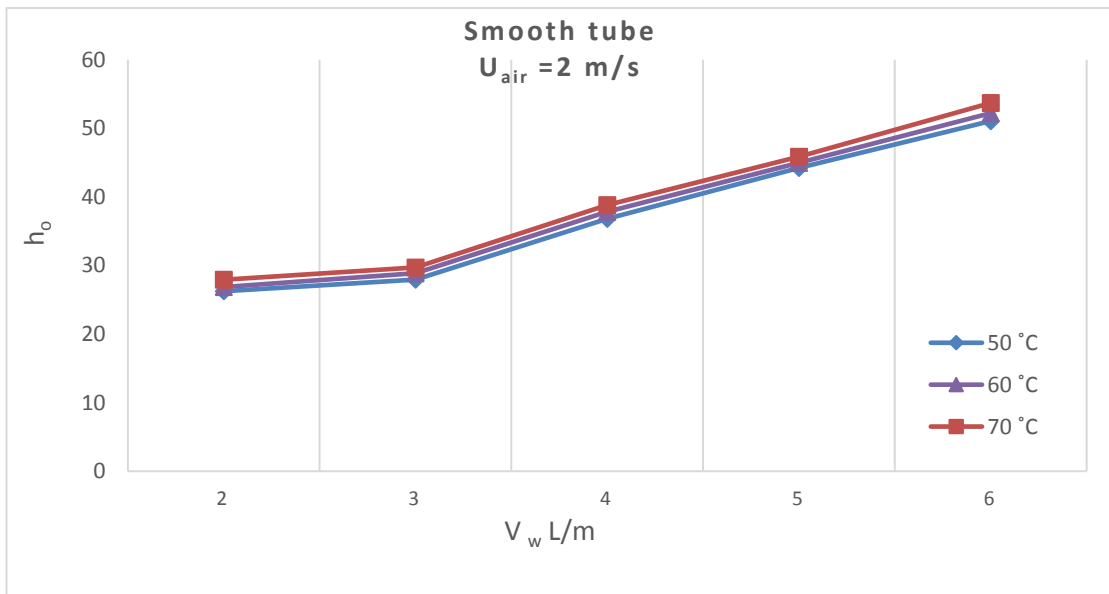


Figure 5.84. The effect of water flow rate on the outlet heat transfer coefficient at air velocity (2 m/s) at different inlet temperatures for smooth tube.

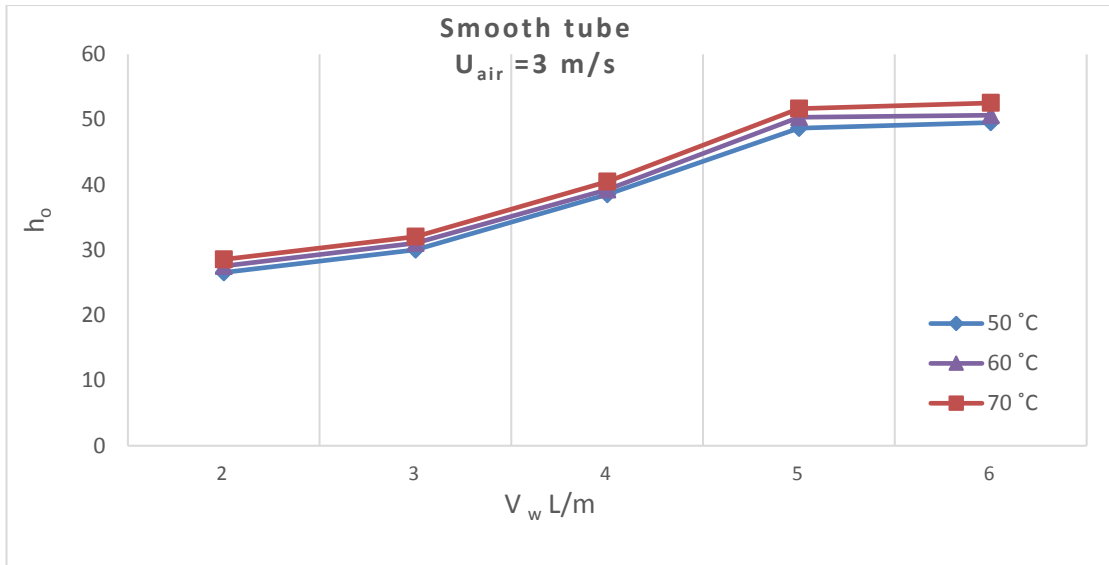


Figure 5.85. The effect of water flow rate on the outlet heat transfer coefficient at air velocity (3 m/s) at different inlet temperatures for smooth tube.

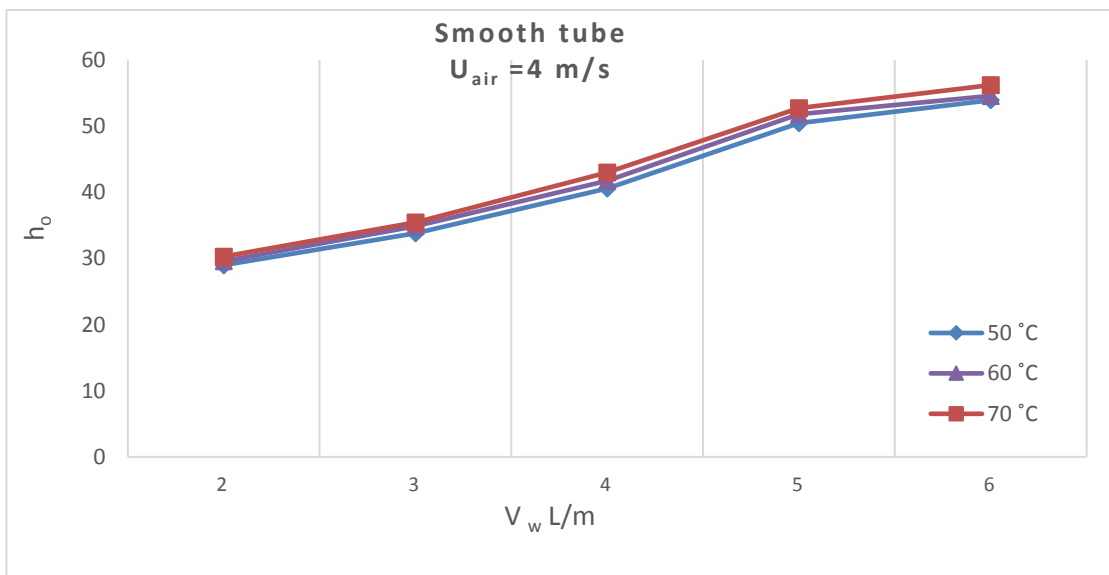


Figure 5.86. The effect of water flow rate on the outlet heat transfer coefficient at air velocity (4 m/s) at different inlet temperatures for smooth tube.

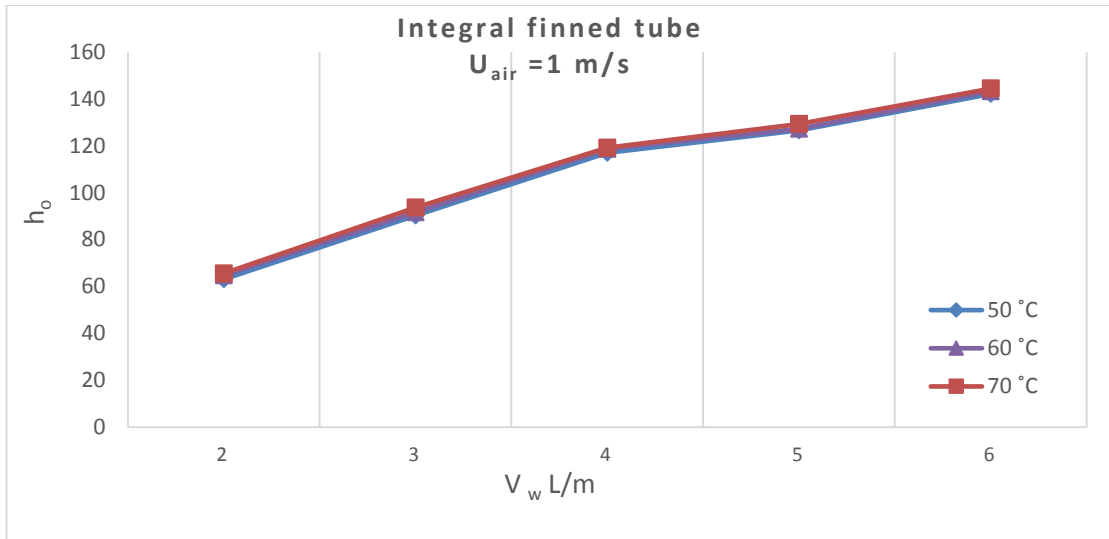


Figure 5.87. The effect of water flow rate on the outlet heat transfer coefficient at air velocity (1 m/s) at different inlet temperatures for integral finned tube with pitch ($P=1.6$ mm).

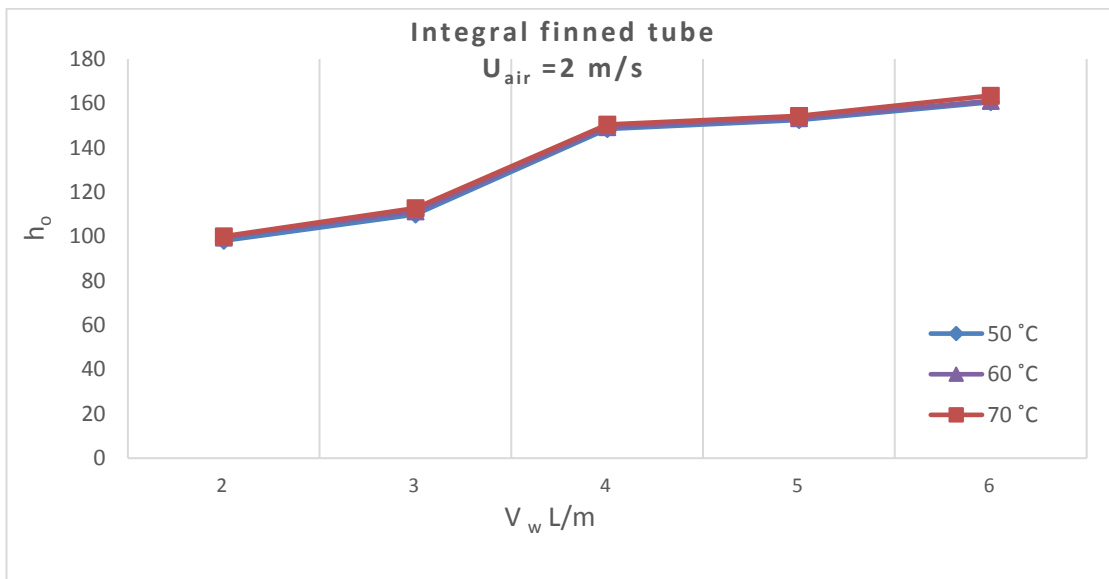


Figure 5.88. The effect of water flow rate on the outlet heat transfer coefficient at air velocity (2 m/s) at different inlet temperatures for integral finned tube with pitch ($P=1.6$ mm).

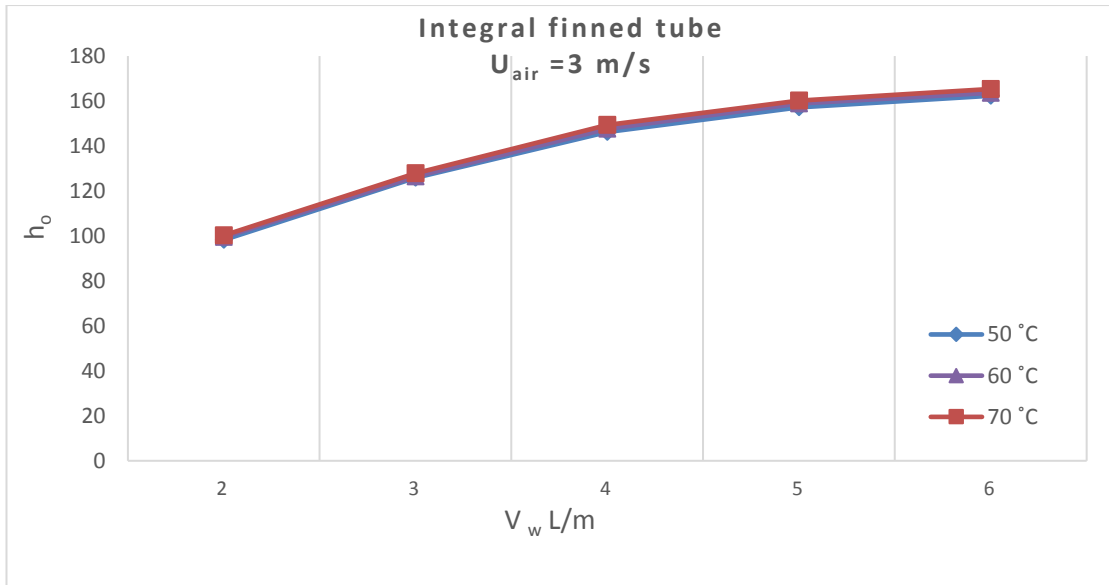


Figure 5.89. The effect of water flow rate on the outlet heat transfer coefficient at air velocity (3 m/s) at different inlet temperatures for integral finned tube with pitch ($P=1.6\text{mm}$).

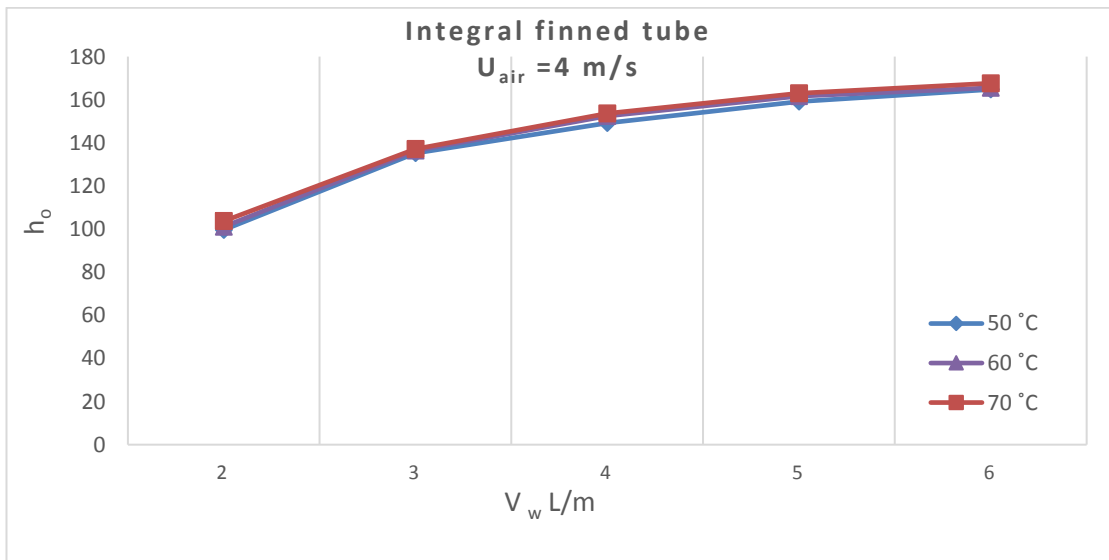


Figure 5.90. The effect of water flow rate on the outlet heat transfer coefficient at air velocity (4 m/s) at different inlet temperatures for integral finned tube with pitch ($P=1.6 \text{ mm}$).

5.4. COMPARING THE THEORETICAL AND EXPERIMENTAL RESULT

Figure (5.91 and 5.92) explain the comparison between the theoretical and experimental results. From the above figures, it is clear that the theoretical and practical behavior of the air-side heat transfer coefficient values behaves in the same

phenomena for both the smooth tube and the integral finned tube with (P=1.6mm), under working condition with the deviation 23.2% for smooth tube and 18.1% for integral finned tube, as shown in the listed calculation below:

for smooth tube

h_o average for experimental was 42.05562 (w/m². s) and the numerical was 54.74593 (w/m². s) for the equation

$$h_{av.} = \frac{\sum_1^n h_o}{n}$$

$$\sigma = \frac{h_{av. numerical} - h_{av. experimental}}{h_{av. numerical}} \times 100 = \left(\frac{54.745 - 42.055}{54.745} \right) \times 100 = 23.18 \%$$

For integral finned tube

h_o average for experimental was 137.86 (w/m². s) and the numerical was 168.4 (w/m². s) for the equation

$$h_{av.} = \frac{\sum_1^n h_o}{n}$$

$$\sigma = \frac{h_{av. numerical} - h_{av. experimental}}{h_{av. numerical}} \times 100 = \left(\frac{168.4 - 137.86}{168.4} \right) \times 100 = 18.134 \%$$

On the other hand, this difference is due to the fact that the theoretical side uses the ANSYS Fluent program, which is an ideal case without any losses. Regarding the results obtained from the practical side, they took into account the losses resulting from the didn't of complete control of the ambient temperature, in addition to the errors in the measuring devices in spite of the calibration of these devices, as well as the human errors

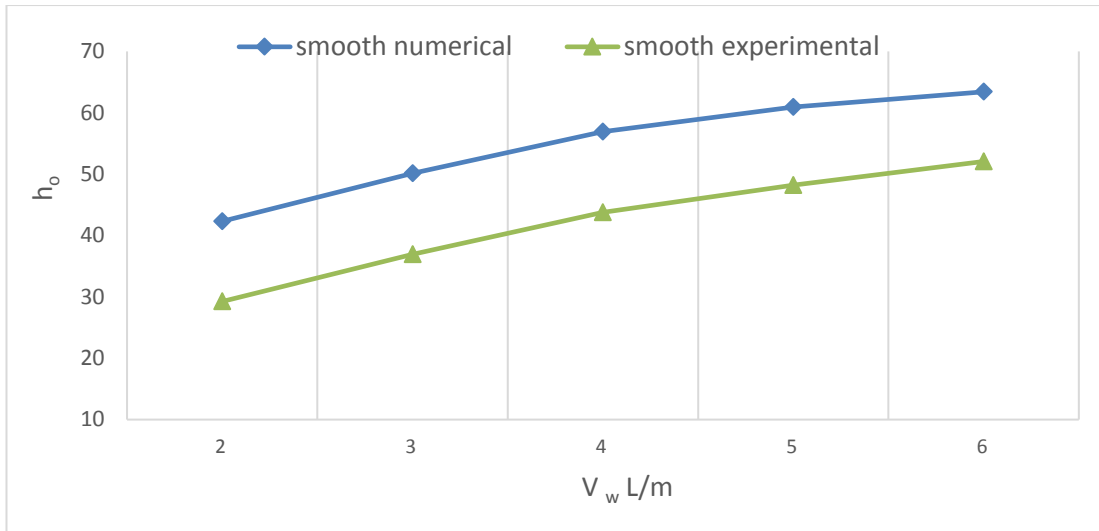


Figure 5.91. Comparing the theoretical and experimental results of the relationship between the outlet heat transfer coefficient at different flow rates for a smooth tube.

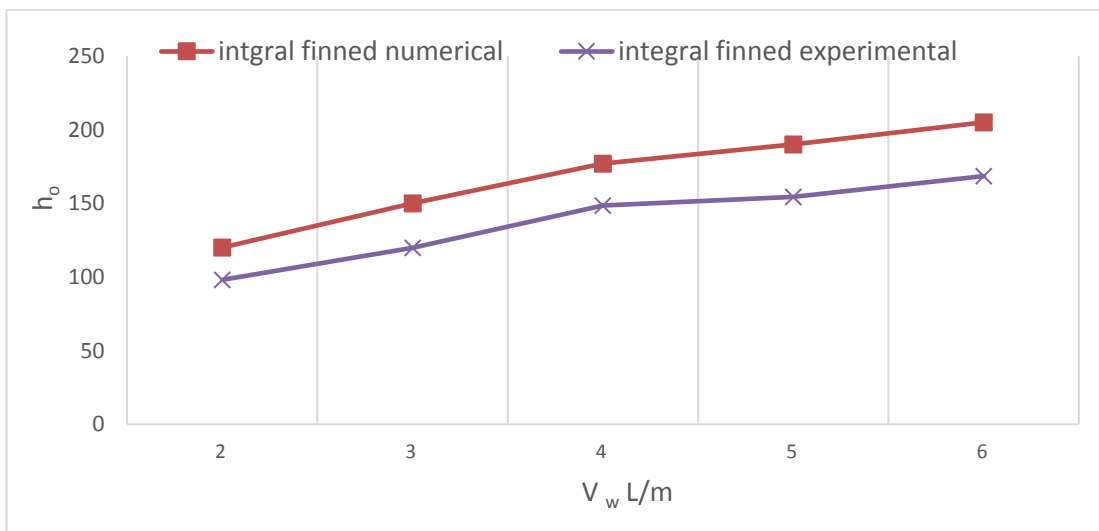


Figure 5.92. Comparing the theoretical and experimental results of the relationship between the outlet heat transfer coefficient at different flow rates for an integral finned tube with pitch fin ($P=1.6$ mm).

5.5. THE VALIDATION FOR CURRENT STUDY WITH PREVIOUS STUDY

The comparison between the current and the previous study [25], shown in Figure 5.93 clarifies an acceptable match appeared in the values of the heat transfer coefficient from the water side with a deviation of (5.7%) under the same working conditions adopted in the two studies. This indicates the accuracy of the results obtained from the current study. In addition to that, Figure 5.94 shows the comparison between the

Nusselt number values with the difference in the Reynolds number of the fluid flow inside the tube for both the current and previous studies. It shows that the deviation in the results does not exceed (8.6%). This confirms the accuracy of the work. Furthermore, Figure 5.95 shows the numerical results for pressure drop with the flow rate of hot water for the two studies even though the diameters are the same and the boundary conditions used in the two studies are similar. This figure clarifies the behavior of the pressure drop at different inlet temperatures and flow rate. The same behavior appears between the two studies with an acceptable deviation, attributed to the difference in the version of the program used in the simulation and the temperature of entering the cold air, as the temperature of entering the cold air in this study is 20°C and the previous study [25].

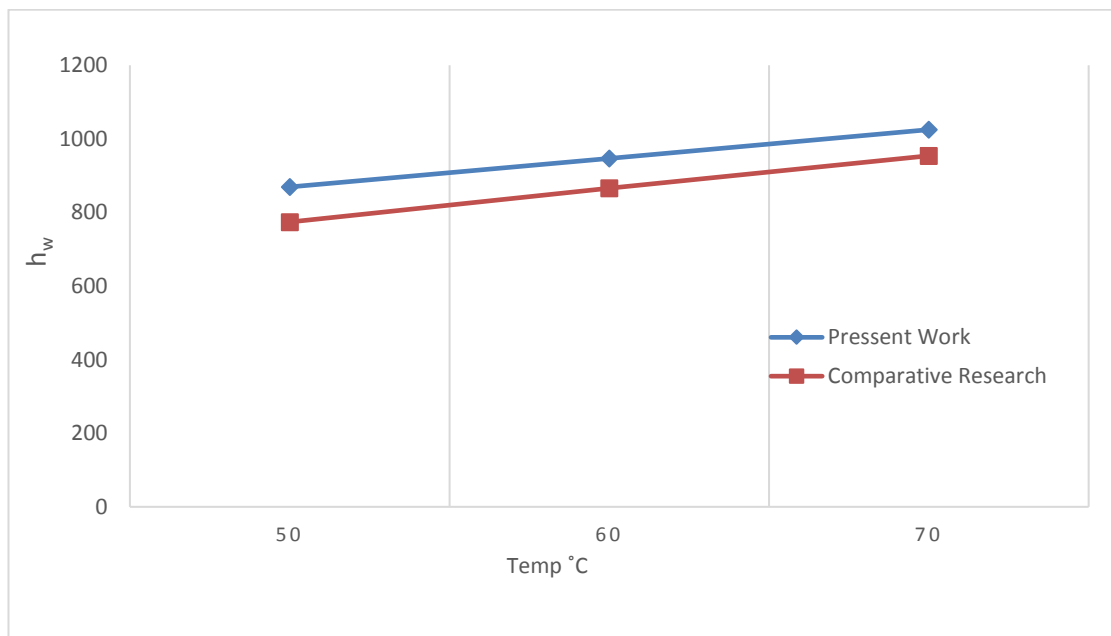


Figure 5.93. Comparing the relationship between the numerical results for internal heat transfer coefficient with the water entry temperatures between the current study and comparative research [25].

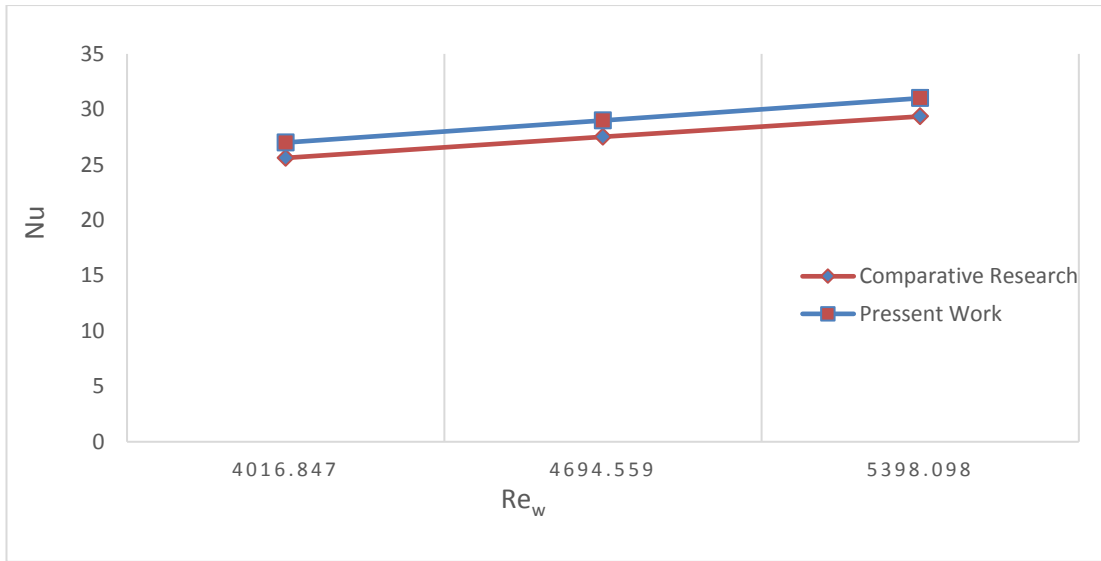


Figure 5.94. Comparing the relationship between the numerical results for Nusselt number with Renolds number between the current study and comparative research [25].

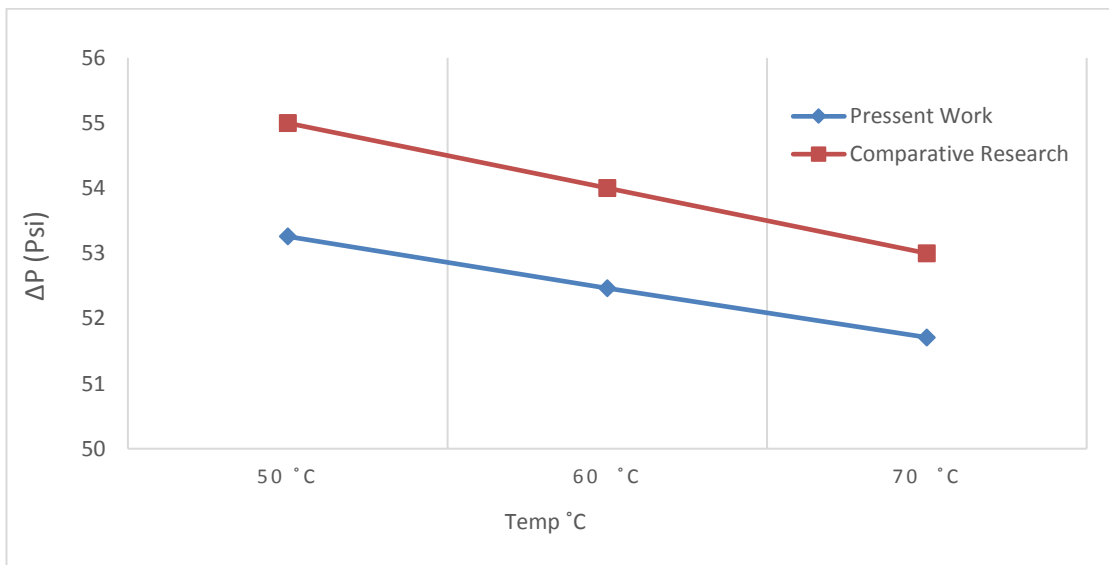


Figure 5.95. Comparing the relationship between the numerical results for pressure drop with the water entry temperatures between the current study and comparative research [25].

PART 6

CONCLUSIONS AND SUGGESTIONS

6.1. CONCLUSIONS

In this chapter, it was presented all the conclusions that obtained through the theoretical and experimental studies for all the models that were tested, which consists of smooth tube, finned tube with pitch ratio of ($P= 3.75, 2.5,$ and 1.6 mm), respectively. The conclusions are as follows:

1. The rate of heat transfer (Q) increases with the increase in the temperature of entering the hot water and the increase in air velocity for all models.
2. The heat transfer rate of the finned tube is higher than the smooth tube for all cases. The finned tube with pitch ratio ($P= 3.75, 2.5,$ and 1.6 mm) enhances the heat transfer rate by percentage of 63.3%, 68.93%, 74.2%, respectively, relative to smooth tube.
3. The distance between the fins (pitch fin) decreases as the number of fins increases, thus increasing the surface area for heat exchange, and this increases the rate of heat transfer.
4. The highest enhancement of the heat transfer rate was reached at the water flow rate of 6 L/min and the enhancement ratio was as follows 313, 361, 438 for the models of ($P= 3.75, 2.5,$ and 1.6 mm), respectively. This gives us confirmation that the best model is the model of pitch 1.6mm.
5. The rate of improvement increases with the increase in the number of fins and the increase in the temperature of entering the hot water, where the highest value is at a temperature of 70°C for entering the water and a flow rate of 6 liters/min. The result is obtained as 4.133%, 4.616%, 6.293% for the models of ($P=3.7, 2.5,$ and 1.6 mm), respectively.

6. The value of pressure drops increases as the flow rate of hot water increases.
7. As the flow rate of hot water increases, the difference in water temperature decreases.
8. Increasing the air velocity increases the temperature difference of hot water and air and increases the rate of heat transfer.
9. The Nusselt number of the air increases with the flow rate of hot water and the velocity of the air. The finned tube is better than the smooth tube by the ratio of 68.1%, 73.5%, 80.4%) for the models of ($P=3.75$, 2.5, and 1.6 mm), respectively.

6.2. SUGGESTIONS FOR LATER STUDIES

1. Nanofluid can be used instead of hot liquid in the heat exchanger.
2. Fin types can be changed.
3. Different heat exchanger types or pipe types can be used.

REFERENCES

1. Bergles, A. E., "Techniques to enhance heat transfer", *Handbook of Heat Transfer*, 3(2): 11-1 (1998).
2. Rahmah, A. M., "Experimental study of an integral finned-tube heat exchanger", *University of Technology, Mechanical Engineering Department, Master Thesis*, Baghdad, Iraq, 12-34 (2011).
3. Wolf I., Franković B., Viličić I., Jurkowski R. and Bailly A., "A numerical and experimental analysis of heat transfer in a wavy fin-and-tube heat exchanger ", *Energy and the Environment*, 2(1): 91-101 (2006).
4. Chaudhari, S., "Experimental investigation of finned tube heat exchanger", *Doctoral Dissertation, University of Vadodara*, India, 12-34 (2014).
5. Pal Durgeshkumar, K., & Umale, S., "Numerical investigation on air side performance of fin and tube heat exchangers with different types of fins", *International Journal of Thermal Engineering*, 1(2): 2395-0250 (2015).
6. Zaid, M. H., & Namasivayam, S., "Semi-empirical model for forced-convection condensation on integral finned-tubes", *In 3rd Engineering Undergraduate Research Catalyst Conference*, Malaysia, 23-31, (2014).
7. Taher, F. A., & Kadhim, Z. K., "Improvement the heat dissipation by using different integral finned tubes for cross flow heat exchanger", *In 2021 International Conference on Advance of Sustainable Engineering and its Application*, Wasit, Iraq, 27-32 (2019).
8. Internet: Makina, M., "Extruded fin tube and heat exchanger", <https://fintube.web.tr/fintube.pdf>(2022).
9. Ameen, M. & Hasan, B. "Heat transfer enhancement using different volume fractions of Nano fluids in heat exchangers", *M.Sc. Thesis, University of Bagdad*, Baghdad, Iraq, 34-44 (2012).
10. Kadhim, Z. K., Kassim, M. S., & Hassan, A. Y. A., "CFD study for cross flow heat exchanger with integral finned tube", *International Journal of Scientific and Research Publications*, 4(3): 6-10 (2016).
11. Jassam, M. J., "Effect of natural nanoparticles on enhancement of heat transfer coefficient in cross flow heat exchanger", *Master Thesis, University of Wasit*, 34-36 (2019).

12. Mon, M. S., & Gross, U., “Numerical study of fin-spacing effects in annular-finned tube heat exchangers”, *International Journal of Heat and Mass Transfer*, 47(9): 1953-1964 (2004).
13. Jung, D., & Assanis, D. N., “Numerical modeling of cross flow compact heat exchanger with louvered fins using thermal resistance concept”, *SAE Paper*, 1(2): 7-26 (2006).
14. Wais, P., “Fluid flow consideration in fin-tube heat exchanger optimization”, *Archives of Thermodynamics*, 31(3): 87-104 (2010).
15. Bhuiyan, A. A., Islam, A. S., & Amin, M. R., “Numerical prediction of laminar characteristics of fluid flow and heat transfer in finned-tube heat exchangers”, *Innovative Systems Design and Engineering*, 2(6): 1-12 (2011).
16. Gunnasegaran, P., Shuaib, N. H., & Abdul Jalal, M. F., “The effect of geometrical parameters on heat transfer characteristics of compact heat exchanger with louvered fins”, *International Scholarly Research Notices*, 2(1):22-34 (2012).
17. Ocloń, P., Łopata, S., Nowak, M., & Benim, A. C., “Numerical study on the effect of inner tube fouling on the thermal performance of high-temperature fin-and-tube heat exchanger”, *Progress in Computational Fluid Dynamics, An International Journal*, 15(5): 290-306 (2015).
18. Dev, A. A., & Ardhapurkar, P. M., “Numerical analysis of multistream cross-counter flow heat exchanger using computational fluid dynamics”, *In International Conference on Recent Advances in Mechanical Engineering*, India, 26-28 (2015).
19. Wais, P., “Correlation and numerical study of heat transfer for single row cross-flow heat exchangers with different fin thickness”, *Procedia Engineering*, 15(7): 177-184 (2016).
20. Ravikumar, K., Raju, C. N., & Saheb, M., “CFD Analysis of a Cross-flow Heat Exchanger with Different fin thickness”, *International Journal of Dynamics of Fluids*, 13(2): 345-362 (2017).
21. Xu, J., Li, J., Ding, Y., Fu, Q., Cheng, M., & Liao, Q., “Numerical simulation of the flow and heat-transfer characteristics of an aligned external three-dimensional rectangular-finned tube bank”, *Applied Thermal Engineering*, 14(5): 110-122 (2018).
22. Rajput, Y. S., & Arya, A., “CFD analysis of cross flow heat exchanger with different fin thickness”, *International Journal of Dynamics of Fluids*, 13(2): 345-362 (2019).

23. Ismail, M. S., Hassab, M., & El-Maghlany, W. M., “Comparative three-dimensional CFD study for inline cross flow plate finned tube heat exchanger”, *Proceedings of the 4th World Congress on Momentum, Heat and Mass Transfer*, Rome, Italy, 23-56 (2019).
24. Sahel, D., Ameer, H., & Mellal, M., “Effect of tube shape on the performance of a fin and tube heat exchanger”, *Journal of Mechanical Engineering and Sciences*, 14(2): 6709-6718 (2020).
25. Merdan, S.H., & Kadhim, Z. K., “Study the flow direction and number of tubes in cross-flow heat exchanger to improve the heat transfer coefficient”, *Wasit Journal of Engineering Sciences*, (2020).
26. Hofmann, R., Frasz, F. & Ponweiser, K., “Heat transfer and pressure drop performance comparison of finned-tube bundles in forced convection”, *WSEAS Trans. Heat Mass Transfer*, 2(4): 72-88 (2007).
27. Nuntaphan, A., & Kiatsiriroat, T., “Effect of fly ash deposit on thermal performance of spiral finned-tube heat exchanger under dehumidifying condition”, *Songklanakarinn J. Sci. Technol*, 26(4): 509-519 (2004).
28. Hofmann, R., Frasz, F., & Ponweiser, K., “Experimental analysis of enhanced heat transfer and pressure-drop of serrated finned-tube bundles with different fin geometries”, *In Proceedings of the 5th WSEAS International Conference on Heat and Mass Transfer*, Vienna, 54-62 (2008).
29. Agrawal, Y., & Bhagoria, J. L., “Heat transfer characteristics of a copper-nickel multi tube with corrugated copper fins in a cross-flow heat exchanger”, *Indian Journal of Science and Technology*, 4(11): 45-67 (2011).
30. Pongsoi, P., Promoppatum, P., Pikulkajorn, S., & Wongwiset, S., “Effect of fin pitches on the air-side performance of L-footed spiral fin-and-tube heat exchangers”, *International Journal of Heat and Mass Transfer*, 5(9): 75-82 (2013).
31. FaJiang, H., WeiWu, C., & Ping, Y., “Experimental investigation of heat transfer and flowing resistance for air flow cross over spiral finned tube heat exchanger”, *Energy Procedia*, 1(7): 741-749 (2012).
32. Ikpotokin, I., & Osueke, C. O., “Heat transfer and fluid flow characteristics study for in-line tube bank in cross-flow”, *International Journal of Mechanical & Mechatronics Engineering*, 14(3): 93-105 (2014).
33. Chaudhari, S., “Experimental investigation of finned tube heat exchanger”, *Doctoral Dissertation, University of Vadodara*, India, 67-89 (2014).
34. Kadhim, Z., Kassim, M., & Hassan, A., “Effect of integral finned tube on heat transfer characteristics for cross flow heat exchanger”, *International Journal of Computer Applications*, 139(3): 20-25 (2016).

35. Dhangar, I. J., & Chopra, M., "Experimental investigation and CFD analysis performance of fin and tube heat exchanger with different types of fins", *Paper Published in International Conference on Emerging and Renewable Energy Generation and Automation*, Beirut, Lebanon, 23-45 (2018).
36. Prajapati, P. A., & Mohite, S. A., "An experimental analysis of the overall heat transfer coefficient on cross flow heat exchanger & fin effectiveness", *International Journal of Research and Analytical Reviews*, 5(3):343- 348 (2018).
37. Arshad, H., Khushnood, S., Ahmad Nizam, L., Ameer Ahsan, M., & Ghufran Bhatti, O., "Effect of fin geometry on flow-induced vibration response of a finned tube in a tube bundle", *Journal of Applied Fluid Mechanics*, 11(4): 1143-1152 (2018).
38. Khitam, F. A. "Design, fabrication and testing of cross flow heat exchanger", *Requirements for the Bachelor's degree of Science in Mechanical Engineering*, University of Al-Qadisiyah, Iraq, 12-19 (2018).
39. Tripathi, A., & Singh, A. K., "A review on heat transfer and pressure drop correlations in solid circular finned tube bundles positioned at inline and staggered arrangement in cross flow", *International Journal of Research in Aeronautical and Mechanical Engineering Mechanical Engineering*, 3(2): 61-67 (2015).
40. Kassim, M. S., & Gaber, H. S., "Investigation of convection heat transfer for high integral finned tube heat exchanger", *Journal of Engineering and Sustainable Development*, 23(6): 123-156 (2019).
41. Farah Abdul Zahra Taher, "**Experimental and Numerical Study of Integrated Finned Heat Exchanger.**" M.Sc. thesis, Wasit University, Iraq, 2019.
42. Zhou, F., Geb, D., & Catton, I., "Numerical investigation on air side performance of fin-and-tube heat exchangers with large diameter tubes and large number of tube rows", *In ASME International Mechanical Engineering Congress and Exposition*, 54(8): 805-813 (2011).
43. Habeeb, L. J., Karamallah, A. A., & Rahmah, A. M., "Heat transfer analysis of integral-fin tubes", *Mechanical Engineering and Technology*, 2(2): 23-34 (2015).
44. Hussein, A. A. H. " Experimental investigation of different types of finned tube", *Master Thesis, University of Technology*, Iraq, 13-19 (2014).
45. Bell, K. J., & Mueller, A. C., "Wolverine engineering data book II", *Wolverine Tube Inc.* USA, 56-77 (2001).
46. Fernández-Seara, J., Uhía, F. J., Diz, R., & Dopazo, A., "Condensation of R-134a on horizontal integral-fin titanium tubes", *Applied Thermal Engineering*, 30(4): 295-301 (2010).

47. Tarrad, A. H., "A numerical model for thermal-hydraulic design of a shell and single pass low finned tube bundle heat exchanger", *Engineering and Technology Journal*, 25(4): 619-645 (2007).
48. Mallikarjuna, S. V., & Raghu, V. B., "Numerical analyses of fin side turbulent flow for round and flat tube heat exchangers", *IJMER*, India, 33-39 (2014).
49. Patil, P. V., & Kumbhar, D. G., "CFD investigation on dimpled FINS with parameter variation for heat transfer augmentation", *Int J Eng Res Technol (IJERT)*, 3(6): 662-6 (2014).
50. Nemati, H., & Moghimi, M., "Numerical study of flow over annular-finned tube heat exchangers by different turbulent models", *CFD Letters*, 6(3): 101-112 (2014).
51. Ahmed J. M., "Heat Transfer of Double Pipe Heat Exchanger Performance by Using Nanofluids and Serrated Fins," MSc thesis, college of engineering-Wasit, Iraq, 2016.
52. Choi, J. M., Kim, Y., Lee, M., & Kim, Y., "Air side heat transfer coefficients of discrete plate finned-tube heat exchangers with large fin pitch", *Applied Thermal Engineering*, 30(3): 174-180 (2010).
53. Tahseen, T. A., Ishak, M., & Rahman, M. M., "An experimental study air flow and heat transfer of air over in-line flat tube bank", *In International Conference on Mechanical Engineering Research*, 1(2): 1-3 (2013).
54. Hasan, W. F., "Theoretical and experimental study to finned tubes cross flow heat exchanger", *University of Technology*, Baghdad, Iraq, 45-62 (2008).
55. Incropera, F. P., DeWitt, D. P., Bergman, T. L., & Lavine, A. S., "Fundamentals of heat and mass transfer", *Wiley*, New York, 116-118 (1996).
56. Holman, J. P., "Heat Transfer", *McGraw-Hill*, USA, 536-537 (1986).
57. IAEA-TECDOC-1585, "Measurement uncertainty", *International Atomic Energy Agency, IAEA-TECDOC-1585*, Austria, 12-78 (2008).
58. Kline, S. J., "Describing uncertainty in single sample experiments", *Mech. Engineering*, 7(5): 3-8 (1953).
59. Moffat, R. J., "Describing the uncertainties in experimental results", *Experimental Thermal and Fluid Science*, 1(1): 3-17(1988).
60. Green, D. W., & Southard, M. Z., "Perry's chemical engineers' handbook", *McGraw-Hill Education*, USA, 12-23 (2019).

61. Snow, F. J., “American society of heating, refrigeration, and air conditioning engineers (ASH RAE) thermographic standard 101 P”, *In Thermal Infrared Sensing Applied to Energy Conservation in Building Envelopes*, 31(3): 94-98 (1982).
62. Haghshenas, F. M., Talaie, M. R., & Nasr, S., “Numerical and experimental investigation of heat transfer of ZnO/water nanofluid in the concentric tube and plate heat exchangers”, *Thermal Science*, 15(1): 183-194 (2011).
63. Versteeg, H. K., & Malalasekera, W., “An introduction to computational fluid dynamics: the finite volume method”, *Pearson Education*, London, 34-55 (2007).
64. Ansys, A. F. U. G., “Southpointe, 275 Technology Drive”, *Canonsburg, USA*, 15-317 (2011).
65. Kline, S. J., “Describing uncertainty in single sample experiments”, *Mech. Engineering*, 7(5): 3-8. (1953).

APPENDIX A.

UNCERTAINTY

For every experiment and study there is an error rate and this percentage increases and decreases according to the variables and according to the accuracy of the devices and because in this study we have many variables, including the temperatures of the inlet water (50, 60, 70) °C and the air speed (1, 2, 3) m/s and the flow rate of water (2, 3, 4, 5) L/m, we have prepared the first three readings to calculate the percentage of error in them using the equations below and as shown in the table (A-1).

Error ratio Equations

The average of measuring parameters (x)

$$X_{av} = \frac{\sum_1^n X_i}{n}$$

Where is

(X_i) is the measurement value of each case

(n) It is the number of cases that have been taken

(σ) standard deviation value

$$\sigma = \frac{\sqrt{(\sum_1^n (X_i - X_{av})^2)}}{n-1}$$

(σ_a) is the mean standard deviation.

$$\sigma_a = \frac{\sigma}{\sqrt{n}}$$

So (X) represents the real value measured by the equation below

$$X = X_{av} \pm \sigma_a$$

Table Appendix 1.1. Calculated for error ratio.

Var.	X1	X2	X3	X _{av}	β	β _a	X+	%
							X-	
Q	42.91	34.107	47.173	41.396	6.663	3.847	45.243	8.502
							37.549	-10.245
U _i	25.513	20.25	28.11	24.625	4.004	2.312	26.937	8.583
							22.313	-10.361
h _i	798.4	798.65	798.283	798.445	0.187	0.108	798.55	0.0135
							798.33	-0.0135
Re _w	3987.781	3989.745	3986.831	3988.12	1.486	0.858	3988.97	0.0215
							3987.261	-0.0215
Nu _w	23.524	23.53	23.521	23.525	0.0047	0.0027	23.527	0.0116
							23.522	-0.0116
U _o	23.083	18.322	25.433	22.279	3.623	2.092	24.371	8.583
							20.187	-10.361
h _o	23.96	18.87	26.502	23.11	3.886	2.243	25.354	8.849
							20.867	-10.752
Re _a	17309.67	17310.53	17304.51	17308.239	3.259	1.881	17310.12	0.011
							17306.36	-0.011
Nu _a	19.457	15.324	21.518	18.766	3.154	1.821	20.587	8.846
							16.945	-10.748

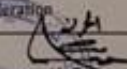


Calibration Certificate
Central Organization for Standardization and Quality Control
Metrology Department - Physics Section (PDM-TC-012)

P.O. Box13032 Aljadriya street, Baghdad, Tel:7785180 - E-Mail : cosqc@cosqc.gov.iq

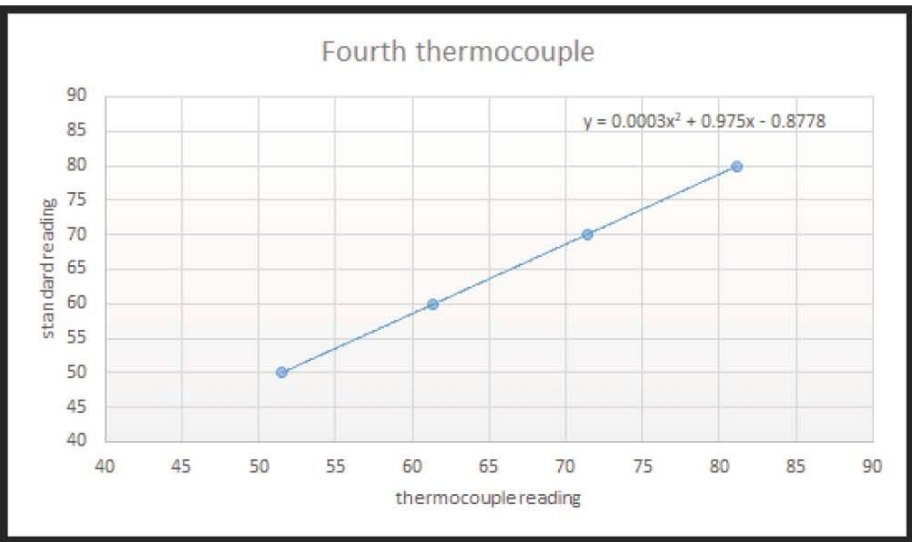
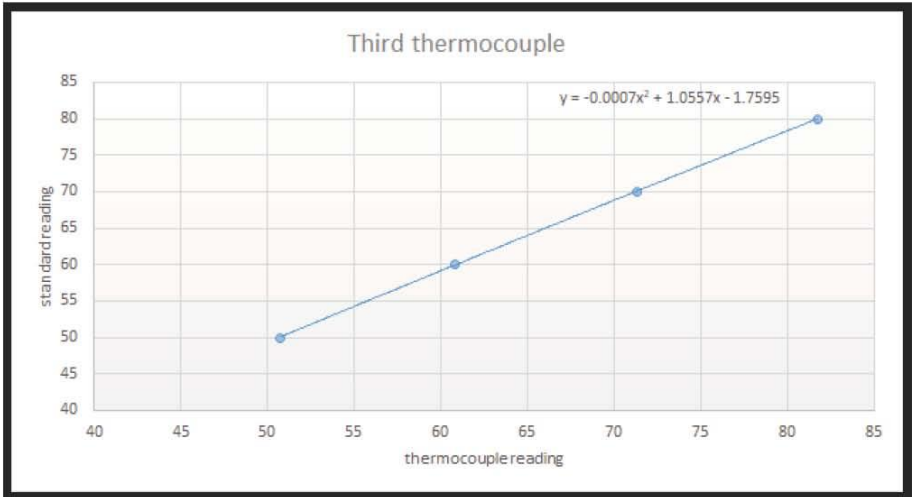
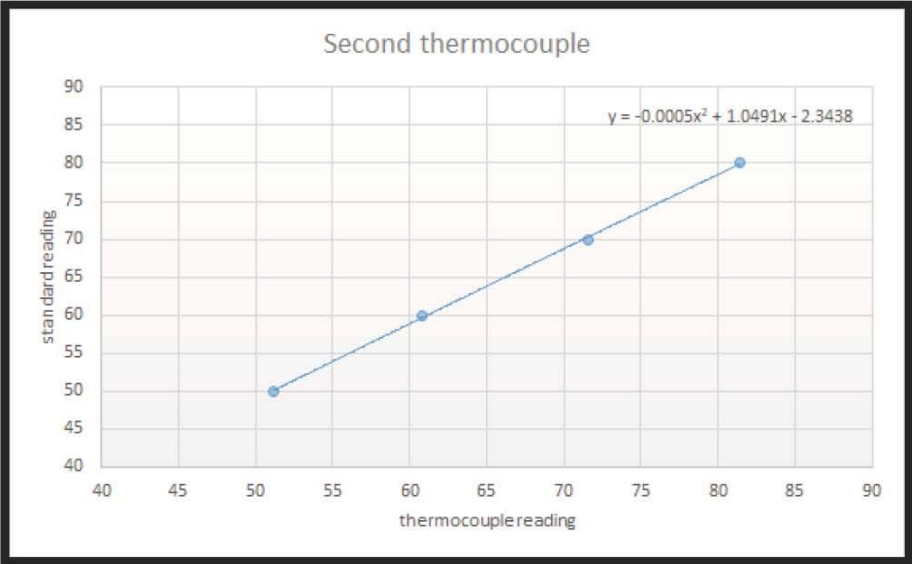
Certificate No.: PHT 360/2020
 Date of issue : 06/09/2020

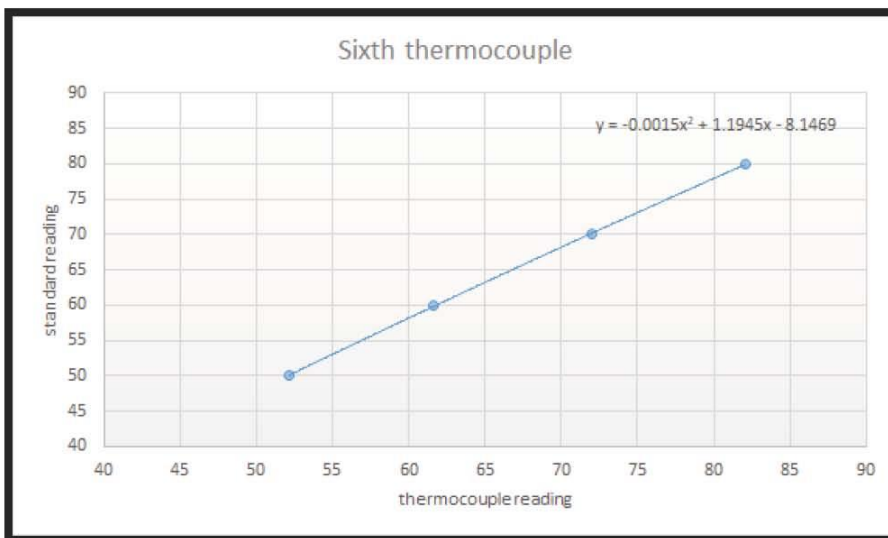
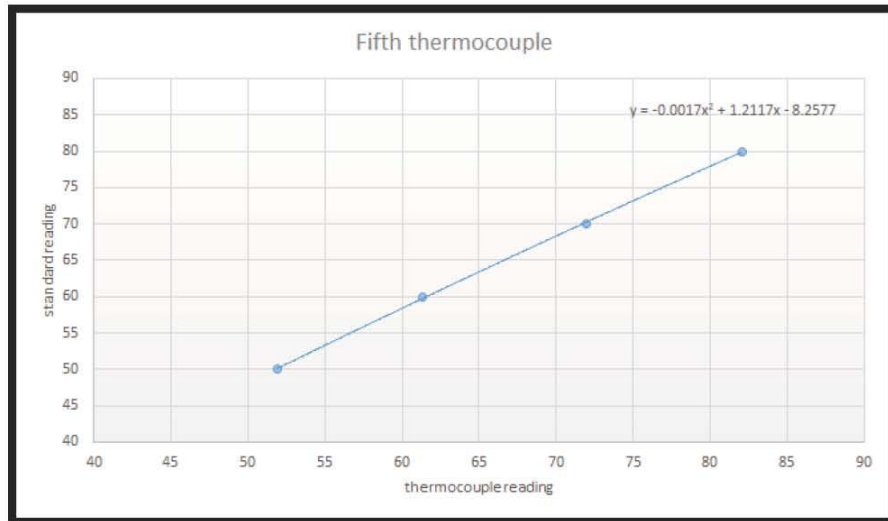
Customer	
Name:	رئاسة جامعة واسط / عمادة كلية الهندسة / شعبة الدراسات العليا / طالبة الماجستير شذى علي مردان
Address:	العراق - واسط
Item under calibration	
Description:	Digital Thermometer with TC(K) Res. : 0.1 °C
Manufacturer:	ROHS
Model:	HT-9815
Serial number:	201809027367
Other identification:	(-200 --- 1372)°C
Date of reception:	Order no. : (187) , Date of Reception : 27/08/2020
Condition of reception:	As Found
Standard(s) used in the calibration	
Description:	Digital Nano volt / Micro Ohm meter PT100
Manufacturer:	Agilent
Model:	34420A
Serial number:	MY42000734 (1)
Other identification:	ID : PHT-01-17 ID : PHT-01-84
Calibration information	
Date of calibration:	31/08/2020 , Due to : 31/08/2021
Place of calibration:	PH LAB. 1
Method(s) of calibration:	Calibration method using - PROC-TC-012 (C)
Calibrated quantity:	Temperature °C
Results of calibration:	Attached a complete result in Annex 1 to 2 of this certificate
Measurement uncertainty:	The reported expanded uncertainty is based on UKAS M3003 Standard and the standard Uncertainty multiplied by coverage factor k=2 to give confidence level of 95%
Metrological traceability:	The traceability of measurement results to the SI units is assured by the National standard maintained at Central Organization for standardization and Quality Control through calibration at :- UME /CER. NO (G1KS-0127)
Environmental conditions of calibration:	Temp. 33.91° C RH. 22.40%
Observations, opinions or recommendations:	The results in Annex 1 should be taken into consideration

Approved by:

 Moyassar Aliq Ali
 Head of Physics Section
 06/09/2020

1 of 2
 This certificate is issued in accordance with the laboratory accreditation requirements. It provides traceability of measurement to recognized national standards and to the units of measurement realized at the COSQC or other recognized national standards laboratories. This certificate may not be reproduced other than in full by photographic process. This certificate refers only to the particular item submitted for calibration.

Appendix A.1. Pictures of the central of standardization and quality control for calibrating reader temperature.





Appendix A.3. Calibration of thermometer type (HT-9815).

APPENDIX B.

THE TABLES FOR EXPERIMENT DATA

Table Appendix B.1. Smooth tube.

$U_{air} = 1 \text{ m/s}$					
$\dot{m} = 2 \text{ L/m}$					
$t_{hi} \text{ }^\circ\text{C}$	$t_{ho} \text{ }^\circ\text{C}$	$Q_w \text{ (Watt)}$	Re_w	$h_i \text{ (W / (m}^2 \cdot \text{ }^\circ\text{C))}$	Nu_w
50	49.688	42.909	3987.781	798.403	23.524
60	59.595	55.479	4648.692	898.683	26.116
70	69.491	69.45	5353.102	1026.023	29.38

$U_{air} = 2 \text{ m/s}$					
$\dot{m} = 2 \text{ L/m}$					
$t_{hi} \text{ }^\circ\text{C}$	$t_{ho} \text{ }^\circ\text{C}$	$Q_w \text{ (Watt)}$	Re_w	$h_i \text{ (W / (m}^2 \cdot \text{ }^\circ\text{C))}$	Nu_w
50	49.638	49.786	3986.248	798.209	23.519
60	59.535	63.699	4646.525	898.425	26.109
70	69.415	79.821	5350.615	1025.741	29.374

$U_{air} = 3 \text{ m/s}$					
$\dot{m} = 2 \text{ L/m}$					
$t_{hi} \text{ }^\circ\text{C}$	$t_{ho} \text{ }^\circ\text{C}$	$Q_w \text{ (Watt)}$	Re_w	$h_i \text{ (W / (m}^2 \cdot \text{ }^\circ\text{C))}$	Nu_w
50	49.632	50.611	3986.064	798.186	23.518
60	59.531	64.247	4646.381	898.408	26.109
70	69.405	81.186	5350.289	1025.704	29.373

$U_{air} = 4 \text{ m/s}$					
$\dot{m} = 2 \text{ L/m}$					
$t_{hi} \text{ }^\circ\text{C}$	$t_{ho} \text{ }^\circ\text{C}$	$Q_w \text{ (Watt)}$	Re_w	$h_i \text{ (W/(m}^2\cdot^\circ\text{C))}$	Nu_w
50	49.598	55.287	3985.023	798.055	23.515
60	59.477	71.645	4644.432	898.176	26.103
70	69.351	88.555	5348.523	1025.504	29.368

$U_{air} = 1 \text{ m/s}$		
$t_h \text{ } 70 \text{ }^\circ\text{C}$		
$\dot{m} \text{ L/m}$	NTU	ε
2	0.017	0.017
3	0.021	0.021
4	0.024	0.024
5	0.025	0.024
6	0.028	0.027

$\dot{m} = 2 \text{ L/m}$		
$t_h \text{ } 70 \text{ }^\circ\text{C}$		
$U_{air} \text{ m/s}$	$\Delta P_{theo.}$	$\Delta P_{exp.}$
1	56.8491	72.6
2	96.5347	132.2
3	140.023	172.3
4	186.184	241.5

$\dot{m} = 2 \text{ L/m}$		
$t_h \text{ } 70 \text{ }^\circ\text{C}$		
$U_{air} \text{ m/s}$	$U_i \text{ (W/(m}^2\cdot^\circ\text{C))}$	$U_o \text{ (W/(m}^2\cdot^\circ\text{C))}$
1	24.534	22.197
2	28.099	25.423
3	28.423	25.716
4	30.929	27.984

Table Appendix B.2. Finned tube.

$U_{air} = 1 \text{ m/s}$					
$\dot{m} = 2 \text{ L/m}$					
$t_{hi} \text{ }^\circ\text{C}$	$t_{ho} \text{ }^\circ\text{C}$	$Q_w \text{ (Watt)}$	Re_w	$h_i \text{ (W / (m}^2 \cdot \text{ }^\circ\text{C))}$	Nu_w
50	49.221	107.144	3973.51	796.601	23.478
60	58.961	142.348	4625.897	895.969	26.048
70	68.677	180.547	5326.597	1023.016	29.313

$U_{air} = 2 \text{ m/s}$					
$\dot{m} = 2 \text{ L/m}$					
$t_{hi} \text{ }^\circ\text{C}$	$t_{ho} \text{ }^\circ\text{C}$	$Q_w \text{ (Watt)}$	Re_w	$h_i \text{ (W / (m}^2 \cdot \text{ }^\circ\text{C))}$	Nu_w
50	48.865	156.118	3962.702	795.234	23.444
60	58.459	211.148	4608.01	893.836	25.995
70	68.038	267.787	5305.982	1020.67	29.261

$U_{air} = 3 \text{ m/s}$					
$\dot{m} = 2 \text{ L/m}$					
$t_{hi} \text{ }^\circ\text{C}$	$t_{ho} \text{ }^\circ\text{C}$	$Q_w \text{ (Watt)}$	Re_w	$h_i \text{ (W / (m}^2 \cdot \text{ }^\circ\text{C))}$	Nu_w
50	48.852	157.906	3962.308	795.184	23.443
60	58.452	212.107	4607.761	893.807	25.994
70	68.029	269.015	5305.693	1020.637	29.26

$U_{air} = 4 \text{ m/s}$					
$\dot{m} = 2 \text{ L/m}$					
$t_{hi} \text{ }^\circ\text{C}$	$t_{ho} \text{ }^\circ\text{C}$	$Q_w \text{ (Watt)}$	Re_w	$h_i \text{ (W / (m}^2 \cdot \text{ }^\circ\text{C))}$	Nu_w
50	48.817	162.722	3961.25	795.05	23.439
60	58.408	218.138	4606.201	893.62	25.99

70	67.993	273.931	5304.537	1020.505	29.257
----	--------	---------	----------	----------	--------

$\dot{m} = 2 \text{ L/m}$			
$t_h \text{ } 70 \text{ } ^\circ\text{C}$			
$U_{air} \text{ m/s}$	Re_a	$h_o \text{ (W/(m}^2 \cdot ^\circ\text{C))}$	Nu_a
1	17184.406	63.402	51.332
2	34412.198	98.069	79.441
3	51669.55	98.217	79.594
4	69011.483	99.636	80.801

$\dot{m} = 2 \text{ L/m}$		
$t_h \text{ } 70 \text{ } ^\circ\text{C}$		
$U_{air} \text{ m/s}$	$U_i \text{ (W/(m}^2 \cdot ^\circ\text{C))}$	$U_o \text{ (W/(m}^2 \cdot ^\circ\text{C))}$
1	64.976	58.788
2	96.634	87.431
3	96.764	87.548
4	98.006	88.673

$U_{air} = 1 \text{ m/s}$		
$t_h \text{ } 70 \text{ } ^\circ\text{C}$		
$\dot{m} \text{ L/m}$	NTU	ε
2	0.047	0.045
3	0.066	0.063
4	0.086	0.081
5	0.094	0.088
6	0.106	0.099

APPENDIX C.

CALCULATION FOR ONE CASE FOR SMOOTH AND FINNED TUBE

C.1. SMOOTH TUBE (EXPERIMENTAL DATA)

C.1.1. Data Case

Table Appendix C.1. Data case.

Parameter	t_{hi} °C	t_{ho} °C	t_{ci} °C	t_{co} °C	$t_{s.av.}$ °C	U_a m/s	\dot{m}_w L/m
Value	50	49.688	20	23.272	48.763	1	2

For first case with smooth tube at boundary condition Inlet temp.=50°C, velocity = 2 l/min for water and inlet temp.=20°C and Air velocity = 1 m/sec.

$$T_{wav.} = \frac{T_{wi} + T_{wo}}{2}$$
$$= \frac{50 + 49.688}{2} \Rightarrow T_{av.} = 49.844 \text{ °C}$$

$$\therefore \rho_{av.} = 988.267 \text{ Kg/m}^3$$

$$Cp_w = 4.175 \text{ kJ/Kg. K}$$

$$K_w = 0.645 \text{ W/m. K}$$

$$\mu_w = 0.00055 \text{ Kg/(m. sec.)}$$

C.1.2. The Rate of Heat Transfer

$$\dot{m}_w = \frac{2}{60 \times 1000} \times 988.267 \Rightarrow \dot{m}_w = 0.033 \text{ Kg/sec}$$

$$Q = \dot{m}_w \times Cp \times (T_{wi} - T_{wo})$$

$$Q = 0.033 \times 4.175 \times 10^3 \times (50 - 49.688)$$

$$Q = 42.909 \text{ W}$$

C.1.3. The Overall Heat Transfer Coefficient for Water

To Find Water Overall Heat Transfer Coefficient (U_i):

$$Q = U_i A_i \Delta T_m.$$

$$A_i = \pi \times d_i \times L \Rightarrow A_i = \pi \times 0.019 \times 1 \Rightarrow A_i = 0.0597 \text{ m}^2$$

$$\text{LMTD} = \frac{\Delta T_1 - \Delta T_2}{\ln\left(\frac{\Delta T_1}{\Delta T_2}\right)}$$

$$\Delta T_1 = T_{hi} - T_{co} \Rightarrow \Delta T_1 = 50 - 23.272 = 28.138^\circ\text{C}$$

$$\Delta T_2 = T_{ho} - T_{ci} \Rightarrow \Delta T_2 = 49.688 - 20 = 29.607^\circ\text{C}$$

$$\Rightarrow \text{LMTD} = 28.182$$

To Find Correction Factor (F):

$$F = \frac{(\sqrt{R^2 + 1}) \times \ln\left(\frac{1 - S}{1 - RS}\right)}{(R - 1) \times \ln\left(\frac{2 - S(R + 1 - (\sqrt{R^2 + 1}))}{2 - S(R + 1 + (\sqrt{R^2 + 1}))}\right)}$$

$$R = \frac{T_{hi} - T_{ho}}{T_{co} - T_{ci}} \Rightarrow R = \frac{50 - 49.688}{23.272 - 20} \Rightarrow R = 0.095$$

$$S = \frac{T_{co} - T_{ci}}{T_{hi} - T_{ci}} \Rightarrow S = \frac{23.272 - 20}{50 - 20} \Rightarrow S = 0.109$$

$$F = \frac{(\sqrt{0.095^2 + 1}) \times \ln\left(\frac{1 - 109066667}{1 - (0.095 \times 109066667)}\right)}{(0.095 - 1) \times \ln\left(\frac{2 - 109066667(0.095 + 1 - (\sqrt{0.095^2 + 1}))}{2 - 109066667(0.095 + 1 + (\sqrt{0.095^2 + 1}))}\right)}$$

$$\Rightarrow F = 0.999$$

$$U_i = \frac{Q}{A_i \times F \times \text{LMTD}} \Rightarrow$$

$$U_i = \frac{42.909}{0.0597 \times 0.999 \times 28.182}$$

$$\Rightarrow U_i = 25.513 \text{ W/m}^2\cdot\text{C}$$

C.1.4. The Average Temperature for Surface

$$T_s = \frac{T_1 + T_2 + T_3 + \dots + T_n}{n}$$

$$T_1 = 49.562^\circ\text{C}, T_2 = 48.981^\circ\text{C}, T_3 = 48.396^\circ\text{C}, T_4 = 48.114^\circ\text{C},$$

$$T_s = \frac{49.562 + 48.981 + 48.396 + 48.114}{4}$$

$$T_s = 48.763 \text{ } ^\circ\text{C}$$

C.1.5. Inside Tube

$$h_i = \frac{Q}{A_i(T_{av} - T_s)}$$

$$h_i = \frac{42.909}{0.0596(49.844 - 48.763)} =$$

$$h_i = 655.152 \frac{\text{W}}{\text{m}^2 \cdot ^\circ\text{C}}$$

$$Re_w = \frac{\rho_w u_w d_i}{\mu_w}$$

$$u_w = \frac{\dot{m}_w}{\rho_w A_{i,c}}$$

$$Pr_w = \frac{\mu_w C p_w}{K_w}$$

$$Nu_w = \frac{h_i d_i}{K_w}$$

C.1.6. Calculations for Air Side

$$U_i A_i = U_o A_o$$

$$U_o = \frac{U_i \times A_i}{A_o}$$

$$A_o = \pi \times d_o \times L \Rightarrow A_o = \pi \times 0.021 \times 1 \Rightarrow A_o = 0.066 \text{ m}^2$$

$$\therefore U_o = \frac{25.513 \times 0.0597}{0.066} \Rightarrow U_o = 23.083 \frac{\text{W}}{\text{m}^2 \cdot ^\circ\text{C}}$$

$$T_{av.} = \frac{T_{ai} + T_{ao}}{2} \Rightarrow T_{av.} = \frac{20 + 23.272}{2} = 21.636 \text{ } ^\circ\text{C}$$

$$C p_a = 1.0056 \text{ J/kg} \cdot ^\circ\text{C}$$

$$K_a = 0.026 \text{ W/m} \cdot ^\circ\text{C}$$

$$\rho_a = 1.203 \text{ Kg/m}^3$$

$$\mu_a = 0.00001820 \text{ Kg/(m. sec.)}$$

$$\alpha_a = 0.20403 \times 10^4 \frac{\text{m}^2}{\text{s}}$$

$$\gamma_a = 14.503 \times 10^6 \frac{m^2}{s}$$

$$h_o = \frac{1}{\left(\frac{1}{U_o}\right) - \left(d_o \times \frac{\ln\left(\frac{d_o}{d_i}\right)}{2 \times K_{cop}}\right) - \left(\frac{d_o}{h_i \times d_i}\right)}$$

$$K_{cop} = 385 \text{ W/m}^\circ\text{C}$$

$$\therefore h_o = \frac{1}{\left(\frac{1}{23.083}\right) - \left(0.021 \times \frac{\ln\left(\frac{0.021}{0.019}\right)}{2 \times 385}\right) - \left(\frac{0.021}{655.152 \times 0.019}\right)}$$

$$h_o = 23.96 \frac{W}{m^2 \cdot ^\circ C}$$

$$Re_a = \frac{\rho_a u_a d_z}{\mu_a}$$

$$d_z = \frac{4 \times (0.25 \times 0.275)}{2 \times (0.25 + 0.275)} = 0.262 \text{ m}$$

$$Re_a = \frac{1.203 \times 1 \times 0.262}{0.00001820} = 17309.673$$

$$Re_a = 17309.673 \quad (\text{turbulent flow})$$

$$Pr_a = \frac{\gamma_a}{\alpha_a} = \frac{14.503 \times 10^6}{0.20403 \times 10^4} = 0.7108$$

$$Pr_a = 0.7108$$

$$Nu_a = \frac{h_o d_o}{K_a} = 19.457$$

C.1.7. Calculations Water Pressure Drop (ΔP)

From Darcy–Weisbach Equation

$$\Delta P_{tube} = F \times \left(\frac{L}{d_i}\right) \times \left(\frac{\rho_w \times U_w^2}{2}\right)$$

$$F = \frac{0.316}{(Re_w)^{0.25}} \Rightarrow F = 0.0397$$

$$\Rightarrow \Delta P_{tube} = 0.0397 \times \left(\frac{1}{0.019}\right) \times \left(\frac{988.267 \times 0.1176^2}{2}\right)$$

$$\Rightarrow \Delta P_{tube} = 14.302 \text{ pa}$$

$$\Delta P_{fitt} = N \times K_1 \times \left(\frac{\rho_w \times U_w^2}{2}\right)$$

$$K_l = 1.9 \quad \text{at} \quad d_i = 19 \text{ mm}$$

$$\Delta P_{fitt} = 3 \times 1.9 \times \left(\frac{988.267 \times 0.1176^2}{2} \right)$$

$$\Rightarrow \Delta P_{fitt} = 38.952 \text{ Pa}$$

$$\Delta P_{Total} = \Delta P_{fitt} + \Delta P_{tube} \Rightarrow \Delta P_{Total} = 53.25479121 \text{ Pa}$$

C.1.8. Calculations for Number of Transfer Unit and Effectiveness

$$C_{hot} = \dot{m}_w \times C_{p_w} \Rightarrow C_{hot} = 0.137 = C_{max}$$

$$C_{cold} = \dot{m}_{air} \times C_{p_{air}} \Rightarrow C_{cold} = 0.083 = C_{min}$$

$$C_r = \frac{C_{min}}{C_{max}} \Rightarrow \frac{0.083}{0.137} \Rightarrow C_r = 0.605$$

$$NTU = \frac{U_o A_{os}}{C_{min}} = \frac{23.083 \times 0.066}{0.083 \times 1000} = 0.0183$$

For C_{min} mixed and C_{max} unmixed:

$$\varepsilon = (1 - \exp(-\frac{1}{C_r})) (1 - e^{-NTU \cdot C_r})$$

$$\varepsilon = (1 - \exp(-\frac{1}{0.605})) (1 - e^{-0.0183 \times 0.605}) = 0.022$$

$$\varepsilon = 0.018$$

C.2. FINNED TUBE WITH PITCH FINNED 1.6 MM (EXPERIMENTAL DATA)

C.2.1. Data Case

Table Appendix C.2. Data case.

Parameter	t_{hi} °C	t_{ho} °C	t_{ci} °C	t_{co} °C	$t_{s.av.}$ °C	U_a m/s	\dot{m}_w L/m
Value	50	49.221	20	24.064	45.086	1	2

$$T_{wav.} = \frac{T_{wi} + T_{wo}}{2} = \frac{50 + 49.221}{2} \Rightarrow T_{av.} = 49.61 \text{ °C}$$

$$\therefore \rho_{av.} = 988.397 \text{ Kg/m}^3$$

$$C_{p_w} = 4.175 \text{ kJ/Kg. K}$$

$$K_w = 0.64465 \text{ W/m. K}$$

$$\mu_w = 0.000556 \text{ Kg/(m. sec.)}$$

C.2.2. The Rate of Heat Transfer

$$\dot{m}_w = \frac{2}{60 \times 1000} \times 988.397 \Rightarrow \dot{m}_w = 0.033 \text{ Kg/sec}$$

$$Q = \dot{m}_w \times Cp \times (T_{wi} - T_{wo})$$

$$Q = 0.033 \times 4.174 \times 10^3 \times (50 - 49.221)$$

$$Q = 107.144 \text{ W}$$

C.2.3. The Overall Heat Transfer Coefficient for water

To Find Water Overall Heat Transfer Coefficient (Ui):

$$Q = U_i A_i \Delta T_m.$$

$$A_i = \pi \times d_i \times L \Rightarrow A_i = \pi \times 0.019 \times 1 \Rightarrow A_i = 0.0597 \text{ m}^2$$

$$LMTD = \frac{\Delta T_1 - \Delta T_2}{\ln\left(\frac{\Delta T_1}{\Delta T_2}\right)}$$

$$\Delta T_1 = T_{hi} - T_{co} \Rightarrow \Delta T_1 = 50 - 24.064 = 25.936^\circ\text{C}$$

$$\Delta T_2 = T_{ho} - T_{ci} \Rightarrow \Delta T_2 = 49.221 - 20 = 29.221^\circ\text{C}$$

$$\Rightarrow LMTD = 28.190728$$

To Find Correction Factor (F):

$$F = \frac{(\sqrt{R^2 + 1}) \times \ln\left(\frac{1 - S}{1 - RS}\right)}{(R - 1) \times \ln\left(\frac{2 - S(R + 1 - (\sqrt{R^2 + 1}))}{(2 - S(R + 1 + (\sqrt{R^2 + 1})))}\right)}$$

$$R = (T_{hi} - T_{ho}) / (T_{co} - T_{ci}) \Rightarrow R = \frac{50 - 49.221}{24.064 - 20} \Rightarrow R = 0.192$$

$$S = (T_{co} - T_{ci}) / (T_{hi} - T_{ci}) \Rightarrow S = \frac{24.064 - 20}{50 - 20} \Rightarrow S = 0.135$$

$$F = \frac{(\sqrt{0.192^2 + 1}) \times \ln\left(\frac{1 - 0.135}{1 - (0.192 \times 0.135)}\right)}{(0.192 - 1) \times \ln\left(\frac{2 - 0.135(0.192 + 1 - (\sqrt{0.192^2 + 1}))}{(2 - 0.135(0.192 + 1 + (\sqrt{0.192^2 + 1})))}\right)}$$

$$\Rightarrow F = 0.999$$

$$U_i = \frac{Q}{A_i \times F \times \text{LMTD}} \Rightarrow U_i = \frac{107.144}{0.0597 \times 0.999 \times 28.191}$$

$$\Rightarrow U_i = 65.209 \text{ W/m}^2 \cdot \text{C}$$

C.2.4. The Average Temperature for Surface

$$T_s = \frac{T_1 + T_2 + T_3 + \dots + T_n}{n}$$

$$T_1 = 47.99 \text{ }^\circ\text{C}, T_2 = 47.377 \text{ }^\circ\text{C}, T_3 = 47.174 \text{ }^\circ\text{C}, T_4 = 46.963 \text{ }^\circ\text{C},$$

$$T_s = \frac{47.99 + 47.377 + 47.174 + 46.963}{4}$$

$$T_s = 47.361 \text{ }^\circ\text{C}$$

C.2.5. Inside Tube

$$h_i = \frac{Q}{A_i(T_m - T_s)}$$

$$h_i = \frac{107.144}{0.0597(49.611 - 47.361)}$$

$$h_i = 796.601 \frac{\text{W}}{\text{m}^2 \cdot \text{C}}$$

$$Re_w = \frac{\rho_w u_w d_i}{\mu_w}$$

$$u_w = \frac{\dot{m}_w}{\rho_w A_{i,c}}$$

$$Pr_w = \frac{\mu_w C p_w}{K_w}$$

$$Nu_w = \frac{h_i d_i}{K_w}$$

C.2.6. Calculations for Air Side

$$U_o = \frac{U_i \times A_i}{A_o}$$

$$A_o = \pi \times d_o \times L \Rightarrow A_o = \pi \times 0.021 \times 1 \Rightarrow A_o = 0.066 \text{ m}^2$$

$$\therefore U_o = \frac{65.209 \times 0.0597}{0.066} \Rightarrow U_o = 58.999 \frac{W}{m^2 \cdot ^\circ C}$$

$$T_{av.} = \frac{T_{ai} + T_{ao}}{2} \Rightarrow T_{av.} = \frac{20 + 24.064}{2} = 22.032^\circ C$$

$$Cp_a = 1.0056 \text{ J/kg} \cdot ^\circ C$$

$$K_a = 0.026 \text{ W/m} \cdot ^\circ C$$

$$\rho_a = 1.2008 \text{ Kg/m}^3$$

$$\mu_a = 0.00001822 \text{ Kg/(m. sec.)}$$

$$\alpha_a = 0.2139 \times 10^4 \frac{m^2}{s}$$

$$\gamma_a = 0.1517 \times 10^4 \frac{m^2}{s}$$

$$h_o = \frac{1}{\left(\frac{1}{U_o}\right) - \left(d_o \times \frac{\ln\left(\frac{d_o}{d_i}\right)}{2 \times K_{cop}}\right) - \left(\frac{d_o}{h_i \times d_i}\right)}$$

$$K_{cop} = 385 \text{ W/m} \cdot ^\circ C$$

$$\therefore h_o = \frac{1}{\left(\frac{1}{58.999}\right) - \left(0.021 \times \frac{\ln\left(\frac{0.021}{0.019}\right)}{2 \times 385}\right) - \left(\frac{0.021}{796.601 \times 0.019}\right)}$$

$$h_o = 65.101 \frac{W}{m^2 \cdot ^\circ C}$$

$$Re_a = \frac{\rho_a u_a d_z}{\mu_a}$$

$$d_z = \frac{4 \times (0.25 \times 0.275)}{2 \times (0.25 + 0.275)} = 0.262 \text{ m}$$

$$Re_a = \frac{1.2007 \times 1 \times 0.262}{0.00001822} = 17379.121$$

$$Re_a = 17264.265 \quad (\text{turbulent flow})$$

$$Pr_a = \frac{\gamma_a}{\alpha_a} = \frac{0.1517 \times 10^4}{0.2139 \times 10^4} = 0.709$$

$$Pr_a = 0.709$$

$$Nu_a = \frac{h_o d_o}{K_a} = 52.809$$

C.2.7. Calculations Water Pressure Drop (ΔP)

For find Water Pressure Drop (ΔP)

From Darcy–Weisbach Equation

$$\Delta P_{tube} = f \times \left(\frac{L}{d_i}\right) \times \left(\frac{\rho_w \times U_w^2}{2}\right)$$

$$f = \frac{0.316}{(Re_w)^{0.25}} \Rightarrow f = 0.0398$$

$$\Rightarrow \Delta P_{tube} = 0.0398 \times \left(\frac{1}{0.019}\right) \times \left(\frac{988.397 \times 0.117^2}{2}\right)$$

$$\Rightarrow \Delta P_{tube} = 14.317 \text{ pa}$$

$$\Delta P_{fitt} = N \times K_1 \times \left(\frac{\rho_w \times U_w^2}{2}\right)$$

$$K_l = 1.9 \quad \text{at} \quad d_i = 19 \text{ mm}$$

$$\Delta P_{fitt} = 3 \times 1.9 \times \left(\frac{988.397 \times 0.117^2}{2}\right)$$

$$\Rightarrow \Delta P_{fitt} = 38.957 \text{ Pa}$$

$$\Delta P_{Total} = \Delta P_{fitt} + \Delta P_{tube} \Rightarrow \Delta P_{Total} = 53.274 \text{ Pa}$$

C.2.8. Calculations for Number of Transfer Unit and Effectiveness

$$C_{hot} = \dot{m}_w \times Cp_w \Rightarrow C_{hot} = 0.137 = C_{max}$$

$$C_{cold} = \dot{m}_{air} \times Cp_{air} \Rightarrow C_{cold} = 0.083 = C_{min}$$

$$C_r = \frac{C_{min}}{C_{max}} \Rightarrow \frac{0.083}{0.137} \Rightarrow C_r = 0.603$$

$$NTU = \frac{U_o A_{os}}{C_{min}} = \frac{58.999 \times 0.066}{0.083 \times 1000} = 0.0468$$

For C_{min} mixed and C_{max} unmixed:

$$\varepsilon = \left(1 - \exp\left(-\frac{1}{C_r}\right)\right) \left(1 - e^{-NTU \cdot C_r}\right)$$

$$\varepsilon = \left(1 - \exp\left(-\frac{1}{0.604}\right)\right) \left(1 - e^{-0.047 \times 0.604}\right)$$

$$\varepsilon = 0.045$$

RESUME

Mohammed Khalid Jar AL-ISAWI was born in Iraq / Al-Fallujah city and he graduated primary, elementary, and high school in this city, after that, he completed his bachelor's degree at the University of Technology, Department of Mechanical Engineering in Baghdad 2003-2004. Then in 2020, he started at Karabuk University Mechanical Engineering to complete his M. Sc. education.